

BULLETIN OF RUSSIAN STATE MEDICAL UNIVERSITY

BIOMEDICAL JOURNAL OF PIROGOV RUSSIAN NATIONAL
RESEARCH MEDICAL UNIVERSITY

EDITOR-IN-CHIEF Denis Rebrikov, DSc, professor

DEPUTY EDITOR-IN-CHIEF Alexander Oettinger, DSc, professor

EDITORS Valentina Geidebrekht, PhD; Nadezda Tikhomirova

TECHNICAL EDITOR Evgeny Lukyanov

TRANSLATORS Nadezda Tikhomirova, Vyacheslav Vityuk

DESIGN AND LAYOUT Marina Doronina

EDITORIAL BOARD

Averin VI, DSc, professor (Minsk, Belarus)
Alipov NN, DSc, professor (Moscow, Russia)
Belousov VV, DSc, professor (Moscow, Russia)
Bogomilskiy MR, corr. member of RAS, DSc, professor (Moscow, Russia)
Bozhenko VK, DSc, CSc, professor (Moscow, Russia)
Bylova NA, CSc, docent (Moscow, Russia)
Gainetdinov RR, CSc (Saint-Petersburg, Russia)
Gendlin GYe, DSc, professor (Moscow, Russia)
Ginter EK, member of RAS, DSc (Moscow, Russia)
Gorbacheva LR, DSc, professor (Moscow, Russia)
Gordeev IG, DSc, professor (Moscow, Russia)
Gudkov AV, PhD, DSc (Buffalo, USA)
Gulyaeva NV, DSc, professor (Moscow, Russia)
Gusev EI, member of RAS, DSc, professor (Moscow, Russia)
Danilenko VN, DSc, professor (Moscow, Russia)
Zarubina TV, DSc, professor (Moscow, Russia)
Zatevakhin II, member of RAS, DSc, professor (Moscow, Russia)
Kagan VE, professor (Pittsburgh, USA)
Kzyzhkowska YuG, DSc, professor (Heidelberg, Germany)
Kobriniskii BA, DSc, professor (Moscow, Russia)
Kozlov AV, MD PhD (Vienna, Austria)
Kotelevtsev YuV, CSc (Moscow, Russia)
Lebedev MA, PhD (Darem, USA)
Manturova NE, DSc (Moscow, Russia)
Milushkina OYu, DSc, professor (Moscow, Russia)
Mitupov ZB, DSc, professor (Moscow, Russia)
Moshkovskii SA, DSc, professor (Moscow, Russia)
Munblit DB, MSc, PhD (London, Great Britain)

Negrebetsky VV, DSc, professor (Moscow, Russia)
Novikov AA, DSc (Moscow, Russia)
Pivovarov YuP, member of RAS, DSc, professor (Moscow, Russia)
Polunina NV, corr. member of RAS, DSc, professor (Moscow, Russia)
Poryadin GV, corr. member of RAS, DSc, professor (Moscow, Russia)
Razumovskii AYU, corr. member of RAS, DSc, professor (Moscow, Russia)
Rebrova OYu, DSc (Moscow, Russia)
Rudoy AS, DSc, professor (Minsk, Belarus)
Rylova AK, DSc, professor (Moscow, Russia)
Savelieva GM, member of RAS, DSc, professor (Moscow, Russia)
Semiglazov VF, corr. member of RAS, DSc, professor (Saint-Petersburg, Russia)
Skoblina NA, DSc, professor (Moscow, Russia)
Slavyanskaya TA, DSc, professor (Moscow, Russia)
Smirnov VM, DSc, professor (Moscow, Russia)
Spallone A, DSc, professor (Rome, Italy)
Starodubov VI, member of RAS, DSc, professor (Moscow, Russia)
Stepanov VA, corr. member of RAS, DSc, professor (Tomsk, Russia)
Suchkov SV, DSc, professor (Moscow, Russia)
Takhchidi KhP, member of RAS, DSc, professor (Moscow, Russia)
Trufanov GE, DSc, professor (Saint-Petersburg, Russia)
Favorova OO, DSc, professor (Moscow, Russia)
Filipenko ML, CSc, leading researcher (Novosibirsk, Russia)
Khazipov RN, DSc (Marsel, France)
Chundukova MA, DSc, professor (Moscow, Russia)
Shimanovskii NL, corr. member of RAS, DSc, professor (Moscow, Russia)
Shishkina LN, DSc, senior researcher (Novosibirsk, Russia)
Yakubovskaya RI, DSc, professor (Moscow, Russia)

SUBMISSION <http://vestnikrgmu.ru/login?lang=en>

CORRESPONDENCE editor@vestnikrgmu.ru

COLLABORATION manager@vestnikrgmu.ru

ADDRESS ul. Ostrovityanova, d. 1, Moscow, Russia, 117997

Indexed in Scopus. CiteScore 2021: 0.5

Scopus[®]

SCImago Journal & Country Rank 2020: 0.14

SJR

Scimago Journal & Country Rank

Indexed in WoS. JCR 2021: 0.5

WEB OF SCIENCE[™]

Listed in HAC 31.01.2020 (№ 507)



ВЫСШАЯ
АТТЕСТАЦИОННАЯ
КОМИССИЯ (ВАК)

Five-year h-index is 8

Google
scholar

Open access to archive

CYBERLENINKA

Issue DOI: 10.24075/brsmu.2022-06

The mass media registration certificate № 012769 issued on July 29, 1994

Founder and publisher is Pirogov Russian National Research Medical University (Moscow, Russia)

The journal is distributed under the terms of Creative Commons Attribution 4.0 International License www.creativecommons.org



Approved for print 31.12.2022
Circulation: 100 copies. Printed by Print.Formula
www.print-formula.ru

ВЕСТНИК РОССИЙСКОГО ГОСУДАРСТВЕННОГО МЕДИЦИНСКОГО УНИВЕРСИТЕТА

НАУЧНЫЙ МЕДИЦИНСКИЙ ЖУРНАЛ РНИМУ ИМ. Н. И. ПИРОГОВА

ГЛАВНЫЙ РЕДАКТОР Денис Ребриков, д. б. н., профессор

ЗАМЕСТИТЕЛЬ ГЛАВНОГО РЕДАКТОРА Александр Эттингер, д. м. н., профессор

РЕДАКТОРЫ Валентина Гейдебрехт, к. б. н.; Надежда Тихомирова

ТЕХНИЧЕСКИЙ РЕДАКТОР Евгений Лукьянов

ПЕРЕВОДЧИКИ Надежда Тихомирова, Вячеслав Витюк

ДИЗАЙН И ВЕРСТКА Марины Дорониной

РЕДАКЦИОННАЯ КОЛЛЕГИЯ

В. И. Аверин, д. м. н., профессор (Минск, Белоруссия)
Н. Н. Алипов, д. м. н., профессор (Москва, Россия)
В. В. Белоусов, д. б. н., профессор (Москва, Россия)
М. Р. Богомилский, член-корр. РАН, д. м. н., профессор (Москва, Россия)
В. К. Боженко, д. м. н., к. б. н., профессор (Москва, Россия)
Н. А. Былова, к. м. н., доцент (Москва, Россия)
Р. Р. Гайнетдинов, к. м. н. (Санкт-Петербург, Россия)
Г. Е. Гендлин, д. м. н., профессор (Москва, Россия)
Е. К. Гинтер, академик РАН, д. б. н. (Москва, Россия)
Л. Р. Горбачева, д. б. н., профессор (Москва, Россия)
И. Г. Гордеев, д. м. н., профессор (Москва, Россия)
А. В. Гудков, PhD, DSc (Буффало, США)
Н. В. Гуляева, д. б. н., профессор (Москва, Россия)
Е. И. Гусев, академик РАН, д. м. н., профессор (Москва, Россия)
В. Н. Даниленко, д. б. н., профессор (Москва, Россия)
Т. В. Зарубина, д. м. н., профессор (Москва, Россия)
И. И. Затевахин, академик РАН, д. м. н., профессор (Москва, Россия)
В. Е. Каган, профессор (Питтсбург, США)
Ю. Г. Кжышковска, д. б. н., профессор (Гейдельберг, Германия)
Б. А. Кобринский, д. м. н., профессор (Москва, Россия)
А. В. Козлов, MD PhD (Вена, Австрия)
Ю. В. Котелевцев, к. х. н. (Москва, Россия)
М. А. Лебедев, PhD (Дарем, США)
Н. Е. Мантурова, д. м. н. (Москва, Россия)
О. Ю. Милушкина, д. м. н., доцент (Москва, Россия)
З. Б. Митупов, д. м. н., профессор (Москва, Россия)
С. А. Мошковский, д. б. н., профессор (Москва, Россия)
Д. Б. Мунблит, MSc, PhD (Лондон, Великобритания)

В. В. Негребцкий, д. х. н., профессор (Москва, Россия)
А. А. Новиков, д. б. н. (Москва, Россия)
Ю. П. Пивоваров, д. м. н., академик РАН, профессор (Москва, Россия)
Н. В. Полунина, член-корр. РАН, д. м. н., профессор (Москва, Россия)
Г. В. Порядин, член-корр. РАН, д. м. н., профессор (Москва, Россия)
А. Ю. Разумовский, член-корр., профессор (Москва, Россия)
О. Ю. Реброва, д. м. н. (Москва, Россия)
А. С. Рудой, д. м. н., профессор (Минск, Белоруссия)
А. К. Рылова, д. м. н., профессор (Москва, Россия)
Г. М. Савельева, академик РАН, д. м. н., профессор (Москва, Россия)
В. Ф. Семглазов, член-корр. РАН, д. м. н., профессор (Санкт-Петербург, Россия)
Н. А. Скоблина, д. м. н., профессор (Москва, Россия)
Т. А. Славянская, д. м. н., профессор (Москва, Россия)
В. М. Смирнов, д. б. н., профессор (Москва, Россия)
А. Спаллоне, д. м. н., профессор (Рим, Италия)
В. И. Стародубов, академик РАН, д. м. н., профессор (Москва, Россия)
В. А. Степанов, член-корр. РАН, д. б. н., профессор (Томск, Россия)
С. В. Сучков, д. м. н., профессор (Москва, Россия)
Х. П. Тахчиди, академик РАН, д. м. н., профессор (Москва, Россия)
Г. Е. Труфанов, д. м. н., профессор (Санкт-Петербург, Россия)
О. О. Фаворова, д. б. н., профессор (Москва, Россия)
М. Л. Филипенко, к. б. н. (Новосибирск, Россия)
Р. Н. Хазипов, д. м. н. (Марсель, Франция)
М. А. Чундокова, д. м. н., профессор (Москва, Россия)
Н. Л. Шимановский, член-корр. РАН, д. м. н., профессор (Москва, Россия)
Л. Н. Шишкина, д. б. н. (Новосибирск, Россия)
Р. И. Якубовская, д. б. н., профессор (Москва, Россия)

ПОДАЧА РУКОПИСЕЙ <http://vestnikrgmu.ru/login>

ПЕРЕПИСКА С РЕДАКЦИЕЙ editor@vestnikrgmu.ru

СОТРУДНИЧЕСТВО manager@vestnikrgmu.ru

АДРЕС РЕДАКЦИИ ул. Островитянова, д. 1, г. Москва, 117997

Журнал включен в Scopus. CiteScore 2021: 0,5

Журнал включен в WoS. JCR 2021: 0,5

Индекс Хирша (h²) журнала по оценке Google Scholar: 8

Scopus[®]

SCImago Journal & Country Rank 2020: 0,14

SJR
Scimago Journal & Country Rank

WEB OF SCIENCE[™]

Журнал включен в Перечень 31.01.2020 (№ 507)



**ВЫСШАЯ
АТТЕСТАЦИОННАЯ
КОМИССИЯ (ВАК)**

Google
scholar

Здесь находится открытый архив журнала

CYBERLENINKA

DOI выпуска: 10.24075/vrgmu.2022-06

Свидетельство о регистрации средства массовой информации № 012769 от 29 июля 1994 г.

Учредитель и издатель — Российский национальный исследовательский медицинский университет имени Н. И. Пирогова (Москва, Россия)

Журнал распространяется по лицензии Creative Commons Attribution 4.0 International www.creativecommons.org



Подписано в печать 31.12.2022
Тираж 100 экз. Отпечатано в типографии Print.Formula
www.print-formula.ru

ORIGINAL RESEARCH

5

The role of *mef* and *ermB* drug resistance genetic markers in the selection of fecal microbiota donors

Gospodaryk AV, Ulakhanova LA, Esiev SS, Polyakova EV, Shansky YD, Bespyatykh JA

Роль генетических маркеров лекарственной устойчивости *mef* и *ermB* при подборе доноров фекальной микробиоты

А. В. Господарик, Л. А. Улаханова, С. С. Есиев, Е. В. Полякова, Я. Д. Шанский, Ю. А. Беспятых

ORIGINAL RESEARCH

12

Gut microbiota alterations in patients with juvenile idiopathic arthritis

Porosyuk MV, Klementiev DD, Hodov NA, Gumenyuk LN, Esatova ES, Sereda EV, Chetveruhina-Malova KS, Sarchuk EV, Ivanov SV

Изменения микробиоты кишечника у больных ювенильным идиопатическим артритом

М. В. Поросюк, Д. Д. Клементьев, Н. А. Ходов, Л. Н. Гуменюк, Э. С. Эсатова, Е. В. Серёда, К. С. Четверухина-Малова, Е. В. Сарчук, С. В. Иванов

ORIGINAL RESEARCH

19

Mutational basis of meropenem resistance in *Pseudomonas aeruginosa*

Chebotar IV, Bocharova YuA, Chaplin AV, Savinova TA, Vasiliadis YuA, Mayansky NA

Мутационные основы формирования устойчивости к меропенему у *Pseudomonas aeruginosa*

И. В. Чеботарь, Ю. А. Бочарова, А. В. Чаплин, Т. А. Савинова, Ю. А. Василиадис, Н. А. Маянский

ORIGINAL RESEARCH

25

Identification of prognostically significant DNA methylation signatures in patients with various breast cancer types

Kalinkin AI, Sigin VO, Nemtsova MV, Strelnikov VV

Определение прогностически значимой сигнатуры ДНК-метилирования у пациенток с различными типами рака молочной железы

А. И. Калинин, В. О. Сигин, М. В. Немцова, В. В. Стрельников

ORIGINAL RESEARCH

35

The rs17713054 and rs1800629 polymorphisms of genes *LZTFL1* and *TNF* are associated with COVID-19 severity

Trasov AA, Minashkin MM, Poyarkov SV, Komarov AG, Shtinova IA, Speshilov GI, Karbyshev IA, Pozdnyakova NV, Godkov MA

Полиморфизмы rs17713054 и rs1800629 генов *LZTFL1* и *TNF* ассоциированы с тяжестью течения COVID-19

А. А. Траслов, М. М. Минашкин, С. В. Поляков, А. Г. Комаров, И. А. Штинова, Г. И. Спешилов, И. А. Карбышев, Н. В. Позднякова, М. А. Годков

ORIGINAL RESEARCH

41

Transgenic mice for study of the CDK8/19 cyclin-dependent kinase independent mechanisms of action

Stavskaya NI, Ilchuk LA, Okulova YuD, Kubekina MV, Varlamova EA, Silaeva YuYu, Bruter AV

Трансгенные мыши для изучения киназа-независимых механизмов действия циклин-зависимых киназ CDK8/19

Н. И. Ставская, Л. А. Ильчук, Ю. Д. Окулова, М. В. Кубекина, Е. А. Варламова, Ю. Ю. Силаева, А. В. Брутер

ORIGINAL RESEARCH

46

Knockout of mutant *TP53* in the HaCaT cells enhances their migration activity

Kozhin PM, Romashin DD, Rusanov AL, Luzgina NG

Нокаут мутантного *TP53* в клетках линии HaCaT усиливает их миграционную активность

П. М. Кожин, Д. Д. Ромашин, А. Л. Русанов, Н. Г. Лузгина

ORIGINAL RESEARCH

52

Peculiarities of amino acid profile in monocytes in breast cancer

Novoselova AV, Yushina MN, Patysheva MR, Prostakishina EA, Bragina OD, Garbukov EY, Kzhyshkowska JG

Особенности профиля аминокислот в моноцитах при раке молочной железы

А. В. Новоселова, М. Н. Юшина, М. Р. Патышева, Е. А. Простакишина, О. Д. Брагина, Е. Ю. Гарбуков, Ю. Г. Кжышкowska

ORIGINAL RESEARCH

60

Role of clusterin in predicting development of early- and late-onset preeclampsia in the first trimester of pregnancy

Timofeeva AV, Fedorov IS, Tarasova AM, Gorina KA, Suhova YuV, Gusar VA, Ivanets TYu

Роль кластерина в прогнозировании развития ранней и поздней преэклампсии в первом триместре беременности

А. В. Тимофеева, И. С. Федоров, А. М. Тарасова, К. А. Горина, Ю. В. Сухова, В. А. Гусар, Т. Ю. Иванец

ORIGINAL RESEARCH

72

Correlation of microembolism risk factors with age in the ischemic stroke recovery period

Orlova EV, Berdalin AB, Lelyuk VG

Взаимосвязь факторов риска микроэмболии с возрастом в восстановительном периоде ишемического инсульта

Е. В. Орлова, А. Б. Бердалин, В. Г. Лелюк

ORIGINAL RESEARCH

80

Neutrophil and monocyte extracellular traps in the diagnosis of post-covid syndrome

Salmasi JM, Poryadin GV, Panina MI, Larina VN, Ryzhikh AA, Stodelova EA, Kazimirskii AN

Нейтрофильные и моноцитарные экстраклеточные ловушки в диагностике постковидного синдрома

Ж. М. Салмаси, Г. В. Порядин, М. И. Панина, В. Н. Ларина, А. А. Рыжих, Е. А. Стоделова, А. Н. Казимирский

ORIGINAL RESEARCH

85

Algorithm of segmentation of OCT macular images to analyze the results in patients with age-related macular degeneration

Ibragimova RR, Gilmanov II, Lopukhova EA, Lakman IA, Bilyalov AR, Mukhamadeev TR, Kutluyarov RV, Idrisova GM

Алгоритм сегментации ОКТ-изображений макулы для анализа пациентов с возрастной макулярной дегенерацией

Р. Р. Ибрагимова, И. И. Гильманов, Е. А. Лопухова, И. А. Лакман, А. Р. Билялов, Т. Р. Мухамадеев, Р. В. Кутлугаров, Г. М. Идрисова

ORIGINAL RESEARCH

92

Justification of use of fixed retainers based on the analysis of size of the incisor and canine crowns

Postnikov MA, Butvilovsky AV, Alsharifi AAM, Madatyay AV, Kopetskiy IS, Eremin DA

Обоснование использования несъемных ретейнеров на основании анализа размеров коронок резцов и клыков

М. А. Постников, А. В. Бутвилковский, А. А. М. Алшарифи, А. В. Мадатян, И. С. Копецкий, Д. А. Еремин

ORIGINAL RESEARCH

99

Amicoumacin-based prodrug development approach

Shmygarev VI, Prokopenko YuA, Terekhov SS, Zakharova MYu, Dubinnyi MA, Smirnov IV, Yampolsky IV, Tsarkova AS

Подход к разработке пролекарства на основе Амикумацина А

В. И. Шмыгарев, Ю. А. Прокопенко, С. С. Терехов, М. Ю. Захарова, М. А. Дубинный, И. В. Смирнов, И. В. Ямпольский, А. С. Царькова

ORIGINAL RESEARCH

106

Efficacy of Favipiravir and Molnupiravir against novel SARS-CoV-2 variants *in vitro* and *in vivo*

Siniavin AE, Russu LI, Vasina DV, Shidlovskaya EV, Kuznetsova NA, Gushchin VA, Gintsburg AL

Эффективность фавипиравира и молнупиравира против новых вариантов SARS-CoV-2 в системах *in vitro* и *in vivo*

А. Э. Синявин, Л. И. Руссу, Д. В. Васина, Е. В. Шидловская, Н. А. Кузнецова, В. А. Гушчин, А. Л. Гинцбург

ORIGINAL RESEARCH

111

Ambient MS profiling of meningiomas: intraoperative oncometabolite-based monitoring

Bormotov DS, Shamraeva MA, Kuzin AA, Shamarina EV, Elifirov VA, Silkin SV, Zhdanova EV, Pekov SI, Popov IA

Прямое масс-спектрометрическое профилирование менингиом: интраоперационный мониторинг на основе онкометаболитов

Д. С. Бормотов, М. А. Шамраева, А. А. Кузин, Е. В. Шамарина, В. А. Елиферов, С. В. Силкин, Е. В. Жданова, С. И. Пеков, И. А. Попов

ORIGINAL RESEARCH

119

Effects of various mRNA-LNP vaccine doses on neuroinflammation in BALB/c mice

Kirshina AS, Kazakova AA, Kolosova ES, Imasheva EA, Vasileva OO, Zaborova OV, Terenin IM, Muslimov AR, Reshetnikov VV

Влияние различных доз мРНК-ЛНЧ-вакцин на нейровоспаление у BALB/c мышей

А. С. Киршина, А. А. Казакова, Е. С. Колосова, Е. А. Имашева, О. О. Васильева, О. В. Заборова, И. М. Теренин, А. Р. Муслимов, В. В. Решетников

OPINION

126

Drug design strategies for the treatment of coronavirus infection

Terekhov SS, Shmygarev VI, Purov KV, Smirnov IV, Yampolsky IV, Tsarkova AS

Стратегии дизайна лекарственных препаратов для лечения коронавирусной инфекции

С. С. Терехов, В. И. Шмыгарев, К. В. Пуртов, И. В. Смирнов, И. В. Ямпольский, А. С. Царькова

THE ROLE OF *MEF* AND *ERMB* DRUG RESISTANCE GENETIC MARKERS IN THE SELECTION OF FECAL MICROBIOTA DONORS

Gospodaryk AV¹ ✉, Ulakhanova LA¹, Esiev SS¹, Polyakova EV¹, Shansky YD¹, Bespyatykh JA^{1,2,3}

¹ Lopukhin Federal Research and Clinical Center Of Physical-Chemical Medicine under the Federal Medical Biological Agency, Moscow, Russia

² Mendeleev University of Chemical Technology of Russia, Moscow, Russia

³ Semashko National Research Institute of Public Health, Moscow, Russia

Fecal microbiota transplantation (FMT) is prescribed to treat various gastrointestinal pathologies. One of the most important and significant stages of FMT is selection of the donor. In recent years, special attention has been paid to checking the biomaterial for genes marking resistance to various groups of antibiotics. This study aimed to analyze the occurrence of *mef* and *ermB* drug resistance genetic markers in population of various age groups, including breastfed infants, and to determine microbiological composition of the flora of distal part of the intestine of potentially healthy volunteering FMT donors. A total of 52 biological samples (46 stool samples and 6 breast milk samples) were analyzed by real-time polymerase chain reaction. The macrolides resistance gene (*mef*) was detected in 97.8% of stool samples (different age groups), the gene marking resistance to macrolides, lincosamides, streptogramin (*ermB*) — in 93.5%. In the isolated "mother-child" group, the *mef* gene was found in all samples of breast milk and feces. The *ermB* gene in this group was found in 3 out of 6 breast milk samples and 4 out of 6 infant stool samples. Since the *mef* and *ermB* genetic determinants were identified not only among in adults but also in infants, it was suggested that transplant material (feces) containing these genes can be used for FMT. The analysis of microbiological composition of stool samples from 23 healthy volunteers (potential FMT donors) revealed that it rarely (in 8.7% of cases only) corresponds to what is considered to be a normal microbiota of the intestine's distal part.

Keywords: FMT, antibiotic resistance gene, *mef*, *ermB*, fecal microbiota donor, PCR

Funding: Grant of ANO Moscow Center for Innovative Technologies in Healthcare (#2412-31).

Author contribution: Gospodaryk AV — selection of study participants, PCR analysis of biological samples, literature analysis, article authoring; Ulakhanova LA — literature analysis, article authoring, fecal culture, bacteriological analysis; Esiev SS — literature analysis, isolation of nucleic acids from biological samples; Polyakova EV — practical part of the bacteriological analysis, isolation of nucleic acids from biological samples; Shansky YD — statistical data processing; Bespyatykh JA — study concept, consulting, article authoring and editing.

Compliance with ethical standards: the study was approved by the Ethics Committee of the Federal Research and Clinical Center Of Physical-Chemical Medicine under the Federal Medical Biological Agency of Russia (Minutes #2022/05/31 of May 31, 2022). All study participants signed the voluntary informed consent form.

✉ **Correspondence should be addressed:** Alina V. Gospodaryk
Krasnogorskoe shosse, 15, Odintsovo, Moscow region, 143007, Russia; alina.gospodarik@rcpcm.org

Received: 20.10.2022 **Accepted:** 25.11.2022 **Published online:** 16.12.2022

DOI: 10.24075/brsmu.2022.059

РОЛЬ ГЕНЕТИЧЕСКИХ МАРКЕРОВ ЛЕКАРСТВЕННОЙ УСТОЙЧИВОСТИ *MEF* И *ERMB* ПРИ ПОДБОРЕ ДОНОРОВ ФЕКАЛЬНОЙ МИКРОБИОТЫ

А. В. Господарик¹ ✉, Л. А. Улаханова¹, С. С. Есиев¹, Е. В. Полякова¹, Я. Д. Шанский¹, Ю. А. Беспятых^{1,2,3}

¹ Федеральный научно-клинический центр физико-химической медицины имени Ю. М. Лопухина Федерального медико-биологического агентства, Москва, Россия

² Российский химико-технологический университет имени Д. И. Менделеева, Москва, Россия

³ Национальный научно-исследовательский институт общественного здоровья имени Н. А. Семашко, Москва, Россия

Трансплантацию фекальной микробиоты (ТФМ) назначают в качестве терапии для лечения различных патологий желудочно-кишечного тракта. Подбор донора является одним из наиболее важных и значимых этапов для ТФМ. Особое внимание в последнее время уделяют проблеме наличия генов устойчивости к разным группам антибиотиков в биоматериале. Целью исследования было провести анализ встречаемости генетических маркеров лекарственной устойчивости *mef* и *ermB* среди разных возрастных групп населения, включая младенцев на грудном вскармливании, а также определить микробиологический состав дистальной части кишечника у потенциально здоровых добровольцев доноров ТФМ. Всего было проанализировано 52 образца биологического материала (46 образцов кала и шесть — грудного молока) методом полимеразной цепной реакции в режиме реального времени. Ген устойчивости к макролидам (*mef*) среди разных возрастных групп был выявлен в 97,8% образцах кала, ген устойчивости к макролидам, линкозамидам, стрептограмину (*ermB*) — в 93,5%. В отдельно выделенной группе «мать – дитя» ген *mef* обнаружен во всех образцах грудного молока и кала. Ген *ermB* в этой группе подтвержден в трех из шести образцов грудного молока и четырех из шести образцов кала младенцев. В результате детекции генетических детерминант *mef* и *ermB* не только среди взрослого населения, но и у младенцев, было выдвинуто предположение, что использование трансплантата (кала), содержащего данные гены допустимо для ТФМ. Анализ микробиологического состава кала 23 здоровых добровольцев — потенциальных доноров ТФМ, показал очень низкий процент соответствия (8,7%) нормам микробиоты дистальной части кишечника.

Ключевые слова: ТФМ, гены резистентности, *mef*, *ermB*, доноры фекальной микробиоты, ПЦР

Финансирование: Грант АНО «Московский центр инновационных технологий в здравоохранении» (№ 2412-31).

Вклад авторов: А. В. Господарик — подбор участников исследования, анализ биологических образцов методом ПЦР, анализ литературы, написание статьи; Л. А. Улаханова — анализ литературы, написание статьи, бактериологический посев кала, бактериологический анализ; С. С. Есиев — анализ литературы, выделение нуклеиновых кислот из биологических образцов; Е. В. Полякова — практическая часть бактериологического анализа, выделение нуклеиновых кислот из биологических образцов; Я. Д. Шанский — статистическая обработка данных; Ю. А. Беспятых — концепция исследования, консультирование, написание и редактирование статьи.

Соблюдение этических стандартов: исследование одобрено этическим комитетом ФГБУ ФНКЦ ФХМ ФМБА России (протокол номер 2022/05/31 от 31 мая 2022 г.). Добровольное информированное согласие подписано всеми участниками исследования.

✉ **Для корреспонденции:** Алина Владимировна Господарик
Красногорское шоссе, д. 15, г. Одинцово, Московская обл., 143007, Россия; alina.gospodarik@rcpcm.org

Статья получена: 20.10.2022 **Статья принята к печати:** 25.11.2022 **Опубликована онлайн:** 16.12.2022

DOI: 10.24075/vrgmu.2022.059

Presently, fecal microbiota transplantation (FMT) is becoming an increasingly popular approach to correcting microbiota dysbiosis caused by various pathologies. FMT is introduction of a suspension of feces from a healthy donor into the intestinal tract of a recipient; the procedure aims to treat or prevent a number of diseases by changing the recipient's microbiome [1–3]. Numerous randomized trials have shown the high efficiency of the method for treatment of refractory and recurrent forms of intestinal infections caused by *Clostridium difficile* [1, 4, 5]. Since 2013, FMT is a procedure officially approved by the US Food & Drug Administration (FDA) [6].

Donor screening and selection is one of the most important stages of FMT, since patient's safety depends thereon. Being the most time-consuming and resource-intensive stage part of the process, this stage consists of two steps: questionnaire filling (to collect the donor's medical history) and laboratory examination (to prevent possible transmission of pathogens to the recipient). Laboratory examination of the donor includes: basic hematological and biochemical blood tests, tests for hepatitis B and C, human immunodeficiency virus, syphilis, general urinalysis, coprogram, occult blood test, tests for protozoa and helminth eggs, fecal culture, PCR test for pathogenic intestinal flora and drug resistance genetic markers (presence of resistance genes) [7, 8].

The microorganisms carrying genes of resistance to antibiotics of various groups have been spreading actively recently [9]. One particular reason behind the spread is the generally more frequent use of broad-spectrum antimicrobial drugs. The pressure exerted by antibiotics on the microbial population translates into mutation or transformation of the genetic material, which leads to the development of new mechanisms enabling adaptation to the changing conditions [10]. In addition, bacteria can share the resistance genes with one another with the help of mobile elements (plasmids, transposons and integrons). The development of various sectors of industry drives outspread of the antibiotic resistance genes not only among microorganisms that directly interact with humans but also in the wild. Resistant bacteria have been found in deep underground trenches, in wastewater, surface and ground water, sediments and soil [11]. They are also present in organisms living in places relatively untouched by human civilization, such as Antarctica and the Arctic [12]. Antibiotic resistance genes are growing more and more common every year. One of the studies (lasted from 2011 through 2015) investigated the mechanisms of resistance to macrolides exhibited by *Streptococcus pyogenes* strains isolated from human microflora, as well as the frequency of occurrence of such resistance. The results of this study show that the pathogen has grown 6.8–12.6% more resistant to macrolides (among the total number of strains studied) [13].

In the context of screening microbiota transplantation donors, genes that determine the resistance of *Streptococcus* and *Staphylococcus* bacteria to macrolides, lincosamides, and streptogramins are of particular interest. The list of such genes includes *mef* (macrolide efflux), which encodes efflux proteins, and *ermB* (erythromycin ribosome methylation), which encodes 23S rRNA methylase that modifies antibacterial drug (ABD) target molecules [14, 15]. Another study has registered prevalence of *mefA* and *ermB* genetic determinants, with both resistance genes found in all intestinal microbiota samples collected from patients with chronic obstructive pulmonary disease that abstained from taking antibiotics for at least three months; the said genes were detected by both metagenomic method and real-time PCR [16, 17]. The resistance genes have also been found in large numbers in stool samples and even meconium collected from newborns [18].

These genes are common in potential FMT donors, which complicates selection of those who can donate healthy microbiota.

The purpose of this study was to analyze the occurrence of *mef* and *ermB* drug resistance genetic markers in population belonging to different age groups, and to determine microbiological composition of the flora of distal part of the intestine of potential FMT donors.

METHODS

Collection of samples

The initial group of donors was selected with the help of questionnaires and an algorithm developed for the purpose [7]. The inclusion criteria were: any gender; age from 18 to 55 years; no history of ABD treatment for a year or more. Stool samples were collected in this group to determine the composition of microflora, detect pathogenic microorganisms and screen for the resistance genes. The exclusion criteria were: a history of diseases associated with intestinal microbiota composition upset, chronic diseases and/or AND courses. In addition, the results of laboratory tests (general blood count, biochemical tests) allowed excluding volunteers that had any deviations from the normal parameters. Ultimately, based on the data obtained, 23 healthy volunteers were selected from the initial group of 53 as potential fecal microbiota donors. Other volunteers were excluded from further analysis due to abnormal blood test results.

Additionally, the study included a "mother-child" group. After receiving informed consent from the participants selected through random sampling, we collected biological material from the following categories of study participants: a) breastfed infants under 1 year of age who have never taken ABD; b) formula-fed infants under 1 year of age who have never taken ABD; c) children aged 1–3 who have never taken ABD; d) children 3 to 7 years old who have not taken ABD for more than a year. The "mother-child" group consisted of six couples (nursing mother/breastfed child); stool (mother and infant) and breast milk samples were taken from all of them.

A total of 52 samples of biological material were included in the study, including 46 stool samples and 6 breast milk samples. Among the stool samples ($n = 46$), 29 were from adults, 9 were from infants (2–11 months; 6 breastfed and 3 formula-fed), 4 from children 1 to 3 years old, 4 more from children aged 3–7 years.

Feces and breast milk were collected into individual sterile plastic containers. The samples (stool sample — 10–20 g, breast milk sample — 10–20 ml) were not frozen but sent to the laboratory in a thermal container immediately or stored for no more than 8 hours at 4 °C before submission to the laboratory.

Stool culture test

The stool culture testing followed provisions of the applicable regulations [19]. One gram of the native stool sample was homogenized in 9 ml of saline (10^{-1}) and left at room temperature for 10–15 minutes. The resulting suspension was plated on the solid nutrient media to detect pathogenic enterobacteria (SS- and XLD-agar (HiMedia Laboratories; India) and selenite broth (Biocompas-S; Russia) to isolate pathogenic *E. coli*. From the initial dilution (10^{-1}), we made a series of subsequent dilutions up to 10^{-9} .

The prepared dilutions were plated on nutrient media to cultivate various groups of microorganisms (1 ml of suspension

Table 1. Stool culture method

Dilution	Group microorganisms tested for	Nutrient medium	Amount of suspension plated, ml	Cultivation time, h	Results evaluation pattern
2	3	4	5	6	7
10 ⁻⁸	<i>Bifidobacterium</i>	Blaurock	1	72	Gram staining, microscopy
10 ⁻⁷	<i>Lactobacillus</i>	MRS-2			
10 ⁻⁵	<i>Clostridium</i>	Iron sulfite agar	1	72	Emission of hydrogen sulfide (black color of the medium), gas formation
	Hemolytic species of bacteria	Blood agar			Type of hemolysis: α, β, γ
10 ⁻³	<i>Enterobacteria</i>	Endo	0.1	20–22	Bacteria counting by lactose fermentation: + pink colonies and nutrient medium; — transparent colonies, no change in colony color
	Pathogenic fungi	Sabouraud			
	<i>Staphylococcus</i>	Yolk-salt agar		48	Chromogenic agar, determined by the color of the colonies
	<i>Enterococcus</i>	Milk inhibitor medium			Growth of colonies, yellow coloration of the medium — assimilation of mannitol, lecithinase activity
10 ⁻¹	Pathogenic enterobacteria	XLD agar	0.1	20–22	<i>Shigella</i> , <i>Salmonella spp.</i> transparent, for salmonella — colorless with a black center, <i>E. coli</i> — opaque yellow with a yellow zone around, <i>Proteus mirabilis</i> — yellow with a black center
		SS agar			<i>Shigella</i> , <i>Salmonella spp.</i> transparent, for salmonella — colorless with a black center, medium color — yellow; <i>E. coli</i> — raspberry, medium color — pink, <i>Proteus mirabilis</i> — brown with a dark center

plated on semi-liquid nutrient media, 0.1 ml on solid media, rubbed with a sterile spatula over the surface of the medium):

– 10⁻⁸ dilution — bifidobacteria on a semi-liquid nutrient medium Blaurock (FBUN GNC PMB Obolensk, Russia);

– 10⁻⁷ dilution — lactobacilli on semi-liquid nutrient medium MRS-2 (FBUN GNC PMB Obolensk, Russia) and bifidobacteria on Blaurock medium (FBUN GNC PMB Obolensk, Russia);

– 10⁻⁵ dilution — clostridia, 1 ml deep plated on iron sulfite agar (Biokompas-S; Russia); gram-negative enterobacteria — Endo medium (HiMedia Laboratories; India); hemolytic bacterial species - blood agar (HiMedia Laboratories; India).

– 10⁻³ dilution — plated on the Endo medium (Biokompas-S; Russia); plated on the Sabouraud medium (Biotechnovatsiya; Russia) to detect pathogenic fungi; plated yolk-salt agar (HiMedia Laboratories; India) to detect on staphylococci; and on milk-inhibitory medium ("Biokompas-S"; Russia) to detect enterococci (Table 1).

Culture test results were evaluated:

– after 20–22 hours for Endo, blood agar, SS- and XLD-agar;

– after 48 hours for Sabouraud, yolk-salt agar and milk inhibitor;

– after 72 hours for Blaurock, MRS-2, iron sulfite agar.

Where Endo media were used, we counted the number and the percentage of lactose-negative (colorless) colonies in relation to the total number of grown colonies. Colonies with mild enzymatic properties (weak decomposition of lactose —

pink colonies) were counted against the total number of *E. coli* colonies. According to the available recommendations, the generic composition of lactose-negative enterobacteria not belonging to the intestinal pathogenic bacteria family can be left undetailed; it is sufficient to count the total amount of lactose-negative colonies on the Endo medium.

Extraction of DNA from biological material

We used the DNA-SORBENT kit (Litech; Russia) and followed the manufacturer's protocol to extract DNA from biological material (feces, breast milk). In case of breast milk, we extracted DNA from saliva, cerebrospinal fluid, and synovial fluid. Prior to submission for PCR testing, the isolated DNA was stored at –20 °C.

Analysis of genetic markers of drug resistance

We used the RESISTOM.mef monoplex kit to detect macrolides resistance mef-genes in *Streptococcus spp.*, RESISTOM.ermB to detect macrolides, lincosamides and streptomycin B resistance erm-genes in *Streptococcus spp.* and *Staphylococcus spp.*; the format was FLUOROPOL-RV (Litech; Russia), method — real-time PCR in a CFX96 amplifier (Bio-Rad Laboratories; USA). A total of 52 DNA samples isolated from biological material (feces and milk) were analyzed. To control the quality of DNA extraction and to prevent the occurrence

Table 2. Bacteria culture test, stool samples from potentially healthy volunteers

№	Microflora	Normal, cfu/g	Number of volunteers, people		p
			Within normal limits	Deviation from the normal	
1	<i>Bifidobacterium spp</i>	10 ⁸ AND ABOVE	13	10	0,678
2	<i>Lactobacillus spp</i>	10 ⁶ -10 ⁷	12	11	0,835
3	Total number of enterobacteria	10 ⁷ -10 ⁸	12	11	0,835
4	<i>Escherichia spp</i>	10 ⁷ -10 ⁸	12	11	0,835
5	<i>Enterococcus spp</i>	10 ⁶ -10 ⁷	4	19	0,004
6	Conditionally pathogenic enterobacteria: <i>Enterobacter cloacae</i> , <i>Enterobacter gergoviae</i> , <i>Citrobacter freundii</i> , <i>Citrobacter amalonaticus</i> , lactose-negative <i>Escherichia coli</i>	< 10 ⁴	8	15	0,211
7	Intestinal pathogenic microorganism	Should be absent	23	0	< 0,001
8	<i>Staphylococcus</i>	≤ 10 ⁴ / Should be absent	9	14	0,404
	<i>S. aureus</i>	≤ 10 ⁴ / Should be absent	21	2	< 0,001
9	<i>Candida spp</i>	≤ 10 ⁴	23	0	< 0,001
10	Non-fermenting gram-negative bacteria incl. <i>Pseudomonas aeruginosa</i> , <i>Pseudomonas putida</i>	≤ 10 ⁴	19	4	0,004
11	Sulfite-reducing anaerobes of the <i>Clostridium</i> genus	≤ 10 ⁶	12	11	0.835

of false negative results in the set we relied on internal exogenous control (detected via the HEX channel) introduced into the studied samples at the DNA extraction stage. The PCR pattern was as follows: 80 °C — 2 minutes, 95 °C — 1 minute 30 seconds, then 40 cycles: 95 °C — 15 seconds, 60 °C — 30 seconds, 72 °C — 40 seconds.

Statistical analysis

Statistical processing was performed with the help of Statistica 10.0 software (StatSoft Inc.; USA). The significance of differences in the registered prevalence of ABD resistance genes (in groups) was assessed by Pearson's χ^2 test with Yates's correction. The significance of differences in the registered prevalence among bacteriological parameters was assessed by McNemar's test. A difference was considered statistically significant at $p < 0.05$.

RESULTS

According to the questionnaire data and the results of clinical studies (complete blood count and blood chemistry tests), 23 volunteers out of 53 were included for further research as potential donors of fecal microbiota.

To determine the probable minimum age when a person becomes a carrier of the studied genes, as well as to identify the ways of transmission of macrolide resistance genes (*mef* and *ermB*), we formed a mother-child group (6 people). Twelve stool samples and six breast milk samples were included in the study from this group.

Bacteriological analysis

In the course of the work, we preliminarily assessed qualitative and quantitative bacteriological composition of the stool samples from potentially healthy volunteers ($n = 23$). The results

of the bacteria culture test corresponded to the values given in regulatory documents [20]; they are presented in Table 2.

Composition of the obligate microflora species, such as *Bifidobacterium*, *Lactobacillus*, *Escherichia*, is normal in 52.2% of the participants, and that of *Enterococcus* — in 8.7%. In 34.8% of the participants the content of conditionally pathogenic bacteria of facultative microflora was normal or below normal; the species of that microflora are *Enterobacter cloacae*, *Staphylococcus aureus*, *Citrobacter freundii*, *Citrobacter amalonaticus*, *Pseudomonas aeruginosa*, *Pseudomonas putida*, *Enterobacter gergoviae*, lactose-negative *Escherichia coli*.

Thus, the bacterial test has shown that only 8.7% of the volunteers met the standards of all indicators, which is only 4 people out of 23 examined.

Molecular genetic analysis

All 23 volunteering donors tested positive for genetic markers of drug resistance to macrolides, both genes (*mef* and *ermB*).

Therefore, in order to identify the age when these genes appear, find out if there is a relationship between their presence and intake of ABD and establish the transmission pathways we formed the "mother-child" sample and samples comprised of children of various ages. Both stool and breast milk samples were tested for *mef* and *ermB* resistance genes. Table 3 presents data on the presence of resistance genes in feces in all volunteers ($n = 46$; different age groups).

The stool sample analysis has revealed the *mef* macrolide resistance gene in 45 (97.8%) out of 46 samples (Tables 3 and 4). Only one sample, that collected from a 7-year old child, did not contain this gene. The presence of the *ermB* gene encoding resistance to macrolides, lincosamides, streptogramin was confirmed in 43 (93.5%) out of 46 cases (Tables 3 and 4). The *ermB* gene was not detected in stool samples from three breastfed and formula-fed infants.

Table 3. Prevalence of *mef* and *ermB* resistance genes in feces, different age groups

Genes	"Mother-child" group		Formula-fed children	Children 1-3 years old	Children 3-7 years old	Adults
	baby's feces	mother's feces				
<i>mef</i>	6/6	6/6	3/3	4/4	3/4	23/23
<i>ermB</i>	4/6	6/6	2/3	4/4	4/4	23/23

Note: * — ratio of the number of samples in which the gene was detected to the total number of samples in the respective group.

Table 4. Prevalence of *mefA* and *ermB* resistance genes in the "mother-child" group

Genes	"Mother-child"		
	Breast milk	Baby's feces	Mother's feces
<i>mef</i>	6/6	6/6	6/6
<i>ermB</i>	3/6	4/6	6/6

Note: * — ratio of the number of samples in which the gene was detected to the total number of samples in the respective group.

Forty-four (84.6%) out of 52 samples had both *mef* and *ermB* resistance genes simultaneously.

Statistical analysis of prevalence of *mef* and *ermB* genes did not reveal significant differences between the age groups ($p = 0.258$).

All breast milk samples collected from mothers breastfeeding their infants in the "mother-child" group (Table 4) contained the genetic determinants (*mef* gene). As for the *ermB* gene, it was found in 3 out of 6 breast milk samples and 4 out of 6 infant stool samples. A noteworthy case is that of a baby who was fed with breast milk that did not contain the *ermB* gene and whose feces proved to have it, nevertheless. There were no significant differences established between the subgroups in studying the joint prevalence of the *mef* and *ermB* resistance genes in the "nursing mother — breastfed child" group ($p = 0.423$).

DISCUSSION

Fecal microbiota transplantation donor screening is one of the most difficult and important stages of the therapy, since it is necessary to exclude or minimize the undesirable consequences of transplantation for the recipient. Special attention should be paid to resistant bacteria that, as a result of transplantation, can trigger emergence of resistant clones in the recipient's microflora [21]. In this connection, it should be remembered that a respective negative result of the bacterial culture test does not guarantee there are no resistance genes in the sample at all.

Bacterial culture allows identifying specifics of the fecal microflora, which reflects the microbial composition of the distal intestines, and to determine the qualitative and quantitative content of the microbiota. Changes in the ratio of certain types of microorganisms allows diagnosing dysbiotic disorders of the digestive tract.

In a healthy person, the colon typically hosts three groups of bacteria: 1) obligate microflora (more than 90%), which includes non-pathogenic types of bacteria (bifidobacteria, bacteroids, lactobacilli, *E. coli*, enterococci) and enables the main physiological functions of the body (digestion, absorption); 2) facultative microflora (less than 10%), which includes conditionally pathogenic microorganisms (clostridia, *Staphylococcus*, proteus, campylobacter, yeast-like fungi, etc.) and is involved in protective and digestive functions; 3) transient (random) microflora (not more than 1%), represented by *Pseudomonas aeruginosa*, fungi of the genus *Candida*, pathogenic enterobacteria, etc. Bacterial culture test has shown that in our sample, the healthy donors (4 out of 23) had a sufficient amount of bifidobacteria, lactobacilli, *Escherichia* and enterococci, and the number of opportunistic bacteria they hosted was within the normal range, which corresponds to regulatory documents [22]. The majority of the examined participants (17 out of 23) had dysbiotic disorders: quantitatively insufficient obligate microflora or overabundant facultative and transient microflora, which can result from an unbalanced diet and frequent stress.

Obviously, a bacteriological study of the feces cannot give a complete picture of the diversity of intestinal microflora,

since microbiota may contain uncultivated bacteria and some bacteria present in small quantities only cannot be cultivated on artificial nutrient media. Currently, the two methods that yield a more accurate data on composition of the intestinal microbiota are whole genome sequencing and metagenomic analysis. However, a standard approach to medical examination of a person includes bacterial culture and biochemical markers tests only, the results thereof being the basis for conclusion about the state of health of the patient. The so-called omics analytical methods are not currently routine in the practice of a clinician. Undoubtedly, to understand the exact mechanism of action of FMT and, possibly, to isolate the most active components thereof, it is necessary to conduct multidisciplinary complex studies. At the same time, more and more medical institutions introduce FMT into their practice and can only rely on routine tests to screen donors. Thus, it is important to understand the significance of testing the potential FMT biomaterial for resistance genes.

In this work, we focused on the analysis of prevalence of *mef* and *ermB* genes, which determine resistance to macrolides, lincosamides, and streptomycin B. According to the data obtained, both of them were detected in stool samples from all 23 healthy volunteers.

In the additionally formed "mother-child" group, we identified the *mef* gene in all breast milk and stool samples of the following categories of participants who had never taken ABD: breastfed infants under 1 year of age; formula-fed babies; children 1–3 years old. This gene was also found in all adults and three children, aged 3 to 7 years, who had not taken ABD for more than a year. The results of our study are consistent with the report on another research effort that saw the *mef* gene in the feces of 100% of newborns participating therein [22].

The *ermB* gene was not detected in stool samples from three infants. Two of them were breastfed and their mothers' milk did not contain this gene, one baby was formula-fed. It should also be noted that feces from one baby has the *ermB* gene, although breast milk of this baby's mother does not have this gene. Two formula-fed children under one year of age have the *ermB* gene in their feces. The issue of the acquisition of genetic determinants in the feces of newborns in the prenatal period, during childbirth or thereafter is not fully understood. Previous studies have confirmed that resistance genes in the feces of newborns were acquired after birth (for example, through breast milk and/or air or drinking water, since resistance genes were not found in the amniotic fluid and meconium of newborns [23–25]).

CONCLUSIONS

The analysis of microbiological composition of feces from 23 potentially healthy volunteers showed that only 8.7% of them had the appropriate microbiota of the intestine's distal part and could be considered as potential FMT donors. This may indicate that population as a whole has a problem with composition of the microbiota. Additionally, the study analyzed the *mef* and *ermB* drug resistance genetic markers occurrence in different age groups, including infants. We have revealed a high prevalence of the macrolide resistance gene, *mef*, which

reached up to 97.8%, while that for *ermB*, gene of resistance to macrolides, lincosamides, streptogramin, was 93.5%. In the "mother-child" group, all stool and breast milk samples had the *mef* gene. Thus, in view of the fact that the *mef* and *ermB* genes can be found not only in the adult population but also

in infants, we suggested that the use of a transplant (feces) containing these genes is acceptable for FMT. These data can help clinicians introducing FMT into their practice in the context of independent search for donors and preparation of biomaterial.

References

1. Cammarota G, Ianiro G, Tilg H, Rajilić-Stojanović M, Kump P, Satokari R, et al. European consensus conference on faecal microbiota transplantation in clinical practice. *Gut*. 2017; 66 (4): 569–80. DOI: 10.1136/gutjnl-2016-313017.
2. Baunwall SMD, Lee MM, Eriksen MK, Mullish BH, Marchesi JR, Dahlerup JF, et al. Faecal microbiota transplantation for recurrent *Clostridioides difficile* infection: An updated systematic review and meta-analysis. *EClinicalMedicine*. 2020; 23: 29–30. PMID: 33437951; PMID: PMC7788438. DOI: 10.1016/j.eclinm.2020.100642.
3. Wang Y, Zhang S, Borody T, Zhang F. Encyclopedia of fecal microbiota transplantation: a review of effectiveness in the treatment of 85 diseases. *Chinese Medical Journal*. 2022; 10.1097/CM9.0000000000002339 DOI: 10.1097/CM9.0000000000002339.
4. Surawicz CM, Brandt LJ, Binion DG, Ananthakrishnan AN, Curry SR, Gilligan PH, et al. Guidelines for diagnosis, treatment, and prevention of *Clostridium difficile* infections. *Am J Gastroenterol*. 2013; 108 (4): 478–98.
5. Debast SB, Bauer MP, Kuijper EJ, European Society of Clinical M, Infectious D: European Society of Clinical Microbiology and Infectious Diseases: update of the treatment guidance document for *Clostridium difficile* infection. *Clin Microbiol Infect*. 2014; 20 (Suppl 2): 1–26.
6. Enforcement Policy Regarding Investigational New Drug Requirements for Use of Fecal Microbiota for Transplantation to Treat *Clostridium difficile* Infection Not Responsive to Standard Therapies. 2013; www.fdagov.
7. Shherbakov PL, Belova ND, Genozov EhV, Zhgun ES, Ivanova OI, Il'ina EN, i dr. Primenenie fekal'noj transplantacii v lechenii zabolevanij pishhevaritel'nogo trakta (pervyj klinicheskij opyt). *Doktor.Ru*. 2019; 3 (158): 40–46. DOI: 10.31550/1727-2378-2019-158-3-40-46. Russian.
8. Yakupova AA, Abdulxakov SR, Safin AG, Alieva IM, Osloпова YuV, Abdulxakov RA. Transplantaciya fekal'noj mikrobioty: kriterii vybora donora, podgotovki i xraneniya biomateriala (obzor sovremennyx rekomendacij). *Terapevticheskij arxiv*. 2021; 93 (2): 215–21. DOI: 10.26442/00403660.2021.02.200615. Russian.
9. Ehjdelshitejn MV. Ehkstremaal'no- i panrezistentnye klony bakterial'nyx vobuditelej v klinike. Tezisy dokladov ezhegodnoj Vserossijskoj nauchno-prakticheskoy konferencii s mezhdunarodnym uchastiem «Kontrol' i profilaktika infekcij, svyazannyx s okazaniem medicinskoj pomoshhi (ISMP-2015)», 25 noyabrya 2015, Moskva Zhurnal Medial'. 2015, 3 (17). Russian.
10. Turkutyukov VB. Molekulyarno-geneticheskij monitoring rezistentnosti mikroorganizmov k antibiotikam. *Tixookeanskij medicinskij zhurnal*. 2011; 2 (44): 28–31. Russian.
11. Zhuangab M, Achmonab Y, Cao Y, Liang X, Chen L, Wange H, et al. Distribution of antibiotic resistance genes in the environment. *Environmental Pollution*. 2021; 285. Article 117402. DOI: org/10.1016/j.envpol.2021.117402.
12. Roberts MC. Environmental macrolide–lincosamide–streptogramin and tetracycline resistant bacteria *Front. Microbiol*. 2011. Available from: <https://doi.org/10.3389/fmicb.2011.00040>.
13. Katosova LK, Lazareva AV, Xoxlova TA., Ponomarenko OA, Alyabeva NM. Rasprostranenie i mexanizmy ustojchivosti k makrolidam *Streptococcus pyogenes*, vydelennyx u detej. *Antibiotiki i ximioterapiya*. 2016; 61 (3–4): 23–29. Russian.
14. Farrell DJ, Morrissey I, Bakker S, Morris L, Buckridge S, Felmingham D. Molecular epidemiology of multiresistant *Streptococcus pneumoniae* with both *erm(B)*- and *mef(A)*-mediated macrolide resistance. *J Clin Microbiol*. 2004; 42 (2): 764–8. DOI: 10.1128/JCM.42.2.764–768.2004. PMID: 14766850; PMID: PMC344484.
15. Reinert RR, Ringelstein A, van der Linden M, Cil MY, Al-Lahham A, Schmitz FJ. Molecular epidemiology of macrolide-resistant *Streptococcus pneumoniae* isolates in Europe. *J Clin Microbiol*. 2005; 43 (3): 1294–300. DOI: 10.1128/JCM.43.3.1294–1300.2005. PMID: 15750098; PMID: PMC1081259.
16. Ikryannikova LN, Senina ME, Lisicina ES, Ogorodova LM, Fedosenko SV, Karnaushkina MA, i dr. Vidovaya identifikaciya i analiz geneticheskix markerov lekarstvennoj ustojchivosti streptokokkov s pomoshh'yu kolichestvennoj mul'tipleksnoj polimeraznoj cepnoj reakcii u pacientov s xronicheskoi obstruktivnoj boleznyu legkix. *Pul'monologiya*. 2014; (6): 40–48. Dostupno po ssylke: <https://doi.org/10.18093/0869-0189-2014-0-6-40-48>. Russian.
17. Fedosenko SV, Ogorodova LM, Ilina EN, Senina ME, Lisicina ES, Karnaushkina MA, i dr. Geneticheskie determinanty ustojchivosti orofaringeal'nyx streptokokkov k antibakterial'nym sredstvam u pacientov s xronicheskoy obstruktivnoj boleznyu legkix i bol'nyx bronxial'noj astmoj. *Terapevticheskij arxiv*. 2015; 87 (8): 51–57. DOI: 10.17116/terarkh201587851-57. Russian.
18. Gosalbes MJ, Vallès Y, Jiménez-Hernández N, Balle C, Riva P, Miravet-Verde S, et al. High frequencies of antibiotic resistance genes in infants' meconium and early fecal samples. *J Dev Orig Health Dis*. 2016; 7: 35–44. DOI: 10.1017/S2040174415001506.
19. Ehpshitejn-Litvak RV, Vilshanskaya FL. Bakteriologicheskaya diagnostika disbakterioza kishhechnika. *Metodicheskie rekomendacii*. M., 1977; 20 s. Russian.
20. Protokol vedeniya bol'nyx. *Disbakterioz kishhechnika: OST 91500.11.0004-2003. Prikaz Minzdrava Rossii # 231 ot 09.06.03. (Otraslevoj standart)*. Russian.
21. U.S. Food and Drug Administration. Information pertaining to additional safety protections regarding use of fecal microbiota for transplantation — screening and testing of stool donors for multi-drug resistant organisms. 2019. Available from: <https://www.fda.gov/vaccines-blood-biologics/safety-availability-biologics/information-pertaining-additional-safety-protections-regarding-use-fecal-microbiota-transplantation>.
22. Klassert TE, Zubiria-Barrera C, Kankel S, Stock M, Neubert R, Lorenzo-Diaz F, et al. Early Bacterial Colonization and Antibiotic Resistance Gene Acquisition in Newborns. *Front Cell Infect Microbiol*. 2020; 10: 332. DOI: 10.3389/fcimb.2020.00332. PMID: 32754449; PMID: PMC7366792.
23. Zhang K, Jin M, Yang D, Shen Z, Liu W, Yin J, et al. Antibiotic resistance genes in gut of breast-fed neonates born by caesarean section originate from breast milk and hospital ward air. *BMC Microbiol*. 2022; 36. DOI: org/10.1186/s12866-022-02447-8.
24. Huang MS, Cheng CC, Tseng SY, Lin YL, Lo HM, Chen PW. Most commensally bacterial strains in human milk of healthy mothers display multiple antibiotic resistance. *Microbiology Open*. 2019; 8 (1): e00618 doi.org/10.1002/mbo3.618.
25. Carvalho MJ, Sands K, Thomson, Portal KE, Mathias J, Milton R, et al. Antibiotic resistance genes in the gut microbiota of mothers and linked neonates with or without sepsis from low- and middle-income countries. *Nat Microbiol*. 2022; 7: 1337–47. Available from: doi.org/10.1038/s41564-022-01184-y.

Литература

- Cammarota G, Ianiro G, Tilg H, Rajilić-Stojanović M, Kump P, Satokari R, et al. European consensus conference on faecal microbiota transplantation in clinical practice. *Gut*. 2017; 66 (4): 569–80. DOI: 10.1136/gutjnl-2016-313017.
- Baunwall SMD, Lee MM, Eriksen MK, Mullish BH, Marchesi JR, Dahlerup JF, et al. Faecal microbiota transplantation for recurrent *Clostridioides difficile* infection: An updated systematic review and meta-analysis. *EClinicalMedicine*. 2020; 23: 29–30. PMID: 33437951; PMCID: PMC7788438. DOI: 10.1016/j.eclinm.2020.100642.
- Wang Y, Zhang S, Borody T, Zhang F. Encyclopedia of fecal microbiota transplantation: a review of effectiveness in the treatment of 85 diseases. *Chinese Medical Journal*. 2022; 10.1097/CM9.0000000000002339 DOI: 10.1097/CM9.0000000000002339.
- Surawicz CM, Brandt LJ, Binion DG, Ananthkrishnan AN, Curry SR, Gilligan PH, et al. Guidelines for diagnosis, treatment, and prevention of *Clostridium difficile* infections. *Am J Gastroenterol*. 2013; 108 (4): 478–98.
- Debast SB, Bauer MP, Kuijper EJ, European Society of Clinical M, Infectious D: European Society of Clinical Microbiology and Infectious Diseases: update of the treatment guidance document for *Clostridium difficile* infection. *Clin Microbiol Infect*. 2014; 20 (Suppl 2): 1–26.
- Enforcement Policy Regarding Investigational New Drug Requirements for Use of Fecal Microbiota for Transplantation to Treat *Clostridium difficile* Infection Not Responsive to Standard Therapies. 2013; www.fdagov.
- Щербakov П. Л., Белова Н. Д., Генерозов Э. В., Жгун Е. С., Иванова О. И., Ильина Е. Н. и др. Применение фекальной трансплантации в лечении заболеваний пищеварительного тракта (первый клинический опыт). *Доктор.Ру*. 2019; 3 (158): 40–46. DOI: 10.31550/1727-2378-2019-158-3-40-46.
- Якупова А. А., Абдулхаков С. Р., Сафин А. Г., Алиева И. М., Ослопова Ю. В., Абдулхаков Р. А. Трансплантация фекальной микробиоты: критерии выбора донора, подготовки и хранения биоматериала (обзор современных рекомендаций). *Терапевтический архив*. 2021; 93 (2): 215–21. DOI: 10.26442/0403660.2021.02.200615.
- Эйдельштейн М. В. Экстремально- и панрезистентные клоны бактериальных возбудителей в клинике. Тезисы докладов ежегодной Всероссийской научно-практической конференции с международным участием «Контроль и профилактика инфекций, связанных с оказанием медицинской помощи (ИСМП-2015)», 25 ноября 2015, Москва Журнал МедиАль. 2015; 3 (17).
- Туркутоков В. Б. Молекулярно-генетический мониторинг резистентности микроорганизмов к антибиотикам. *Тихоокеанский медицинский журнал*. 2011; 2 (44): 28–31.
- Zhuangab M, Achmonab Y, Cao Y, Liang X, Chen L, Wange H, et al. Distribution of antibiotic resistance genes in the environment. *Environmental Pollution*. 2021; 285. Article 117402. DOI: org/10.1016/j.envpol.2021.117402.
- Roberts MC. Environmental macrolide–lincosamide–streptogramin and tetracycline resistant bacteria. *Front. Microbiol*. 2011. Available from: <https://doi.org/10.3389/fmicb.2011.00040>.
- Катосова Л. К., Лазарева А. В., Хохлова Т. А., Пономаренко О. А., Алябьева Н. М. Распространение и механизмы устойчивости к макролидам *Streptococcus pyogenes*, выделенных у детей. *Антибиотики и химиотерапия*. 2016; 61 (3–4): 23–29.
- Farrell DJ, Morrissey I, Bakker S, Morris L, Buckridge S, Felmingham D. Molecular epidemiology of multiresistant *Streptococcus pneumoniae* with both erm(B)- and mef(A)-mediated macrolide resistance. *J Clin Microbiol*. 2004; 42 (2): 764–8. DOI: 10.1128/JCM.42.2.764–768.2004. PMID: 14766850; PMCID: PMC344484.
- Reinert RR, Ringelstein A, van der Linden M, Cil MY, Al-Lahham A, Schmitz FJ. Molecular epidemiology of macrolide-resistant *Streptococcus pneumoniae* isolates in Europe. *J Clin Microbiol*. 2005; 43 (3): 1294–300. DOI: 10.1128/JCM.43.3.1294-1300.2005. PMID: 15750098; PMCID: PMC1081259.
- Икрянникова Л. Н., Сенина М. Е., Лисицина Е. С., Огородова Л. М., Федосенко С. В., Карнаушкина М. А. и др. Видовая идентификация и анализ генетических маркеров лекарственной устойчивости стрептококков с помощью количественной мультиплексной полимеразной цепной реакции у пациентов с хронической обструктивной болезнью легких. *Пульмонология*. 2014; (6): 40–48. Доступно по ссылке: <https://doi.org/10.18093/0869-0189-2014-0-6-40-48>.
- Федосенко С. В., Огородова Л. М., Ильина Е. Н., Сенина М. Е., Лисицина Е. С., Карнаушкина М. А. и др. Генетические детерминанты устойчивости орофарингеальных стрептококков к антибактериальным средствам у пациентов с хронической обструктивной болезнью легких и больных бронхиальной астмой. *Терапевтический архив*. 2015; 87 (8): 51–57. DOI: 10.17116/terarkh201587851-57.
- Gosalbes MJ, Vallès Y, Jiménez-Hernández N, Balle C, Riva P, Miravet-Verde S, et al. High frequencies of antibiotic resistance genes in infants' meconium and early fecal samples. *J Dev Orig Health Dis*. 2016; 7: 35–44. DOI: 10.1017/S2040174415001506.
- Эпштейн-Литвак Р. В., Вильшанская Ф. Л. Бактериологическая диагностика дисбактериоза кишечника. *Методические рекомендации*. М., 1977; 20 с.
- Протокол ведения больных. Дисбактериоз кишечника: ОСТ 91500.11.0004-2003. Приказ Минздрава России № 231 от 09.06.03. (Отраслевой стандарт).
- U.S. Food and Drug Administration. Information pertaining to additional safety protections regarding use of fecal microbiota for transplantation — screening and testing of stool donors for multi-drug resistant organisms. 2019. Available from: <https://www.fda.gov/vaccines-blood-biologics/safety-availability-biologics/information-pertaining-additional-safety-protections-regarding-use-fecal-microbiota-transplantation>.
- Klassert TE, Zubiria-Barrera C, Kankel S, Stock M, Neubert R, Lorenzo-Diaz F, et al. Early Bacterial Colonization and Antibiotic Resistance Gene Acquisition in Newborns. *Front Cell Infect Microbiol*. 2020; 10: 332. DOI: 10.3389/fcimb.2020.00332. PMID: 32754449; PMCID: PMC7366792.
- Zhang K, Jin M, Yang D, Shen Z, Liu W, Yin J, et al. Antibiotic resistance genes in gut of breast-fed neonates born by caesarean section originate from breast milk and hospital ward air. *BMC Microbiol*. 2022; 36. DOI: org/10.1186/s12866-022-02447-8.
- Huang MS, Cheng CC, Tseng SY, Lin YL, Lo HM, Chen PW. Most commensally bacterial strains in human milk of healthy mothers display multiple antibiotic resistance. *Microbiology Open*. 2019; 8 (1): e00618 doi.org/10.1002/mbo3.618.
- Carvalho MJ, Sands K, Thomson, Portal KE, Mathias J, Milton R, et al. Antibiotic resistance genes in the gut microbiota of mothers and linked neonates with or without sepsis from low- and middle-income countries. *Nat Microbiol*. 2022; 7: 1337–47. Available from: doi.org/10.1038/s41564-022-01184-y.

GUT MICROBIOTA ALTERATIONS IN PATIENTS WITH JUVENILE IDIOPATHIC ARTHRITIS

Porosyuk MV, Klementiev DD, Hodov NA, Gumenyuk LN [✉], Esatova ES, Sereda EV, Chetveruhina-Malova KS, Sarchuk EV, Ivanov SV

Georgievsky Medical Academy, Vernadsky Crimean Federal University, Simferopol, Russia

Currently, the issue of the relationship between gut microbiota and juvenile idiopathic arthritis (JIA) is still relevant. The study was aimed to assess alterations in the gut microbiota taxonomic composition and estimate the relationship between these alterations and cortisol, melatonin, and TNF α at the genus level in patients with JIA. The comparative cross-sectional study involved 65 patients with JIA (index group) and 60 healthy children (control group). The gut microbiota taxonomic composition and plasma levels of cortisol, melatonin, and TNF α were assessed. The following alterations of the gut microbiota taxonomic composition were found in patients with JIA: the significantly decreased abundance of *Anaerostipes* ($p = 0.042$), *Lachnospira* ($p = 0.034$), *Roseburia* ($p = 0.002$), *Coprococcus* ($p = 0.014$), *Dialister* ($p = 0.003$) and the increase in the abundance of *Ruminococcus* ($p = 0.012$). There were significant correlations of cortisol levels with the abundance of *Lachnospira* ($r = -0.44$; $p = 0.001$), melatonin concentrations and the abundance of *Coprococcus* ($r = -0.48$; $p = 0.023$), the levels of TNF α and the abundance of *Ruminococcus* ($r = 0.52$; $p = 0.001$). The association of the *Lachnospira*, *Roseburia*, and *Ruminococcus* abundance with the higher DAS28 scores was discovered ($r = -0.57$; $p = 0.002$; $r = -0.44$; $p = 0.002$; $r = 0.54$; $p = 0.032$, respectively). The findings provide additional information about the features of gut microbiota alterations and their correlation with some hormone and inflammatory biomarkers associated with JIA, that could provide the basis for further research and possibly for new approaches to treatment of this disorder.

Keywords: juvenile idiopathic arthritis, gut microbiota, cortisol, melatonin, TNF α

Author contribution: Porosyuk MV, Klementiev DD — data acquisition, analysis, and interpretation; Gumenyuk LN — study concept and design; Hodov NA, Esatova ES, Sereda EV — statistical data processing; Chetveruhina-Malova KS, Sarchuk EV, Ivanov SV — manuscript writing

Compliance with ethical standards: the study was approved by the Ethics Committee of the S.I. Georgievsky Medical Academy, V. I. Vernadsky Crimean Federal University (protocol № 10 of 16 November 2020), planned and conducted in accordance with the Declaration of Helsinki. The informed consent was submitted by all the subjects enrolled.

✉ **Correspondence should be addressed:** Lesya N. Gumenyuk
Lenina bulvar, 5/7, Simferopol, 295006, Republic of Crimea; lesya_gumenyuk@mail.ru

Received: 01.11.2022 **Accepted:** 29.11.2022 **Published online:** 19.12.2022

DOI: 10.24075/brsmu.2022.060

ИЗМЕНЕНИЯ МИКРОБИОТЫ КИШЕЧНИКА У БОЛЬНЫХ ЮВЕНИЛЬНЫМ ИДИОПАТИЧЕСКИМ АРТРИТОМ

М. В. Поросюк, Д. Д. Клементьев, Н. А. Ходов, Л. Н. Гуменюк [✉], Э. С. Эсатова, Е. В. Середина, К. С. Четверухина-Малова, Е. В. Сарчук, С. В. Иванов

Медицинская академия имени С. И. Георгиевского, Крымский федеральный университет имени В. И. Вернадского, Симферополь, Россия

На сегодняшний день остается актуальной проблема взаимосвязи микробиоты кишечника и ювенильного идиопатического артрита (ЮИА). Целью исследования было изучить изменения таксономического состава микробиоты кишечника и оценить на уровне родов характер их взаимосвязи с кортизолом, мелатонином и TNF α у больных ЮИА. В одномоментном сравнительном исследовании приняли участие 65 больных ЮИА (основная группа) и 60 здоровых детей (контрольная группа). Оценивали таксономический состав микробиоты кишечника, уровни кортизола, мелатонина и TNF α в плазме крови. У больных ЮИА обнаружены изменения таксономического состава микробиоты кишечника: статистически значимое снижение численности *Anaerostipes* ($p = 0,042$), *Lachnospira* ($p = 0,034$), *Roseburia* ($p = 0,002$), *Coprococcus* ($p = 0,014$), *Dialister* ($p = 0,003$) и повышение численности *Ruminococcus* ($p = 0,012$). Установлена статистически значимая корреляция значений кортизола с уровнем бактерий *Lachnospira* ($r = -0,44$; $p = 0,001$), концентрации мелатонина и уровнем бактерий *Coprococcus* ($r = -0,48$; $p = 0,023$), значений TNF α и уровнем бактерий *Ruminococcus* ($r = 0,52$; $p = 0,001$). Также выявлена сопряженность численности бактерий *Lachnospira*, *Roseburia* и *Ruminococcus* с более высокими показателями по DAS28 ($r = -0,57$; $p = 0,002$; $r = -0,44$; $p = 0,002$; $r = 0,54$; $p = 0,032$ соответственно). Результаты предоставляют дополнительные данные об особенностях изменений микробиоты кишечника и их связи с некоторыми гормональными и воспалительными биомаркерами при ЮИА, что может стать обоснованием для проведения дальнейших исследований, а также, возможно, открывает новые подходы к терапии этого заболевания.

Ключевые слова: ювенильный идиопатический артрит, микробиота кишечника, кортизол, мелатонин, TNF α

Вклад авторов: М. В. Поросюк, Д. Д. Клементьев — сбор, анализ и интерпретация данных; Л. Н. Гуменюк — идея и дизайн исследования; Н. А. Ходов, Э. С. Эсатова, Е. В. Середина — статистическая обработка данных; К. С. Четверухина-Малова, Е. В. Сарчук, С. В. Иванов — подготовка статьи.

Соблюдение этических стандартов: исследование одобрено этическим комитетом Крымской медицинской академии имени С. И. Георгиевского ФГАУ ВО «Крымский федеральный университет им. В. И. Вернадского» (протокол № 10 от 16 ноября 2020 г.), спланировано и проведено в соответствии с Хельсинкской декларацией. Все лица, включенные в исследование, подписали добровольное информированное согласие.

✉ **Для корреспонденции:** Леся Николаевна Гуменюк
бул. Ленина, 5/7, г. Симферополь, 295006, Республика Крым; lesya_gumenyuk@mail.ru

Статья получена: 01.11.2022 **Статья принята к печати:** 29.11.2022 **Опубликована онлайн:** 19.12.2022

DOI: 10.24075/vrgmu.2022.060

Juvenile idiopathic arthritis (JIA) is arthritis of unknown etiology that persists for more than six weeks and occurs in children under the age of 16 [1]. The incidence of JIA all over the world varies between 0.8–22.6 cases per 100,000 children annually, and the prevalence is 7–401 cases per 100,000 children a year [2]. JIA remains one of the vital sociomedical issues due to high prevalence and high levels of early disability [3].

It has been proven that JIA is a multifactorial disease with the complex and poorly understood pathophysiology. In the light of the current concept, aberrant cytokine production along with the dysregulated immune response is a key element of the disease process associated with JIA [4]. In this regard, tumor necrosis factor — (TNF α) that is considered as the “early” cytokine emerging at the onset of inflammatory response [5] and

playing a vital part in the disease process chronification [6], is of special interest. There is evidence that in patients with JIA the levels of TNF α are associated with the activity of inflammation, including cartilage and bone destruction, bone tissue losses [5], while the significantly increased level of TNF α is a predictor of severe complication, the macrophage activation syndrome [5]. Furthermore, the immune system is closely linked with the neuroendocrine system. The pineal-pituitary-adrenal axis deep involvement in the mechanisms underlying the emergence and progression of the JIA clinical symptoms is actively discussed in the literature, and alterations in the melatonin and cortisol secretion are of particular importance [7, 8]. Assessment of blood hormone profiles in patients with JIA revealed the elevated levels of cortisol and the decreased melatonin levels [7, 8]. Moreover, the elevated cortisol levels were related to the clinical markers of inflammation [8], while the levels of melatonin were associated with the process activity, erythrocyte sedimentation rate (ESR), and the levels of immunoglobuline M [8].

Current research suggests that gut microbiota plays a certain role in the development and progression of JIA, resulting from its key role in the neuroendocrine regulation. Thus, the changes in the microbial landscape and disbalance between the members of gut microbiota [9–11], some of which strongly correlate with such biomarkers of inflammation, as anti-cyclic citrullinated peptide antibody, rheumatoid factor, and C-reactive protein [12], are typical for patients with JIA. Furthermore, some microbial representatives are found in the synovial fluid of patients with rheumatoid arthritis [13] and liver tissue of humans and mice [14], which can be the cause of autoimmune reactions [13, 14]. Finally, it was shown that treatment of gut dysbiosis using the specific four-week carbohydrate diet contributed to the decreased plasma levels of TNF α , number of swollen joints, pain syndrome severity, and morning stiffness, as well as to the increased physical activity in patients with JIA [15]. However, many aspects of the relationship between gut microbiota and hormonal biomarkers in patients with JIA are still poorly understood. There is no information about the relationship between the gut microbiota members and the levels of cortisol, melatonin, and TNF α in JIA.

Thus, the issue of the relationship between gut microbiota and JIA is still relevant. The study was aimed to assess alterations in the gut microbiota taxonomic composition and estimate the relationship between these alterations and cortisol, melatonin, and TNF α at the genus level in patients with JIA.

METHODS

The comparative cross-sectional study involved 65 patients with JIA (index group) (39 girls (60.0%), 26 boys (40.0%); average age 10.3 [3.1; 11.6] years), who sought help in the Children's Outpatient Clinic № 1 and Children's Outpatient Clinic № 3 (Simferopol, Republic of Crimea), and 60 healthy children (control group, CG) (35 girls (58.3%), 25 boys (41.7%); average age 9.9 [3.2; 11.8] years), who underwent their annual medical check-up at the Gemokod medical center (Simferopol, Republic of Crimea) and met the inclusion and exclusion criteria.

Inclusion criteria: first verified case of JIA; child's age 1–16 years; JIA duration 6 weeks to 6 months; no treatment with non-steroidal anti-inflammatory drugs (NSAIDs), genetically engineered biological preparations (GEBPs), and steroids; availability of the parents' informed consent to the child's participation in the study.

Exclusion criteria: systemic JIA, deficit [16] — the criteria for verification of underweight and overweight in children are

provided [17]; concomitant somatic diseases; irritable bowel syndrome; chronic disorders of gastrointestinal tract and liver; bacterial, viral, and fungal infections; mental disorders; stool disorders (constipation / diarrhea) within a month before the study; taking antibiotics, probiotics, prebiotics, antivirals, symbiotic or acid-suppression drugs within three months before the study; taking drugs that affect the stool within a month before the study; refusal to participate in the study.

Inclusion criteria for healthy volunteers: age 1–16 years; no chronic disorders or allergy; no more than three respiratory diseases a year; no infectious or acute disorders within two months before the study; no stool disorders (constipation / diarrhea) within a month before the study; refusal to take probiotics, prebiotics, symbiotic drugs within three months before the study; refusal to take drugs that affect the stool within a month before the study; no history of mental disorders; availability of the parents' informed consent to the child's participation in the study.

Exclusion criteria for healthy children: body temperature above 36.9 °C; refusal to participate in the study.

The diagnosis of JIA was verified in accordance with the classification criteria proposed by the International League of Associations for Rheumatology (ILAR), Second Revision (2001) [18]. To provide the disease activity objective assessment, we used the disease activity score (DAS) for 28 joints (DAS28); scores < 2.6 corresponded to remission, 2.6–3.0 to low activity, 3.1–5.0 to moderate activity, 5.1 or more to high disease activity [19].

To assess the gut microbiota taxonomic composition, faecal samples were collected in the morning on the day of admission (between 8 am and 11 am), that were frozen and stored in the disposable plastic containers at a temperature of –80 °C until the metagenomic analysis. Total DNA was isolated by the phenol extraction. The fragments of the V3–V4 variable regions of gene encoding 16S rRNA was amplified using universal primers. The V3–V4 region of 16S rRNA of gut microbiota was analyzed in the SOLiD5500 Wildfire sequencer (AppliedBiosystems; USA) by the paired-end sequencing with the total coverage of at least 10,000 pairs of reads per sample [20].

Filtration of the reads based on the quality and taxonomic classification were provided using the QIIME software, v. 1.9.1 [21]. The approach that involved the use of two taxonomic databases was used to define the taxonomic status of the reads. During the first stage we selected the reference set of bacterial operational taxonomic units (OTUs) based on the comparison of the 16S rRNA gene reads obtained with the GreenGenes database, v. 13.5 [22]. During the second phase we defined the taxonomic status of these OTUs based on the HITdb specialized database of human microbiota using the RDP algorithm [23].

The qualitative and quantitative gut microbiota composition was assessed by defining microbial species, genera, and phyla. Assessment of community α -diversity by calculating the Chao1 index, the number of taxa observed (Sobs), and the abundance-based coverage estimator (ACE) was performed using the Mothur software, v.1.22.0 (<http://www.mothur.org>).

The serum levels of cortisol, melatonin, and TNF α were assessed by enzyme-linked immunosorbent assay using the test systems (Vector-Best; Russia) and (Immuno Biological Laboratories; Germany). Blood was collected from the cubital vein in the morning (7.00–9.00) after fasting in a resting state (for at least 15 min).

Statistical processing was performed using the STATISTICA 8.0 software package (StatSoft Inc.; USA). When the data were

Table 1. Characteristics of patients with JIA and healthy children

Parameter	Patients with JIA (<i>n</i> = 65)	Control group (<i>n</i> = 60)
Girls/boys, <i>n</i> (%)	39 (60,0)/26 (40,0)	35 (58,3)/25 (41,7)
Average age, years, median [25%; 75%]	10,3 [3,1; 11,6]	9,9 [3,2; 11,8]
Body mass index, kg/m ² , median [25%; 75%]	16,2 [15,1; 18,3]	16,6 [15,7; 18,1]

Table 2. Clinical characteristics of patients with juvenile idiopathic arthritis

Parameter	Patients with JIA (<i>n</i> = 65)
Disease duration, months (M ± CD)	2,5 ± 1,5
Oligoarthritis, <i>n</i> (%)	38 (58,5)
Polyarthritis, <i>n</i> (%)	27 (41,5)
Rheumatoid factor (+), <i>n</i> (%)	8 (12,3)
Anti-CCP (+), <i>n</i> (%)	5(7,7)
Low disease activity based on the DAS28 score, <i>n</i> (%)	49 (75,3)
Moderate disease activity based on the DAS28 score, <i>n</i> (%)	12 (18,5)
High disease activity based on the DAS28 score, <i>n</i> (%)	4 (6,2)
Total DAS28 score, median [25%; 75%]	3,4 [2,9; 4,2]

Note: Anti-CCP — anti-cyclic citrullinated peptide (anti-CCP) antibody

normally distributed, mean values and standard deviations were defined, while in case of non-normal distribution median values, 25th and 75th percentiles were calculated. Distributions were tested for normality using the Gaussian functions. Shares and absolute values were defined for qualitative traits. Comparative analysis of the normally distributed quantitative traits was performed using the parametric Student's *t*-test, Mann–Whitney U test was used for non-normal distributions, and the chi-squared (χ^2) test was used for qualitative traits. Spearman's rank correlation coefficient was used for assessment of correlations between traits. The correlation analysis and multiple rank correlation analysis were performed, the correlation reliability was tested using the correlation reliability tables. The multiple comparisons were adjusted using the Bonferroni test. The differences were considered significant at $p < 0.05$.

RESULTS

The characteristics of patients with JIA and healthy children are provided in Table 1. The groups were matched for gender ($p = 0.97$; χ^2), age ($p = 0.92$; χ^2), and body mass index ($p = 0.054$; χ^2).

The clinical characteristics of patients with JIA are provided in Table 2. Children with oligoarthritis and low level inflammation prevailed among patients.

Comparison of the gut microbiota taxonomic composition in patients with JIA and children in the CG revealed a significant decrease in the microbial community α -diversity (Chao1 index; $p = 0.017$). The ACE and Sobs indices were slightly decreased in the group of patients with JIA compared to controls, however, there were no significant differences ($p = 0.055$; $p = 0.049$, respectively) (Fig. 1).

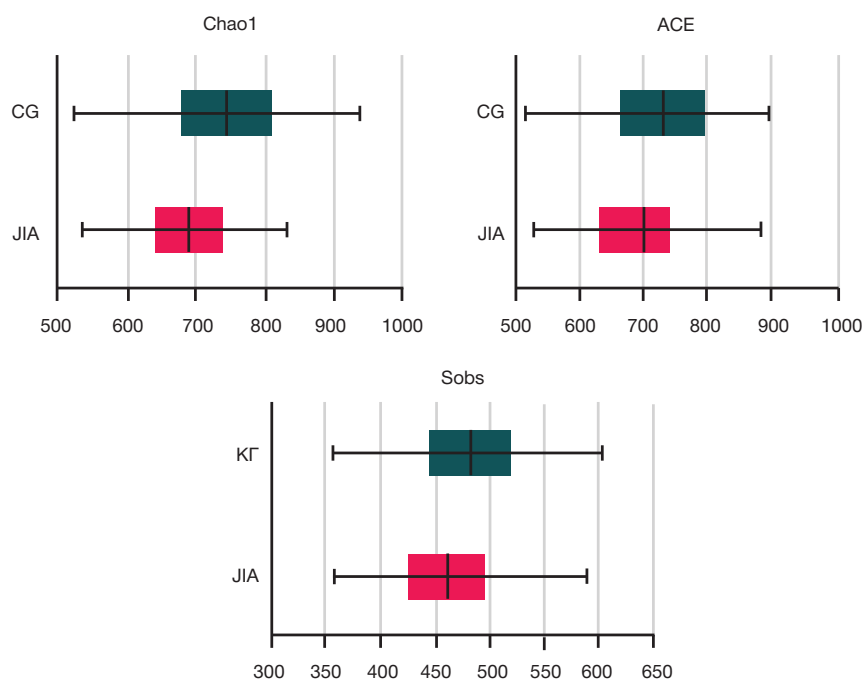


Fig. 1. Comparative analysis of the gut microbiota phylogenetic composition in patients with juvenile idiopathic arthritis and healthy children. JIA — juvenile idiopathic arthritis, CG — control group

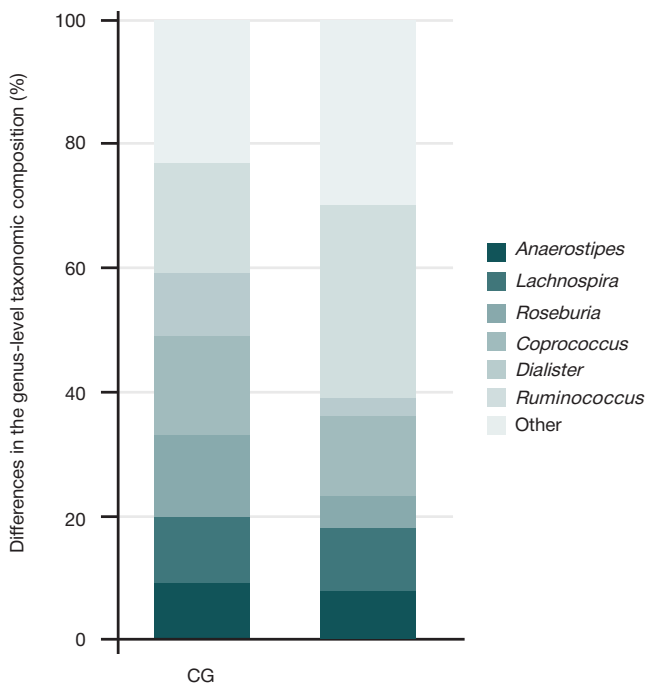


Fig. 2. Comparative analysis of the gut microbiota genus-level taxonomic composition in patients with JIA and healthy children. JIA — juvenile idiopathic arthritis, CG — control group

Comparison of the gut microbiota genus-level taxonomic composition in the surveyed groups revealed that the patients with JIA showed lower abundance of *Anaerostipes* ($p = 0.042$), *Lachnospira* ($p = 0.034$), *Roseburia* ($p = 0.002$), *Coprococcus* ($p = 0.014$), *Dialister* ($p = 0.003$) and higher abundance of *Ruminococcus* ($p < 0.001$) compared to the control group (Fig. 2).

Patients with JIA had the significantly higher plasma levels of cortisol and TNF α and the significantly lower levels of melatonin compared to controls (Table 3).

The cortisol levels and total DAS28 scores strongly correlated with the abundance of *Lachnospira* ($r = -0.44$ at $p = 0.001$; $r = -0.57$ at $p = 0.002$, respectively). We also managed to establish a relationship between the levels of melatonin and the abundance of *Coprococcus* ($r = -0.48$; $p = 0.023$). The correlations of the TNF α levels and total DAS28 scores with the abundance of *Ruminococcus* were established ($r = 0.52$ at $p = 0.001$; $r = 0.54$ at $p = 0.032$, respectively). The total DAS28 scores negatively correlated with the abundance of *Roseburia* ($r = -0.44$; $p = 0.002$).

DISCUSSION

In this study we have clarified alterations in the gut microbiota taxonomic composition and assessed the relationship between these alterations and plasma levels of cortisol, melatonin, and TNF α at the genus level in the group of patients with JIA.

A number of earlier papers report alterations in gut microbiota composition in patients with JIA [9–11]. Our findings also show that the gut microbiota composition of patients with JIA differs significantly from that of healthy children. According to our data, patients with JIA show lower bacterial α -diversity compared to healthy children. This is consistent with the results of the previous studies [9, 10]. Furthermore, dysbiotic alterations of the gut observed in patients with JIA are characterized by the reduced abundance of bacteria having immunomodulatory potential (members of the *Anaerostipes*, *Lachnospira*, *Roseburia*, *Coprococcus*, and *Dialister* genera) that are known to produce the short-chain fatty acids (SCFAs)

(butyrate and propionate). The reduced levels of the latter result in activation of histone deacetylase and inhibition of the GPR41, GPR43, and GPR109A G protein coupled receptors, thus promoting chronic inflammation [24]. At the same time, we have discovered high abundance of potential pathobionts, bacteria of the genus *Ruminococcus*. Our findings are partially in line with the number of earlier studies. For example, the decrease in the relative abundance of *Anaerostipes* and *Lachnospira* is typical for patients with JIA [11, 25], however, these data are opposite to the results obtained in patients with rheumatoid arthritis [26]. The other paper reports that the decreased abundance of *Anaerostipes*, *Lachnospira*, and *Roseburia* is typical for patients with COVID-19 [9]. In contrast to our data, the paper [27] reports the increased relative abundance of *Dialister* in patients with JIA. Such conflicting results may be due to the fact that, first, the studies were carried out in different geographic regions, and, second, unlike the abovementioned authors, we included children, who matched patients with JIA for age, gender, and body mass index, in the CG, because the impact of these factors on the gut microbiota composition was proven. Moreover, we did not include the patients with JIA, who used NSAIDs, GEBPs, steroids, and antibacterials in order to neutralize the effects of these drugs on the study results.

Regardless of the fact that some bacteria we have identified can be common for a number of other bowel diseases and systemic disorders, the correlation of the decreased abundance of *Lachnospira* and *Roseburia* and the increased abundance of *Ruminococcus* with the higher DAS28 scores we have discovered suggests that the changes in the abundance of these bacteria may be typical for this cohort of patients with JIA, and may also provide the basis for these alterations to be considered as predictors of the disease progression. The associations revealed were compared with the results of the earlier studies. Thus, in patients with JIA admitted to the hospitals of the Zhejiang Province, the abundance of *Lachnospira* and *Roseburia* negatively correlated with the disease activity, anti-CCP antibody levels, and ESR [9]. Based on the data on the causal relationships between gut dysbiosis and metabolic disorders [28], it can be assumed that the following sequential transformations could be observed in patients with JIA: gut microbiota alterations, specifically, the reduced abundance of bacteria producing SCFAs — the decrease in the concentrations of SCFAs — immune dysfunctions, and eventually the disease. Furthermore, it may be that the therapeutic increase in the abundance of *Lachnospira* и *Roseburia* and the decrease in the abundance of *Ruminococcus* effectively reduce the disease severity, however, further research with appropriate design is necessary to confirm this hypothesis.

As stated earlier, the patients with JIA show the significantly increased levels of cortisol, melatonin, and TNF α , the role of which in the development and progression of the disease has been proven [7, 8]. Our findings are in line with the literature data: there are significant differences in the levels of cortisol, melatonin, and TNF α between patients with JIA and healthy children. It is worth mentioning, that some gut microbiota representatives found in patients with JIA are associated with plasma levels of the studied biomarkers; this could be indicative of the correlation between the gut microbiota composition and abundance and this disorder. The negative correlation with the plasma cortisol levels have been shown for the genus *Lachnospira*, which confirms the likelihood of these bacteria being actively involved in the hypothalamic-pituitary-adrenal (HPA) axis dysregulation associated with JIA. We have found no studies focused on assessing the relationship between gut microbiota and cortisol in patients with JIA. However, it

Table 3. Comparative analysis of cortisol, melatonin and TNF α levels in blood plasma of patients with JIA and healthy children

Parameter	Patients with JIA (n = 65)	Control group (n = 60)	p
Cortisol, nmol/L (m \pm CD)	617,5 \pm 17,6	326,1 \pm 30,8	p < 0,001
Melatonin, pg/mL (m \pm CD)	21,1 \pm 6,1	35,5 \pm 9,2	p = 0,038
TNF α , pg/mL (m \pm CD)	63,3 \pm 1,8	4,6 \pm 0,3	p < 0,001

Note: p — significance of differences between the JIA group and the control group.

has been reported that *Lachnospira* negatively correlates with cortisol production in healthy children aged 8–16 [29]. Similar data are provided in the paper [30]: the decreased abundance of *Lachnospira* bacteria is associated with the higher cortisol levels in infants. We have found a possible explanation of this relationship in the literature. It is known that *Lachnospira* are among major butyrate-producing bacteria. In turn, SCFAs are capable of affecting the synthesis of cortisol: intracolonic administration of the physiologic doses of SCFAs for seven days resulted in the increased levels of SCFAs in the systemic circulation and reduced cortisol response to acute psychosocial stress in healthy men [31]. It has been found that oral administration of SCFAs (67.5 mmol acetate, 25 mmol propionate, 25 mmol butyrate) for 7 days in mice promoted inhibition of the corticosterone secretion potentiated by acute stress [32]. Since SCFAs are capable of crossing the blood–brain barrier (through the circumventricular organs), it can be assumed that these are involved in modulation of the HPA axis activity via direct effects on the secretory tone in the hypophysiotrophic neurons of the medial parvocellular paraventricular nucleus [33].

The association of melatonin levels with the abundance of *Coprococcus* bacteria has been revealed that can be mediated by blocking signal in the p-CREB-binding protein and arylalkylamine-N-acetyltransferase system due to the decreased secretion of tryptophan [34], being the precursor of

serotonin that is subsequently used for synthesis of melatonin. We have found a similar association in patients with type 2 diabetes mellitus in the literature, that is confirmed by positive correlations of the abundance of *Coprococcus* with the levels of tryptophan metabolites and plasma levels of melatonin [35].

A strong positive correlation between the levels of TNF α and the abundance of *Ruminococcus* bacteria suggests that these bacteria play a negative role in the JIA immunogenesis. This could be explained by the following: glucorhamnan, the inflammatory lipopolysaccharide produced by *Ruminococcus* bacteria, induces the synthesis of pro-inflammatory cytokines, such as TNF α and IL6, by the bone marrow dendritic cells through activation of the TLR4-mediated reactions [36].

CONCLUSIONS

The pronounced disorders of the gut microbiota abundance and taxonomic composition have been found in patients with JIA. The discovered significant correlations of some microbiota representatives with the DAS28 scores and the hormonal and inflammatory biomarkers testify in favor of the concept that the gut microbiota abundance and composition are associated with JIA. The issue of the correlation between the gut microbiota alterations and hormone biomarkers is still relevant. The targeted correction of gut microbiota may improve the JIA therapy efficiency.

References

- Rigante D, Bosco A, Esposito S. The Etiology of Juvenile Idiopathic Arthritis. *Clin Rev Allergy Immunol*. 2015; 49 (2): 253–61. DOI: 10.1007/s12016-014-8460-9.
- Shiff NJ, Oen K, Kroeker K, Lix LM. Trends in population-based incidence and prevalence of juvenile idiopathic arthritis in Manitoba, Canada. *Arthritis Care Res*. 2019; 71 (3): 413–8.
- Gumenyuk LN, Kabatova IN. Osobennosti kachestva zhizni bol'nykh yuvenil'nym revmatoidnym artritom na sanatorno-kurortnom lechenii. *Tavrisheskiĭ mediko-biologicheskiĭ vestnik*. 2017; 20 (2): 32–35. Russian.
- Raghavendra VV, Singh AV, Shaji H Vohra, Kulkarni SK, Agrewala JN. Melatonin provides signal 3 to unprimed CD4(+) T cells but failed to stimulate LPS primed B cells. *Clin Exp Immunol*. 2001; 124: 414–22.
- Fedorov ES, Salugina SO, Kuzmina NN. Rol' citokinovoj seti v regulyacii vospaleniya pri razlichnykh variantax yuvenil'nogo artrita. 2009; 3: 74–89. Russian.
- Belyaeva LM, Chizhevskaya ID, Filonovich RM, i dr. Sovremennye podxody k terapii revmaticheskix boleznej u detej. *Mezhdunarodnyĭ zhurnal pediatrii, akusherstva i ginekologii*. 2013; 3 (3): 25–34. Russian.
- Kabatova IN. Sostoyanie gormonal'nogo komponenta adaptacii u detej s yuvenil'nym revmatoidnym artritom. *Tavrisheskiĭ mediko-biologicheskiĭ vestnik*. 2017; 20 (3): 43–48. Russian.
- Skoronnaya NN. Rol' ehpfizarnogo gormona melatonina v regulyacii razlichnykh zven'ev ehndokrinnoj sistemy u bol'nykh yuvenil'nym revmatoidnym artritom. *Zdorov'e rebenka*. 2012; 8 (43): 65–70. Russian.
- Qian X, Liu YX, Ye X, et al. Gut microbiota in children with juvenile idiopathic arthritis: characteristics, biomarker identification, and usefulness in clinical prediction. *BMC Genomics*. 2020; 21: 286.
- Di Paola M, Cavalieri D, Albanese D, et al. Alteration of fecal microbiota profiles in juvenile idiopathic arthritis. Associations with HLA-B27 allele and disease status. *Front Microbiol*. 2016; 7: 1703.
- Tejesvi MV, Arvonen M, Kangas SM, et al. Faecal microbiome in new-onset juvenile idiopathic arthritis. *Eur J Clin Microbiol Infect Dis*. 2016; 35 (3): 363–70.
- Zhang X, Zhang D, Jia H, et al. The oral and gut microbiomes are perturbed in rheumatoid arthritis and partly normalized after treatment. *Nat Med*. 2015; 21 (8): 895–905.
- Pianta A, Arvikar S, Strle K, et al. Evidence of the immune relevance of *Prevotella copri*, a gut microbe, in patients with rheumatoid arthritis. *Arthritis Rheumatol*. 2017; 69 (5): 964–75.
- Manfredo Vieira S, Hiltensperger M, Kumar V, et al. Translocation of a gut pathobiont drives autoimmunity in mice and humans. *Science*. 2018; 359 (6380): 1156–61.
- Berntson L. A pilot study of possible anti-inflammatory effects of the specific carbohydrate diet in children with juvenile idiopathic arthritis. *Pediatr Rheumatol Online J*. 2021; 19 (1): 88.
- Ashworth A. Nutrition, food security, and health. In: Kliegman RM, Stanton BF, St Geme III JW, Schor NF, editors. *Nelson textbook of pediatrics*. 20th ed. New York: Elsevier, 2015.
- Gahagan S. Overweight and obesity. In: Kliegman RM, Stanton BF, St Geme III JW, Schor NF, editors. *Nelson textbook of pediatrics*.

- 20th ed. New York: Elsevier, 2015; 307–16.
18. Petty RE, Southwood TR, Manners P, et al. International League of Associations for Rheumatology. International League of Associations for Rheumatology classification of juvenile idiopathic arthritis: second revision, Edmonton, 2001. *J Rheumatol.* 2004; 31: 390–2
 19. Smolen JS, Breedveld FC, Eberl G, et al. Validity and reliability of the twenty-eight-joint count for the assessment of rheumatoid arthritis activity. *Arthritis Rheum.* 1995; 38: 38–43.
 20. Mitra S, Forster-Fromme K, Damms-Machado A, et al. Analysis of the intestinal microbiota using SOLiD16S rRNA gene sequencing and SOLiD shotgun sequencing. *BMC Genomics.* 2013; 14 (5): 16.
 21. Caporaso JG, Kuczynski J, Stombaugh J, et al. QIIME allows analysis of high-throughput community sequencing data. *Nat Methods.* 2010; 7 (5): 335–6.
 22. DeSantis TZ, Hugenholtz P, Larsen N. Greengenes, a chimera-checked 16S rRNA gene database and workbench compatible with ARB. *Appl Environ Microbiol.* 2006; 72: 5069–72.
 23. Ritari J, Salojärvi J, Lahti L, de Vos WM. Improved taxonomic assignment of human intestinal 16S rRNA sequences by a dedicated reference database. *BMC Genomics.* 2015; 16 (1): 1056.
 24. Vinolo MAR, Rodrigues HG, Nachbar RT, Curi R. Regulation of Inflammation by Short Chain Fatty Acids. *Nutrients.* 2011; 3 (10): 858–76.
 25. Stoll ML, Weiss PF, Weiss JE, et al. Age and fecal microbial strain-specific differences in patients with spondyloarthritis. *Arthritis Res Ther.* 2018; 20 (1): 14.
 26. Breban M, Tap J, Leboime A, et al. Faecal microbiota study reveals specific dysbiosis in spondyloarthritis. *Ann Rheum Dis.* 2017; 76 (9): 1614–22.
 27. Tito RY, Cypers H, Joossens M, et al. Brief report: dialister as a microbial marker of disease activity in Spondyloarthritis. *Arthritis Rheumatol.* 2017; 69 (1): 114–21.
 28. Sanna S, van Zuydam NR, Mahajan A, et al. Causal relationships among the gut microbiome, short-chain fatty acids and metabolic diseases. *Nat Genet.* 2019; 51 (4): 600–5.
 29. Michels N, Van de Wiele T, Fouhy F, et al. Gut microbiome patterns depending on children's psychosocial stress: Reports versus biomarkers. *Brain Behav Immun.* 2019; 80: 751–62.
 30. Rosin S, Xia K, Azcarate-Peril MA, et al. A preliminary study of gut microbiome variation and HPA axis reactivity in healthy infants. *Psychoneuroendocrinology.* 2021; 124: 105046.
 31. Dalile B, Vervliet B, Bergonzelli G, et al. Colon-delivered short-chain fatty acids attenuate the cortisol response to psychosocial stress in healthy men: a randomized, placebo-controlled trial. *Neuropsychopharmacol.* 2020; 45: 2257–66.
 32. Van de Wouw M, Boehme M, Lyte JM, et al. Short-chain fatty acids: microbial metabolites that alleviate stress-induced brain-gut axis alterations. *J Appl Physiol.* 2018; 596: 4923–44.
 33. Ziegler DR, Herman JP. Neurocircuitry of stress integration: anatomical pathways regulating the hypothalamo-pituitary-adrenocortical axis of the rat. *Integr Comp Biol.* 2002; 42: 541–51.
 34. Song L, He M, Sun Q, et al. Roseburia hominis Increases Intestinal Melatonin Level by Activating p-CREB-AANAT Pathway. *Nutrients.* 2022; 14: 117.
 35. Huang X, Qiu Y, Gao Y, et al. Gut microbiota mediate melatonin signalling in association with type 2 diabetes. *Diabetologia.* 2022; 65 (10): 1627–41.
 36. Henke MT, Kenny, DJ, Cassilly CD, et al. Ruminococcus gnavus, a member of the human gut microbiome associated with Crohn's disease, produces an inflammatory polysaccharide. *Proc Natl Acad Sci.* 2019; 116: 12672–7.

Литература

1. Rigante D, Bosco A, Esposito S. The Etiology of Juvenile Idiopathic Arthritis. *Clin Rev Allergy Immunol.* 2015; 49 (2): 253–61. DOI: 10.1007/s12016-014-8460-9.
2. Shiff NJ, Oen K, Kroeker K, Lix LM. Trends in population-based incidence and prevalence of juvenile idiopathic arthritis in Manitoba, Canada. *Arthritis Care Res.* 2019; 71 (3): 413–8.
3. Гуменок Л. Н., Кабатова И. Н. Особенности качества жизни больных ювенильным ревматоидным артритом на санаторно-курортном лечении. *Таврический медико-биологический вестник.* 2017; 20 (2): 32–35.
4. Raghavendra VV, Singh AV, Shaji H Vohra, Kulkarni SK, Agrewala JN. Melatonin provides signal 3 to unprimed CD4(+) T cells but failed to stimulate LPS primed B cells. *Clin Exp Immunol.* 2001; 124: 414–22.
5. Федоров Е. С., Салугина С. О., Кузьмина Н. Н. Роль цитокиновой сети в регуляции воспаления при различных вариантах ювенильного артрита. 2009; 3: 74–89.
6. Беляева Л. М., Чижевская И. Д., Филонович Р. М. и др. Современные подходы к терапии ревматических болезней у детей. *Международный журнал педиатрии, акушерства и гинекологии.* 2013; 3 (3): 25–34.
7. Кабатова И. Н. Состояние гормонального компонента адаптации у детей с ювенильным ревматоидным артритом. *Таврический медико-биологический вестник.* 2017; 20 (3): 43–48.
8. Скоромная Н. Н. Роль эпифизарного гормона мелатонина в регуляции различных звеньев эндокринной системы у больных ювенильным ревматоидным артритом. *Здоровье ребенка.* 2012; 8 (43): 65–70.
9. Qian X, Liu YX, Ye X, et al. Gut microbiota in children with juvenile idiopathic arthritis: characteristics, biomarker identification, and usefulness in clinical prediction. *BMC Genomics.* 2020; 21: 286.
10. Di Paola M, Cavalieri D, Albanese D, et al. Alteration of fecal microbiota profiles in juvenile idiopathic arthritis. Associations with HLA-B27 allele and disease status. *Front Microbiol.* 2016; 7: 1703.
11. Tejesvi MV, Arvonen M, Kangas SM, et al. Faecal microbiome in new-onset juvenile idiopathic arthritis. *Eur J Clin Microbiol Infect Dis.* 2016; 35 (3): 363–70.
12. Zhang X, Zhang D, Jia H, et al. The oral and gut microbiomes are perturbed in rheumatoid arthritis and partly normalized after treatment. *Nat Med.* 2015; 21 (8): 895–905.
13. Pianta A, Arvikar S, Strle K, et al. Evidence of the immune relevance of *Prevotella copri*, a gut microbe, in patients with rheumatoid arthritis. *Arthritis Rheumatol.* 2017; 69 (5): 964–75.
14. Manfredo Vieira S, Hiltensperger M, Kumar V, et al. Translocation of a gut pathobiont drives autoimmunity in mice and humans. *Science.* 2018; 359 (6380): 1156–61.
15. Berntson L. A pilot study of possible anti-inflammatory effects of the specific carbohydrate diet in children with juvenile idiopathic arthritis. *Pediatr Rheumatol Online J.* 2021; 19 (1): 88.
16. Ashworth A. Nutrition, food security, and health. In: Kliegman RM, Stanton BF, St Geme III JW, Schor NF, editors. *Nelson textbook of pediatrics.* 20th ed. New York: Elsevier, 2015.
17. Gahagan S. Overweight and obesity. In: Kliegman RM, Stanton BF, St Geme III JW, Schor NF, editors. *Nelson textbook of pediatrics.* 20th ed. New York: Elsevier, 2015; 307–16.
18. Petty RE, Southwood TR, Manners P, et al. International League of Associations for Rheumatology classification of juvenile idiopathic arthritis: second revision, Edmonton, 2001. *J Rheumatol.* 2004; 31: 390–2.
19. Smolen JS, Breedveld FC, Eberl G, et al. Validity and reliability of the twenty-eight-joint count for the assessment of rheumatoid arthritis activity. *Arthritis Rheum.* 1995; 38: 38–43.
20. Mitra S, Forster-Fromme K, Damms-Machado A, et al. Analysis of the intestinal microbiota using SOLiD16S rRNA gene sequencing and SOLiD shotgun sequencing. *BMC Genomics.* 2013; 14 (5): 16.
21. Caporaso JG, Kuczynski J, Stombaugh J, et al. QIIME allows analysis of high-throughput community sequencing data. *Nat Methods.* 2010; 7 (5): 335–6.
22. DeSantis TZ, Hugenholtz P, Larsen N. Greengenes, a chimera-checked 16S rRNA gene database and workbench compatible with ARB. *Appl Environ Microbiol.* 2006; 72: 5069–72.
23. Ritari J, Salojärvi J, Lahti L, de Vos WM. Improved taxonomic assignment of human intestinal 16S rRNA sequences by a

- dedicated reference database. *BMC Genomics*. 2015; 16 (1): 1056.
24. Vinolo MAR, Rodrigues HG, Nachbar RT, Curi R. Regulation of Inflammation by Short Chain Fatty Acids. *Nutrients*. 2011; 3 (10): 858–76.
 25. Stoll ML, Weiss PF, Weiss JE, et al. Age and fecal microbial strain-specific differences in patients with spondyloarthritis. *Arthritis Res Ther*. 2018; 20 (1): 14.
 26. Breban M, Tap J, Leboime A, et al. Faecal microbiota study reveals specific dysbiosis in spondyloarthritis. *Ann Rheum Dis*. 2017; 76 (9): 1614–22.
 27. Tito RY, Cypers H, Joossens M, et al. Brief report: dialister as a microbial marker of disease activity in Spondyloarthritis. *Arthritis Rheumatol*. 2017; 69 (1): 114–21.
 28. Sanna S, van Zuydam NR, Mahajan A, et al. Causal relationships among the gut microbiome, short-chain fatty acids and metabolic diseases. *Nat Genet*. 2019; 51 (4): 600–5.
 29. Michels N, Van de Wiele T, Fouhy F, et al. Gut microbiome patterns depending on children's psychosocial stress: Reports versus biomarkers. *Brain Behav Immun*. 2019; 80: 751–62.
 30. Rosin S, Xia K, Azcarate-Peril MA, et al. A preliminary study of gut microbiome variation and HPA axis reactivity in healthy infants. *Psychoneuroendocrinology*. 2021; 124: 105046.
 31. Dalile B, Vervliet B, Bergonzelli G, et al. Colon-delivered short-chain fatty acids attenuate the cortisol response to psychosocial stress in healthy men: a randomized, placebo-controlled trial. *Neuropsychopharmacol*. 2020; 45: 2257–66.
 32. Van de Wouw M, Boehme M, Lyte JM, et al. Short-chain fatty acids: microbial metabolites that alleviate stress-induced brain-gut axis alterations. *J Appl Physiol*. 2018; 596: 4923–44.
 33. Ziegler DR, Herman JP. Neurocircuitry of stress integration: anatomical pathways regulating the hypothalamo-pituitary-adrenocortical axis of the rat. *Integr Comp Biol*. 2002; 42: 541–51.
 34. Song L, He M, Sun Q, et al. Roseburia hominis Increases Intestinal Melatonin Level by Activating p-CREB-AANAT Pathway. *Nutrients*. 2022; 14: 117.
 35. Huang X, Qiu Y, Gao Y, et al. Gut microbiota mediate melatonin signalling in association with type 2 diabetes. *Diabetologia*. 2022; 65 (10): 1627–41.
 36. Henke MT, Kenny, DJ, Cassilly CD, et al. Ruminococcus gnavus, a member of the human gut microbiome associated with Crohn's disease, produces an inflammatory polysaccharide. *Proc Natl Acad Sci*. 2019; 116: 12672–7.

MUTATIONAL BASIS OF MEROPENEM RESISTANCE IN *PSEUDOMONAS AERUGINOSA*

Chebotar IV , Bocharova YuA, Chaplin AV, Savinova TA, Vasiliadis YuA, Mayansky NA

Pirogov Russian National Research Medical University, Moscow, Russia

The carbapenem-resistant strains of *Pseudomonas aeruginosa* are considered as the dangerous pathogens of critical priority. Deciphering the mechanisms underlying the development of carbapenem resistance is an urgent challenge faced by modern medical science. The study was aimed to describe the diversity and fixation of mutations associated with the development of carbapenem resistance during the *P. aeruginosa* adaptation to the increasing meropenem concentrations. The objects of the study were *P. aeruginosa* isolates obtained by growing the ATCC 27853 *P. aeruginosa* reference strain exposed to increasing concentrations of meropenem. The isolates were tested for meropenem susceptibility using E-tests (Epsilon meter tests) and by the agar dilution method. Genomes of the isolates were sequenced in the MGISEQ-2000 whole-genome sequencer. The findings show that in experimental settings *P. aeruginosa* develops high meropenem resistance very quickly (in 6 days). Evolution of resistance is associated with cloning involving the emergence of multiple clones with various genotypes. Mutagenesis that involves 11 genes, including *oprD*, *pbuE*, *nalD*, *nalC*, *spoT*, *miaA*, *mexD*, *mexR*, *oprM*, *mraY*, *pbp3*, provides the basis for cloning. Regardless of the levels of their meropenem resistance, some of the emerging clones do not progressively develop and are replaced by more successful clones.

Keywords: antibiotics, resistance, *Pseudomonas aeruginosa*, meropenem, mutation

Funding: the study was supported by the Russian Science Foundation (project No. 20-15-00235).

Acknowledgements: the authors thank the Center of Precision Genome Editing and Genetic Technologies for Biomedicine of the Pirogov Russian National Research Medical University for their advice on the research methods.

Author contribution: Chebotar IV — concept, manuscript writing; Bocharova YuA — methods, formal analysis; Chaplin AV — formal analysis of sequencing data; Savinova TA — formal analysis of sequencing data; Vasiliadis YuA — methods, sequencing; Mayansky NA — concept, manuscript editing.

Compliance with ethical standards: the study was performed in full compliance with the principles of the Declaration of Helsinki and the standards for handling opportunistic pathogens.

 **Correspondence should be addressed:** Igor V. Chebotar
Ostrovityanova, 1, Moscow, 117997, Russia: nizarnn@yandex.ru

Received: 25.11.2022 **Accepted:** 11.12.2022 **Published online:** 28.12.2022

DOI: 10.24075/brsmu.2022.063

МУТАЦИОННЫЕ ОСНОВЫ ФОРМИРОВАНИЯ УСТОЙЧИВОСТИ К МЕРОПЕНЕМУ У *PSEUDOMONAS AERUGINOSA*

И. В. Чеботарь , Ю. А. Бочарова, А. В. Чаплин, Т. А. Савинова, Ю. А. Василиадис, Н. А. Маянский

Российский национальный исследовательский медицинский университет имени Н. И. Пирогова, Москва, Россия

Резистентные к карбапенемам штаммы *Pseudomonas aeruginosa* расценивают в качестве критически опасных патогенов первого уровня приоритета. Расшифровка механизмов формирования устойчивости к карбапенемам является актуальной задачей современной медицинской науки. Целью работы было описать разнообразие и закрепление мутаций, ассоциированных с формированием карбапенемрезистентности в процессе адаптации *P. aeruginosa* к повышающимся концентрациям меропенема. Объектами исследования были изоляты *P. aeruginosa*, полученные при росте референтного штамма *P. aeruginosa* ATCC 27853 в градиенте возрастающих концентраций меропенема. Оценку чувствительности изолятов к меропенему выполняли при помощи е-тестов (эпсилонметрический метод) с меропенемом и при помощи метода дилуции антибиотика в агаре. Геномы изолятов были секвенированы на полногеномном секвенаторе MGISEQ-2000. Полученные результаты показали, что формирование высоких уровней резистентности к меропенему у *P. aeruginosa* в эксперименте происходит в короткие сроки (6 суток). Эволюция резистентности сопряжена с процессом клонирования, при котором происходит возникновение множества клонов с различными генотипами. Основой клонирования является мутагенез, в который вовлечены 11 генов, включая *oprD*, *pbuE*, *nalD*, *nalC*, *spoT*, *miaA*, *mexD*, *mexR*, *oprM*, *mraY*, *pbp3*. Часть образовавшихся клонов, независимо от уровня их резистентности к меропенему, не получают прогрессивного развития и вытесняются более успешными клонами.

Ключевые слова: антибиотики, резистентность, *Pseudomonas aeruginosa*, меропенем, мутации

Финансирование: работа выполнена при поддержке гранта Российского научного фонда (проект № 20-15-00235).

Благодарности: авторы благодарят Центр высокоточного редактирования и генетических технологий для биомедицины ФГАОУ ВО РНИМУ им. Н. И. Пирогова Минздрава РФ за консультации по методической части исследования.

Вклад авторов: И. В. Чеботарь — концептуализация, подготовка рукописи; Ю. А. Бочарова — методология, формальный анализ; А. В. Чаплин — формальный анализ данных секвенирования; Т. А. Савинова — формальный анализ данных секвенирования; Ю. А. Василиадис — методология, выполнение секвенирования; Н. А. Маянский — концептуализация, редактирование рукописи.

Соблюдение этических стандартов: исследование выполнено с соблюдением принципов Хельсинкской декларации и норм работ с условно-патогенными организмами.

 **Для корреспонденции:** Игорь Викторович Чеботарь
ул. Островитянова, д. 1, г. Москва, 117997, Россия: nizarnn@yandex.ru

Статья получена: 25.11.2022 **Статья принята к печати:** 11.12.2022 **Опубликована онлайн:** 28.12.2022

DOI: 10.24075/vrgmu.2022.063

Pseudomonas aeruginosa is one of the major opportunistic pathogens [1]. The carbapenem-resistant *P. aeruginosa* strains are especially dangerous for patients, that is why these strains have been included in the WHO priority list for R&D of new antibiotics for antibiotic-resistant bacteria as dangerous

pathogens of critical priority [2]. Carbapenem resistance can be developed in two ways. The first way is implemented by acquiring resistance genes from external sources via horizontal transfer. This resistance mechanism that is often referred to as plasmid-borne resistance provides high levels of resistance.

Studying this mechanism is more popular among scientists. Enzymes, the heterogenous β -lactamases of various Ambler classes combined into a group of carbapenemases based on the function, provide the main molecular basis for the horizontally transferred carbapenem resistance. However, there is one more way of developing carbapenem resistance that is not associated with horizontal gene transfer. It is based on the *P. aeruginosa* unique adaptive potential and is implemented through mutational variation in the chromosome genes [3]. Among clinical isolates, *P. aeruginosa* strains isolated from patients with cystic fibrosis are the most vivid examples of mutational antibiotic resistance. Highly resistant strains have been reported, which contain more than 60 genes disrupted by mutations. These genes can be the cause of resistance to various classes of antibiotics [4]. Of those 26 mutant genes can cause carbapenem resistance.

Studying the diversity of mutations that occur during the *P. aeruginosa* adaptation to carbapenems is of interest for prediction of carbapenem resistance evolution among clinical strains. The mechanisms underlying carbapenem resistance are assessed using two methodological approaches: 1) studying genetic and phenotypic characteristics of the clinical carbapenem-resistant isolates; 2) targeted *in vitro* modeling of carbapenem resistance that involves *P. aeruginosa* exposure to antibiotic.

The study was aimed to describe the diversity and fixation of mutations associated with the development of carbapenem resistance during the *P. aeruginosa* adaptation to the increasing meropenem concentrations.

The targeted creation of resistant *P. aeruginosa* strains is more often modelled using a series of consecutive transfers of bacteria in the liquid growth media containing the increasing concentrations of antibiotic (from 0 $\mu\text{g}/\text{mL}$ to the concentrations that are tens and hundreds of times greater than the minimum inhibitory concentration (MIC)) [5]. We used the other model [6] that was based on evolution of motile bacteria exposed to the increasing antibiotic concentrations. Such an approach makes it possible to isolate the larger number of clones with various genotypes.

METHODS

The ATCC 27853 *P. aeruginosa* reference strain used as a standard of carbapenem susceptibility (The European Committee on Antimicrobial Susceptibility Testing (EUCAST). EUCAST Clinical Breakpoint Tables v. 12.0. Available at: www.eucast.org) was the object of the study.

The study was carried out using the spatiotemporal model of antibiotic resistance in motile bacteria in accordance with the earlier reported method [7]. We formed five compartments divided by partitions with the depth of 2.0 cm in the 20.0 \times 40.0 cm container and filled these compartments with the solid growth medium containing Luria Bertani broth (LB Miller, Becton Dickinson and Co.; USA). The growth medium in the compartments contained sequential concentrations (0, 0.2, 20, 200, 2000 $\mu\text{g}/\text{mL}$) of meropenem (Supelco[®] Analytical Products, Merck & Co. Inc.; USA). A single layer (about 0.6 cm high) of solid growth medium containing Luria Bertani broth with no meropenem was formed atop of the compartments. It was covered with the layer of semi-solid agar (0.28% of agar) containing Luria Bertani broth with no meropenem. This layer was about 0.8 cm high. The culture of *P. aeruginosa* was adapted to semi-solid growth medium by the earlier reported method before starting the experiment [7].

Bacterial suspension with optical density equivalent to 0.5 MacFarland standard was used for inoculation. Inoculation was

performed by injection into the semi-solid agar to a depth of about 1–2 mm in the A sector (Fig. 1).

Every 24 h, samples were collected from the propagating *P. aeruginosa* growth front and inoculated to Mueller–Hinton agar plates (Becton Dickinson and Co.; USA) in order to gather enough biomaterial for further assessment of phenotypic characteristics (antibiotic resistance profile) and bacterial genome alterations.

Isolates were tested for meropenem susceptibility by determining MICs in two ways: 1) using meropenem E-tests (Epsilon meter tests) in accordance with the manufacturer's guidelines (BioMerieux SA; France); 2) using the agar dilution method [8]. The MIC values were not interpreted from a clinical perspective, these were analyzed solely in terms of the MIC dynamics.

Trough meropenem concentrations in the semi-solid agar were assessed 240 h after the start of the experiment by high-performance liquid chromatography (HPLC) using a well-known technique [9].

Bacterial DNA was isolated from the 24-h culture of *P. aeruginosa* isolates grown on Mueller–Hinton agar (Becton Dickinson and Co.; USA) using the QIAamp DNA Mini Kit (Qiagen; Germany) in accordance with the manufacturer's protocol. DNA samples were stored at $-20\text{ }^{\circ}\text{C}$. Ultrasonic fragmentation (Covaris; USA) of bacterial DNA (400 ng) with subsequent end repair and adapter ligation (MGI Tech; China) were used to prepare genomic DNA libraries. DNA libraries were washed with the Agencourt AMPure XP magnetic beads (Beckman Coulter; USA). The concentrations of bacterial DNA and DNA libraries were measured using the Qubit 4 fluorometer (Thermo Fisher Scientific; USA). Whole-genome sequencing was performed using the MGISEQ-2000 platform (MGI Tech; China). The read length was 250 bp. The quality was tested using the FASTQC (Babraham Institute; UK) and Trimmomatic v.0.38 (Usadel Lab; USA) software. Genomes were assembled *de novo* using the SPAdes 3.14 software [10]. The Contest16S web server was used to control the assembly completeness and eliminate the possibility of contamination. The quality of assemblies was evaluated in QUAST 5.0 [11]. Genomes were annotated using the RAST server [12] and the Prokka software [13].

To detect single nucleotide polymorphisms (SNPs), the short reads were mapped to the reference genome in Snippy [14]. The genome of "null" isolate, i.e. the isolate obtained after the ATCC 27853 *P. aeruginosa* strain adaptation to semi-solid agar that was used to launch the experiment, was used as a reference genome. The SnpEff software was used for annotation of the variants identified and prediction of their effects on the genes [15].

BLASTn tools (<https://blast.ncbi.nlm.nih.gov/Blast.cgi>) were used to analyze genes in the genomes of all the isolates obtained and amino acid sequences of the gene products. The ResFinder service and AMRFinderPlus algorithm included in the NCBI Pathogen Detection pipeline were used for assessment of resistance determinants [16, 17].

RESULTS

The dynamics of the *P. aeruginosa* propagation across the surface of semi-solid agar towards higher meropenem concentrations is provided in Fig. 1. The edge of the *P. aeruginosa* growth reached the zone with the maximum meropenem concentration in 168 h (7 days), and growth on the entire area of culture medium was observed within 240 h (10 days). At the end of the experiment meropenem concentration in the E sector of semi-solid agar (Fig. 1) was 56 $\mu\text{g}/\text{mL}$.

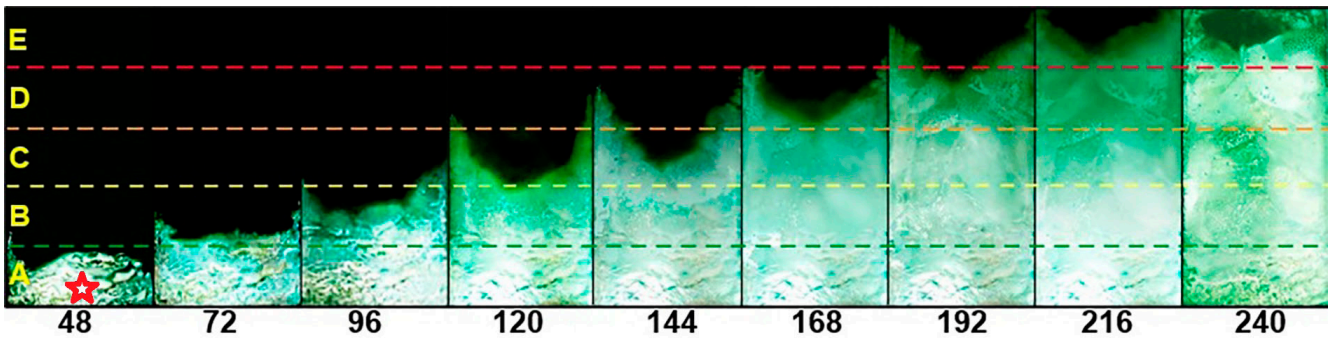


Fig. 1. The dynamics of *P. aeruginosa* propagation across the surface of semi-solid agar towards the higher concentrations of meropenem. The images were acquired after incubation for 48, 72, 96, 120, 144, 168, 192, 216, 240 h from the start of the experiment. The dashed lines refer to the boundaries which divide sectors A, B, C, D, E with various meropenem concentrations (0, 0.2, 20, 200, 2000 $\mu\text{g/mL}$, respectively) in the lower layer of solid growth medium (see Methods). Asterisk refers to the starting point (inoculation of the culture of *P. aeruginosa* ATCC 27853)

A total of 92 isolates were collected from the propagating *P. aeruginosa* growth front. Meropenem resistance of the isolates increased as the bacteria propagated towards higher meropenem concentrations (Fig. 2). The increase in MICs from 0.5 $\mu\text{g/mL}$ to 2, 4, and 8 $\mu\text{g/mL}$ was observed within 72 h after the start of the experiment. Isolates with MIC = 16 $\mu\text{g/mL}$ and MIC = 32 $\mu\text{g/mL}$ emerged after 144 h, while isolates with MIC = 64 $\mu\text{g/mL}$ emerged after 216 h. The meropenem MICs > 8 $\mu\text{g/mL}$ were reported in 61 isolates, and MICs \geq 32 were reported in 45 isolates.

Nonsynonymous mutations were found in 11 genes, including *oprD*, *pbuE*, *nalD*, *nalC*, *spoT*, *miaA*, *mexD*, *mexR*, *oprM*, *mraY*, *pbp3*. Mutations of these genes were not detected in four genomes out of 92 (4.3%), these were genomes of isolates obtained in the first 48 h of growth. In other 88 genomes out of 92 (95.7%), various combinations of genes disrupted by mutations were detected (Table 1). The most frequent disrupted genes were *oprD*, *pbuE*, *nalD* (Table 2). Mutations of genes *nalD*, *spoT*, *miaA*, *mexR*, *mraY*, *pbp3* were associated with high levels of resistance in the isolates carrying these mutations, the meropenem MICs of which exceeded 8 $\mu\text{g/mL}$ (Table 2). In contrast, the *oprM* gene mutations were found only in four strains out of 92 (4.3%) with meropenem MICs exceeding 8 $\mu\text{g/mL}$. Among 84 strains carrying *oprD* mutations four highly susceptible isolates with meropenem MICs of 0.5–2 $\mu\text{g/mL}$ were found. In these isolates *oprD* mutations resulted in L292Q, L252P, G307D substitutions in three cases and in premature termination of protein synthesis (W138stop) in one case. The genotype carrying a combination of mutations in *oprD*, *pbuE*, *nalD* was the most common (Table 1).

The dynamics of mutation emergence at various stages of biomaterial collection is provided in Table 2. The first stable mutations emerged in the *oprD* and *pbuE* genes within 72 h after the start of the experiment. The *pbuE* mutation resulting in the A261D substitution was represented by only one variant and was combined with different variants of other mutations evenly in 77 isolates out of 92 (83.7%). The *oprD* mutations were represented by nine variants. However, only two variants of mutations resulting in the G307D (*oprD*-G307D) and L238P (*oprD*-L238P) substitutions were found in the majority of isolates carrying *oprD* mutations (73 out of 84; 86.9%). The other seven variants of *oprD* mutations were relatively rare, these were found in 11 isolates with mutant *oprD* genes out of 84 (13.1%). Thus, the original strain produced two clones, *oprD*-G307D and *oprD*-L238P (Fig. 2). The strain that was a direct ancestor of the clone *oprD*-G307D emerged within 96 h of the experiment and its meropenem MIC was 2 $\mu\text{g/mL}$. The strain that was a direct ancestor of the clone *oprD*-L238P was not isolated during the experiment. Hypothetically, it could

emerge within 120 h after the start of the experiment. Evolution of the main clones, *oprD*-G307D and *oprD*-L238P, was associated with reduction of their meropenem susceptibility (Fig. 2) and accumulation of mutations in other genes important for development of carbapenem resistance.

Starting from hour 144 of the experiment, isolates carrying *nalD* mutation resulting in the G172D substitution emerged among strains of the *oprD*-G307D clone. By the end of the experiment, 14 strains of the *oprD*-G307D clone out of 34 were carriers of this mutation.

The *oprD*-L238P clone was related to the other *nalD* mutations resulting in the T11N (24 isolates of the clone out of 39) and H56P (4 isolates of the clone out of 39) substitutions. The deletion in the *miaA* gene (5 bp del (nucleotides 423–427)) resulting in the open reading frame shift was also found only in isolates (11 out of 39) of the clone *oprD*-L238P. The *miaA* deletion was combined with the T11N mutation of the *nalD* gene in all cases.

Mutations of genes *mexR*, *oprM*, *mraY*, *pbp3*, *nalC* were found only in few isolates.

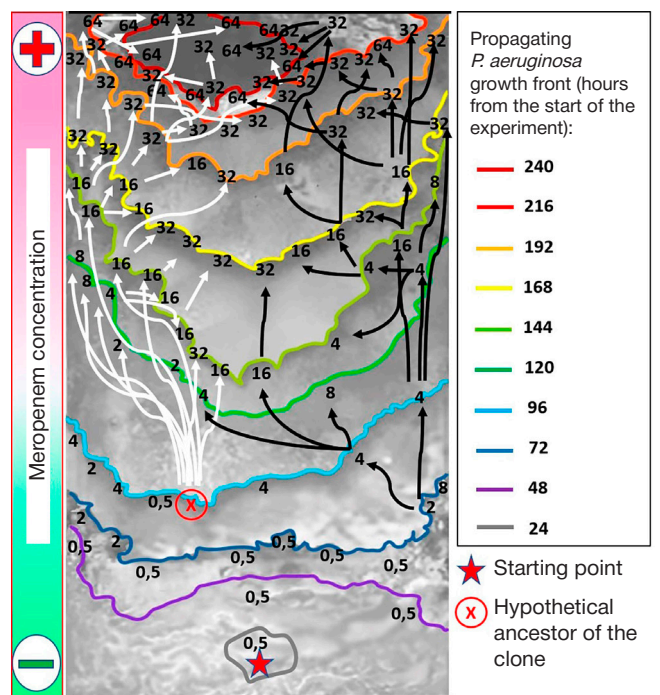


Fig. 2. Topology of *P. aeruginosa* clones on the surface of semi-solid agar with the increasing meropenem concentrations after 240 h of incubation. The numbers refer to meropenem MICs ($\mu\text{g/mL}$) of isolates collected from the sites designated with the numbers. White arrows demonstrate the *oprD*-L238P clone propagation, black arrows demonstrate the *oprD*-G307D clone propagation

Table 1. Genes and gene combinations where nonsynonymous mutations were found

№	Combinations of genes carrying mutations	Number of strains (% of all strains, <i>n</i> = 92)
1	<i>oprD, pbuE, nalD</i>	20 (22.2)
2	<i>oprD, pbuE</i>	11 (12.0)
3	<i>oprD, pbuE, nalD, spoT</i>	10 (10.9)
4	<i>oprD, pbuE, nalD, mlaA</i>	11 (12.0)
5	<i>oprD, pbuE, mexD</i>	9 (10)
6	<i>oprD</i>	6 (7)
7	<i>oprD, pbuE, spoT</i>	4 (4)
8	<i>oprD, pbuE, mexR</i>	3 (3)
9	<i>pbuE</i>	3 (3)
10	<i>oprD, nalD</i>	2 (2)
11	<i>oprD, pbuE, mexR, mraY</i>	2 (2)
12	<i>oprD, oprM</i>	2 (2)
13	<i>oprM</i>	1 (1)
14	<i>oprD, nalC, pbuE</i>	1 (1)
15	<i>oprD, pbuE, oprM</i>	1 (1)
16	<i>oprD, pbuE, spoT, mexD</i>	1 (1)
17	<i>oprD, pbuE, pbp3</i>	1 (1)
18	No mutations	4 (4)

DISCUSSION

When discussing phenotypic traits of the *P. aeruginosa* adaptation to meropenem, the focus should be placed on the rate of developing resistance. The resistance levels of certain isolates obtained at this stage reached meropenem MICs of 32 µg/mL within 6 days. The maximum meropenem MICs were 64 µg/mL, these were 128 times higher than the MIC values registered in isolates obtained within the first 48 h of the experiment. The fact of finding isolates with MIC values of 32 µg/mL in the zone with the actual meropenem content of 56 µg/mL can be explained by the differences between the conditions of determining MICs by reference methods (Epsilon test and agar dilution method) and the experimental conditions (growth medium, incubation time).

Gene mutation was revealed along with the meropenem MIC increase in distinct strains on the term of 72 h. A total of 11 mutated genes were found during the experiment. Among those the association with carbapenem resistance was proven only for *oprD, nalC, nalD, mexD, mexR, and pbp3* [18–21]. The

role of *oprM, pbuE, spoT, mraY, mlaA* genes in the development of antibiotic resistance has not been reported before, however, this does not eliminate their indirect effects on adaptation to carbapenems.

When considering the mutation pattern as a whole, attention should be paid to the phenomenon of cloning. Two major clonal lines emerged within 72–96 h. All the members of the first clonal line carried the *oprD* mutation resulting in the G307D substitution. The *oprD* mutation resulted in the L238P substitution in all representatives of the other clonal line. New mutations, that resulted in the increased phenotypic resistance to meropenem, emerged and were partially fixed in the clones produced. Along with these lines, single clones carrying other *oprD* mutations emerged. These clones showed no progressive spread, while some of the clones had higher meropenem MICs than the surrounding representatives of the clones *oprD*-G307D and *oprD*-L238P (Fig. 2). Perhaps, mutations in the non-successful but highly resistant clones were the factor adversely affecting the outcome of intraspecific competition. It is worth mentioning that *oprD* disruption in the

Table 2. Meropenem resistant phenotypes of *P. aeruginosa* and genes that can possibly determine carbapenem resistance

№	Gene	Time of mutation emergence (hours since the start)	Number of strains (% of the group) carrying mutations in the groups with various meropenem MICs (µg/mL)			Number of strains carrying mutations (% of all strains, <i>n</i> = 92)
			≤ 8, <i>n</i> = 31	> 8 < 32, <i>n</i> = 16	≥ 32, <i>n</i> = 45	
1	<i>oprD</i>	72	23 (74,2)	16 (100)	45 (100)	84 (91,3)
2	<i>pbuE</i>	72	16 (51,6)	16 (100)	45 (100)	77 (83,7)
3	<i>nalD</i>	120	1 (3)	12 (75)	30 (66,7)	43 (46,7)
4	<i>spoT</i>	192	0 (0)	1 (6)	14 (31,1)	15 (16,3)
5	<i>mlaA</i>	144	0 (0)	1 (6)	10 (22,2)	11 (12,0)
6	<i>mexD</i>	120	3 (10)	3 (29)	4 (9)	10 (10,9)
7	<i>mexR</i>	144	0 (0)	2 (13)	3 (7)	5 (5)
8	<i>oprM</i>	72	4 (13)	0 (0)	0 (0)	4 (4)
9	<i>mraY</i>	168	0 (0)	0 (0)	2 (4)	2 (2)
10	<i>pbp3</i>	144	0 (0)	0 (0)	1 (2)	1 (1)
11	<i>nalC</i>	72	1 (3)	0 (0)	0 (0)	0 (0)

P. aeruginosa meropenem resistant isolates is observed not only in experimental settings. Thus, five highly meropenem resistant (MIC > 32 µg/mL) *P. aeruginosa* strains out of six, which were found in individuals with cystic fibrosis and produced no carbapenemases, carried mutations in the *oprD* genes [4]. At the same time, disruption of one gene (*oprD*) is insufficient for development of meropenem resistance. Even the strain carrying the *oprD* nonsense mutation (W138stop termination codon) remained highly susceptible to meropenem. Accumulation of chromosomal mutations in multiple chromosome genes directly or indirectly affecting antibiotic susceptibility is essential for resistance.

We do not exclude the possibility that some isolates with unique genotypes have not been selected during the experiment, and information about these isolates has been lost. The example of this is uncertainty about the progenitor of the *oprD*-L238P clone being an intermediate between the highly susceptible and highly resistant strains. However, in contrast

to evolution in liquid medium, spatiotemporal resistance model makes it possible to isolate a larger number of clones and avoid the loss of information about possible mutations leading to resistance.

CONCLUSIONS

In experimental settings *P. aeruginosa* develops high meropenem resistance very quickly (in 6 days). Evolution of resistance is associated with cloning involving the emergence of multiple clones with various genotypes. Mutagenesis that involves 11 genes, including *oprD*, *pbuE*, *nalD*, *nalC*, *spoT*, *mIaA*, *mexD*, *mexR*, *oprM*, *mraY*, *pbp3*, provides the basis for cloning. Regardless of the levels of their meropenem resistance, some of the emerging clones do not progressively develop and are replaced by the more successful clones. The model used during the experiment is a convenient tool to obtain the set of variants with various resistant genotypes.

References

- Lazareva AV, Chebotar IV, Kryzhanovskaya OA, Chebotar VI, Mayanskiy NA. Pseudomonas aeruginosa: patogennost', patogenez i patologiya. Klin Mikrobiol Antimikrob Ximioter. 2015; 17 (3): 170–86. Russian.
- WHO priority list for research and development of new antibiotics for antibiotic-resistant bacteria. Geneva: World Health Organization; 2017. Available from: <https://www.who.int/news/item/27-02-2017-who-publishes-list-of-bacteria-for-which-new-antibiotics-are-urgently-needed> (accessed September 1, 2012).
- Oliver A, Mulet X, López-Causapé C, Juan C. The increasing threat of Pseudomonas aeruginosa high-risk clones. Drug Resistance Updates. 2015; 21: 41–59. Available from: <https://doi.org/10.1016/j.drug.2015.08.002>.
- López-Causapé C, Sommer LM, Cabot G, Rubio R, Ocampo-Sosa AA, Johansen H et al. Evolution of the Pseudomonas aeruginosa mutational resistome in an international cystic fibrosis clone. Sci Rep. 2017; 7: 5555. Available from: <https://doi.org/10.1038/s41598-017-05621-5>.
- Barbosa C, Trebosc V, Kemmer C, Rosenstiel P, Beardmore R, Schulenburg H, et al. Alternative evolutionary paths to bacterial antibiotic resistance cause distinct collateral effects. Mol Biol Evol. 2017; 34 (9): 2229–44. Available from: <https://doi.org/10.1093/molbev/msx158>.
- Baym M, Lieberman TD, Kelsic ED, Chait R, Gross R, Yelin I, et al. Spatiotemporal microbial evolution on antibiotic landscapes. Science. 2016; 353 (6304): 1147–51. Available from: <https://doi.org/10.1126/science.aag0822>.
- Savinova TA, Bocharova YA, Chaplin AV, Korostin DO, Shamina OV, Mayanskiy NA, et al. Meropenem-induced reduction in colistin susceptibility in Pseudomonas aeruginosa strain ATCC 27853. Bulletin of RSMU. 2022; 1: 30–4. Available from: <https://doi.org/10.24075/brsmu.2022.001>.
- European Committee for Antimicrobial Susceptibility Testing (EUCAST) of the European Society of Clinical Microbiology and Infectious Diseases (ESCMID). Determination of minimum inhibitory concentrations (MICs) of antibacterial agents by agar dilution. Clin Microbiol Infect. 2000; 6 (9): 509–15. Available from: <https://doi.org/10.1046/j.1469-0691.2000.00142.x>.
- Kazanova AM, Stepanova ES, Makarenkova LM, Chistyakov VV, Zyryanov SK, Senchenko SP. Razrabotka i validaciya metodiki kolichestvennogo opredeleniya meropenema v plazme krovi dlya terapevticheskogo lekarstvennogo monitoringa. Ximikofarmaceuticheskij zhurnal. 2020; 54 (4): 56–60. Available from: <https://doi.org/10.30906/0023-1134-2020-54-4-56-60>. Russian.
- Bankevich A, Nurk S, Antipov D, Gurevich AA, Dvorkin M, Kulikov AS et al. SPAdes: a new genome assembly algorithm and its applications to single-cell sequencing. J Comput Biol. 2012; 19: 455–77. Available from: <https://doi.org/10.1089/cmb.2012.0021>.
- Gurevich A, Saveliev V, Vyahhi N, Tesler G. QUASt: quality assessment tool for genome assemblies. Bioinformatics. 2013; 29 (8): 1072–5. Available from: <https://doi.org/10.1093/bioinformatics/btt086>.
- Overbeek R, Olson R, Pusch GD, Olsen GJ, Davis JJ, Disz T et al. The SEED and the Rapid Annotation of microbial genomes using Subsystems Technology (RAST). Nucleic Acids Res. 2014; 42: D206–14. Available from: <https://doi.org/10.1093/nar/gkt1226>.
- Seemann T. Prokka: rapid prokaryotic genome annotation. Bioinformatics. 2014; 30 (14): 2068–9. Available from: <https://doi.org/10.1093/bioinformatics/btu153>.
- Seemann T. 2015. Snippy: fast bacterial variant calling from NGS reads. GitHub. Available at: <https://github.com/tseemann/snippy> (accessed November 2022).
- Cingolani P, Platts A, Wang LL, Coon M, Nguyen T, Wang L, et al. A program for annotating and predicting the effects of single nucleotide polymorphisms, SnpEff: SNPs in the genome of Drosophila melanogaster strain w1118; iso-2; iso-3. Fly. 2012; 6 (2): 80–92. Available from: <https://doi.org/10.4161/fly.19695>.
- Afgan E, Baker D, Batut B, van den Beek M, Bouvier D, Cech M, et al. The Galaxy platform for accessible, reproducible and collaborative biomedical analyses: 2018 update. Nucleic Acids Res. 2018; 46 (W1): W537–44. Available from: <https://doi.org/10.1093/nar/gky379>.
- Bortolaia V, Kaas RS, Ruppe E, Roberts MC, Schwarz S, Cattor V, et al. ResFinder 4.0 for predictions of phenotypes from genotypes. J Antimicrob Chemother. 2020; 75 (12): 3491–500. Available from: <https://doi.org/10.1093/jac/dkaa345>.
- Li H, Luo YF, Williams BJ, Blackwell TS, Xie CM. Structure and function of OprD protein in Pseudomonas aeruginosa: from antibiotic resistance to novel therapies. Int J Med Microbiol. 2012; 302 (2): 63–8. Available from: <https://doi.org/10.1016/j.ijmm.2011.10.001>.
- Lister PD, Wolter DJ, Hanson ND. Antibacterial-resistant Pseudomonas aeruginosa: clinical impact and complex regulation of chromosomally encoded resistance mechanisms. Clin Microbiol Rev. 2009; 22 (4): 582–610. Available from: <https://doi.org/10.1128/CMR.00040-09>.
- Srikumar R, Kon T, Gotoh N, Poole K. Expression of Pseudomonas aeruginosa multidrug efflux pumps MexA-MexB-OprM and MexC-MexD-OprJ in a multidrug-sensitive Escherichia coli strain. Antimicrob Agents Chemother. 1998; 42 (1): 65–71. Available from: <https://doi.org/10.1128/AAC.42.1.65>.
- Glen KA, Lamont IL. β-lactam Resistance in Pseudomonas aeruginosa: Current Status, Future Prospects. Pathogens. 2021; 10 (12): 1638. Available from: <https://doi.org/10.3390/pathogens10121638>.

Литература

1. Лазарева А. В., Чеботарь И. В., Крыжановская О. А., Чеботарь В. И., Маянский Н. А. *Pseudomonas aeruginosa*: патогенность, патогенез и патология. *Клин Микробиол Антимикроб Химиотер.* 2015; 17 (3): 170–86.
2. WHO priority list for research and development of new antibiotics for antibiotic-resistant bacteria. Geneva: World Health Organization, 2017. Available from: <https://www.who.int/news/item/27-02-2017-who-publishes-list-of-bacteria-for-which-new-antibiotics-are-urgently-needed> (accessed September 1, 2012).
3. Oliver A, Mulet X, López-Causapé C, Juan C. The increasing threat of *Pseudomonas aeruginosa* high-risk clones. *Drug Resistance Updates.* 2015; 21: 41–59. Available from: <https://doi.org/10.1016/j.drug.2015.08.002>.
4. López-Causapé C, Sommer LM, Cabot G, Rubio R, Ocampo-Sosa AA, Johansen H et al. Evolution of the *Pseudomonas aeruginosa* mutational resistome in an international cystic fibrosis clone. *Sci Rep.* 2017; 7: 5555. Available from: <https://doi.org/10.1038/s41598-017-05621-5>.
5. Barbosa C, Trebosc V, Kemmer C, Rosenstiel P, Beardmore R, Schulenburg H, et al. Alternative evolutionary paths to bacterial antibiotic resistance cause distinct collateral effects. *Mol Biol Evol.* 2017; 34 (9): 2229–44. Available from: <https://doi.org/10.1093/molbev/msx158>.
6. Baym M, Lieberman TD, Kelsic ED, Chait R, Gross R, Yelin I, et al. Spatiotemporal microbial evolution on antibiotic landscapes. *Science.* 2016; 353 (6304): 1147–51. Available from: <https://doi.org/10.1126/science.aag0822>.
7. Savinova TA, Bocharova YA, Chaplin AV, Korostin DO, Shamina OV, Mayanskiy NA, et al. Meropenem-induced reduction in colistin susceptibility in *Pseudomonas aeruginosa* strain ATCC 27853. *Bulletin of RSMU.* 2022; 1: 30–4. Available from: <https://doi.org/10.24075/brsmu.2022.001>.
8. European Committee for Antimicrobial Susceptibility Testing (EUCAST) of the European Society of Clinical Microbiology and Infectious Diseases (ESCMID). Determination of minimum inhibitory concentrations (MICs) of antibacterial agents by agar dilution. *Clin Microbiol Infect.* 2000; 6 (9): 509–15. Available from: <https://doi.org/10.1046/j.1469-0691.2000.00142.x>.
9. Казанова А. М., Степанова Е. С., Макаренкова Л. М., Чистяков В. В., Зырянов С. К., Сенченко С. П.. Разработка и валидация методики количественного определения меропенема в плазме крови для терапевтического лекарственного мониторинга. *Химико-фармацевтический журнал.* 2020; 54 (4): 56–60. Available from: <https://doi.org/10.30906/0023-1134-2020-54-4-56-60>.
10. Bankevich A, Nurk S, Antipov D, Gurevich AA, Dvorkin M, Kulikov AS et al. SPAdes: a new genome assembly algorithm and its applications to single-cell sequencing. *J Comput Biol.* 2012; 19: 455–77. Available from: <https://doi.org/10.1089/cmb.2012.0021>.
11. Gurevich A, Saveliev V, Vyahhi N, Tesler G. QUAST: quality assessment tool for genome assemblies. *Bioinformatics.* 2013; 29 (8): 1072–5. Available from: <https://doi.org/10.1093/bioinformatics/btt086>.
12. Overbeek R, Olson R, Pusch GD, Olsen GJ, Davis JJ, Disz T et al. The SEED and the Rapid Annotation of microbial genomes using Subsystems Technology (RAST). *Nucleic Acids Res.* 2014; 42: D206–14. Available from: <https://doi.org/10.1093/nar/gkt1226>.
13. Seemann T. Prokka: rapid prokaryotic genome annotation. *Bioinformatics.* 2014; 30 (14): 2068–9. Available from: <https://doi.org/10.1093/bioinformatics/btu153>.
14. Seemann T. 2015. Snippy: fast bacterial variant calling from NGS reads. GitHub. Available at: <https://github.com/tseemann/snippy> (accessed November 2022).
15. Cingolani P, Platts A, Wang LL, Coon M, Nguyen T, Wang L, et al. A program for annotating and predicting the effects of single nucleotide polymorphisms, SnpEff: SNPs in the genome of *Drosophila melanogaster* strain w1118; iso-2; iso-3. *Fly.* 2012; 6 (2): 80–92. Available from: <https://doi.org/10.4161/fly.19695>.
16. Afgan E, Baker D, Batut B, van den Beek M, Bouvier D, Cech M, et al. The Galaxy platform for accessible, reproducible and collaborative biomedical analyses: 2018 update. *Nucleic Acids Res.* 2018; 46 (W1): W537–44. Available from: <https://doi.org/10.1093/nar/gky379>.
17. Bortolaia V, Kaas RS, Ruppe E, Roberts MC, Schwarz S, Cattoir V, et al. ResFinder 4.0 for predictions of phenotypes from genotypes. *J Antimicrob Chemother.* 2020; 75 (12): 3491–500. Available from: <https://doi.org/10.1093/jac/dkaa345>.
18. Li H, Luo YF, Williams BJ, Blackwell TS, Xie CM. Structure and function of OprD protein in *Pseudomonas aeruginosa*: from antibiotic resistance to novel therapies. *Int J Med Microbiol.* 2012; 302 (2): 63–8. Available from: <https://doi.org/10.1016/j.ijmm.2011.10.001>.
19. Lister PD, Wolter DJ, Hanson ND. Antibacterial-resistant *Pseudomonas aeruginosa*: clinical impact and complex regulation of chromosomally encoded resistance mechanisms. *Clin Microbiol Rev.* 2009; 22 (4): 582–610. Available from: <https://doi.org/10.1128/CMR.00040-09>.
20. Srikumar R, Kon T, Gotoh N, Poole K. Expression of *Pseudomonas aeruginosa* multidrug efflux pumps MexA-MexB-OprM and MexC-MexD-OprJ in a multidrug-sensitive *Escherichia coli* strain. *Antimicrob Agents Chemother.* 1998; 42 (1): 65–71. Available from: <https://doi.org/10.1128/AAC.42.1.65>.
21. Glen KA, Lamont IL. β -lactam Resistance in *Pseudomonas aeruginosa*: Current Status, Future Prospects. *Pathogens.* 2021; 10 (12): 1638. Available from: <https://doi.org/10.3390/pathogens10121638>.

IDENTIFICATION OF PROGNOSTICALLY SIGNIFICANT DNA METHYLATION SIGNATURES IN PATIENTS WITH VARIOUS BREAST CANCER TYPES

Kalinkin AI¹✉, Sigin VO¹, Nemtsova MV^{1,2}, Strelnikov VV^{1,3}

¹ Research Centre of Medical Genetics, Moscow, Russia

² Sechenov First Moscow State Medical University (Sechenov University), Moscow, Russia

³ Pirogov Russian National Research Medical University, Moscow, Russia

Breast cancer (BC) is the most frequently diagnosed cancer and one of the major causes of female mortality. The development of prognostic models based on multiomics data is the main goal of precision oncology. Aberrant DNA methylation in BC is a diagnostic marker of carcinogenesis. Despite the existing factors of BC prognosis, introduction of methylation markers would make it possible to obtain more accurate prognostic scores. The study was aimed to assess DNA methylation signatures in various BC subtypes for clinical endpoints and patients' clinicopathological characteristics. The data on methylation of CpG dinucleotides (probes) and clinical characteristics of BC samples were obtained from The Cancer Genome Atlas Breast Cancer database. CpG dinucleotides associated with the selected endpoints were chosen by univariate Cox regression method. The LASSO method was used to search for stable probes, while further signature construction and testing of the clinical characteristics independence were performed using multivariate Cox regression. The diagnostic and prognostic potential of the signatures was assessed using ROC analysis and Kaplan–Meier curves. It has been shown that the signatures of selected probes have a significant diagnostic (AUC 0.76–1) and prognostic ($p < 0.05$) potential. This approach has made it possible to identify 47 genes associated with good and poor prognosis, among these five genes have been described earlier. If the genome-wide DNA analysis results are available, the research approach applied can be used to study molecular pathogenesis of BC and other disorders.

Keywords: breast cancer, molecular subtypes, survival analysis, DNA methylation, prognostic markers

Funding: the study was supported by the Ministry of Science and Higher Education of the Russian Federation within the framework of the Federal Scientific and Technical Program for the Development of Genetic Technologies in 2019–2027 (agreement № 075-15-2021-1073).

Author contribution: Kalinkin AI — study design, data acquisition, analysis and interpretation, manuscript writing; Sigin VO — manuscript writing; Nemtsova MV — study concept and design; Strelnikov VV — study concept and design, scientific editing.

✉ **Correspondence should be addressed:** Alexey I. Kalinkin
Moskvorechye, 1, Moscow, 115522; alexeika2@yandex.ru

Received: 18.10.2022 **Accepted:** 11.11.2022 **Published online:** 25.11.2022

DOI: 10.24075/brsmu.2022.056

ОПРЕДЕЛЕНИЕ ПРОГНОСТИЧЕСКИ ЗНАЧИМОЙ СИГНАТУРЫ ДНК-МЕТИЛИРОВАНИЯ У ПАЦИЕНТОК С РАЗЛИЧНЫМИ ТИПАМИ РАКА МОЛОЧНОЙ ЖЕЛЕЗЫ

А. И. Калинин¹✉, В. О. Сигин¹, М. В. Немцова^{1,2}, В. В. Стрельников^{1,3}

¹ Медико-генетический научный центр имени Н. П. Бочкова, Москва, Россия

² Первый Московский государственный медицинский университет имени И. М. Сеченова (Сеченовский университет), Москва, Россия

³ Российский национальный исследовательский медицинский университет имени Н. И. Пирогова, Москва, Россия

Рак молочной железы (РМЖ) — наиболее часто диагностируемое онкологическое заболевание и одна из ведущих причин смертности среди женского населения. Разработка прогностических моделей с использованием мультиомиксных данных является главной целью прецизионной онкологии. Аберрантное метилирование ДНК в РМЖ представляет собой информативный маркер канцерогенеза. Несмотря на существующие факторы прогноза РМЖ, введение маркеров метилирования позволит получать более точную прогностическую оценку. Целью работы было изучить сигнатуры метилирования ДНК в различных подтипах РМЖ для клинических конечных точек и клинико-патологических характеристик пациенток. Данные об уровнях метилирования CpG-динуклеотидов (зондов) и клинические характеристики образцов РМЖ были получены из базы данных The Cancer Genome Atlas Breast Cancer. С помощью метода одномерной регрессии Кокса были выбраны CpG-динуклеотиды, ассоциированные с выбранными конечными точками. Методом LASSO осуществляли поиск стабильных зондов, а дальнейшее построение сигнатур и независимость клинических характеристик выполняли с помощью многофакторной регрессии Кокса. Диагностический и прогностический потенциал сигнатур оценивали с помощью метода ROC-анализа и кривых Каплан–Майера. Показано, что сигнатуры отобранных зондов обладают значимым диагностическим (AUC от 0,76 до 1) и прогностическим ($p < 0,05$) потенциалом. С помощью данного подхода удалось идентифицировать 47 генов, связанных с хорошим и плохим прогнозом, из которых пять уже были описаны ранее. При наличии результатов широкогеномного анализа ДНК примененный исследовательский подход можно использовать для изучения не только молекулярного патогенеза РМЖ, но и для других заболеваний.

Ключевые слова: рак молочной железы, молекулярные подтипы, выживаемость, метилирование ДНК, прогностические маркеры

Финансирование: работа выполнена при финансовой поддержке Министерства науки и высшего образования Российской Федерации в рамках Федеральной научно-технической программы развития генетических технологий на 2019–2027 годы (соглашение № 075-15-2021-1073).

Вклад авторов: А. И. Калинин — дизайн исследования, сбор, анализ и интерпретация данных, написание статьи; В. О. Сигин — написание статьи; М. В. Немцова — концепция и дизайн исследования; В. В. Стрельников — концепция и дизайн исследования, научное редактирование.

✉ **Для корреспонденции:** Алексей Игоревич Калинин
ул. Москворечье, д. 1, г. Москва, 115522; alexeika2@yandex.ru

Статья получена: 18.10.2022 **Статья принята к печати:** 11.11.2022 **Опубликована онлайн:** 25.11.2022

DOI: 10.24075/vrgmu.2022.056

According to the Global Cancer Observatory (GLOBOCAN), about 2.3 million of new breast cancer (BC) cases and 684,996 deaths from BC were reported in 2020. BC, being the most

common type of cancer all over the world [1], is a highly heterogeneous disease with varying molecular and clinical characteristics [2].

Today, BC subtypes are defined by immunohistochemical (IHC) staining of tumor tissue [3], particularly based on the estrogen, progesterone, HER2 receptor protein expression in the tumor and on the cancer cell proliferation rate. The development of methods for gene expression analysis involving the use of DNA microarrays played a major role in determining BC molecular subtypes. The use of the classifier based on the expression of 50 PAM50 genes makes it possible to clearly distinguish luminal A (LumA), luminal B (LumB), HER2-enriched (HER2+) molecular subtypes, as well as basal-like or triple-negative breast cancer (TNBC) [4]. TNBC that comprises 15–20% of all BC cases is characterized by aggressiveness, high metastasis rate, frequent relapses, and low survival rate compared to other BC subtypes [5]. Multigene microarray-based test systems make it possible to obtain prognostic information that is important for cancer patients, especially in cases of equivocal predictions made based on the clinical characteristics and IHC markers. Such systems include MammaPrint/Blueprint and Prosigna/PAM50, which, in addition

to their predictive value, provide the possibility of division into molecular subtypes [6]. These systems can be used to define high or low risk of relapse in female BC patients, however, this option is not yet available for TNBC and HER2+ molecular subtypes due to a lack of clinical trials.

Epigenetic changes modulate genome utilization through histone modification, changes in histone variant composition, chromatin remodeling, DNA methylation, positioning of nucleosomes and non-coding RNAs (expression of specific miRNAs). For the effect to become manifest, all of the above mentioned epigenetic alterations act in concert. DNA methylation is one of the best known factors of gene expression regulation. It occurs due to covalent modification of cytosines through the methyl group attachment to the C5-positions of cytosine residues in the context of CpG dinucleotides [7]. CpG dinucleotides tend to concentrate in the GC-rich DNA regions known as CpG islands, many of which are located in promoter gene regions and long repeat regions, such as retrotransposable elements or centromere

Table 1. Clinicopathological characteristics and data on the clinical endpoint status of patients with LumAB, TNBC and HER2-enriched BC molecular subtypes taken from open source (TCGA-BRCA)

Characteristics	LumAB	TNBC	HER2-enriched
Number of samples (%)	555	134	46
Age (median), years	59	54	58
T (%)			
T1	148 (26.49)	26 (19.4)	12 (26.09)
T2	310 (55.86)	87 (64.93)	28 (60.87)
T3	81 (14.59)	16 (11.94)	3 (6.52)
T4	14 (2.52)	4 (2.99)	3 (6.52)
No information	2 (0.36)	1 (0.75)	–
N (%)			
N0	233 (41.98)	78 (58.21)	16 (34.78)
N1	197 (35.5)	41 (30.6)	17 (36.96)
N2	75 (13.51)	11 (8.21)	6 (13.04)
N3	42 (7.57)	4 (2.99)	4 (8.7)
No information	8 (1.44)	–	3 (6.52)
M (%)			
M0	431 (77.66)	110 (82.09)	37 (80.43)
M1	6 (1.08)	3 (2.24)	1 (2.17)
No information	118 (21.26)	21 (15.67)	8 (17.39)
Grade (%)			
I	98 (17.66)	16 (11.94)	4 (8.7)
II	291 (52.43)	94 (70.15)	28 (60.87)
III	154 (27.75)	19 (14.18)	12 (26.09)
IV	5 (0.9)	2 (1.49)	1 (2.17)
No information	7 (1.26)	3 (2.24)	1 (2.17)
Clinical endpoint			
Overall survival (%)			
No event	490 (88.29)	113 (84.33)	37 (80.43)
Death	65 (11.71)	21 (15.67)	9 (19.57)
Disease-free survival (%)			
No relapse	445 (80.18)	102 (76.12)	35 (76.09)
Relapse	39 (7.03)	20 (14.93)	4 (8.7)
No information	71 (12.79)	12 (8.96)	7 (15.22)
Progression-free survival (%)			
No progression	486 (87.57)	109 (81.34)	38 (82.61)
Progression	69 (12.43)	25 (18.66)	8 (17.39)

Table 2. Total number of signatures and CpG pairs obtained by the LASSO Cox regression method for each survival outcome and BC molecular subtype. For some CpG pairs it was impossible to define genes these belonged to

Clinical endpoint + molecular subtype	ID's of HM450 probes	Genes	Number of combinations obtained
OS + LumAB	cg02287630; cg20417424 cg05828605 cg00297993 cg20471297 cg08133669 cg17323488 cg08241401 cg00815177 cg08442529 cg20746134 cg01821113 cg04523731 cg11140305 cg22067527	<i>SLC30A7; EXTL2; ST6GALNAC5; C15orf41; DYNC1H1; MIA3; NIPAL3; HEY2; HK1; DIRC3; TMEM41A; SH3BP5L; RFX2</i>	32752
DFS + LumAB	cg22790777 cg23667405 cg01017355 cg09561458 cg08128789 cg27304144 cg08039281 cg13486627 cg04833210 cg27439396 cg24347894	<i>SLC25A39; BAT2; ZNF417; LRRC8B; HSPG2; PSMA6; RG9MTD3; RBM19; N6AMT2; ZNF827</i>	2036
PFS + LumAB	cg13792075 cg08128789 cg13447284 cg00815177 cg10466124 cg13486627 cg15481636 cg00120948 cg05564086 cg23667405 cg17960080	<i>LRRC8B; HIST3H2A; ABCC5; BAT2; SPAG5; RERE; NIPAL3; HLA-DRB5; RG9MTD3</i>	2036
OS + TNBC	cg03512997 cg07804617 cg12814969 cg14293027 cg15355719 cg17053075 cg19002462 cg26401512 cg02567719	<i>FAM136A; HNRPDL; ENOPH1; LIN54; DNAJB4; ZNF643; TAP1; RASGRP2; LDLRAD3</i>	502
DFS + TNBC	cg20154816 cg02927111 cg18701707 cg12484411 cg20222926 cg02338142 cg06667406 cg13420273 cg22512222 cg17804981 cg13745678	<i>FEZF1; PLIN5; KCNMB2; AASS; HDAC9; ZFAND1; TRHR; PKNOX1</i>	2036
PFS + TNBC	cg01652244 cg02927111 cg20154816 cg00355315 cg24083274 cg23390595 cg13420273 cg10170774 cg01323371	<i>SSU72; DPPA5; PEX5L; HDAC9; CADPS2; STC1; PKNOX1</i>	502
OS + HER2-enriched	cg19236995 cg01564068 cg07351262 cg23409370 cg26290926 cg22043168 cg19986472 cg01647795	<i>GSTM4; BDNF; SLC43A1; PATL2; DHX8</i>	247
DFS + HER2-enriched	cg02327465 cg11261264 cg23302638 cg27252154 cg10660854 cg02796790 cg04407660 cg23183932	<i>BIRC5; EDARADD; TAPBPL; QTRT1; PTPRH; SNRPB</i>	247
PFS + HER2-enriched	cg20662988 cg23409370 cg23757489 cg03880890 cg04073970 cg22284390 cg27020573 cg00297843 cg17258551	<i>KCNN1; BOD1; SLC35F1; HTR5A; SLC45A1; CCDC49</i>	502

repeats. Methylation of cytosine is mediated by the enzyme class known as methyltransferases (DNMT) [7]. A total of five DNMT family members have been identified in mammals: DNMT1, DNMT2, DNMT3a, DNMT3b, and DNMT3L. DNMT3a and DNMT3b are *de novo* methyltransferases that interact with non-methylated CpG dinucleotides. DNMT1 is responsible for methylation maintenance during replication in S phase. It has been shown that DNMT3L stimulates *de novo* methylation that involves DNMT3a and mediates transcriptional repression with the help of histone deacetylase 1 (HDAC1) [7]. Aberrant DNA methylation is associated with a wide range of diseases and appears to be most marked in malignant tumors [8]. Studies of recent years show that every epithelial tumor contains about 10–15 genes inactivated by the genome structural changes and hundreds of genes inactivated by DNA hypermethylation. This demonstrates the importance of this modification for

tumor development. Total hypomethylation is one more feature of tumor genomes. This is a genome-wide hypomethylation that results mainly from the loss of methylation at repetitive elements and leads to genome instability and chromosomal rearrangement [8]. The increased promoter methylation in the tumor suppressor genes suppressing various mechanisms of tumor progression, that results in epigenetic silencing and reversible inactivation of these genes, plays an important role in BC pathogenesis [8]. Identification of the tumor-specific aberrant DNA methylation patterns can be useful for early diagnosis of cancer, differential diagnosis of malignant neoplasms, in the capacity of prognostic and predictive markers [9]. The study of specific DNA methylation patterns identified by genome-wide analysis makes an important contribution to understanding of BC pathogenesis [10]. As noted above, each cancer type is divided into subtypes. There are genomic patterns, including

Table 3. The best signature, number of probes in the signature, values of cvAUC (cross-validated area under curve; the average area under curve obtained at all stages of cross-validation), sensitivity, specificity and accuracy for each survival outcome and BC molecular subtype

Clinical endpoint + molecular subtype	Number of probes in the combination	Genes in the combination	cvAUC	Sensitivity	Specificity	Accuracy
OS + LumAB	12	<i>SLC30A7, EXTL2, C15orf41, MIA3, NIPAL3, HEY2, HK1, DIRC3, TMEM41A, SH3BP5L, RFX2</i>	0.797	0.829	0.629	0.805
DFS + LumAB	6	<i>SLC25A39, BAT2, ZNF417, PSMA6, RG9MTD3, ZNF827</i>	0.831	0.838	0.716	0.828
PFS + LumAB	9	<i>ABCC5, NIPAL3, HLA-DRB5, RG9MTD3, HIST3H2A, RERE, SPAG5, BAT2, cg13447284</i>	0.761	0.875	0.562	0.836
OS + TNBC	5	<i>cg03512997, LIN54, RASGRP2, LDLRAD3, ZNF643</i>	0.969	0.864	0.939	0.876
DFS + TNBC	5	<i>PKNOX1, KCNMB2, ZFAND1, HDAC9, cg13745678</i>	0.834	0.902	0.673	0.865
PFS + TNBC	6	<i>DPPA5, cg02927111, PKNOX1, SSU72, CADPS2, PEX5L</i>	0.844	0.952	0.674	0.900
OS + HER2-enriched	3	<i>GSTM4 (TSS200), GSTM4 (Body), cg26290926</i>	0.898	1	0.883	0.977
DFS + HER2-enriched	2	<i>BIRC5, cg10660854</i>	1	1	1	1
PFS + HER2-enriched	4	<i>SLC43A1, BOD1, cg00297843, KCNN1</i>	1	0.947	1	0.956

epigenetic ones, that are typical for these subtypes. Thus, it is necessary to perform specific genome-wide DNA methylation profiling in cancer patients, along with the conventional assessment of the promoter hypermethylation point events in certain genes [11].

Prognosis involves prediction of the possible course and outcome of cancer. Survival analysis that is based on mathematical approach to cancer prognosis makes it possible to predict the likelihood of staying alive after a certain time. Because of their biological importance and stability, DNA methylation markers are an effective prognostic factor [12]. In one of the studies, the data of the genome-wide DNA methylation analysis of BC samples from The Cancer Genome Atlas Breast Cancer (TCGA-BRCA) database were used to construct a model of seven CpG dinucleotides that made it possible to clearly distinguish breast tumors of all subtypes and normal tissues, and to identify six methylation sites that strongly correlated with overall survival (OS) [13]. The analysis of methylation data from open sources by LASSO regression and boosting revealed 29 and 11 CpG dinucleotides associated with OS, respectively [14]. The study of data taken from the open source (TCGA-BRCA) also made it possible to identify three genes (*TDRD10, PRAC2, and TMEM132C*), the methylation status of which had some predictive value, however, this was true mostly for estrogen receptor-positive breast tumors [15]. A prognostic model that comprises five genes (*TGFBR2, EIF4EBP1, FOSB, BCL2A1, ADRB2*) has been developed for TNBC based on the data obtained from TCGA-BRCA. The model is equally well suited for prediction of OS and disease free survival (DFS) [16].

Research is necessary due to the lack of such signatures for HER2-enriched subtype and a rather limited number of signatures for other BC molecular subtypes. The diagnostic potential of the existing survival prediction models is also uncertain, that is why we have used a modified algorithm to search for CpG dinucleotides associated with all available clinical endpoints found in the TCGA-BRCA database.

The study was aimed to obtain various signatures based on the open data on DNA methylation in BC from The Cancer Genome Atlas Breast Cancer for prediction of various

clinical endpoints (overall survival, disease-free survival, and progression-free survival) for BC molecular subtypes and test the relationship between the clinicopathological characteristics and the signatures obtained.

METHODS

The publicly available clinical parameters and the data of the genome-wide DNA methylation profiling obtained using the HumanMethylation450 (HM450) hybridization chips (Illumina Inc.; USA) within the framework of The Cancer Genome Atlas Breast Cancer (TCGA-BRCA) project (<https://portal.gdc.cancer.gov/projects/TCGA-BRCA>) were acquired and processed using the TCGAbiolinks software package [17]. Inclusion criteria for patients to be used for further selection of candidate CpG pairs were as follows: appropriate BC molecular subtype, availability of accessible clinicopathological information, availability of the DNA methylation profiling data obtained using the Illumina HumanMethylation450 chips. Exclusion criteria: no data on the time values for clinical endpoints, patient's age, TNM stage and grade. Then the results obtained using the patients' FFPE (formalin fixed paraffin-embedded) blocks and cross-hybridization probes were excluded from the profiling data matrix.

Selection of CpG pairs associated with OS, DFS or progression-free survival (PFS) was performed by univariate Cox regression method [18]. Of all the selected CpG pairs, those subjected to multiple testing adjustment (adjusted value $p < 0.05$, Wald test was used) by the false discovery rate (FDR) method were further analyzed. The LASSO Cox regression [19] method implemented in the SurvHiDim software package [20] was used to select the most stable CpG pairs. Multivariate Cox regression [21] was used to calculate the CpG-based signatures and to test the independence between the patients' clinical parameters and these signatures. The ability to classify various outcomes was defined by logistic regression method. Stratification into the high- and low-risk categories was performed using the median. The cvROC (cross-validated receiver operative curve) method [22] was used to test the quality of the models constructed and to plot the ROC curves.

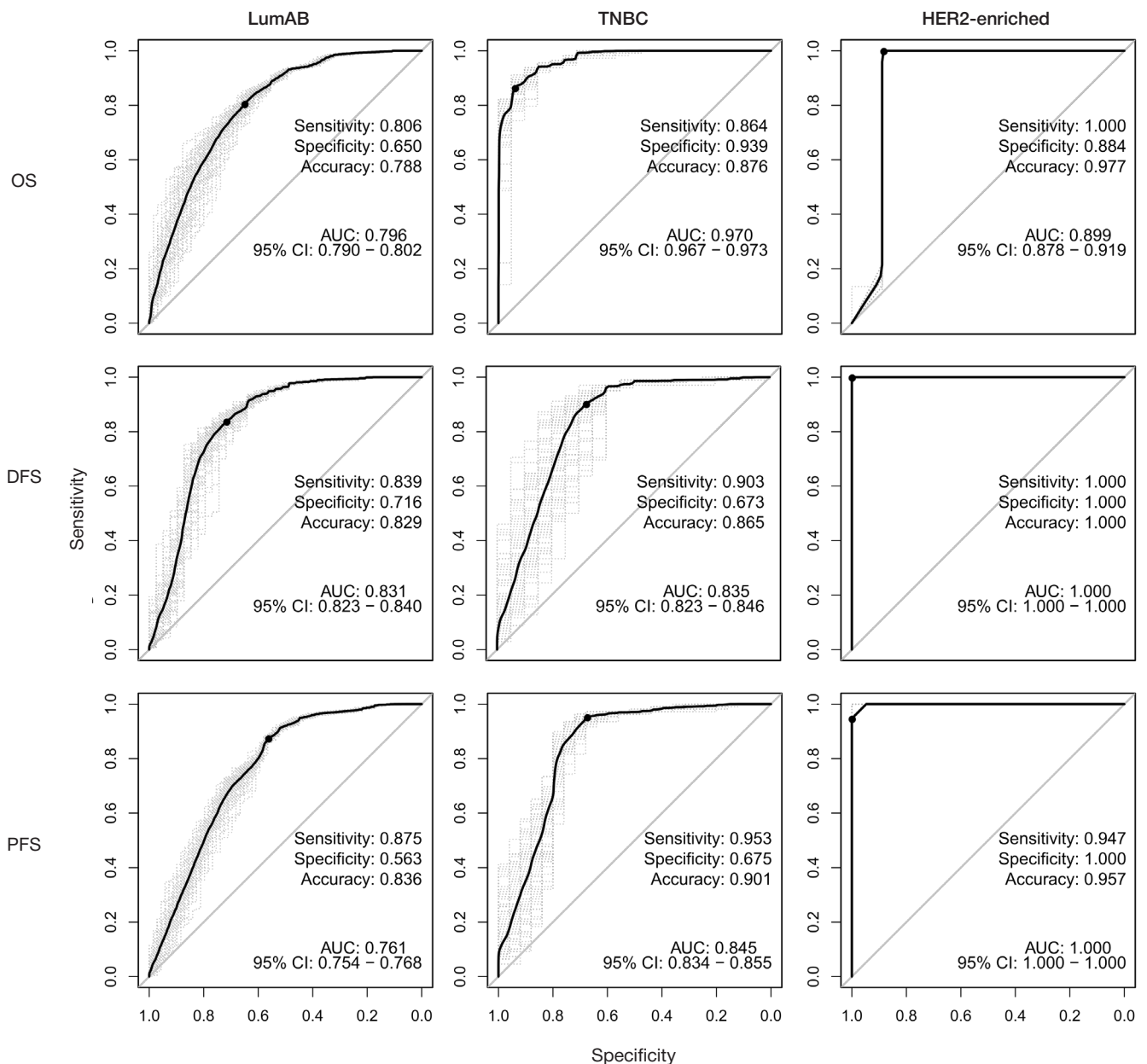


Fig. 1. cvROC curves (cross-validated receiver operative curve; ROC curve is plotted at every stage of cross-validation, then the resulting curve is constructed) for the best signatures. The vertical axis shows sensitivity (0–1), the horizontal axis shows specificity (0–1), rows show survival outcomes, columns show BC molecular subtypes

The best sensitivity and specificity values were defined by the Youden's index method. The Kaplan–Meier curves were constructed using the *survminer* software package [23]. The Mantel–Cox test was used to compare two survival curves. The 10-fold cross-validation method was used throughout all stages of marker selection and signature calculation. All the listed above calculations were performed using the R statistical programming language [24].

RESULTS

The studied TCGA-BRCA data set included the DNA methylation profile obtained using the HM450 chips and the clinicopathological characteristics of 735 primary BC samples. After exclusion of paraffin-embedded samples, there were a total of 555 LumA+B subtype (LumAB) samples, 134 TN subtype samples, and 46 HER2-enriched subtype samples (Table 1). Prior to selection of traits for further analysis, cross-hybridization probes were excluded from the methylation data

matrix, so that the number of probes reduced from 485,577 to 456,344, respectively.

The next stage of analysis involved using univariate Cox regression to search for methylation sites that correlate with the duration of OS, DFS and PFS in various BC molecular subtypes. After the initial selection with allowance for the multiple testing adjusted p-value, the following probes were selected:

- 10,433 probes associated with OS in the LumAB subtypes, 3214 probes in the TN subtype, 6471 probes in the HER2-enriched subtype;
- 4419 probes associated with DFS in the LumAB subtypes, 168 probes in the TN subtype, 483 probes in the HER2-enriched subtype;
- 2345 probes associated with PFS in the LumAB subtypes, 43 probes in the TN subtype, 3216 probes in the HER2-enriched subtype.

LASSO Cox regression was used for each of the listed sets, allowing for selection of CpG dinucleotides that were most important for analysis. Different numbers of such CpG pairs

Table 4. Multivariate Cox regression results for the best signatures and clinicopathological characteristics. HR — hazard ratio (relative risk), P — responsible for *p*-val

Variable/clinical endpoint + molecular subtype	OS + LumAB		DFS + LumAB		PFS + LumAB		OS + TNBC		DFS + TNBC		PFS + TNBC		OS + HER2-enriched		DFS + HER2-enriched		PFS + HER2-enriched	
	HR (95% confidence interval)	P	HR (95% confidence interval)	P	HR (95% confidence interval)	P	HR (95% confidence interval)	P										
Risk indicator	1 (1-1)	<0.001	1.1 (1.05-1.10)	<0.001	1.03 (1.02-1.04)	<0.001	1.1 (1.004-1.2)	<0.001	1.02 (1.01-1.03)	<0.001	1.02 (1.001-1.03)	<0.001	1.0 (1-1)	0.03	1.02 (1.009-1.03)	0.006	1.005 (1.001-1.000)	0.01
Age (below median/over median)	1.38 (0.84-2.30)	0.201	1.2 (0.58-2.40)	0.638	2 (0.9-3.30)	0.231	0.76 (0.28-2.00)	0.575	0.51 (0.160-1.600)	0.25	0.66 (0.270-1.600)	0.35	6.2 (0.619-62.900)	0.12	1.9 (0.878-2.344)	0.512	2.06 (0.27-15)	0.47
T (T1-2/3-4)	0.87 (0.48-1.60)	0.64	1.1 (0.48-2.60)	0.78	0.77 (0.38-1.60)	0.463	2.52 (0.75-8.40)	0.134	1.06 (0.310-3.600)	0.93	1.50 (0.430-5.200)	0.52	2.6 (0.169-39.900)	0.49	0.9 (0.625-1.932)	0.404	7.00 (0.50-98)	0.14
N (N0/N1-3)	1.23 (0.74-2.00)	0.42	2.1 (0.73-6.00)	0.16	1.1 (0.56-2.20)	0.097	2.95 (0.88-9.90)	0.08	0.96 (0.280-3.300)	0.95	1.14 (0.390-3.300)	0.81	1.1 (0.174-7.500)	0.89	0.34 (0.120-1.500)	0.463	1.09 (0.07-16)	0.94
M (M0/M1)	1.03 (0.51-2.10)	0.94	1.6 (0.66-3.80)	0.30	1.9 (0.90-2.20)	0.076	0.36 (0.09-1.30)	0.125	1.56 (0.360-6.700)	0.55	0.89 (0.290-2.800)	0.83	1.2 (0.089-15.300)	0.90	0.63 (0.105-2.000)	0.376	0.02 (0.00-1.05)	0.053
Grade (I-II/III-IV)	1.20 (0.71-2.00)	0.49	2.3 (0.95-5.50)	0.06	1.54 (0.80-2.90)	0.19	1.48 (0.36-6.00)	0.58	4.19 (0.94-18.60)	0.06	3.76 (0.97-14.50)	0.055	1.10 (0.09-14.30)	0.91	2.6 (0.78-2.80)	0.16	1.83 (0.12-27.00)	0.66

were identified during each stage of cross-validation. CpG pairs found in more than 50% of cross-validation data splits were selected (Table 2).

To select the combinations of CpG dinucleotides showing significant correlations with various survival outcomes, we assessed all possible combinations (signatures) of such CpG dinucleotides in various BC molecular subtypes. For each clinical endpoint and BC molecular subtype, cvAUC (cross-validated area under curve, the average area under curve at all stages of cross-validation), sensitivity, specificity and accuracy were defined for various combinations. The first 10 combinations showing high cvAUC values were tested for independence of the clinicopathological characteristics. The diagnostic characteristics of these combinations along with the number of probes and genes belonging to the probes are provided in Table 3.

The combination of 12 CpG dinucleotides for prediction of OS in the LumAB subtype was the largest defined combination, while the combination of two CpG dinucleotides for prediction of DFS in the HER2-expressing subtype was the smallest one. The cvROC (cross-validated receiver operative characteristics: ROC curve is plotted at every stage of cross-validation, then the average curve is constructed) curves and the Kaplan–Meier curves were plotted for each signature to show the diagnostic

potential and estimate the survival function. The LumAB combinations showed lower cvAUC values (0.76–0.83), while the combinations for TN and HER2-expressing subtypes showed high cvAUC values with fewer number of combinations (0.83–1) (Fig. 1).

Our combinations are independent of the clinical characteristics (Table 4). This makes it possible to use the risk indicators of these clinical endpoints in any group of patients.

The Kaplan–Meier curve analysis revealed a significant (*p* < 0.05) decrease in OS, DFS and PFS in the group of patients with high risk of death, relapse and disease progression compared to the group of patients with low risk. This was true for all BC molecular subtypes and all selected combinations (Fig. 2).

DISCUSSION

In this study, we considered the possibility of identifying the CpG dinucleotide differentially methylated sites to predict survival outcomes in various BC molecular subtypes using the methods of survival analysis and DNA methylation data. The approach to calculation of differential methylation based on univariate Cox regression is widely used in a variety of studies. Thus, this method was used for identification of 249,810 and 249,811 probes based on DNA methylation data

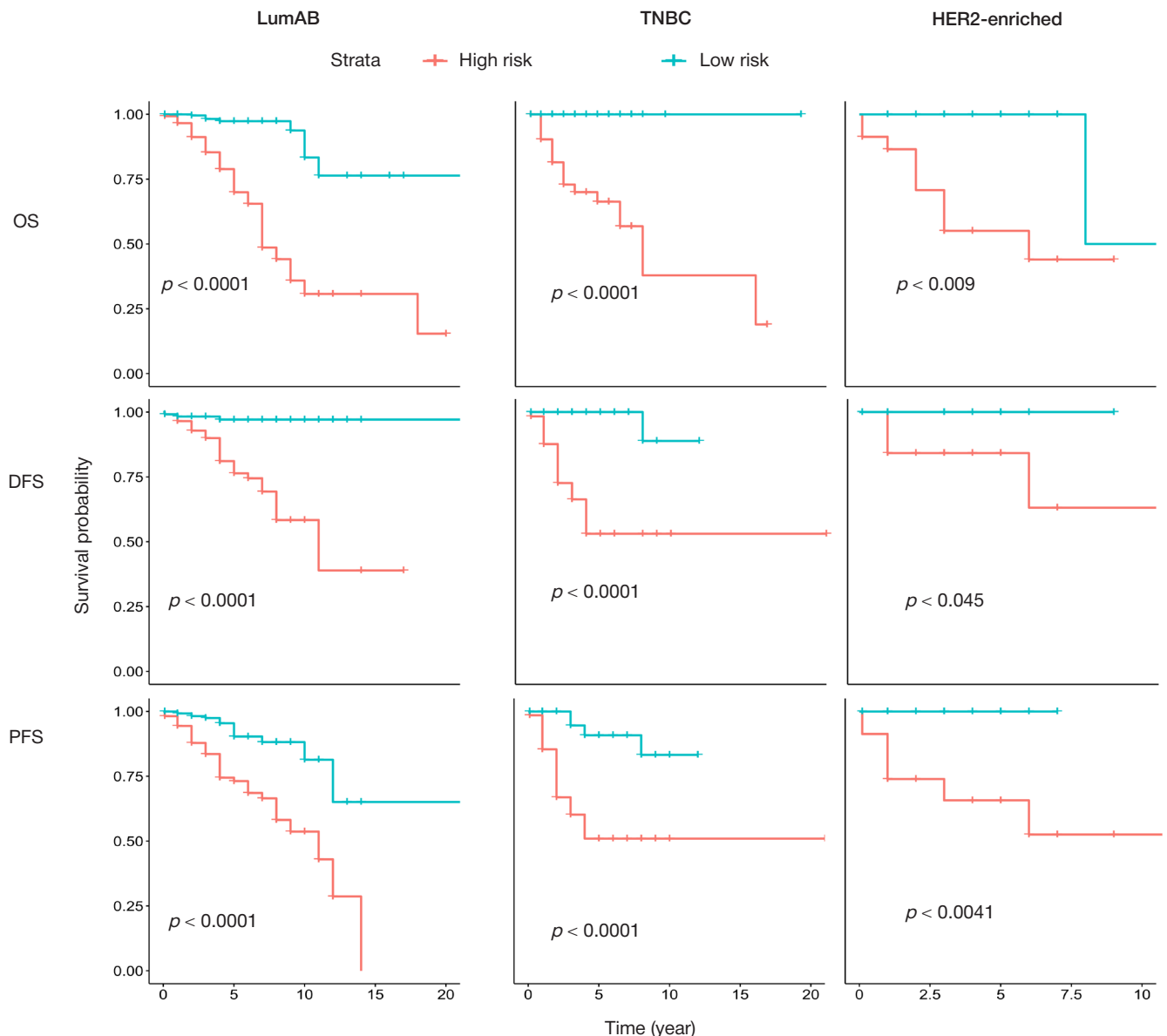


Fig. 2. Kaplan–Meier curves for the best signatures. The horizontal axis shows time (years), the vertical axis shows the likelihood of staying alive (0–1). High risk of death, progression and relapse is highlighted in red, low risk of death, progression and relapse is highlighted in turquoise. Rows show survival outcomes, and columns show BC molecular subtypes

associated with ovarian cancer and BC, respectively [12], and for identification of probes based on DNA methylation data associated with cutaneous melanoma [25].

We have shown that the use of various combinations (2–12 CpG dinucleotides) makes it possible to achieve acceptable (cvAUC 0.7–0.8), high (0.8–0.9) and very high quality (0.9–1) of classification into high and low risk of death, relapse and progression. During the study we have identified 47 probes/genes (*SLC30A7*, *EXTL2*, *C15orf41*, *MIA3*, *NIPAL3*, *HEY2*, *HK1*, *DIRC3*, *TMEM41A*, *SH3BP5L*, *RFX2*, *SLC25A39*, *BAT2*, *ZNF417*, *PSMA6*, *RG9MTD3*, *ZNF827*, *ABCC5*, *HLA-DRB5*, *HIST3H2A*, *RERE*, *SPAG5*, *cg13447284*, *cg03512997*, *LIN54*, *RASGRP2*, *LDLRAD3*, *ZNF643*, *PKNOX1*, *KCNMB2*, *ZFAND1*, *HDAC9*, *cg13745678*, *DPPA5*, *cg02927111*, *PKNOX1*, *SSU72*, *CADPS2*, *PEX5L*, *GSTM4*, *cg26290926*, *BIRC5*, *cg10660854*, *SLC43A1*, *BOD1*, *cg00297843*, *KCNN1*), the methylation of which is associated with OS, DFS and PFS. We failed to define which genes seven probes (*cg13447284*, *cg03512997*, *cg13745678*, *cg02927111*, *cg26290926*, *cg10660854*, *cg00297843*) belonged to. Five of these probes (*BIRC5*, *PKNOX1*, *SPAG5*, *HDAC9*, *PSMA6*) have been

previously reported in scientific literature as molecular markers of BC patients' survival based on the data of gene expression quantification [26–31].

It is noteworthy that in our study we found the same number of CpG dinucleotides (HM450 probes) for prediction of OS and DFS (based on five probes) as other researchers [16], but the probes varied according to genes they belonged to. According to our data, the signature for prediction of PFS consists of six probes; no PFS signature was calculated during the study [16]. Other researchers suggest using individual markers of promoter hypermethylation in seven genes (*RASSF1*, *BRCA1*, *PITX2*, *RARB*, *PGR*, *CDH1*, and *PCDH10*) for prediction of OS and DFS outcome in patients with ER+ BC, they also consider using the panel of three genes (*GSTP1*, *RASSF1*, and *RARB*) for prediction of OS based on the literature data analysis (systematic review of the reports) [26], while we have used a strategy of developing panels of six, nine and 12 methylation markers based on the marker diagnostic potential defined by statistical analysis of the experimental data set.

Among genes included in our combinations, attention is drawn to *BIRC5* (encodes baculoviral IAP repeat-containing

protein 5) that is overexpressed in the majority of tumors, including BC, and is associated with poorer prognosis of overall, disease-free and progression-free survival. It has been shown that the use of taxane chemotherapy drugs may increase the expression of this gene [27]. *PKNOX1* (gene of the short arm of chromosome 21 that encodes eponymous protein and plays an important role in embryogenesis) is a tumor suppressor gene, while the increased expression of this gene is associated with poorer survival rate [28]. The increased expression of *SPAG5* (encodes protein associated with the mitotic spindle apparatus), associated with poorer prognosis of OS, DFS and PFS only in estrogen receptor-positive (ER⁺) breast tumors, is also a prognostic factor [29], which is confirmed by our study. The findings of the study that involved ER⁺ BC samples show that the increased expression of *HDAC9* epigenetic enzyme (encodes protein, histone deacetylase 9) in tumors is associated with the poorer prognosis of DFS [30]. Our study shows the association between the abnormal methylation

of this gene and survival of patients with estrogen receptor-negative (ER⁻) tumors, and more precisely with TNBC. The reduced DFS of patients with ER⁺ BC was associated with the increased expression of *PSMA6* (encodes proteasome subunit alpha type-6) [31], which was also confirmed by our findings.

CONCLUSIONS

Molecular epigenetic signatures for various BC types were discovered using the survival analysis methods, combinations of various methylation sites, and estimation of diagnostic parameters. This method may be recommended to search for signatures typical for BC and other tumor diseases. In the future the discovered epigenetic signatures may be used to develop the methylation-sensitive quantitative PCR assays. After clinical trials, such assays may become a cheaper and more practical alternative to gene expression microarrays, without reducing diagnostic performance.

References

- Sung H, Ferlay J, Siegel RL, Laversanne M, Soerjomataram I, Jemal A, et al. Global Cancer Statistics 2020: GLOBOCAN Estimates of Incidence and Mortality Worldwide for 36 Cancers in 185 Countries. *CA Cancer J Clin.* 2021; 71 (3): 209–49. DOI: 10.3322/caac.21660
- Bernhardt SM, Dasari P, Walsh D, Townsend AR, Price TJ, Ingman WW. Hormonal Modulation of Breast Cancer Gene Expression: Implications for Intrinsic Subtyping in Premenopausal Women. *Front Oncol.* 2016; 6: 241. DOI: 10.3389/fonc.2016.00241.
- Zaha DC. Significance of immunohistochemistry in breast cancer. *World J Clin Oncol.* 2014; 5 (3): 382–92. DOI: 10.5306/wjco.v5.i3.382. PMID: 25114853; PMCID: PMC4127609.
- Perou CM, Sørlie T, Eisen MB, van de Rijn M, Jeffrey SS, Rees CA, et al. Molecular portraits of human breast tumours. *Nature.* 2000; 406 (6797): 747–52. DOI: 10.1038/35021093.
- Echeverria GV, Ge Z, Seth S, Zhang X, Jeter-Jones S, Zhou X, et al. Resistance to neoadjuvant chemotherapy in triple-negative breast cancer mediated by a reversible drug-tolerant state. *Sci Transl Med.* 2019; 11 (488): eaav0936. DOI: 10.1126/scitranslmed.aav0936.
- Blanchette P, Sivajohanathan D, Bartlett J, Eisen A, Feilotter H, Pezo R, et al. Clinical Utility of Multigene Profiling Assays in Early-Stage Invasive Breast Cancer: An Ontario Health (Cancer Care Ontario) Clinical Practice Guideline. *Curr Oncol.* 2022; 29 (4): 2599–615. DOI: 10.3390/curroncol29040213.
- Edwards JR, Yarychkivska O, Boulard M, Bestor TH. DNA methylation and DNA methyltransferases. *Epigenetics Chromatin.* 2017; 10: 23. DOI: 10.1186/s13072-017-0130-8.
- Vietri MT, D'Elia G, Benincasa G, Ferraro G, Caliendo G, Nicoletti GF, et al. DNA methylation and breast cancer: A way forward (Review). *Int J Oncol.* 2021; 59 (5): 98. DOI: 10.3892/ijo.2021.5278.
- Esteller M. Cancer epigenomics: DNA methylomes and histone-modification maps. *Nat Rev Genet.* 2007; 8 (4): 286–98. DOI: 10.1038/nrg2005.
- Karami Fath M, Azarjoojahromi A, Kiani A, Jalalifar F, Osati P, Akbari Oryani M, et al. The role of epigenetic modifications in drug resistance and treatment of breast cancer. *Cell Mol Biol Lett.* 2022; 27 (1): 52. DOI: 10.1186/s11658-022-00344-6.
- Lee G, Bang L, Kim SY, Kim D, Sohn KA. Identifying subtype-specific associations between gene expression and DNA methylation profiles in breast cancer. *BMC Med Genomics.* 2017; 10 (Suppl 1): 28. DOI: 10.1186/s12920-017-0268-z.
- Hu WL, Zhou XH. Identification of prognostic signature in cancer based on DNA methylation interaction network. *BMC Med Genomics.* 2017; 10 (Suppl 4): 63. DOI: 10.1186/s12920-017-0307-9.
- Zhang M, Wang Y, Wang Y, Jiang L, Li X, Gao H, et al. Integrative Analysis of DNA Methylation and Gene Expression to Determine Specific Diagnostic Biomarkers and Prognostic Biomarkers of Breast Cancer. *Front Cell Dev Biol.* 2020; 8: 529386. DOI: 10.3389/fcell.2020.529386.
- Hao X, Luo H, Krawczyk M, Wei W, Wang W, Wang J, et al. DNA methylation markers for diagnosis and prognosis of common cancers. *Proc Natl Acad Sci U S A.* 2017; 114 (28): 7414–9. DOI: 10.1073/pnas.1703577114.
- de Almeida BP, Apolônio JD, Binnie A, Castelo-Branco P. Roadmap of DNA methylation in breast cancer identifies novel prognostic biomarkers. *BMC Cancer.* 2019; 19 (1): 219. DOI: 10.1186/s12885-019-5403-0.
- Gao Y, Wang X, Li S, Zhang Z, Li X, Lin F. Identification of a DNA Methylation-Based Prognostic Signature for Patients with Triple-Negative Breast Cancer. *Med Sci Monit.* 2021; 27: e930025. DOI: 10.12659/MSM.930025.
- Colaprico A, Silva TC, Olsen C, Garofano L, Cava C, Garolini D, et al. TCGAbiolinks: an R/Bioconductor package for integrative analysis of TCGA data. *Nucleic Acids Res.* 2016; 44 (8): e71. DOI: 10.1093/nar/gkv1507.
- Abd ElHafeez S, D'Arrigo G, Leonardi D, Fusaro M, Tripepi G, Roumeliotis S. Methods to Analyze Time-to-Event Data: The Cox Regression Analysis. *Oxid Med Cell Longev.* 2021; 2021: 1302811. DOI: 10.1155/2021/1302811.
- Utazirubanda JC, Leon T, Ngom P. Variable selection with Group LASSO approach: Application to Cox regression with frailty model. *Commun Stat Simul Comput.* 2021; 50 (3): 881–901. DOI: 10.1080/03610918.2019.1571605.
- Bhattacharjee A, Pawar A. SurvHiDim: high dimensional survival data analysis. R package version 0.1.1. 2021. Available from: <https://CRAN.R-project.org/package=SurvHiDim>.
- Bradburn MJ, Clark TG, Love SB, Altman DG. Survival analysis part II: multivariate data analysis — an introduction to concepts and methods. *Br J Cancer.* 2003; 89 (3): 431–6. DOI: 10.1038/sj.bjc.6601119.
- LeDell E, Petersen M, van der Laan M. cvAUC: Cross-Validated Area Under the ROC Curve Confidence Intervals. R package version 1.1-4. 2022 Available from: <http://CRAN.R-project.org/package=cvAUC>.
- Kassambara A, Kosinski M, Biecek P. survminer: Drawing Survival Curves using 'ggplot2'. R package version 0.4.6. Available from: <https://CRAN.R-project.org/package=survminer>.
- Team RCR Foundation for Statistical Computing; Vienna, Austria: 2015.
- Guo W, Zhu L, Zhu R, Chen Q, Wang Q, Chen JQ. A four-DNA methylation biomarker is a superior predictor of survival of patients

- with cutaneous melanoma. *Elife*. 2019; 8: e44310. DOI: 10.7554/eLife.44310.
26. de Ruijter TC, van der Heide F, Smits KM, Aarts MJ, van Engeland M, Heijnen VCG. Prognostic DNA methylation markers for hormone receptor breast cancer: a systematic review. *Breast Cancer Res*. 2020; 22 (1): 13. DOI: 10.1186/s13058-020-1250-9.
 27. Dai JB, Zhu B, Lin WJ, Gao HY, Dai H, Zheng L, et al. Identification of prognostic significance of BIRC5 in breast cancer using integrative bioinformatics analysis. *Biosci Rep*. 2020; 40 (2): BSR20193678. DOI: 10.1042/BSR20193678.
 28. Jiang S, Bu X, Tang D, Yan C, Huang Y, Fang K. A tumor suppressor gene-based prognostic classifier predicts prognosis, tumor immune infiltration, and small molecule compounds in breast cancer. *Front Genet*. 2022; 12: 783026. DOI: 10.3389/fgene.2021.783026.
 29. Mohamadlizada-Hanjani Z, Shahbazi S, Geranpayeh L. Investigation of the SPAG5 gene expression and amplification related to the NuMA mRNA levels in breast ductal carcinoma. *World J Surg Oncol*. 2020; 18 (1): 225. DOI: 10.1186/s12957-020-02001-8.
 30. Linares A, Assou S, Lapierre M, Thouennon E, Duraffourd C, Fromaget C, et al. Increased expression of the HDAC9 gene is associated with antiestrogen resistance of breast cancers. *Mol Oncol*. 2019; 13 (7): 1534–47. DOI: 10.1002/1878-0261.
 31. Li Y, Huang J, Sun J, Xiang S, Yang D, Ying X, et al. The transcription levels and prognostic values of seven proteasome alpha subunits in human cancers. *Oncotarget*. 2017 Jan 17; 8 (3): 4501–19. DOI: 10.18632/oncotarget.13885.

Литература

1. Sung H, Ferlay J, Siegel RL, Laversanne M, Soerjomataram I, Jemal A, et al. Global Cancer Statistics 2020: GLOBOCAN Estimates of Incidence and Mortality Worldwide for 36 Cancers in 185 Countries. *CA Cancer J Clin*. 2021; 71 (3): 209–49. DOI: 10.3322/caac.21660
2. Bernhardt SM, Dasari P, Walsh D, Townsend AR, Price TJ, Ingman WV. Hormonal Modulation of Breast Cancer Gene Expression: Implications for Intrinsic Subtyping in Premenopausal Women. *Front Oncol*. 2016; 6: 241. DOI: 10.3389/fonc.2016.00241.
3. Zaha DC. Significance of immunohistochemistry in breast cancer. *World J Clin Oncol*. 2014; 5 (3): 382–92. DOI: 10.5306/wjco.v5.i3.382. PMID: 25114853; PMCID: PMC4127609.
4. Perou CM, Sørlie T, Eisen MB, van de Rijn M, Jeffrey SS, Rees CA, et al. Molecular portraits of human breast tumours. *Nature*. 2000; 406 (6797): 747–52. DOI: 10.1038/35021093.
5. Echeverria GV, Ge Z, Seth S, Zhang X, Jeter-Jones S, Zhou X, et al. Resistance to neoadjuvant chemotherapy in triple-negative breast cancer mediated by a reversible drug-tolerant state. *Sci Transl Med*. 2019; 11 (488): eaav0936. DOI: 10.1126/scitranslmed.aav0936.
6. Blanchette P, Sivajohanathan D, Bartlett J, Eisen A, Feilotter H, Pezo R, et al. Clinical Utility of Multigene Profiling Assays in Early-Stage Invasive Breast Cancer: An Ontario Health (Cancer Care Ontario) Clinical Practice Guideline. *Curr Oncol*. 2022; 29 (4): 2599–615. DOI: 10.3390/curroncol29040213.
7. Edwards JR, Yarychivska O, Boulard M, Bestor TH. DNA methylation and DNA methyltransferases. *Epigenetics Chromatin*. 2017; 10: 23. DOI: 10.1186/s13072-017-0130-8.
8. Vietri MT, D'Elia G, Benincasa G, Ferraro G, Caliendo G, Nicoletti GF, et al. DNA methylation and breast cancer: A way forward (Review). *Int J Oncol*. 2021; 59 (5): 98. DOI: 10.3892/ijo.2021.5278.
9. Esteller M. Cancer epigenomics: DNA methylomes and histone-modification maps. *Nat Rev Genet*. 2007; 8 (4): 286–98. DOI: 10.1038/nrg2005.
10. Karami Fath M, Azargoonyahromi A, Kiani A, Jalalifar F, Osati P, Akbari Oryani M, et al. The role of epigenetic modifications in drug resistance and treatment of breast cancer. *Cell Mol Biol Lett*. 2022; 27 (1): 52. DOI: 10.1186/s11658-022-00344-6.
11. Lee G, Bang L, Kim SY, Kim D, Sohn KA. Identifying subtype-specific associations between gene expression and DNA methylation profiles in breast cancer. *BMC Med Genomics*. 2017; 10 (Suppl 1): 28. DOI: 10.1186/s12920-017-0268-z.
12. Hu WL, Zhou XH. Identification of prognostic signature in cancer based on DNA methylation interaction network. *BMC Med Genomics*. 2017; 10 (Suppl 4): 63. DOI: 10.1186/s12920-017-0307-9.
13. Zhang M, Wang Y, Wang Y, Jiang L, Li X, Gao H, et al. Integrative Analysis of DNA Methylation and Gene Expression to Determine Specific Diagnostic Biomarkers and Prognostic Biomarkers of Breast Cancer. *Front Cell Dev Biol*. 2020; 8: 529386. DOI: 10.3389/fcell.2020.529386.
14. Hao X, Luo H, Krawczyk M, Wei W, Wang W, Wang J, et al. DNA methylation markers for diagnosis and prognosis of common cancers. *Proc Natl Acad Sci U S A*. 2017; 114 (28): 7414–9. DOI: 10.1073/pnas.1703577114.
15. de Almeida BP, Apolônio JD, Binnie A, Castelo-Branco P. Roadmap of DNA methylation in breast cancer identifies novel prognostic biomarkers. *BMC Cancer*. 2019; 19 (1): 219. DOI: 10.1186/s12885-019-5403-0.
16. Gao Y, Wang X, Li S, Zhang Z, Li X, Lin F. Identification of a DNA Methylation-Based Prognostic Signature for Patients with Triple-Negative Breast Cancer. *Med Sci Monit*. 2021; 27: e930025. DOI: 10.12659/MSM.930025.
17. Colaprico A, Silva TC, Olsen C, Garofano L, Cava C, Garolini D, et al. TCGAAbiolinks: an R/Bioconductor package for integrative analysis of TCGA data. *Nucleic Acids Res*. 2016; 44 (8): e71. DOI: 10.1093/nar/gkv1507.
18. Abd ElHafeez S, D'Arrigo G, Leonardis D, Fusaro M, Tripepi G, Roumeliotis S. Methods to Analyze Time-to-Event Data: The Cox Regression Analysis. *Oxid Med Cell Longev*. 2021; 2021: 1302811. DOI: 10.1155/2021/1302811.
19. Utazirubanda JC, Leon T, Ngom P. Variable selection with Group LASSO approach: Application to Cox regression with frailty model. *Commun Stat Simul Comput*. 2021; 50 (3): 881–901. DOI: 10.1080/03610918.2019.1571605.
20. Bhattacharjee A, Pawar A. SurvHiDim: high dimensional survival data analysis. R package version 0.1.1. 2021. Available from: <https://CRAN.R-project.org/package=SurvHiDim>.
21. Bradburn MJ, Clark TG, Love SB, Altman DG. Survival analysis part II: multivariate data analysis — an introduction to concepts and methods. *Br J Cancer*. 2003; 89 (3): 431–6. DOI: 10.1038/sj.bjc.6601119.
22. LeDell E, Petersen M, van der Laan M. cvAUC: Cross-Validated Area Under the ROC Curve Confidence Intervals. R package version 1.1-4. 2022 Available from: <http://CRAN.R-project.org/package=cvAUC>.
23. Kassambara A, Kosinski M, Bieчек P. survminer: Drawing Survival Curves using 'ggplot2'. R package version 0.4.6. Available from: <https://CRAN.R-project.org/package=survminer>.
24. Team RCR Foundation for Statistical Computing; Vienna, Austria: 2015.
25. Guo W, Zhu L, Zhu R, Chen Q, Wang Q, Chen JQ. A four-DNA methylation biomarker is a superior predictor of survival of patients with cutaneous melanoma. *Elife*. 2019; 8: e44310. DOI: 10.7554/eLife.44310.
26. de Ruijter TC, van der Heide F, Smits KM, Aarts MJ, van Engeland M, Heijnen VCG. Prognostic DNA methylation markers for hormone receptor breast cancer: a systematic review. *Breast Cancer Res*. 2020; 22 (1): 13. DOI: 10.1186/s13058-020-1250-9.
27. Dai JB, Zhu B, Lin WJ, Gao HY, Dai H, Zheng L, et al. Identification of prognostic significance of BIRC5 in breast cancer using integrative bioinformatics analysis. *Biosci Rep*. 2020; 40 (2): BSR20193678. DOI: 10.1042/BSR20193678.
28. Jiang S, Bu X, Tang D, Yan C, Huang Y, Fang K. A tumor suppressor gene-based prognostic classifier predicts prognosis, tumor immune infiltration, and small molecule compounds in breast cancer. *Front Genet*. 2022; 12: 783026. DOI: 10.3389/

- fgene.2021.783026.
29. Mohamadalizadeh-Hanjani Z, Shahbazi S, Geranpayeh L. Investigation of the SPAG5 gene expression and amplification related to the NuMA mRNA levels in breast ductal carcinoma. *World J Surg Oncol.* 2020; 18 (1): 225. DOI: 10.1186/s12957-020-02001-8.
 30. Linares A, Assou S, Lapierre M, Thouennon E, Duraffourd C, Fromaget C, et al. Increased expression of the HDAC9 gene is associated with antiestrogen resistance of breast cancers. *Mol Oncol.* 2019; 13 (7): 1534–47. DOI: 10.1002/1878-0261.
 31. Li Y, Huang J, Sun J, Xiang S, Yang D, Ying X, et al. The transcription levels and prognostic values of seven proteasome alpha subunits in human cancers. *Oncotarget.* 2017 Jan 17; 8 (3): 4501–19. DOI: 10.18632/oncotarget.13885.

THE RS17713054 AND RS1800629 POLYMORPHISMS OF GENES *LZTFL1* AND *TNF* ARE ASSOCIATED WITH COVID-19 SEVERITY

Traspov AA¹, Minashkin MM¹, Poyarkov SV¹, Komarov AG², Shtinova IA², Speshilov GI², Karbyshev IA², Pozdnyakova NV^{1✉}, Godkov MA³

¹ Sistema BioTech LLC, Moscow, Russia

² Diagnostic Center (Center of Laboratory Testing) of the Moscow Department of Health, Moscow, Russia

³ Sklifosovsky Research Institute for Emergency Medicine, Moscow, Russia

Both genetic and non-genetic factors are responsible for high interindividual variability in response to SARS-CoV-2. Despite the fact that multiple genetic polymorphisms have been identified as risk factors of severe COVID-19, such polymorphisms are still insufficiently studied in the Russian population. The study was aimed to identify genetic determinants associated with severe COVID-19 in the sample of patients from the Russian Federation. The correlation of the rs17713054 polymorphism in gene *LZTFL1* and rs1800629 polymorphism in gene *TNF* (tumor necrosis factor) with the COVID-19 severity was assessed. DNA samples obtained from 713 patients (324 males and 389 females) aged 18–95 with COVID-19 of varying severity were analyzed. The rs1800629 polymorphism of gene *TNF* (OR = 1.5; $p = 0.02$) and rs17713054 polymorphism of gene *LZTFL1* (OR = 1.60; $p = 0.0043$) were identified as risk factors of severe disease. The *TNF* polymorphism rs1800629 and *LZTFL1* polymorphism rs17713054 could be considered as potential predictive biomarkers. The rs17713054 G > A polymorphism was strongly associated with severe disease. In the future the findings may provide the basis for the development of test-systems for prediction of the risk of severe viral respiratory diseases.

Keywords: COVID-19, SARS-CoV-2, SNP, *LZTFL1*, *TNF*, severity, genetic determinants

Funding: the study was supported by the major Sistema BioTech LLC shareholder, the Sistema Public Joint Stock Financial Corporation. The study was funded by the Moscow Department of Health as part of the double blind clinical trial.

Acknowledgements: the authors express their gratitude to Antipova YuO, Deputy Head of the Moscow Department of Health, for organizing the blind clinical trial of COVID-19 severity and the patients of the Diagnostic Center (Center of Laboratory Testing) of the Moscow Department of Health for the provided biomaterial samples.

Author contribution: Pozdnyakova NV, Poyarkov SV — study concept and design; Minashkin MM — molecular genetic research, laboratory tests; Poyarkov SV, Traspov AA — literature review, manuscript writing; Traspov AA — statistical processing of the results, manuscript editing; Komarov AG — project management, planning the experiment, data analysis; Shtinova IA, Speshilov GI, Karbyshev IA — providing clinical data and metadata; Godkov MA — control over clinical sample collection at the Sklifosovsky Research Institute for Emergency Medicine, providing anonymized data.

Compliance with ethical standards: the study did not need to be approved by the Ethics Committee because of dealing with anonymized patient data and the double blind study format.

✉ **Correspondence should be addressed:** Natalia V. Pozdnyakova
1 Kurjanovskaja, 34, korp. 11, Moscow, Russia; n.pozdnyakova@sistemabiotech.ru

Received: 18.11.2022 **Accepted:** 14.12.2022 **Published online:** 28.12.2022

DOI: 10.24075/brsmu.2022.065

ПОЛИМОРФИЗМЫ RS17713054 И RS1800629 ГЕНОВ *LZTFL1* И *TNF* АССОЦИИРОВАНЫ С ТЯЖЕЛЫМ ТЕЧЕНИЕМ COVID-19

А. А. Траспов¹, М. М. Минашкин¹, С. В. Поляков¹, А. Г. Комаров², И. А. Штинова², Г. И. Спешилов², И. А. Карбышев², Н. В. Позднякова^{1✉}, М. А. Годков³

¹ «Система-БиоТех», Москва, Россия

² Диагностический центр (Центр лабораторных исследований) Департамента здравоохранения города Москвы, Москва, Россия

³ Научно-исследовательский институт скорой помощи имени Н. В. Склифосовского

Генетические и негенетические факторы ответственны за высокую межиндивидуальную вариабельность ответа на SARS-CoV-2. Хотя многочисленные генетические полиморфизмы были идентифицированы как факторы риска тяжелого течения COVID-19, они остаются недостаточно изученными в российской популяции. Целью данного исследования было выявить генетические детерминанты, ассоциированные с тяжелым течением COVID-19 на выборке пациентов из Российской Федерации. Проведена оценка связи генетических полиморфизмов rs17713054 в гене *LZTFL1* и rs1800629 в гене *TNF* (фактор некроза опухоли) с тяжестью COVID-19. Были исследованы образцы ДНК 713 пациентов (324 мужчины и 389 женщины) возрастом 18–95 лет с COVID-19, протекавшей с разной степенью тяжести. Идентифицированы rs1800629 *TNF* (OR = 1,5; $p = 0,02$) и rs17713054 *LZTFL1* (OR = 1,60; $p = 0,0043$) как факторы риска тяжелого течения. Полиморфизмы *TNF* rs1800629 и *LZTFL1* rs17713054 могут быть потенциальным предиктивным и предиктивным биомаркерами. Показана сильная ассоциация rs17713054 G > A с тяжелым течением. Полученные данные могут в дальнейшем стать основой для разработки тест-систем предсказания рисков тяжести течения вирусных заболеваний респираторного тракта.

Ключевые слова: COVID-19, SARS-CoV-2, SNP, *LZTFL1*, *TNF*, тяжесть течения, генетические детерминанты

Финансирование: исследование профинансировано главным акционером компании ООО «Система-БиоТех», АФК «Система». Исследование профинансировано в рамках двойного слепого клинического исследования Департаментом здравоохранения г. Москвы

Благодарности: авторы благодарят заместителя руководителя Департамента здравоохранения г. Москвы Ю. О. Антипову за организацию исследования; за предоставление образцов биологических материалов пациентов ГБУЗ «Диагностический центр (Центр лабораторных исследований) г. Москвы».

Вклад авторов: Н. В. Позднякова, С. В. Поляков — концепция и дизайн исследования; М. М. Минашкин — выполнение молекулярно-генетических работ, лабораторная постановка; С. В. Поляков, А. А. Траспов — обзор литературы, написание статьи; А. А. Траспов — статистическая обработка и редактирование статьи; А. Г. Комаров — руководство, планирование эксперимента, анализ данных; И. А. Штинова, Г. И. Спешилов и И. А. Карбышев — предоставление клинического материала и метаданных; М. А. Годков — контроль за сбором образцов, предоставление обезличенных данных.

Соблюдение этических стандартов: одобрение этического комитета не требовалось в связи с работой с обезличенными данными пациентов и двойным слепым форматом исследования.

✉ **Для корреспонденции:** Наталья Вячеславовна Позднякова
1-я Курьяновская ул., д. 34, кор.11, Москва, Россия; n.pozdnyakova@sistemabiotech.ru

Статья получена: 18.11.2022 **Статья принята к печати:** 14.12.2022 **Опубликована онлайн:** 28.12.2022

DOI: 10.24075/vrgmu.2022.065

In the past decades it was shown that human genome variation contributes to heterogeneity emerging in response to infectious diseases.

The pandemic of severe acute respiratory syndrome caused by the SARS-CoV-2 coronavirus has killed millions of people all over the world.

The disease caused by the novel coronavirus infection (COVID-19) is characterized by high variability of clinical manifestations (World Health Organization, 2021). The majority of patients, specifically 81%, are asymptomatic or develop mild disease, while 14% have severe disease and 5% develop critical illness [1]. The most common symptoms include fever, dry cough, and fatigue; ageusia, anosmia, and gastrointestinal symptoms have been also reported. Severe COVID-19 is characterized by respiratory failure requiring mechanical ventilation or the use of high flow oxygen.

There is a constant search for the risk factors associated with the disease. Initially it was assumed that elderly males having a history of cardiovascular disorders developed severe disease, but it turned out that genetic background contributed just as much. Numerous studies have shown that polymorphisms of genes encoding the host factors essential for realization of the viral life cycle, such as *ACE2*, *TMPRSS2*, *AR*, and genes involved in the innate immunity, such as *TNF*, *TLR7*, may be associated with the COVID-19 severity [2].

The first genome-wide association study (GWAS) of the COVID-19 severity that compared 1980 patients from Italy and Spain who developed severe infection with the control population with the unknown status of the SARS-CoV-2 infection revealed two loci significant at the genome-wide level, which were mapped to the 3p21.31 region comprising six genes (*SLC6A26*, *LZTFL1*, *CXCR6*, *CCR1*, *CCR3*, *CCR9*) and the 9q34.2 region comprising the ABO blood group locus [3].

The signal at the 3p21.31 locus remains the most stable and strong in numerous studies, this is associated with both susceptibility to infection and the disease severity. In this locus, allele C of the rs10490770 variant is associated with the highest risk of severe COVID-19-associated pneumonia [4].

The genome-wide association studies (GWAS) have shown that the 3p21.31 region is associated with the twofold increased risk of respiratory failure [5].

The role of the host factors determining both susceptibility and infection severity has been shown for many pathogens, including *Mycobacterium tuberculosis*, HIV, *Candida albicans*, and many more [6].

It is known that the risk of severe infection is associated with the genes involved in the immune and inflammatory responses. Thus, the role of the minor alleles of TLR7 [7] and the interferon system genes [8] is well-known.

Along with the risk alleles, there are variants that have a protective effect. Thus, the TT genotype of the rs5443 SNP in the gene *GNB3* is associated with protection against COVID-19 fatality [9]. Polymorphisms in the regulatory regions of the genes encoding pro-inflammatory cytokines capable of affecting the expression of mRNA of this genes, such as C-572G rs1800796 in the promoter region of the gene *IL-6*, are associated with protection against severe COVID-19 and COVID-19 fatality in the Asian population [10].

METHODS

Clinical and demographic characteristics of surveyed patients

The patients admitted to the intensive care units (ICU) of the Sklifosovsky Research Institute for Emergency Medicine, Medsi

Clinical Hospital № 1, City Clinical Hospital № 40 together with the staff members of the Sistema Public Joint Stock Financial Corporation and the Sistema BioTech laboratory were enrolled. A retrospective study was carried out (the disease outcome was known) that involved 713 patients ($n = 713$). Inclusion criteria: coronavirus infection of varying severity. Exclusion criteria: comorbidities of various types capable of dramatically affecting the patient's overall condition (cancer, CAD, immune defects).

To reveal the association of the studied variants with the severe and critical course of the disease, we divided the patients into two groups: the control group that included two categories of patients (patients with mild-to-moderate disease) and the experimental group (patients with severe disease). The patients were allocated to groups in accordance with the computed tomography-based (or MSCT-based) visual assessment scale for the lung damage developed during the pandemic of novel coronavirus infection by the experts of the US center for diagnosis and telemedicine after assessing CT images of 13,003 people who constituted the core sample. This classification is also widely used in the Russian practice [24]. The lung CT scan data were the criteria of the disease severity: CT1 and 2 for the control group, CT3 and 4 for the group of patients with the severe disease. The main characteristics of the studied cohort are provided in Table. 1.

Genomic DNA isolation

Venous blood stabilized with EDTA was used as biomaterial for extraction of genomic DNA.

DNA was extracted using the DiaGene kit (Dia-M; Russia) for DNA isolation from whole blood. The extracted DNA purity was determined with the NanoDrop OneC spectrophotometer (Thermo FS; USA). The A260/280 ratio was between 1.8–1.91, and the A260/230 ratio was between 1.62–2.28. DNA concentration was measured using the dsDNA BR kit in the Qubit Flex fluorometer (Thermo FS; USA). The concentration values varied between 15–300 ng/μL. The concentrations of all DNA samples were adjusted to 2 ng/μL.

DNA genotyping

DNA genotyping in the region of the studied polymorphic markers was performed by the real-time PCR with fluorescence detection using the TaqMan SNP kits for genotyping analysis (Thermo FS; USA). PCR was performed in the CFX96Touch System (BioRad; USA).

A number of markers was genotyped that was later confirmed by Sanger sequencing. The primers were constructed using PrimerBlast (<https://www.ncbi.nlm.nih.gov/tools/primer-blast/> (as at 24 September 2020)). The BigDye Terminator v3.1 kit (Thermo FS; USA) was used for cycle sequencing; sequencing was performed in the Genetic Analyzer 3500 system (Thermo FS; USA).

Statistical data processing

The two-tailed Fischer's exact test and chi-squared (χ^2) test were used to calculate the statistical significance of differences in allele frequency. The calculations were performed for both minor allele (AA vs. Aa+aa; dominant model) and the minor allele homozygous genotypes (AA+Aa vs. aa; recessive model). The odds ratios (OR), 95% confidence intervals (CI), and significance levels were calculated for the groups in which significant differences were revealed. Calculations were performed using the SNPStats web tool (<https://www.snpstats.net/> (as at

Table 1. The main age and gender parameters selected for the study. The patients are divided into two groups based on the disease severity (the control group and the group of patients with severe disease), gender, and age

	<i>n</i> = 713	
	Control group	Group with severe disease
Total	373 (52.31%)	340 (47.69%)
MALES	154 (41%)	170 (50%)
FEMALES	219 (59%)	170 (50%)
Age	21–94	18–95

20 September 2021)) designed to reveal the associations between the single nucleotide polymorphisms and the risk of the disease. The Holm–Bonferroni method was used to adjust the OR values of significant polymorphisms for multiple comparisons. The samples, including all polymorphisms, were tested for the sample size sufficiency. The analysis was performed in the Statsoft Statistica 12 software package. To analyze the sample size required to achieve a power of 80%, we used the two-sample t-test for comparison of two population means (the null hypothesis was $\mu_1 = \mu_2$). The features of the SNPstats software package were taken into account, along with the values used: the means with the Akaike information criterion (AIC) values and Bayesian information criterion (BIC) values.

RESULTS

Table 1 describes the studied sample in terms of the sample diversity.

The two-tailed Fischer's exact test and χ^2 test were used to calculate the statistical significance of differences in allele frequency. Statistical calculations were based on the dominant model (involving identification of the risk allele) and recessive model (involving identification of the risk genotype). Furthermore, the odds ratios (OR), 95% confidence intervals (CI), and significance levels (*p*) were calculated for the groups in which significant differences were revealed.

Statistical significance was calculated using two models, the dominant and recessive ones, for all polymorphisms (depending on the patients' division into groups). The model was based on estimation of the risk of transition from mild to severe disease; allele frequencies were compared in patients of the control group and patients of the group with severe disease (Table 2).

Table 2. SNPs used in the model for assessment of the risk of severe disease in two groups (control and experimental)

Gene/SNP	Dominant model (AA vs. Aa+aa)			Recessive model (AA+Aa vs. aa)		
	OR (95% CI)	CI	<i>P</i> -value	OR (95% CI)	CI	<i>P</i> -value
<i>TNF</i> /rs1800629	1.5	1.06–2.12	0.02	1.1	0.35–3.44	0.87
<i>IFIH1</i> /rs1990760	1.2	0.88–1.63	0.26	1.4	0.98–2.01	0.07
<i>IFITM3</i> /rs12252	0.87	0.55–1.38	0.56	1.66	0.46–5.92	0.43
<i>CCR2</i> /rs1799864	1.27	0.91–1.78	0.16	1.33	0.57–3.11	0.51
<i>STAT3</i> /rs744166	0.94	0.70–1.27	0.71	0.53	0.32–0.88	0.01
<i>STAT6</i> /rs324011	0.93	0.68–1.26	0.62	1.17	0.75–1.81	0.48
<i>TLR2</i> /rs1898830	0.72	0.53–0.98	0.04	0.73	0.48–1.11	0.13
<i>C3AR1</i> /rs7842	1.13	0.84–1.52	0.41	1.37	0.77–2.42	0.28
<i>TMPRSS2</i> /rs75603675	1.23	0.90–1.68	0.19	0.85	0.57–1.27	0.43
<i>LZTFL1</i> /rs17713054	1.6	1.16–2.21	0.0043	4.56	1.51–13.76	0.0025

Note: CI values are provided only for odds ratios.

Since multiple hypotheses were tested during the study using the same dataset, the Holm–Bonferroni correction was used due to the multiple comparison problem in order to avoid type I errors.

As for two markers, the presence of the minor allele and homozygous genotype were associated with the increased risk of severe disease. These were rs1800629 in the gene *TNF* (OR = 1.5; *p* = 0.02) and rs17713054 in the gene *LZTFL1* (OR = 1.60; *p* = 0.0043), however rs17713054 appeared to be pathogenic in the recessive model (OR = 4.56; *p* = 0.0025).

As for marker *TLR2*, the minor allele homozygous genotype exerted protective effect in the dominant model.

All the markers identified are the risk factors of both disease susceptibility and the transition from mild to more severe disease, however, only the variants provided in the above tables are significant.

Furthermore, the studied sample was also tested for deviations from Hardy–Weinberg equilibrium (*n* = 713), the analysis was performed for 10 studied markers (Table 3).

Summation of the Hardy–Weinberg disequilibrium coefficients and their significance levels (*P*) revealed deviation from equilibrium for *IFIH1* (*p* = 0.0047), *CCR2* (*p* = 0.049), and significant deviation from equilibrium for *IFITM3* (*p* = 0.00053).

Thus, the *TNF* rs1800629 and *LZTFL1* rs17713054 variants may be considered as probable candidates for further assessment involving larger samples (Table 4).

DISCUSSION

Our study demonstrates evidence of the human 3p21.31 locus involvement in pathophysiology of COVID-19 based on assessing the independent cohort of patients and the control group comprising people from the Russian Federation.

Our previous research has analysed the distribution of 10 SNPs and the association of these SNPs with the disease

Table 3. Estimation of allele frequencies of 10 studied markers based on the dominant and recessive models, HOM1/HET/HOM2 genotype distribution, and significance of deviations from Hardy–Weinberg equilibrium (HWE *p*-value). Assessment was performed in the experimental (*n* = 340), control (*n* = 373), and combined (*n* = 713) groups

Comparison of the control group and the group of patients with severe disease									
Gene/allele variants	Allele frequency			Genotype distribution			HWE <i>p</i> -value		
	all	control	experiment	all	control	experiment	all	control	experiment
<i>TNF</i> (G/A)	0.87/0.13	0.89/0.11	0.85/0.15	0.02/0.22/0.76	0.02/0.18/0.8	0.02/0.26/0.73	0.86	0.42	0.83
<i>IFIH1</i> (T/C)	0.57/0.43	0.59/0.41	0.54/0.46	0.21/0.44/0.35	0.18/0.45/0.37	0.24/0.43/0.33	0.0047	0.13	0.016
<i>IFITM3</i> (A/G)	0.93/0.07	0.93/0.07	0.94/0.06	0.88/0.11/0.01	0.87/0.12/0.01	0.89/0.09/0.02	0.00053	0.081	0.0012
<i>CCR2</i> (G/A)	0.85/0.15	0.87/0.13	0.84/0.16	0.03/0.23/0.74	0.03/0.21/0.76	0.04/0.25/0.71	0.049	0.12	0.22
<i>STAT3</i> (A/G)	0.66/0.34	0.64/0.36	0.68/0.32	0.42/0.47/0.11	0.42/0.45/0.13	0.43/0.49/0.08	0.24	0.65	0.019
<i>STAT6</i> (C/T)	0.62/0.38	0.62/0.38	0.62/0.38	0.37/0.5/0.13	0.36/0.51/0.12	0.38/0.48/0.14	0.13	0.078	0.82
<i>TLR2</i> (A/G)	0.59/0.41	0.57/0.43	0.62/0.38	0.34/0.52/0.15	0.3/0.53/0.17	0.37/0.5/0.13	0.062	0.11	0.25
<i>C3AR1</i> (T/C)	0.72/0.28	0.73/0.27	0.71/0.29	0.07/0.42/0.51	0.06/0.41/0.53	0.08/0.42/0.5	0.46	0.43	0.9
<i>TMPRSS2</i> (C/A)	0.59/0.41	0.6/0.4	0.58/0.42	0.16/0.5/0.34	0.17/0.46/0.36	0.15/0.53/0.32	0.54	0.52	0.094
<i>LZTFL1</i> (C/T)	0.84/0.16	0.87/0.13	0.8/0.2	0.7/0.27/0.03	0.75/0.24/0.01	0.65/0.3/0.05	0.68	0.37	0.39

severity [11]. In this study involving the use of the larger sample and the extended set of polymorphisms, the *TLR7* polymorphism was excluded, and the polymorphism *LZTFL1* polymorphism was added; the study revealed that only two polymorphisms in the genes *LZTFL1* and *TNF* showed a strong association with severe COVID-19.

Among the studied polymorphisms, only two were strongly associated with severe disease. It is interesting to note that the results for some polymorphisms obtained during the earlier study [11] turned out to be non-significant after the sample expansion to 713 patients. However, the equally strong signal was found in the rs17713054 (gene *LZTFL1*, locus 3p21.3). The second most important was the *TNF* rs1800629. It is known that both polymorphisms are associated with severe COVID-19, and carriers of the minor alleles are at high risk of developing severe COVID-19 [12]. The rs17713054 polymorphism is located in the enhancer that regulates gene

expression in this locus, including the expression of *LZTFL1*, *SLC6A20*, and genes encoding chemokines.

This polymorphism results in the emergence of the new binding site for the C/EBP beta transcription factor, which leads to the increased expression of *LZTFL1* and neighbouring genes in this locus [13]. The *LZTFL1* gene is involved in the ciliary function of the lung epithelial cells, which is important for airway virus clearance [14].

LZTFL1 is widely expressed in the lung epithelial cells, including the ciliated epithelial cells that have been identified as one of the key cellular targets of the SARS-CoV-2 infection. Furthermore, a homozygous deletion of *LZTFL1* causes the classic ciliopathy, the Bardet–Biedl syndrome [15]; it is known that respiratory viruses may affect mucociliary clearance. *LZTFL1* encodes the cytosole leucine zipper protein that binds to E-cadherin (epithelial marker) and is involved in the transport of numerous signaling molecules. It is also known that *LZTFL1*

Table 4. Estimation of the significance of differences between the experimental and control groups in 10 studied polymorphisms

Gene/SNP	Allele	Experiment	Control	<i>P</i> -value	Odds ratio	CI
<i>TNF</i> /rs1800629	G	665	581	0.03801	1.398585	1.009831–1.941277
	A	81	99			
<i>IFIH1</i> /rs1990760	T	442	370	0.06881	1.217995	0.9818877–1.5111842
	C	304	310			
<i>IFITM3</i> /rs12252	A	695	636	0.8319	0.9427985	0.6060591–1.4617779
	G	51	44			
<i>CCR2</i> /rs1799864	G	647	571	0.1536	1.247354	0.9192725–1.6940554
	A	99	109			
<i>STAT3</i> /rs744166	A	478	460	0.1627	0.8531148	0.6806029–1.0687811
	G	268	220			
<i>STAT6</i> /rs1898830	C	464	423	1	0.999678	0.8020877–1.2457747
	T	282	257			
<i>TLR2</i> /rs1898830	A	423	424	0.03094	0.7908369	0.6357947–0.9831671
	G	323	256			
<i>C3AR1</i> /rs7842	T	547	481	0.2877	1.137109	0.8959515–1.4432459
	C	199	199			
<i>TMPRSS2</i> /rs75603675	C	445	397	0.628	1.053809	0.8482685–1.3092215
	A	301	283			
<i>LZTFL1</i> /rs17713054	C	649	546	0.0007003	1.641442	1.223191–2.208574
	T	97	134			

activation in the context of malignant neoplasms inhibits the epithelial-mesenchymal transition (EMT) pathway, which is known to be a part of the mechanisms underlying both wound healing and immune response [16]. The study of postmortem lung biopsies obtained from patients who died from the COVID-19 complications showed a widespread epithelial dysfunction with the signs of EMT [13]. According to several studies, the signal in the 3p21.31 locus remains the most stable and strong. This is associated with both susceptibility to infection and the disease severity [17].

It has been shown that the rs17713054 risk allele A in the *LZTFL1* gene enhancer is largely responsible for the increased risk of respiratory failure in COVID-19 patients that is associated with 3p21.31 [13]. *LZTFL1* is widely expressed in the lung epithelial cells, including the ciliated epithelial cells that have been identified as one of the key cellular targets of the SARS-CoV-2 infection SARS-CoV-2 [18].

The analysis of other *LZTFL1* polymorphisms, such as rs11385942, revealed the increased risk of hospitalization ($p < 0.01$; OR = 5.73; 95% CI: 1.2–26.5 based on the allelic test) in the Colombian [19] and Latvian [20] populations; the rs35280891 intronic variant ($p = 6.88 \times 10^{-7}$; OR = 19.846, 95% CI: 5.728–68.761) was associated with severe disease in the Serbian population [21].

It is interesting to note that the rs17713054 minor allele A is a part of the extended haplotype inherited from the Neanderthals. Today, this haplotype is the major risk factor associated with developing severe symptoms after the SARS-CoV-2 infection. The differences in the haplotype frequencies between the populations of South Asia and East Asia led to a speculation that certain selective pressure, probably related to cholera, resulted in the haplotype spread across the population of South Asia [22].

Our study confirmed the rs17713054 strong association with severe disease (OR = 4.56; $p = 0.0025$) in the recessive model.

It was also shown that both the minor allele T of the *TNF* rs1800629 variant and the minor TT genotype were the risk factors of severe disease in all the variants of samples (OR = 1.5; $p = 0.02$).

It is known that the rs1800629 variant of the gene *TNF* is associated with the need for respiratory support and the longer duration of respiratory support in patients with COVID-19 [23]. Along with the pathogenic variants, we also found the *TLR2* rs1898830 variant that exerted protective effect (OR = 0.72).

The association study of 10 SNPs showed that two polymorphisms had enough power to be used for assessment of the risk of severe disease.

The association study of the *LZTFL1* rs17713054 in the RF that involved the balanced sample of patients with severe and mild course of the disease revealed a strong association with the disease severity. This confirmed the hypothesis about the functional significance of this polymorphism.

A simple, rapid, and affordable test for prediction of the risk of severe COVID-19 based on the individual DNA polymorphisms would be useful for both stratification of patients at high and low risk of complications and, which is more important, for assessment of the disease severity in the population of healthy people in case of infection followed by the disease as a promising predictive test.

CONCLUSIONS

The genetic testing of the sample of 713 patients with the confirmed diagnosis of COVID-19 revealed the key *TNF* and *LZTFL1* SNPs associated with severe disease. The new genetic marker in the gene *LZTFL1* with the predictive value exceeding 91% was characterized. The deviation of the allele frequencies of the genetic polymorphisms associated with the risk of severe COVID-19 from the Hardy-Weinberg equilibrium are of great epidemiological significance and require further research. The *TNF* rs1800629 variants and *LZTFL1* rs17713054 variants may be considered as probable candidates for further analysis involving larger samples. The clinical study conducted makes it possible to draw a number of conclusions for further clinical practice. The overall flow of patients admitted to the clinics due to the acute respiratory coronavirus infection is heterogeneous, it can be divided into the groups of patients with the potentially mild and potentially severe disease based on the presence or absence of the selected *TNF* rs1800629 and *LZTFL1* rs17713054 polymorphisms in the patient's genotype at an early stage. The *LZTFL1* and *TNF* polymorphisms may be used as both prognostic and predictive biomarkers. These markers can provide scientific grounds for the new approaches to the genotype-directed treatment of patients with the severe COVID-19-associated lung damage. The study entails a promising opportunity to organize the apparently affordable and efficient screening studies.

References

- Hu B, et al., Characteristics of SARS-CoV-2 and COVID-19. *Nat Rev Microbiol.* 2021; 19 (3): 141–54.
- Gupta K, et al., Systematic review and meta-analysis of human genetic variants contributing to COVID-19 susceptibility and severity. *Gene.* 2022; 844: 146790.
- Severe Covid GG, et al., Genomewide Association Study of Severe Covid-19 with Respiratory Failure. *N Engl J Med.* 2020; 383 (16): 1522–34.
- Colona VL, Vasiliou V, Watt J, Novelli G, Reichardt JKV. Update on human genetic susceptibility to COVID-19: susceptibility to virus and response. *Hum Genomics.* 2021; 15 (1): 57.
- Nakanishi T, Pigazzini S, Degenhardt F, Cordioli M, Butler-Laporte G, Maya-Miles D, et al. Age-dependent impact of the major common genetic risk factor for COVID-19 on severity and mortality. *J Clin Invest.* 2021; 131 (23): e152386.
- Kwok AJ, Mentzer A, Knight JC. Host genetics and infectious disease: new tools, insights and translational opportunities. *Nat Rev Genet.* 2021; 22 (3): 137–53.
- El-Hefnawy SM, et al, COVID-19 susceptibility, severity, clinical outcome and Toll-like receptor (7) mRNA expression driven by *TLR7* gene polymorphism (rs3853839) in middle-aged individuals without previous comorbidities. *Gene Rep.* 2022; 27: 101612.
- Casanova JL, Abel L. From rare disorders of immunity to common determinants of infection: Following the mechanistic thread. *Cell.* 2022; 185 (17): 3086–103.
- Mohlendick B, et al. The *GNB3* c.825C>T (rs5443) polymorphism and protection against fatal outcome of corona virus disease 2019 (COVID-19). *Front Genet.* 2022; 13: 960731.
- Chen T, et al. A Low-Producing Haplotype of Interleukin-6 Disrupting CTCF Binding Is Protective against Severe COVID-19. *mBio.* 2021; 12 (5): e0137221.
- Minashkin MM, et al. The Role of Genetic Factors in the Development of Acute Respiratory Viral Infection COVID-19: Predicting Severe Course and Outcomes. *Biomedicines.* 2022; 10 (3).
- Fricke-Galindo I, Buendía-Roldán I, Ruiz A, Palacios Y, Pérez-Rubio G, de Jesus Hernández-Zenteno R, et al. *TNFRSF1B* and *TNF* Variants Are Associated With Differences in Levels of

- Soluble Tumor Necrosis Factor Receptors in Patients With Severe COVID-19. *J Infect Dis.* 2022; 226 (5): 778–87.
13. Downes DJ, et al. Identification of LZTFL1 as a candidate effector gene at a COVID-19 risk locus. *Nat Genet.* 2021; 53 (11): 1606–15.
 14. Fink-Baldauf IM, et al. CRISPRi links COVID-19 GWAS loci to LZTFL1 and RAVR1. *EBioMedicine.* 2022; 75: 103806.
 15. Marion V, et al., Exome sequencing identifies mutations in LZTFL1, a BBSome and smoothed trafficking regulator, in a family with Bardet-Biedl syndrome with situs inversus and insertional polydactyly. *J Med Genet.* 2012; 49 (5): 317–21.
 16. Stewart CA, Gay CM, Ramkumar K, Cargill KR, Cardnell RJ, Nilsson MB, et al. Lung Cancer Models Reveal Severe Acute Respiratory Syndrome Coronavirus 2-Induced Epithelial-to-Mesenchymal Transition Contributes to Coronavirus Disease 2019 Pathophysiology. *J Thorac Oncol.* 2021; 16 (11): 1821–39.
 17. Redin C, CW. Thorball, and J. Fellay, Host genomics of SARS-CoV-2 infection. *Eur J Hum Genet.* 2022; 30 (8): 908–14.
 18. Wei Q, Chen ZH, Wang L, Zhang T, Duan L, Behrens C, et al. LZTFL1 suppresses lung tumorigenesis by maintaining differentiation of lung epithelial cells. *Oncogene.* 2016; 35 (20): 2655–63.
 19. Angulo-Aguado M, et al., Association Between the LZTFL1 rs11385942 Polymorphism and COVID-19 Severity in Colombian Population. *Front Med (Lausanne).* 2022; 9: 910098.
 20. Rescenko R, et al. Replication of LZTFL1 Gene Region as a Susceptibility Locus for COVID-19 in Latvian Population. *Virology.* 2021; 36 (5): 1241–4.
 21. Zecevic M, et al. Genome-Wide Association Study of COVID-19 Outcomes Reveals Novel Host Genetic Risk Loci in the Serbian Population. *Front Genet.* 2022; 13: 911010.
 22. Niemi MEK, Daly MJ, Ganna A. The human genetic epidemiology of COVID-19. *Nat Rev Genet.* 2022; 23 (9): 533–46.
 23. Fishchuk L, et al. Modifying effects of TNF-alpha, IL-6 and VDR genes on the development risk and the course of COVID-19. Pilot study. *Drug Metab Pers Ther.* 2021; 37 (2): 133–9.
 24. Kudryavtsev YS, Beregov MM, Berdalín AB, Lelyuk VG. Comparison of the Main Staging Systems for Assessing the Severity of Lung Injury in Patients with COVID-19 and Evaluation of Their Predictive Value. *Journal of radiology and nuclear medicine.* 2021; 102 (5): 296–303.

Литература

1. Hu B, et al., Characteristics of SARS-CoV-2 and COVID-19. *Nat Rev Microbiol.* 2021; 19 (3): 141–54.
2. Gupta K, et al., Systematic review and meta-analysis of human genetic variants contributing to COVID-19 susceptibility and severity. *Gene.* 2022; 844: 146790.
3. Severe Covid GG, et al., Genomewide Association Study of Severe Covid-19 with Respiratory Failure. *N Engl J Med.* 2020; 383 (16): 1522–34.
4. Colona VL, Vasiliou V, Watt J, Novelli G, Reichardt JKV. Update on human genetic susceptibility to COVID-19: susceptibility to virus and response. *Hum Genomics.* 2021; 15 (1): 57.
5. Nakanishi T, Pigazzini S, Degenhardt F, Cordioli M, Butler-Laporte G, Maya-Miles D, et al. Age-dependent impact of the major common genetic risk factor for COVID-19 on severity and mortality. *J Clin Invest.* 2021; 131 (23): e152386.
6. Kwok AJ, Mentzer A, Knight JC. Host genetics and infectious disease: new tools, insights and translational opportunities. *Nat Rev Genet.* 2021; 22 (3): 137–53.
7. El-Hefnawy SM, et al. COVID-19 susceptibility, severity, clinical outcome and Toll-like receptor (7) mRNA expression driven by TLR7 gene polymorphism (rs3853839) in middle-aged individuals without previous comorbidities. *Gene Rep.* 2022; 27: 101612.
8. Casanova JL, Abel L. From rare disorders of immunity to common determinants of infection: Following the mechanistic thread. *Cell.* 2022; 185 (17): 3086–103.
9. Mohlendick B, et al. The GNB3 c.825C>T (rs5443) polymorphism and protection against fatal outcome of corona virus disease 2019 (COVID-19). *Front Genet.* 2022; 13: 960731.
10. Chen T, et al. A Low-Producing Haplotype of Interleukin-6 Disrupting CTCF Binding Is Protective against Severe COVID-19. *mBio.* 2021; 12 (5): e0137221.
11. Minashkin MM, et al. The Role of Genetic Factors in the Development of Acute Respiratory Viral Infection COVID-19: Predicting Severe Course and Outcomes. *Biomedicine.* 2022; 10 (3).
12. Fricke-Galindo I, Buendía-Roldán I, Ruiz A, Palacios Y, Pérez-Rubio G, de Jesus Hernández-Zenteno R, et al. TNFRSF1B and TNF Variants Are Associated With Differences in Levels of Soluble Tumor Necrosis Factor Receptors in Patients With Severe COVID-19. *J Infect Dis.* 2022; 226 (5): 778–87.
13. Downes DJ, et al. Identification of LZTFL1 as a candidate effector gene at a COVID-19 risk locus. *Nat Genet.* 2021; 53 (11): 1606–15.
14. Fink-Baldauf IM, et al. CRISPRi links COVID-19 GWAS loci to LZTFL1 and RAVR1. *EBioMedicine.* 2022; 75: 103806.
15. Marion V, et al., Exome sequencing identifies mutations in LZTFL1, a BBSome and smoothed trafficking regulator, in a family with Bardet-Biedl syndrome with situs inversus and insertional polydactyly. *J Med Genet.* 2012; 49 (5): 317–21.
16. Stewart CA, Gay CM, Ramkumar K, Cargill KR, Cardnell RJ, Nilsson MB, et al. Lung Cancer Models Reveal Severe Acute Respiratory Syndrome Coronavirus 2-Induced Epithelial-to-Mesenchymal Transition Contributes to Coronavirus Disease 2019 Pathophysiology. *J Thorac Oncol.* 2021; 16 (11): 1821–39.
17. Redin C, CW. Thorball, and J. Fellay, Host genomics of SARS-CoV-2 infection. *Eur J Hum Genet.* 2022; 30 (8): 908–14.
18. Wei Q, Chen ZH, Wang L, Zhang T, Duan L, Behrens C, et al. LZTFL1 suppresses lung tumorigenesis by maintaining differentiation of lung epithelial cells. *Oncogene.* 2016; 35 (20): 2655–63.
19. Angulo-Aguado M, et al., Association Between the LZTFL1 rs11385942 Polymorphism and COVID-19 Severity in Colombian Population. *Front Med (Lausanne).* 2022; 9: 910098.
20. Rescenko R, et al. Replication of LZTFL1 Gene Region as a Susceptibility Locus for COVID-19 in Latvian Population. *Virology.* 2021; 36 (5): 1241–4.
21. Zecevic M, et al. Genome-Wide Association Study of COVID-19 Outcomes Reveals Novel Host Genetic Risk Loci in the Serbian Population. *Front Genet.* 2022; 13: 911010.
22. Niemi MEK, Daly MJ, Ganna A. The human genetic epidemiology of COVID-19. *Nat Rev Genet.* 2022; 23 (9): 533–46.
23. Fishchuk L, et al. Modifying effects of TNF-alpha, IL-6 and VDR genes on the development risk and the course of COVID-19. Pilot study. *Drug Metab Pers Ther.* 2021; 37 (2): 133–9.
24. Kudryavtsev YS, Beregov MM, Berdalín AB, Lelyuk VG. Comparison of the Main Staging Systems for Assessing the Severity of Lung Injury in Patients with COVID-19 and Evaluation of Their Predictive Value. *Journal of radiology and nuclear medicine.* 2021; 102 (5): 296–303.

TRANSGENIC MICE FOR STUDY OF THE CDK8/19 CYCLIN-DEPENDENT KINASE KINASE-INDEPENDENT MECHANISMS OF ACTION

Stavskaya NI¹, Ilchuk LA²✉, Okulova YuD², Kubekina MV², Varlamova EA², Silaeva YuYu¹, Bruter AV²

¹ Institute of Gene Biology, Russian Academy of Sciences, Moscow, Russia

² Center for Precision Genome Editing and Genetic Technologies for Biomedicine, Institute of Gene Biology, Russian Academy of Sciences, Moscow, Russia

The CDK8 cyclin-dependent transcription-associated kinase and its less studied paralog, CDK19, regulate the expression of the dependant genes via several mechanisms. CDK8/19 can directly phosphorylate some transcription factors (ICN, STAT1), but at the same time these kinases being a component of the mediator complex regulate transcription via interaction with chromatin in the promoter and enhancer regions of appropriate genes. Recently the papers have appeared showing that CDK8/19 has kinase-independent mechanisms of action through comparison of the effects of the kinase activity genetic inactivation and chemical inhibition. The study was aimed to generate transgenic mice capable of the induced and tissue-specific expression of the kinase-negative (showing no phosphorylation activity) form of CDK8, CDK8 (D173A), which could be later used to study the CDK8 kinase-independent mechanisms of action *in vivo*. We obtained four F₀ transgenic animals by microinjection of linear DNA into the pronucleus, two of these animals became the ancestors of two distinct lines. The copy number of the integrated construct was measured for all F₀ and the lines generated. This model may be used to study the kinase-independent properties of the CDK8/19 proteins.

Keywords: transgenesis, transcription regulation, Cdk8, mediator kinase, kinase-independent functions

Funding: RSF grant, project № 22-15-00227.

Author contribution: Stavskaya NI — experimental procedure, working with animals; Ilchuk LA — manuscript writing, design of genotyping systems, data analysis; Okulova YuD — working with embryos; Kubekina MV — preparation of genetically engineered construct, experimental procedure; Varlamova EA — experimental procedure; Silaeva YuYu — literature analysis, study planning; Bruter AV — literature analysis, study planning, data analysis and interpretation, manuscript editing.

Compliance with ethical standards: the study was approved by the Ethics Committee of the Institute of Gene Biology RAS (protocol № 1 of 10 November 2021) and conducted in full compliance with the Directive 2010/63/EU of the European Parliament and of the Council of 22 September 2010 on the protection of animals used for scientific purposes.

✉ **Correspondence should be addressed:** Leonid A. Ilchuk
Prospekt Mira, 124, Moscow, 129164, Russia; lechuk12@gmail.com

Received: 22.11.2022 **Accepted:** 19.12.2022 **Published online:** 28.12.2022

DOI: 10.24075/brsmu.2022.066

ТРАНСГЕННЫЕ МЫШИ ДЛЯ ИЗУЧЕНИЯ КИНАЗА-НЕЗАВИСИМЫХ МЕХАНИЗМОВ ДЕЙСТВИЯ ЦИКЛИН-ЗАВИСИМЫХ КИНАЗ CDK8/19

Н. И. Ставская¹, Л. А. Ильчук²✉, Ю. Д. Окулова², М. В. Кубекина², Е. А. Варламова², Ю. Ю. Силаева¹, А. В. Брутер²

¹ Институт биологии гена Российской академии наук, Москва, Россия

² Центр высокоточного редактирования и генетических технологий для биомедицины, Институт биологии гена Российской академии наук, Москва, Россия

Циклин-зависимая транскрипционная киназа CDK8 и ее менее изученный паралог CDK19 регулируют экспрессию зависимых генов посредством нескольких механизмов. CDK8/19 могут напрямую фосфорилировать некоторые транскрипционные факторы (ICN, STAT1), но в то же время в составе медиаторного комплекса эти киназы регулируют транскрипцию за счет взаимодействия с хроматином в области промоторов и энхансеров соответствующих генов. В последнее время появляются работы, демонстрирующие путем сравнения эффектов генетической инактивации и химического ингибирования киназной активности наличие у CDK8/19 киназа-независимых механизмов действия. Целью работы было получить трансгенных мышей, способных к индуцируемой и тканеспецифичной экспрессии киназонегативной (лишенной фосфорилирующей активности) формы CDK8 — CDK8 (D173A), которых впоследствии можно будет использовать для изучения киназа-независимых механизмов действия CDK8 *in vivo*. Методом случайного трансгенеза в результате микроинъекций линейной ДНК в пронуклеус нами получены четыре трансгенных особи F₀, две из которых стали родоначальниками отдельных линий. Для всех F₀ и полученных линий измерена копийность интегрировавшейся конструкции. Данная модель может быть использована для изучения киназа-независимых свойств белков CDK8/19.

Ключевые слова: трансгенез, регуляция транскрипции, Cdk8, киназа медиатора, киназа-независимые функции

Финансирование: грант РФФ#22-15-00227.

Вклад авторов: Н. И. Ставская — проведение экспериментов, работа с животными; Л. А. Ильчук — написание рукописи, разработка систем генотипирования, анализ результатов; Ю. Д. Окулова — с эмбрионами; М. В. Кубекина — подготовка генно-инженерной конструкции, проведение экспериментов; Е. А. Варламова — проведение экспериментов; Ю. Ю. Силаева — анализ литературы, планирование исследования; А. В. Брутер — анализ литературы, планирование исследования, анализ и интерпретация результатов, редактирование рукописи.

Соблюдение этических стандартов: исследование одобрено этическим комитетом ИБГ РАН (протокол № 1 от 10 ноября 2021 г.) и проведено в строгом соответствии с положениями Директивы 2010/63/EU Европейского Парламента и Совета Европейского союза от 22 сентября 2010 г. по охране животных, используемых в научных целях.

✉ **Для корреспонденции:** Леонид Альбертович Ильчук
проспект Мира, д. 124, г. Москва, 129164, Россия; lechuk12@gmail.com

Статья получена: 22.11.2022 **Статья принята к печати:** 19.12.2022 **Опубликована онлайн:** 28.12.2022

DOI: 10.24075/vrgmu.2022.066

The CDK8 cyclin-dependent kinase and its paralog, CDK19, are not directly involved in regulation of the cell cycle phase transitions and belong to the so-called transcription-associated kinases that regulate gene transcription [1]. However, the

mechanisms underlying such regulation are diverse. On the one hand CDK8/19 as part of a complex with cyclin C, MED12, and MED13 directly phosphorylate some transcription factors, such as intracellular domain NOTCH [2] or STAT1 [3]. On the other

hand, together these four proteins form the kinase module of the Mediator complex that regulates gene expression via binding to the promoter and enhancer regions [1]. Despite the fact that *in vitro* studies have shown that, just like the CDK7 and CDK9 transcription-associated kinases, CDK8/19 can phosphorylate the RNA polymerase II C-terminal region, which represents an important event during transition to the elongation stage. This mechanism is likely to play no significant role in the cell [4]. At the same time it has been shown that CDK8/19 play an important role in expression of certain genes, especially in activation of expression of the earlier inactivated genes [5–7] and the major oncogenes, such as c-Myc [8, 9] and genes of the Wnt/ β -catenin signaling pathway [10]. In some cases the expression levels correlate with the presence of CDK8/19 in the enhancers and super-enhancers of the corresponding genes [11]. However, despite the important fundamental role played by CDK8/19 and their potential as therapeutic targets, specific molecular mechanism underlying the relationship between the expression of certain genes and CDK8/19 are unknown.

Recently there are papers reporting the comparison of chemical inhibition and genetic inactivation that show that genetic inactivation provides much larger effects in some models [7, 12, 13]. It must follow from this fact that CDK8/19 has some kinase-independent mechanisms of action. However, such comparison is not always precise, even in *in vitro* studies, due to limited selectivity and efficiency of inhibitors and is almost impossible in *in vivo* studies due to the features of biodistribution and metabolism of chemical inhibitors and the difficulties associated with crossing the blood-brain and blood–testis barriers by the substances.

The study was aimed to generate transgenic mice capable of tissue-specific induced expression of the CDK8 (D173A) mutant kinase-negative form for further identification of possible CDK8/19 kinase-independent mechanisms of action.

METHODS

The construct

Transgenesis involved the pKB2 vector that, in contrast to the previously used vector pKB1 [14, 15], was characterized by the absence of the reporter gene. The open reading frame was amplified using the KapaHiFi polymerase (Kapa Biosystems; USA) and primers P1 and P2 (hereinafter all oligonucleotides, the sequences of which are provided in Table 1, have been synthesized by Evrogen, Russia) with cDNA. cDNAs were obtained by reverse transcription using the RevertAid reverse transcriptase (Thermo Scientific; USA) based on the RNA extracted from the murine brain using the ExtractRNA reagent (Evrogen; Russia). When performing amplification, the AgeI and MluI restriction sites were added to the 5' and 3' ends of the reading frame for further transfer to the final vector, along with

the Kozak consensus sequence. The amplified reading frame was cloned into the CloneJet vector (Thermo Scientific; USA) and sequenced. The c.A518C mutation was created by site-directed mutagenesis during the polymerase chain reaction with the previously phosphorylated primers P3 and P4. The presence of target mutation and the absence of additional mutations were confirmed by sequencing. Then the ORF of the obtained *mCdk8kd* gene variant (kinase-dead) was re-cloned by the AgeI and MluI sites (all the restriction endonucleases were manufactured by Thermo Scientific, USA) into the pKB2 vector. The construct was linearized by sites Sall and NotI, separated by electrophoresis, extracted from the gel with the Cleanup Mini kit (Evrogen; Russia), further purified using the spin column with the Corning Costar Spin-X 0.22 μ m nylon filter (Corning; USA), and diluted in the microinjection buffer (10 mmol Tris, 1 mmol EDTA) to the DNA concentration of 2 ng/ μ L.

Mice housing conditions

Embryos were obtained from 30 immature (weight 12–13 g) females (F1 hybrids CBA \times C57BL/6) and similar males aged 6–8 weeks (Stolbovaya breeding station; Russia). The CD1 outbred mice (Stolbovaya breeding station; Russia) were used as recipients and foster mothers. The mice that were kept in the vivarium of the Institute of Gene Biology RAS had free access to water and food. The 22–24 °C ambient temperature was maintained, and the light/dark cycle (day/night) was 14/10 h.

Microinjections and embryo transfer

Microinjections and embryo transfer were performed as described previously [16]. On day 19 after the embryo transfer, recipients underwent caesarean section, and the newborn mouse pups were housed together with foster mothers.

Genotyping and copy number measurement

Animal genotyping was performed in accordance with the previously used protocol [14]. A STOP cassette (primers P5 and P6) and a terminator (primers P7 and P8) being parts of the pKB2 vector were simultaneously detected in transgenic animals by multiplex polymerase chain reaction (PCR). The copy number of the inserted construct was defined by comparison with genes with the known varying copy numbers (HPRT, HbA, H3C7) based on the results of the real-time PCR [14].

RESULTS

To generate transgenic mice capable of induced and tissue-specific expression of the kinase-negative CDK8 variant, we created a genetic construct containing the open reading frame of the *mCdk8* gene with the c.A518C substitution in the DNA

Table 1. Oligonucleotide sequences

	Sequence	Designation
P1	attaaccggtGCACCATGGACTATGACTTTAAAGTGAAG	Amplification of the CDK8kd ORF
P2	taatacgogtTCAGTACCGATGTGTCT	Amplification of the CDK8kd ORF
P3	CCATGGGCTTTGCCCGATTAT	Creation of the A518C mutation
P4	CAGCAATTTTACTCTTCCTCG	Creation of the A518C mutation
P5	GTTAGATCTGCTGCCACCGT	Genotyping (STOP cassette)
P6	AGGTGGCAAGTGGTATCCG	Genotyping (STOP cassette)
P7	GCGAGTCCATGTCACCTCAGG	Genotyping (terminator)
P8	GTGTTGCCCTTTGGAGCTTG	Genotyping (terminator)

Table 2. Results of activities on generating primary transgenic animals

Recipients used	Cells transferred	Number of mice that gave birth	Number of newborn mouse pups	Number of newborn transgenic animals
41	487	7	14	6

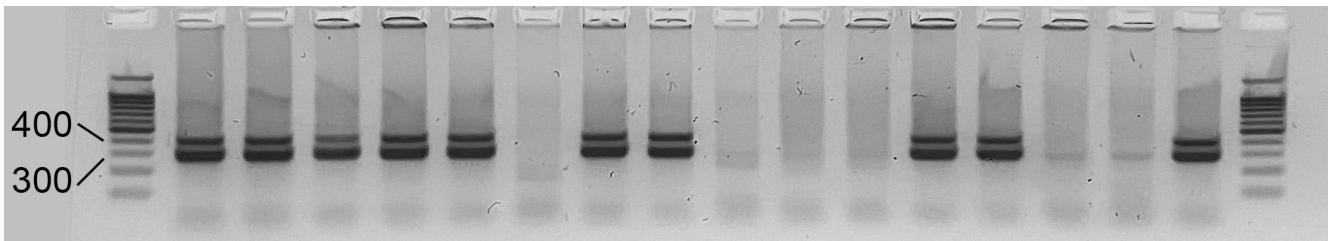


Fig. 1. F₁ mouse genotyping by gel electrophoresis. The lanes with the bands of PCR products with the size of about 300 bp (fragment of STOP cassette) and about 400 bp (fragment of terminator) correspond to transgenic mice. The lanes with no bands correspond to the wild type mice. The first and the last lanes contain the size markers

(and, consequently, with the D173A substitution in the protein) based on the pKB2 vector [17]. Along with the insulator and terminators which are protection against the position effect during insertion, the vector used contains the CAG promoter and the STOP cassette flanked by LoxP sites that separates promoter from the ORF. The STOP cassette inserted in such a way significantly reduces the transgene transcription and makes further translation of the transcript impossible [14].

The linearized construct was microinjected into the zygotes, among which 487 zygotes survived and were transferred to recipients. As a result, 14 mouse pups were born, among which six pups were transgenic. The presence of the transgene was confirmed by PCR in all newborn animals (Fig. 1). A numerical representation of the results of activities on generating transgenic animals is provided in Table 2.

Among six primary transgenic animals, two died before puberty and four produced offspring when bred with the C57BL/6J mice. To date, four independent substrains have been generated: «369», «372», «375», «376». When random integration takes place in the genome, multimers of the construct can be formed and then inserted in chromosomes. In turn, the expression levels can be a function of the number of monomers. Furthermore, since insertion in distinct blastomeres may occur independently, F₀ animals may be mosaic due to the varying copy numbers of the construct in various cells. We have defined the average copy number of insertion for F₀ and the copy number for the substrains obtained (Fig. 2). The resulting values can be non-integers because of using exponential approximation when assessing the copy numbers and averaging the values of various cells. However, in fact this is due to the measurement error. Starting from the F₁ generation, the copy numbers are constant integer values. Two substrains of F₁ hybrids with the copy numbers of about 2, which correspond to the copy

numbers of the majority of genes in diploid genomes, were selected for further breeding.

DISCUSSION

We have generated the mice line capable of the induced and tissue-specific expression of the kinase-negative mCDK8 form: six F₀ animals, among which four animals have produced offspring and two have become the founders of substrains by now. Furthermore, the efficiency of obtaining transgenes was 50% (6 out of 12), and further segregation compared to F₁ that was associated with mosaicism in F₀ together with the wide range of copy numbers of the inserted construct (1–17) was found in the animals generated. This allowed us to select the lines with the copy numbers most close to natural for further studies.

A series of studies consider the consequences of the CDK8 and/or CDK19 genetic knockout [18–20], however, the models used in these studies make it impossible to draw a final conclusion about the role played by the lack of CDK8/19 proteins and impossibility of the Mediator complex kinase module assembly in the observed phenotypes, and about the role of appropriate phosphorylation. Moreover, the use of the CDK8/19 inhibitors in animals has resulted in the effects that are different from that reported in knockout animals [21]. The animal line we have generated is a right tool for distinguishing between kinase-dependent and kinase independent CDK8/19 functions.

CONCLUSIONS

During the study transgenic mice were generated providing the possibility of the tissue-specific and induced expression of the kinase-negative form of the CDK8 cyclin-dependent kinase.

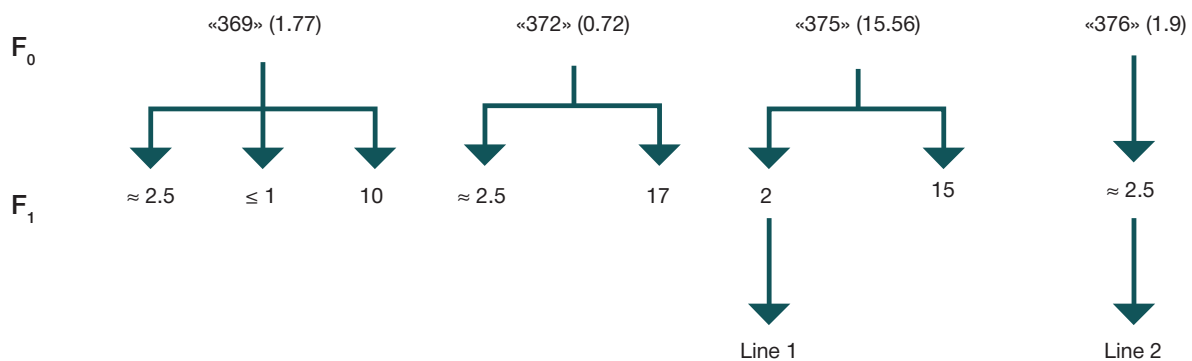


Fig. 2. Scheme of the substrains obtained and copy numbers of the substrain members. The names of substrains are put in quotes. The average copy numbers of ancestors (F₀) are put in parentheses. Only the copy numbers are provided for F₁

In the future, after breeding with the CDK19^{-/-}, CDK8^{fl/fl} mice and various activators, animals will be generated, in which the wild type CDK8 and CDK19 could be replaced by the kinase-

negative variant in the ubiquitous or tissue-specific manner. The experiments involving such animals can possibly reveal the CDK8/19 kinase-independent mechanisms of action.

References

- Dannappel MV, Sooraj D, Loh JJ, Firestein R. Molecular and in vivo Functions of the CDK8 and CDK19 Kinase Modules. *Frontiers in Cell and Developmental Biology*. 2019; 6. DOI: 10.3389/fcell.2018.00171.
- Li N, Fassi A, Chick J, Inuzuka H, Li X, Mansour MR, et al. Cyclin C is a haploinsufficient tumour suppressor. *Nature cell biology*. 2014; 16 (11): 1080–91. Epub 2014/10/27. DOI: 10.1038/ncb3046. PubMed PMID: 25344755; PubMed Central PMCID: PMC35773.
- Bancerek J, Poss ZC, Steinparzer I, Sedlyarov V, Pfaffenwimmer T, Mikulic I, et al. CDK8 kinase phosphorylates transcription factor STAT1 to selectively regulate the interferon response. *Immunity*. 2013; 38 (2): 250–62. Epub 2013/01/29. DOI: 10.1016/j.immuni.2012.10.017. PubMed PMID: 23352233; PubMed Central PMCID: PMC3580287.
- Galbraith MD, Donner AJ, Espinosa JM. CDK8: a positive regulator of transcription. *Transcription*. 2010; 1 (1): 4–12. Epub 2011/02/18. DOI: 10.4161/trns.1.1.12373. PubMed PMID: 21327159; PubMed Central PMCID: PMC3035184.
- Chen M, Liang J, Ji H, Yang Z, Altilla S, Hu B, et al. CDK8/19 Mediator kinases potentiate induction of transcription by NFκB. *Proceedings of the National Academy of Sciences*. 2017; 114 (38): 10208–13. DOI: 10.1073/pnas.1710467114.
- Galbraith Matthew D, Allen Mary A, Bensard Claire L, Wang X, Schwinn Marie K, Qin B, et al. HIF1A Employs CDK8-Mediator to Stimulate RNAPII Elongation in Response to Hypoxia. *Cell*. 2013; 153 (6): 1327–39. DOI: <https://doi.org/10.1016/j.cell.2013.04.048>.
- Steinparzer I, Sedlyarov V, Rubin JD, Eismayr K, Galbraith MD, Levandowski CB, et al. Transcriptional Responses to IFN-γ Require Mediator Kinase-Dependent Pause Release and Mechanistically Distinct CDK8 and CDK19 Functions. *Molecular Cell*. 2019; 76 (3): 485–99. Available from: <https://doi.org/10.1016/j.molcel.2019.07.034>.
- Adler AS, McClelland ML, Truong T, Lau S, Modrusan Z, Soukup TM, et al. CDK8 Maintains Tumor Dedifferentiation and Embryonic Stem Cell Pluripotency. *Cancer Research*. 2012; 72 (8): 2129–39. DOI: 10.1158/0008-5472.CAN-11-3886.
- Fukasawa K, Kadota T, Horie T, Tokumura K, Terada R, Kitaguchi Y, et al. CDK8 maintains stemness and tumorigenicity of glioma stem cells by regulating the c-MYC pathway. *Oncogene*. 2021; 40 (15): 2803–15. DOI: 10.1038/s41388-021-01745-1.
- Firestein R, Bass AJ, Kim SY, Dunn IF, Silver SJ, Guney I, et al. CDK8 is a colorectal cancer oncogene that regulates beta-catenin activity. *Nature*. 2008; 455 (7212): 547–51. Epub 2008/09/17. DOI: 10.1038/nature07179. PubMed PMID: 18794900; PubMed Central PMCID: PMC2587138.
- Bruter AV, Rodionova MD, Varlamova EA, Shtil AA. Super-Enhancers in the Regulation of Gene Transcription: General Aspects and Antitumor Targets. *Acta naturae*. 2021; 13 (1): 4–15. Epub 2021/05/08. DOI: 10.32607/actanaturae.11067. PubMed PMID: 33959383; PubMed Central PMCID: PMC8084300.
- Audetat KA, Galbraith Matthew D, Odell Aaron T, Lee T, Pandey A, Espinosa Joaquin M, et al. A Kinase-Independent Role for Cyclin-Dependent Kinase 19 in p53 Response. *Molecular and Cellular Biology*. 2017; 37 (13): e00626–16. DOI: 10.1128/MCB.00626-16.
- Menzl I, Zhang T, Berger-Becvar A, Grausenburger R, Heller G, Prchal-Murphy M, et al. A Kinase-independent role for CDK8 in BCR-ABL1(+) leukemia. *Nature communications*. 2019; 10 (1): 4741. Epub 2019/10/20. DOI: 10.1038/s41467-019-12656-x. PubMed PMID: 31628323.
- Bruter AV, Korshunova DS, Kubekina MV, Sergiev PV, Kalinina AA, Ilchuk LA, et al. Novel transgenic mice with Cre-dependent co-expression of GFP and human ACE2: a safe tool for study of COVID-19 pathogenesis. *Transgenic research*. 2021; 30 (3): 289–301. Epub 2021/04/16. DOI: 10.1007/s11248-021-00249-8. PubMed PMID: 33855640; PubMed Central PMCID: PMC8045570.
- Kubekina MV, Silaeva YY, Bruter AV, Korshunova DS, Ilchuk LA, Okulova YD, et al. Transgenic mice Cre-dependently expressing mutant polymerase-gamma: novel test-system for pharmacological study of mitoprotective drugs. *Research Results in Pharmacology*. 2021; 7 (3): 33–9.
- Silaeva YY, Kirikovich YK, Skuratovskaya LN, Deikin AV. Optimal Number of Embryos for Transplantation in Obtaining Genetic-Modified Mice and Goats. *Russian Journal of Developmental Biology*. 2018; 49 (6): 356–61. DOI: 10.1134/S106236041806005X.
- Akoulitchev S, Chuikov S, Reinberg D. TFIIH is negatively regulated by cdk8-containing mediator complexes. *Nature*. 2000; 407 (6800): 102–6. DOI: 10.1038/35024111. PMID: 10993082.
- McClelland ML, Soukup TM, Liu SD, Esenstein JH, de Sousa e Melo F, Yaylaoglu M, et al. Cdk8 deletion in the Apc(Min) murine tumour model represses EZH2 activity and accelerates tumourigenesis. *The Journal of pathology*. 2015; 237 (4): 508–19. Epub 2015/08/04. DOI: 10.1002/path.4596. PubMed PMID: 26235356.
- Dannappel MV, Zhu D, Sun X, Chua HK, Poppelaars M, Suehiro M, et al. CDK8 and CDK19 regulate intestinal differentiation and homeostasis via the chromatin remodeling complex SWI/SNF. *The Journal of clinical investigation*. 2022; 132 (20). Epub 2022/08/26. DOI: 10.1172/jci158593. PubMed PMID: 36006697; PubMed Central PMCID: PMC9566890.
- Prieto S, Dubra G, Camasses A, Aznar AB, Begon-Pescia C, Simboeck E, et al. CDK8 and CDK19 act redundantly to control the CFTR pathway in the intestinal epithelium. *EMBO reports*. n/a (n/a): e54261. DOI: <https://doi.org/10.15252/embr.202154261>.
- Clarke PA, Ortiz-Ruiz MJ, TePoele R, Adeniji-Popoola O, Box G, Court W, et al. Assessing the mechanism and therapeutic potential of modulators of the human Mediator complex-associated protein kinases. *eLife*. 2016; 5. Epub 2016/12/10. DOI: 10.7554/eLife.20722. PubMed PMID: 27935476; PubMed Central PMCID: PMC5224920.

Литература

- Dannappel MV, Sooraj D, Loh JJ, Firestein R. Molecular and in vivo Functions of the CDK8 and CDK19 Kinase Modules. *Frontiers in Cell and Developmental Biology*. 2019; 6. DOI: 10.3389/fcell.2018.00171.
- Li N, Fassi A, Chick J, Inuzuka H, Li X, Mansour MR, et al. Cyclin C is a haploinsufficient tumour suppressor. *Nature cell biology*. 2014; 16 (11): 1080–91. Epub 2014/10/27. DOI: 10.1038/ncb3046. PubMed PMID: 25344755; PubMed Central PMCID: PMC35773.
- Bancerek J, Poss ZC, Steinparzer I, Sedlyarov V, Pfaffenwimmer T, Mikulic I, et al. CDK8 kinase phosphorylates transcription factor STAT1 to selectively regulate the interferon response. *Immunity*. 2013; 38 (2): 250–62. Epub 2013/01/29. DOI: 10.1016/j.immuni.2012.10.017. PubMed PMID: 23352233; PubMed Central PMCID: PMC3580287.
- Galbraith MD, Donner AJ, Espinosa JM. CDK8: a positive regulator of transcription. *Transcription*. 2010; 1 (1): 4–12.

- Epub 2011/02/18. DOI: 10.4161/trns.1.1.12373. PubMed PMID: 21327159; PubMed Central PMCID: PMC3035184.
5. Chen M, Liang J, Ji H, Yang Z, Altilia S, Hu B, et al. CDK8/19 Mediator kinases potentiate induction of transcription by NF κ B. *Proceedings of the National Academy of Sciences*. 2017; 114 (38): 10208–13. DOI: 10.1073/pnas.1710467114.
 6. Galbraith Matthew D, Allen Mary A, Bensard Claire L, Wang X, Schwinn Marie K, Qin B, et al. HIF1A Employs CDK8-Mediator to Stimulate RNAPII Elongation in Response to Hypoxia. *Cell*. 2013; 153 (6): 1327–39. DOI: <https://doi.org/10.1016/j.cell.2013.04.048>.
 7. Steinparzer I, Sedlyarov V, Rubin JD, Eismayr K, Galbraith MD, Levandowski CB, et al. Transcriptional Responses to IFN- γ Require Mediator Kinase-Dependent Pause Release and Mechanistically Distinct CDK8 and CDK19 Functions. *Molecular Cell*. 2019; 76 (3): 485–99. Available from: <https://doi.org/10.1016/j.molcel.2019.07.034>.
 8. Adler AS, McClelland ML, Truong T, Lau S, Modrusan Z, Soukup TM, et al. CDK8 Maintains Tumor Dedifferentiation and Embryonic Stem Cell Pluripotency. *Cancer Research*. 2012; 72 (8): 2129–39. DOI: 10.1158/0008-5472.CAN-11-3886.
 9. Fukasawa K, Kadota T, Horie T, Tokumura K, Terada R, Kitaguchi Y, et al. CDK8 maintains stemness and tumorigenicity of glioma stem cells by regulating the c-MYC pathway. *Oncogene*. 2021; 40 (15): 2803–15. DOI: 10.1038/s41388-021-01745-1.
 10. Firestein R, Bass AJ, Kim SY, Dunn IF, Silver SJ, Guney I, et al. CDK8 is a colorectal cancer oncogene that regulates beta-catenin activity. *Nature*. 2008; 455 (7212): 547–51. Epub 2008/09/17. DOI: 10.1038/nature07179. PubMed PMID: 18794900; PubMed Central PMCID: PMC2587138.
 11. Bruter AV, Rodionova MD, Varlamova EA, Shtil AA. Super-Enhancers in the Regulation of Gene Transcription: General Aspects and Antitumor Targets. *Acta naturae*. 2021; 13 (1): 4–15. Epub 2021/05/08. DOI: 10.32607/actanaturae.11067. PubMed PMID: 33959383; PubMed Central PMCID: PMC8084300.
 12. Audetat KA, Galbraith Matthew D, Odell Aaron T, Lee T, Pandey A, Espinosa Joaquin M, et al. A Kinase-Independent Role for Cyclin-Dependent Kinase 19 in p53 Response. *Molecular and Cellular Biology*. 2017; 37 (13): e00626–16. DOI: 10.1128/MCB.00626-16.
 13. Menzl I, Zhang T, Berger-Becvar A, Grausenburger R, Heller G, Prchal-Murphy M, et al. A kinase-independent role for CDK8 in BCR-ABL(+) leukemia. *Nature communications*. 2019; 10 (1): 4741. Epub 2019/10/20. DOI: 10.1038/s41467-019-12656-x. PubMed PMID: 31628323.
 14. Bruter AV, Korshunova DS, Kubekina MV, Sergiev PV, Kalinina AA, Ilchuk LA, et al. Novel transgenic mice with Cre-dependent co-expression of GFP and human ACE2: a safe tool for study of COVID-19 pathogenesis. *Transgenic research*. 2021; 30 (3): 289–301. Epub 2021/04/16. DOI: 10.1007/s11248-021-00249-8. PubMed PMID: 33855640; PubMed Central PMCID: PMC8045570.
 15. Kubekina MV, Silaeva YY, Bruter AV, Korshunova DS, Ilchuk LA, Okulova YD, et al. Transgenic mice Cre-dependently expressing mutant polymerase-gamma: novel test-system for pharmacological study of mitoprotective drugs. *Research Results in Pharmacology*. 2021; 7 (3): 33–9.
 16. Silaeva YY, Kirikovich YK, Skuratovskaya LN, Deikin AV. Optimal Number of Embryos for Transplantation in Obtaining Genetic-Modified Mice and Goats. *Russian Journal of Developmental Biology*. 2018; 49 (6): 356–61. DOI: 10.1134/S106236041806005X.
 17. Akoulitchev S, Chuikov S, Reinberg D. TFIIH is negatively regulated by cdk8-containing mediator complexes. *Nature*. 2000; 407 (6800): 102–6. DOI: 10.1038/35024111. PMID: 10993082.
 18. McClelland ML, Soukup TM, Liu SD, Esensten JH, de Sousa e Melo F, Yaylaoglu M, et al. Cdk8 deletion in the Apc(Min) murine tumour model represses EZH2 activity and accelerates tumourigenesis. *The Journal of pathology*. 2015; 237 (4): 508–19. Epub 2015/08/04. DOI: 10.1002/path.4596. PubMed PMID: 26235356.
 19. Dannappel MV, Zhu D, Sun X, Chua HK, Poppelaars M, Suehiro M, et al. CDK8 and CDK19 regulate intestinal differentiation and homeostasis via the chromatin remodeling complex SWI/SNF. *The Journal of clinical investigation*. 2022; 132 (20). Epub 2022/08/26. DOI: 10.1172/jci158593. PubMed PMID: 36006697; PubMed Central PMCID: PMC9566890.
 20. Prieto S, Dubra G, Camasses A, Aznar AB, Begon-Pescia C, Simboeck E, et al. CDK8 and CDK19 act redundantly to control the CFTR pathway in the intestinal epithelium. *EMBO reports*. n/a (n/a): e54261. DOI: <https://doi.org/10.15252/embr.202154261>.
 21. Clarke PA, Ortiz-Ruiz MJ, TePoele R, Adeniji-Popoola O, Box G, Court W, et al. Assessing the mechanism and therapeutic potential of modulators of the human Mediator complex-associated protein kinases. *eLife*. 2016; 5. Epub 2016/12/10. DOI: 10.7554/eLife.20722. PubMed PMID: 27935476; PubMed Central PMCID: PMC5224920.

KNOCKOUT OF MUTANT *TP53* IN THE HACAT CELLS ENHANCES THEIR MIGRATION ACTIVITYKozhin PM¹, Romashin DD¹, Rusanov AL¹ ✉, Luzgina NG¹¹ Institute of Biomedical Chemistry, Moscow, Russia

The HaCaT cell line represents the spontaneously immortalized non-carcinogenic human keratinocytes that are used as a model for studying the function of normal human keratinocytes. There are two *TP53* alleles in the HaCaT cell genome, which comprise two gain-of-function (GOF) mutations acquired through spontaneous immortalization (*mutTP53*). Mutations result in the increased proliferation rate and violation of the stratification program. The study was aimed to assess the effects of the *mutTP53* gene knockout on the HaCaT keratinocytes capability of proliferation and migration in the in vitro model of epidermal injury and regeneration (scratch test), and on the ability to form stratified epithelium in the organotypic epidermal model. To perform the scratch-test, cells were cultured until monolayer was formed, then the standardized wound was created. The organotypic model was obtained by growing keratinocytes in the polycarbonate membrane inserts with the pore size of 0.4 μm at the interface between the phases (air-liquid). It has been shown that the mutant *TP53* gene knockout results in the increased migration capability of the HaCaT keratinocytes: in the *mutTP53* knockout HaCaT, the defect closure occurred faster than in the appropriate group of the WT HaCaT ($p < 0.05$), on day three the defect size was $12\% \pm 3\%$ and $66\% \pm 5\%$ of the initial size. There is evidence that mutant *TP53* in the HaCaT cells is a negative regulator of the laminin-5 expression (*LAMC2* expression was 9.96 ± 1.92 times higher in the cells with the *mutTP53* knockout, $p < 0.05$), however, this does not promote normalization of the program of epithelial differentiation and stratification followed by formation of the stratum corneum in the organotypic model.

Keywords: HaCaT, keratinocyte differentiation, p53, CRISPR/Cas9, knockout, migration

Funding: the study was carried out as part of the Program for fundamental research in the Russian Federation for the long-term period (2021–2030) (№ 122022800481-0).

Author contribution: Luzgina NG, Rusanov AL — study concept; Romashin DD, Kozhin PM, Luzgina NG, Rusanov AL — study design and literature review; Romashin DD, Kozhin PM — study planning and execution; Kozhin PM, Romashin DD, Luzgina NG, Rusanov AL — data analysis and interpretation; Kozhin PM, Romashin DD — manuscript writing; Kozhin PM, Romashin DD, Luzgina NG, Rusanov AL — manuscript editing.

Compliance with ethical standards: the study was carried out in accordance with the Declaration of Helsinki of the World Medical Association and all its revisions.

✉ **Correspondence should be addressed:** Alexander L. Rusanov
Pogodinskaya, 10, str. 8, Moscow, 119121, Russia; alexander.l.rusanov@gmail.com

Received: 09.12.2022 **Accepted:** 24.12.2022 **Published online:** 30.12.2022

DOI: 10.24075/brsmu.2022.070

НОКАУТ МУТАНТНОГО *TP53* В КЛЕТКАХ ЛИНИИ НАСАТ УСИЛИВАЕТ ИХ МИГРАЦИОННУЮ АКТИВНОСТЬП. М. Кожин¹, Д. Д. Ромашин¹, А. Л. Русанов¹ ✉, Н. Г. Лузгина¹¹ Научно-исследовательский институт биомедицинской химии имени В. Н. Ореховича, Москва, Россия

Линия HaCaT — спонтанно immortalized неканцерогенные кератиноциты человека, широко используемые в качестве модели для изучения функций нормальных кератиноцитов человека. В геноме клеток HaCaT присутствуют две аллели гена *TP53*, которые содержат две gain-of-function (GOF) мутации, приобретенные в результате спонтанной immortalization (*mutTP53*). Наличие мутаций приводит к увеличению скорости пролиферации и нарушению программы стратификации. Целью исследования было изучить влияние нокаута гена *mutTP53* на способность кератиноцитов линии HaCaT к пролиферации и миграции в модели повреждения и регенерации эпидермиса *in vitro* (скретч-тест), а также на способность формировать многослойный эпителий в органотипической модели эпидермиса. Для проведения скретч-теста клетки культивировали до образования монослоя, затем наносили стандартизованное повреждение. Органотипическую модель получали культивированием кератиноцитов в поликарбонатных мембранных вставках с диаметром пор 0,4 мкм на границе раздела фаз (воздух-жидкость). Продемонстрировано, что нокаут мутантного гена *TP53* приводит к увеличению миграционной способности кератиноцитов линии HaCaT: для HaCaT с нокаутом *mutTP53* закрытие дефекта происходило быстрее по сравнению с соответствующей группой WT HaCaT ($p < 0,05$), на третьи сутки размер дефекта составлял $12\% \pm 3\%$ и $66\% \pm 5\%$ от первоначального. Получены данные, что мутантный *TP53* в клетках HaCaT является негативным регулятором экспрессии ламинина-5 (экспрессия *LAMC2* была выше в клетках с нокаутом *mutTP53* в $9,96 \pm 1,92$ раз, $p < 0,05$), однако это не способствует нормализации программы дифференцировки и стратификации эпителия с образованием рогового слоя в органотипической модели.

Ключевые слова: HaCaT, дифференцировка кератиноцитов, p53, CRISPR/Cas9, нокаут, миграция

Финансирование: работа выполнена в рамках Программы фундаментальных научных исследований в Российской Федерации на долгосрочный период (2021–2030 годы) (№ 122022800481-0).

Вклад авторов: Н. Г. Лузгина, А. Л. Русанов — концепция исследования; Д. Д. Ромашин, П. М. Кожин, Н. Г. Лузгина, А. Л. Русанов — дизайн исследования и анализ литературы; Д. Д. Ромашин, П. М. Кожин — планирование и проведение исследования; П. М. Кожин, Д. Д. Ромашин, Н. Г. Лузгина, А. Л. Русанов — анализ и интерпретация полученных данных; П. М. Кожин, Д. Д. Ромашин — подготовка текста статьи; П. М. Кожин, Д. Д. Ромашин, Н. Г. Лузгина, А. Л. Русанов — редактирование рукописи.

Соблюдение этических стандартов: исследование проведено в соответствии с принципами Хельсинкской декларации Всемирной медицинской ассоциации и всех ее пересмотров.

✉ **Для корреспонденции:** Александр Леонидович Русанов
ул. Погодинская, д. 10, стр. 8, г. Москва, 119121, Россия; alexander.l.rusanov@gmail.com

Статья получена: 09.12.2022 **Статья принята к печати:** 24.12.2022 **Опубликована онлайн:** 30.12.2022

DOI: 10.24075/vrgmu.2022.070

The HaCaT cell line (spontaneously immortalized non-carcinogenic human keratinocytes) is widely considered a model for studying the function of normal human keratinocytes [1, 2]. However, stratification program and differentiation marker expression are abnormal in the HaCaT line keratinocytes [3].

It is known that there are two alleles of the *TP53* gene the HaCaT keratinocyte genome that comprise two gain-of-function (GOF) mutations acquired via spontaneous immortalization (H179Y and R282Q) [4]. *MutTP53* exerts significant effects on the increase in proliferation rate and cell growth in the HaCaT

cell line and has more than 7000 DNA binding sites. Furthermore, protein functions associated with apoptosis triggering are preserved [5]. It is known that mutant p53 functions in at least two ways: it affects the function of p63/p73 inhibiting their binding to DNA [6] or binds to new DNA sites via interaction with other transcription factors (NF-Y, E2F1, NF-KB, VDR, p63) [7, 8].

Among fundamental physiological characteristics of the HaCaT cells, the most interesting are as follows: proliferation, migration, stratification, and creation of three-dimensional organotypic structures.

We have shown previously that alterations in *mutp53* activity in the HaCaT cells result in the altered expression of differentiation markers (such as caspase 14, involucrin and transglutaminase 1) and are associated with altered expression of p63 [9].

Understanding the features of the HaCaT cell physiology and underlying mechanisms is essential for assessment of limitations associated with using such cells as model ones. Moreover, studying cells containing *mutTP53* makes it possible to obtain new data for carcinogenesis studies [10, 11].

The study was aimed to assess the features of alterations in migration capabilities of the *mutTP53* knockout HaCaT cells.

METHODS

Cell lines and culture conditions

The HaCaT cell line was acquired from the cell culture collection of the German Cancer Research Center (DKFZ, Heidelberg; Germany). The cell culture of the *mutTP53* knockout (dp53) HaCaT keratinocytes was obtained earlier [13]. The cells were cultured at 37 °C with 5% CO₂ in the DMEM/F12 medium (1:1, Gibco; USA) supplemented with 1% GlutaMAX (Thermo Fisher Scientific; USA), penicillin/streptomycin solution with a concentration of 100 U/mL and 100 µg/mL, respectively (Gibco; USA), and 10% fetal bovine serum (Dia-M; Russia).

The cell culture of normal human keratinocytes (NHK, pool of five donors) was acquired from Perspektiva SPA LLC (Novosibirsk, Russia). The cells were cultured at 37 °C with 5% CO₂ in the Keratinocyte SFM medium (Gibco; USA) containing 1% GlutaMAX (Gibco; USA), 1% antibiotic/antifungal (Gibco; USA), 50 µg/mL of BPE (Gibco; USA), 10 ng/mL of EGF (Gibco; USA).

The cells were grown in culture flasks with a surface area of 25 cm² or in Petri dishes with a diameter of 60 mm (Corning; USA). The medium was replaced with the fresh one every other day.

Cell cycle analysis

The cell cycle was assessed based on the Edu incorporation (Click-iT Plus Edu Alexa Fluor 488; ThermoFisher, USA) and the amount of DNA estimated by staining with Propidium Iodide (PI) (Sigma; USA). The cells were seeded into wells of the six-well plate and grown before reaching 50% confluency. Then Edu was added, and the cells were stained in accordance with the manufacturer's guidelines. After that the cells were incubated with RNase solution (100 µg/mL) and PI (1 µg/mL) for 30 min. Detection was performed using the ZE5 flow cytometer (Bio-Rad; USA) and the Everest 2.4.0.1365 software (Bio-Rad; USA).

The strongly positive Edu staining was typical for cells in S phase. The strongly positive PI staining was typical for cells with the doubled DNA content being through the G₂/M phase of cell cycle.

Comparison of cell proliferation rates

The cell proliferation rates of the wild type (WT) HaCaT cells and *mutTP53* knockout (dp53) cells were compared using

CytoTrace Red CMTPX (AAT Bioquest; USA). The cells were seeded into wells of the six-well plate and grown before reaching 50% confluency. Then the cells were stained with CellTracer (according to the manufacturer's guidelines) and cultured for 24 h. Detection was performed using the ZE5 flow cytometer (Bio-Rad; USA) and the Everest 2.4.0.1365 software (Bio-Rad; USA). The decrease in fluorescence intensity (dilution of the label) reflects the number of cell divisions.

Scratch test: assessment of the cell monolayer defect closure rate

To perform the scratch test, 50,000 of the wild type (WT) HaCaT cells, *mutTP53* knockout (dp53) HaCaT cells or normal human keratinocytes (NHK) were added to the wells of the 24-well plate and pre-incubated in the complete culture medium at 37 °C with 5% CO₂ until the monolayer was formed in the well. Then standardized damage to the monolayer was caused using the plastic scraper, the cells were washed with the DPBS solution and grown in the complete culture medium for three days. Each well was photographed along the entire length of the scratch every day. The images were processed using the skimage library [12]. The area not occupied by cells (defect area) was calculated 0, 24, 48, and 72 h after scratching, and the ratio compared to the baseline defect area (relative defect area) was defined. The experiment was run in triplicate.

Proteomics data

The analysis of the earlier acquired proteomics data [13] deposited in the ProteomeXchange Consortium (available from <http://proteomecentral.proteomexchange.org/cgi/GetDataset?ID=PX030700>) was carried out using the MaxQuant software (v1.6.3.4). Three biological replicates per line (wild type HaCaT cells or *mutTP53* knockout HaCaT cells) were analyzed in three technical replicates.

Estimation of gene expression

RNA was extracted using the RNeasy Kit (QIAGEN; USA) in accordance with the manufacturer's protocol. The amount of RNA obtained was measured with the NanoDrop 2000c spectrophotometer (Thermo Scientific; USA). The reaction of reverse transcription was carried out using the MMLV RT kit (Evrogen; Russia) according to the standard protocol by adding 1 µg of RNA at a time to the reaction. qPCR was performed using qPCRmix-HS SYBR+LowROX (Evrogen; Russia). The reaction was repeated three times for every gene and sample. *GAPDH* was used as a reference gene. The primers used are provided in Table 1.

Generation of multilayered skin equivalent

To generate the organotypic model, wild type (WT) HaCaT cells, *mutTP53* knockout HaCaT cells or normal human keratinocytes (NHK) were grown in the Millipore PIHP01250 polycarbonate cell culture inserts with the pore size of 0.4 µm used in a 24-well plate. The membrane inserts were placed in the plate wells, after that 700,000 HaCaT cells (wild type or *mutTP53* knockout cells) were added to the apical compartment and 700 µL of the Submerge medium (EpiLife (Gibco; USA) containing 1% GlutaMAX (Gibco; USA), 1% antibiotic-antimycotic (Gibco; USA), 1% HKGS (Gibco; USA), 10 ng/mL of EGF (Gibco; USA), and 1.5 mmol of CaCl₂ (Sigma; USA) were added to the basolateral compartment. The cells were incubated for 24 h (37 °C, 5% CO₂) to ensure cell attachment and proliferation activation.

Table 1. Primers used during the study

Gene	Primer sequences
<i>GAPDH</i>	Forward 5'-TCGACAGTCAGCCGCATCTTCTTT-3' Reverse 5'-ACCAAATCCGTTGACTCCGACCTT-3'
<i>LAMB3</i>	Forward 5'-TGGCTGAAGATGAGACCATT-3'; Reverse 5'-GGTAGATGAAGCTCGGAGAAAC-3'
<i>LAMC2</i>	Forward 5'-TGGATGAGTTCAAGCGTACAC-3'; Reverse 5'-CTTTTAGCAAGATTGGCACGG-3'

After 24 h the medium was completely removed from the apical compartment, while in the basolateral compartment it was replaced with 450 μ L of the growth medium at the interface of phases (ALI-medium: Submerge + 10 ng/mL of KGF (Gibco; USA) and 1 mmol of L-ascorbic acid (Sigma; USA)). The cells were grown for 10 days, and the growth medium was replaced by fresh medium every day.

Immunofluorescence staining

The cell models obtained were fixed in 4% formalin and processed by standard histology methods: dehydrated in the series of alcohols with the increasing concentrations, embedded in paraffin blocks, and sliced using microtome.

To perform immunofluorescence staining, the cells were incubated with primary antibodies against KRT5 (ab52635; Abcam, USA), CK10 (ab9025; Abcam, USA) and Alexa Fluor 488-conjugated (ab150105; Abcam, USA) or Texas Red-conjugated (ab6793; Abcam, USA) secondary antibodies. All the specimens were stained simultaneously using the same reagent kit (dilutions of antibodies and buffers).

Estimation of electrical resistance

Transepithelial electrical resistance (TEER) of the skin models generated using cells of various types was defined with the EVOM voltmeter (World Precision Instruments, Inc.; USA). For that growth medium in the basal compartment was replaced with 0.9% NaCl and 300 μ L of 0.9% NaCl were added to the apical compartment of the membrane insert. After that electrodes were placed in the apical and basolateral compartments of the membrane insert, and electrical resistance (TEER) of the membrane insert with the cultured cells (skin equivalent) was measured.

Data analysis

The results obtained were processed using R programming language for statistical analysis [14]. The intergroup differences between the studied parameter values were defined using

the t-test with the Benjamini-Hochberg procedure for multiple testing correction. The differences were considered significant at $p < 0.05$. The data are presented as $M \pm m$.

RESULTS

Assessment of the actively proliferating cells based on the Edu (analogue of Brdu) incorporation in DNA showed that the wild type HaCaT proliferated more actively than the *mutTP53* knockout cells. In S phase there were $45.6 \pm 3.2\%$ wild type cells (HaCaT WT) on average, while the average number of *mutTP53* knockout cells (HaCaT dp53) was $34.1 \pm 2.9\%$ (Fig. 1). These data were also confirmed by the results of the CellTracer label dilution assay performed after 24 h of cell growth.

The scratch test showed that the defect closure rates of the NHK and WT HaCaT cell lines were almost equal. On day three there were $54\% \pm 9\%$ and $66\% \pm 5\%$ of the baseline defect areas for NHK and WT HaCaT, respectively. At the same time the *mutTP53* knockout HaCaT cells showed a significant increase in the defect closure rate: on day three there were $12\% \pm 3\%$ ($p < 0.05$ compared to the corresponding group of WT HaCaT) of the baseline defect area (Fig. 2A, B).

A comparative panoramic proteome study of the wild type and *mutp53* knockout HaCaT cells was previously conducted [13]. When performing data analysis a total of 2080 proteins were identified based on two or more peptides (potential contaminants, proteins identified based on one site, and false-positives were excluded). Among the proteins identified, 27 proteins showed differences in expression between the assessed lines (FDR < 0.05). Alterations in expression of *LAMC2* and *LAMB3* proteins were the most interesting: the expression was significantly higher in the *mutTP53* knockout cells (4.95 and 4.58 times higher, respectively).

The data of proteomics study focused on *LAMC2* were confirmed by real-time PCR (Fig. 2): the *LAMC2* expression was significantly higher in the *mutTP53* knockout cells (9.96 ± 1.92 , $p < 0.05$). However, there were no significant differences in the *LAMB3* expression between the lines assessed.

When growing 3D cultures, all three lines formed multilayered skin equivalents (Fig. 3A). However, only normal human

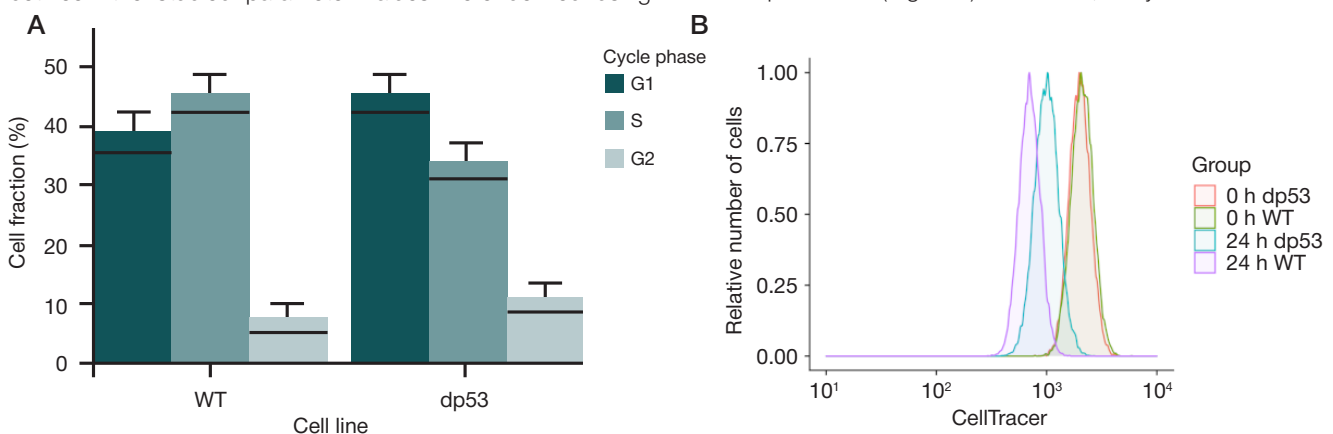


Fig. 1. Proliferative activity of HaCaT cells. **A.** Distribution of wild type (WT) HaCaT cells and *mutTP53* knockout (dp53) HaCaT cells by cell cycle phases. **B.** Proliferative activity of wild type (WT) HaCaT cells and *mutTP53* knockout (dp53) HaCaT cells

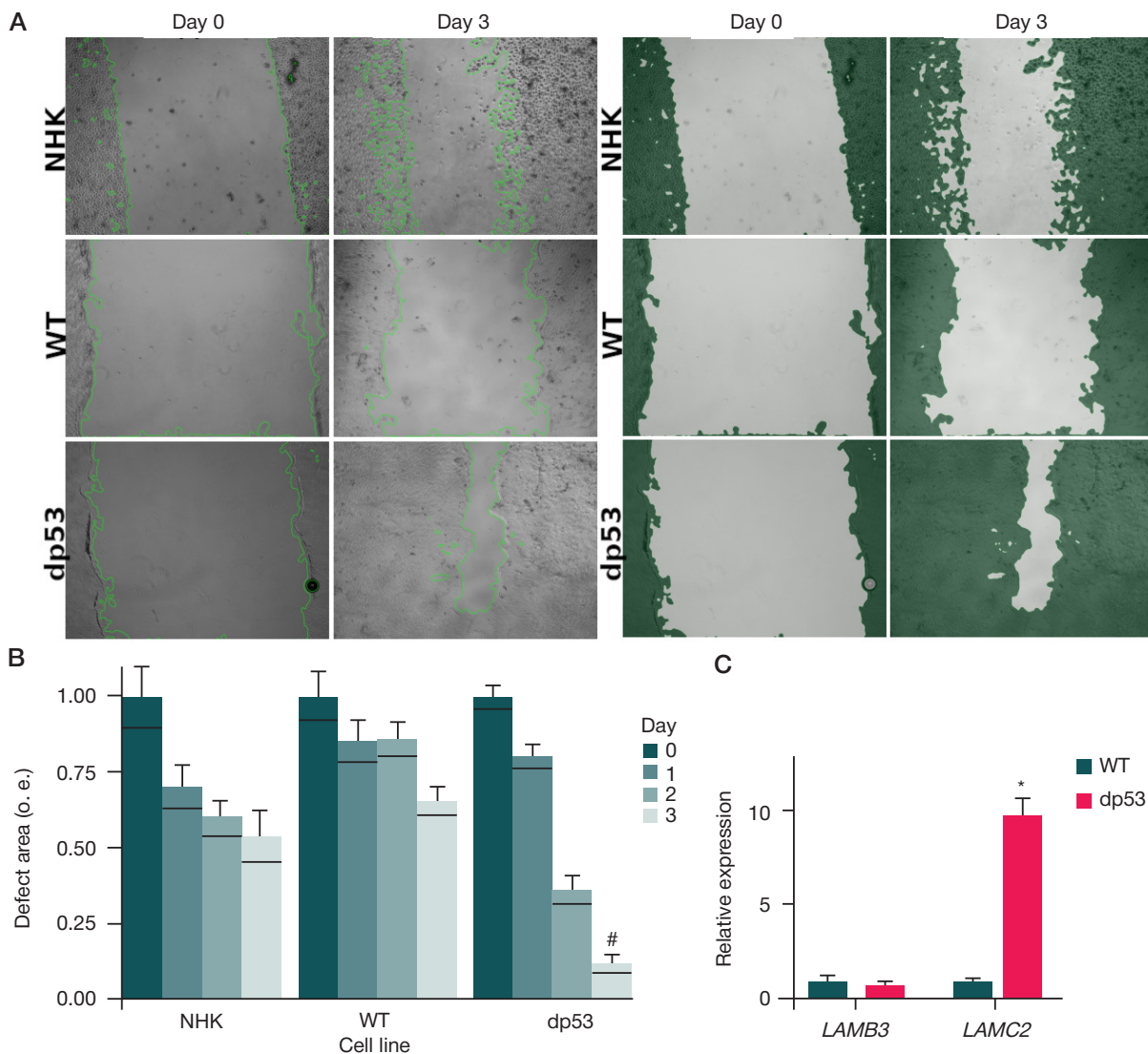


Fig. 2. Scratch test. Rates of monolayer defect closure by various cell lines: normal keratinocytes (NHK), wild type (WT) HaCaT cells, and *mutTP53* knockout (dp53) HaCaT cells. **A.** Light microscopy; magnification $\times 40$; day 0 (immediately after injury) and day 3 after scratching. **B.** Generalized chart of the relative defect area observed on days 1, 2, 3 after scratching. **C.** Relative expression of genes *LAMB3*, *LAMC2*. * — significant differences compared to wild type HaCaT ($p < 0.05$); # — significant differences compared to NHK on the corresponding day ($p < 0.05$)

keratinocytes (NHK) showed stratification typical for normal human epidermal cells and formed the stratum corneum.

The well-defined stratum corneum was observed in the organotypic model of epidermis formed by normal human keratinocytes (NHK).

There were no clear cell stratification and stratum corneum formation in the organotypic models of epidermis formed by the wild type (WT) HaCaT keratinocytes and *mutTP53* knockout HaCaT cells. KRT5 expression was observed in all layers, and the expression levels were comparable (Fig. 3A).

When measuring transepithelial electrical resistance (TEER) in the organotypic model of epidermis formed by normal keratinocytes, electrical resistance increased throughout the observation period.

Organotypic models of epidermis formed by various cell types were different in terms of both maximum transepithelial electrical resistance values and the dynamic changes in transepithelial electrical resistance observed within five days (Fig. 3B).

The highest transepithelial electrical resistance (TEER) value was found in the model of epidermis formed by normal keratinocytes (NHK): $5712 \pm 146 \text{ ohm}\cdot\text{cm}^2$. In the models formed by the wild type HaCaT keratinocytes and *mutTP53* knockout

HaCaT cells, the TEER values were almost five times lower: 964 ± 82 and 1088 ± 91 , respectively ($p < 0.05$ compared to NHK).

Transepithelial electrical resistance increased faster between days two and four with subsequent getting to plateau in the organotypic model of epidermis formed by normal human keratinocytes. The values of this parameter in the model of epidermis formed by the wild type HaCaT keratinocytes and *mutTP53* HaCaT cells were lower compared to the model formed by NHK and got to plateau by day two.

The increase in transepithelial potential is associated with the formation of intercellular contacts and stratification of epithelium followed by the stratum corneum formation [15] that is observed in the model of epidermis formed by normal keratinocytes and is absent in the models formed by HaCaT keratinocytes, regardless of the *mutTP53* knockout (Fig. 3A).

DISCUSSION

It is known that mutant p53 in the HaCaT cells is associated with the increased cell growth and proliferation rates, which has been confirmed experimentally in the previously reported studies [5]. It is also associated with the cells' inability to normally differentiate and form the full-fledged stratum corneum.

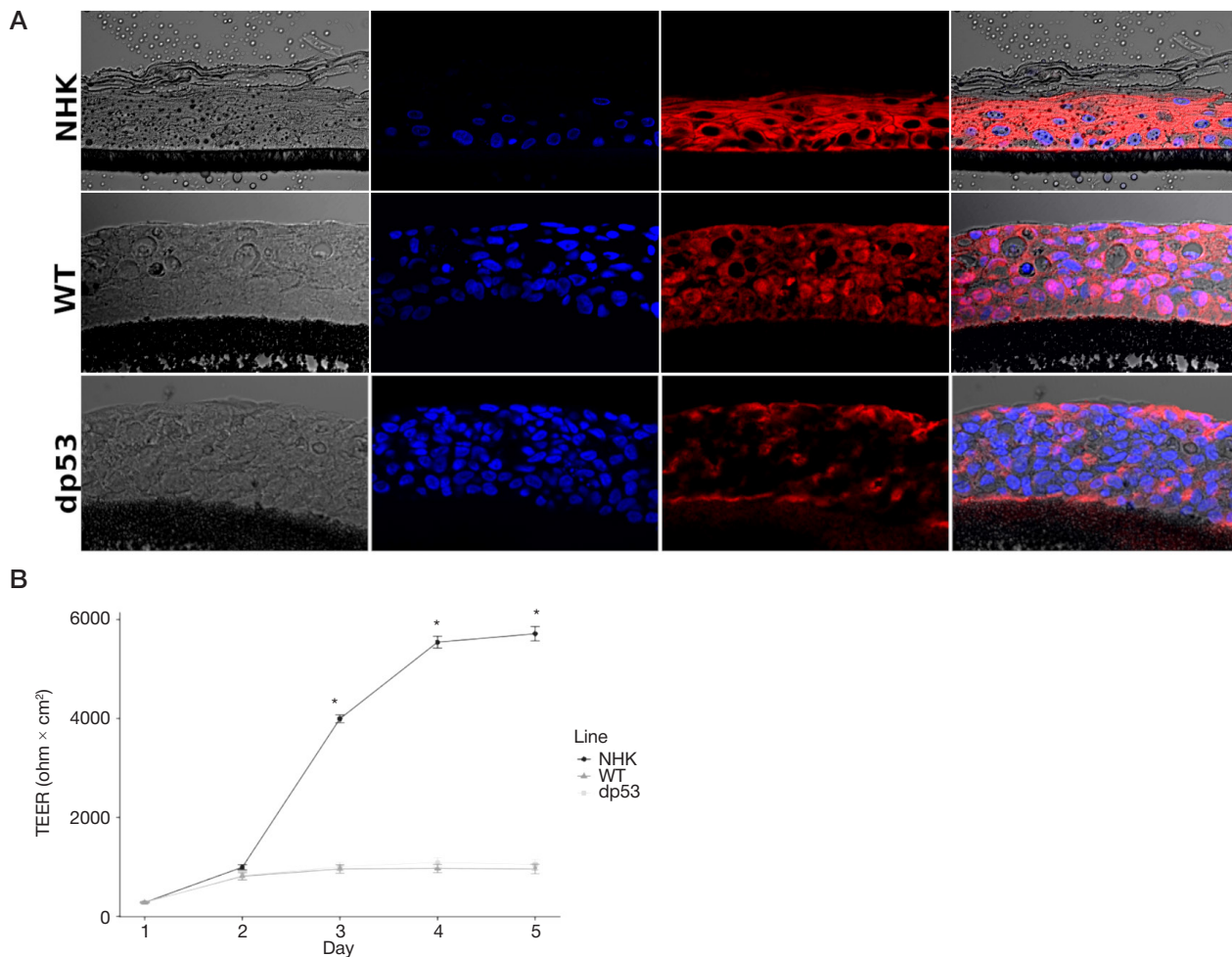


Fig. 3. Multilayered skin equivalent formation by keratinocytes of different lines: normal keratinocytes (NHK), wild type (WT) HaCaT cells, and *mutTP53* knockout (dp53) HaCaT cells. **A.** Immunofluorescence microscopy. Stain: nuclei (DAPI) — blue, KRT5 — red; magnification ×400. **B.** Transepithelial electrical resistance (TEER) values

According to the comparative proteomics study of primary human keratinocytes and HaCaT keratinocytes, one of the most noticeable differences is the expression of laminin-5 subunits, the $\alpha 3$, $\beta 3$, and $\gamma 2$ chains (LAMA3, LAMB3, LAMC2), that is significantly decreased in the HaCaT cells [16]. When discussing the findings, the authors of the above paper assume that this feature determines the aberrant nature of the HaCaT cells' differentiation program.

Laminins, being the main component of extracellular matrix, play an important role in cell adhesion, differentiation, and signal transmission [17]. The laminin-5 complex is essential for stabilization of dermoepidermal junction via binding to integrins $\alpha 3\beta 1$, $\alpha 6\beta 4$ and type VII collagen. Laminin-5 also plays a vital role in cell migration. It has been shown that downregulation of the gene encoding laminin-5 in keratinocytes results in reduced keratinocyte adhesion and impaired epidermal regeneration [18]. However, the increased expression of LAMB3 and LAMC2 subunits is often associated with cancer. As a result, tumor cells are characterized by higher migration rate and invasiveness [19].

Our findings show that *mutTP53* knockout in the HaCaT cells does result in the increased expression of LAMB3 and LAMC2 (the data of cell proteomics study). However, it is worth mentioning that the scratch test has revealed no significant differences in the defect closure rates between normal keratinocytes and the wild type HaCaT cells on day three after scratching, while the defect closure rate of the *mutTP53* knockout cells is significantly higher. High defect closure rate shown by the *mutTP53* knockout HaCaT cells in the scratch test should be associated with the cells' migration activity,

but not with their proliferation rate, since in these cells it is significantly lower than in the wild type HaCaT cells.

Apparently, mutations in *TP53* have no significant effect on the gene's ability to regulate migration, while gene inactivation (knockout) results in the significantly increased cells' ability to migrate, including compared to normal human keratinocytes. As a result, the *mutTP53* knockout HaCaT cells acquire the features of cells with pro-carcinogenic phenotype.

It should be also noted that the elevated expression of laminin-5 resulting from the *mutTP53* knockout has shown no effect on the HaCaT keratinocytes' ability to form the full-fledged stratified epithelium in the organotypic model of epidermis. This is manifested in the lack of the stratum corneum formation and low transepithelial electrical resistance (TEER) comparable to that of the wild type cells.

Thus, our findings confirm the regulatory role of mutant p53 in the HaCaT cells in terms of laminin-5 expression, but make it impossible to associate low expression levels with aberrant differentiation program in these cells.

CONCLUSIONS

Mutant *TP53* in the HaCaT cells is a negative regulator of laminin-5 expression. The *mutTP53* gene knockout results in the increased HaCaT cells' migration activity, but does not promote normalization of differentiation program. The data obtained supplement the information about the functional features of mutant *TP53* in the HaCaT cells.

References

- Petushkova NA, Rusanov AL, Pyatnitskiy MA, et al. Proteomic characterization of HaCaT keratinocytes provides new insights into changes associated with SDS exposure. *Biomed Dermatol.* 2020; 4 (1): 4. DOI:10.1186/s41702-019-0054-y.
- Rusanov AL, Nakhod KV, Nakhod VI, Poverennaya EV, Petushkova NA, Luzgina NG. Changes in the Proteome of HaCaT Keratinocytes Induced by Cytotoxic Substance Triton X-100. *Bull Exp Biol Med.* 2017; 163 (5): 620–22. DOI: 10.1007/s10517-017-3863-2.
- Smits JPH, Niehues H, Rikken G, et al. Immortalized N/TERT keratinocytes as an alternative cell source in 3D human epidermal models. *Sci Rep.* 2017; 7 (1): 11838. DOI: 10.1038/s41598-017-12041-y.
- Lehman TA, Modali R, Boukamp P, et al. p53 mutations in human immortalized epithelial cell lines. *Carcinogenesis.* 1993; 14 (5): 833–9. DOI: 10.1093/carcin/14.5.833.
- Martynova E, Pozzi S, Basile V, et al. Gain-of-function p53 mutants have widespread genomic locations partially overlapping with p63. *Oncotarget.* 2012; 3 (2): 132–43. DOI: 10.18632/oncotarget.447.
- Xu J, Reumers J, Couceiro JR, et al. Gain of function of mutant p53 by coaggregation with multiple tumor suppressors. *Nat Chem Biol.* 2011; 7 (5): 285–95. DOI: 10.1038/nchembio.546.
- Cordani N, Pozzi S, Martynova E, et al. Mutant p53 subverts p63 control over KLF4 expression in keratinocytes. *Oncogene.* 2011; 30 (8): 922–32. DOI: 10.1038/onc.2010.474.
- Neilsen PM, Noll JE, Suetani RJ, et al. Mutant p53 uses p63 as a molecular chaperone to alter gene expression and induce a pro-invasive secretome. *Oncotarget.* 2011; 2 (12): 1203–17. DOI: 10.18632/oncotarget.382.
- Rusanov AL, Kozhin PM, Romashin DD, Karagyaur MN, Luzgina NG. Impact of p53 modulation on interactions between p53 family members during HaCaT keratinocytes differentiation. *Bulletin of RSMU.* 2020; (6): 58–65. DOI: 10.24075/brsmu.2020.082.
- Goh AM, Coffill CR, Lane DP. The role of mutant p53 in human cancer. *J Pathol.* 2011; 223 (2): 116–26. DOI: 10.1002/path.2784.
- Muller PAJ, Vousden KH, Norman JC. p53 and its mutants in tumor cell migration and invasion. *J Cell Biol.* 2011; 192 (2): 209. DOI: 10.1083/jcb.201009059.
- van der Walt S, Schönberger JL, Nunez-Iglesias J, et al. scikit-image: image processing in Python. *PeerJ.* 2014; 2: e453. DOI: 10.7717/peerj.453.
- Rusanov AL, Romashin DD, Kozhin PM, et al. Impact of p53 Knockout on Protein Data Set of HaCaT Cells in Confluent and Subconfluent Conditions. *Data.* 2022; 7 (3). DOI: 10.3390/data7030027.
- Wickham H, Averick M, Bryan J, et al. Welcome to the Tidyverse. *J Open Source Softw.* 2019; 4: 1686. DOI: 10.21105/joss.01686.
- Rusanov AL, Luzgina ED, Vakhrushev IV, Nakhod KV, Luzgina NG. A Cell Model of Human Small Intestinal Wall Based on Genetically Modified Caco-2 Cells. *Bull Exp Biol Med.* 2018; 166 (1): 174–7. DOI: 10.1007/s10517-018-4308-2.
- Sprenger A, Weber S, Zarai M, et al. Consistency of the proteome in primary human keratinocytes with respect to gender, age, and skin localization. *Mol Cell Proteomics MCP.* 2013; 12 (9): 2509–21. DOI: 10.1074/mcp.M112.025478.
- Rousselle P, Beck K. Laminin 332 processing impacts cellular behavior. *Cell Adhes Migr.* 2013; 7 (1): 122–34. DOI: 10.4161/cam.23132.
- Natsumi A, Sugawara K, Yasumizu M, et al. Re-investigating the Basement Membrane Zone of Psoriatic Epidermal Lesions: Is Laminin-511 a New Player in Psoriasis Pathogenesis? *J Histochem Cytochem.* 2018; 66 (12): 847–62. DOI: 10.1369/0022155418782693.
- Huang C, Chen J. Laminin-332 mediates proliferation, apoptosis, invasion, migration and epithelial-to-mesenchymal transition in pancreatic ductal adenocarcinoma. *Mol Med Rep.* 2021; 23 (1): 11. DOI: 10.3892/mmr.2020.11649.

Литература

- Petushkova NA, Rusanov AL, Pyatnitskiy MA, et al. Proteomic characterization of HaCaT keratinocytes provides new insights into changes associated with SDS exposure. *Biomed Dermatol.* 2020; 4 (1): 4. DOI:10.1186/s41702-019-0054-y.
- Rusanov AL, Nakhod KV, Nakhod VI, Poverennaya EV, Petushkova NA, Luzgina NG. Changes in the Proteome of HaCaT Keratinocytes Induced by Cytotoxic Substance Triton X-100. *Bull Exp Biol Med.* 2017; 163 (5): 620–22. DOI: 10.1007/s10517-017-3863-2.
- Smits JPH, Niehues H, Rikken G, et al. Immortalized N/TERT keratinocytes as an alternative cell source in 3D human epidermal models. *Sci Rep.* 2017; 7 (1): 11838. DOI: 10.1038/s41598-017-12041-y.
- Lehman TA, Modali R, Boukamp P, et al. p53 mutations in human immortalized epithelial cell lines. *Carcinogenesis.* 1993; 14 (5): 833–9. DOI: 10.1093/carcin/14.5.833.
- Martynova E, Pozzi S, Basile V, et al. Gain-of-function p53 mutants have widespread genomic locations partially overlapping with p63. *Oncotarget.* 2012; 3 (2): 132–43. DOI: 10.18632/oncotarget.447.
- Xu J, Reumers J, Couceiro JR, et al. Gain of function of mutant p53 by coaggregation with multiple tumor suppressors. *Nat Chem Biol.* 2011; 7 (5): 285–95. DOI: 10.1038/nchembio.546.
- Cordani N, Pozzi S, Martynova E, et al. Mutant p53 subverts p63 control over KLF4 expression in keratinocytes. *Oncogene.* 2011; 30 (8): 922–32. DOI: 10.1038/onc.2010.474.
- Neilsen PM, Noll JE, Suetani RJ, et al. Mutant p53 uses p63 as a molecular chaperone to alter gene expression and induce a pro-invasive secretome. *Oncotarget.* 2011; 2 (12): 1203–17. DOI: 10.18632/oncotarget.382.
- Русанов А. Л., Кожин П. М., Ромашин Д. Д., Карагяур М. Н., Лузгина Н. Г. Влияние модуляции активности p53 на взаимодействие членов семейства p53 в процессе дифференцировки кератиноцитов линии HaCaT. *Вестник РГМУ.* 2020; (6): 60–67. DOI: 10.24075/vrgmu.2020.082.
- Goh AM, Coffill CR, Lane DP. The role of mutant p53 in human cancer. *J Pathol.* 2011; 223 (2): 116–26. DOI: 10.1002/path.2784.
- Muller PAJ, Vousden KH, Norman JC. p53 and its mutants in tumor cell migration and invasion. *J Cell Biol.* 2011; 192 (2): 209. DOI: 10.1083/jcb.201009059.
- van der Walt S, Schönberger JL, Nunez-Iglesias J, et al. scikit-image: image processing in Python. *PeerJ.* 2014; 2: e453. DOI: 10.7717/peerj.453.
- Rusanov AL, Romashin DD, Kozhin PM, et al. Impact of p53 Knockout on Protein Data Set of HaCaT Cells in Confluent and Subconfluent Conditions. *Data.* 2022; 7 (3). DOI: 10.3390/data7030027.
- Wickham H, Averick M, Bryan J, et al. Welcome to the Tidyverse. *J Open Source Softw.* 2019; 4: 1686. DOI: 10.21105/joss.01686.
- Rusanov AL, Luzgina ED, Vakhrushev IV, Nakhod KV, Luzgina NG. A Cell Model of Human Small Intestinal Wall Based on Genetically Modified Caco-2 Cells. *Bull Exp Biol Med.* 2018; 166 (1): 174–7. DOI: 10.1007/s10517-018-4308-2.
- Sprenger A, Weber S, Zarai M, et al. Consistency of the proteome in primary human keratinocytes with respect to gender, age, and skin localization. *Mol Cell Proteomics MCP.* 2013; 12 (9): 2509–21. DOI: 10.1074/mcp.M112.025478.
- Rousselle P, Beck K. Laminin 332 processing impacts cellular behavior. *Cell Adhes Migr.* 2013; 7 (1): 122–34. DOI: 10.4161/cam.23132.
- Natsumi A, Sugawara K, Yasumizu M, et al. Re-investigating the Basement Membrane Zone of Psoriatic Epidermal Lesions: Is Laminin-511 a New Player in Psoriasis Pathogenesis? *J Histochem Cytochem.* 2018; 66 (12): 847–62. DOI: 10.1369/0022155418782693.
- Huang C, Chen J. Laminin-332 mediates proliferation, apoptosis, invasion, migration and epithelial-to-mesenchymal transition in pancreatic ductal adenocarcinoma. *Mol Med Rep.* 2021; 23 (1): 11. DOI: 10.3892/mmr.2020.11649.

PECULIARITIES OF AMINO ACID PROFILE IN MONOCYTES IN BREAST CANCER

Novoselova AV¹, Yushina MN¹, Patysheva MR^{2,3}, Prostakishina EA^{2,3}, Bragina OD², Garbukov EY², Kzhyshkowska JG^{3,4,5,6}¹ Kulakov National Medical Research Center for Obstetrics, Gynecology and Perinatology, Moscow, Russia² Cancer Research Institute, Tomsk National Research Medical Center, Tomsk, Russia³ Tomsk National State University, Tomsk, Russia⁴ Siberian State Medical University, Tomsk, Russia⁵ Institute of Transfusion Medicine and Immunology, Faculty of Medicine Mannheim, University of Heidelberg, Heidelberg, Germany⁶ German Red Cross Blood Service Baden-Württemberg-Hesse, Mannheim, Germany

Monocytes are large circulating white blood cells that are the main precursors of tissue macrophages as well as tumor-associated macrophages in the adult body. Different types of monocytes have multidirectional effects on the growth and metastatic spread of cancer cells, both activating and inhibiting these processes. Tumor progression is associated with the triggering of a whole cascade of inflammatory and immune reactions. These pathological processes are associated with changes in the amino acid content of monocytes, which can lead to disruption of their function, in particular their migration, division and maturation. The aim of the work was to profile the amino acids of monocytes, followed by a study of the amino acid composition of monocytes from patients with breast cancer using liquid chromatography with mass spectrometric detection. Significant differences in metabolite levels in monocytes of breast cancer patients and monocytes of healthy donors were found for glycine (p -value = 0.0127), asparagine (p -value = 0.0197), proline (p -value = 0.0159), methionine (p -value = 0.0357), tryptophan (p -value = 0.0028), tyrosine (p -value = 0.0127). In the study, we identified biological networks that could potentially be involved in altering the phenotype of monocytes affected by breast cancer (BC), using bioinformatic analysis of metabolic pathways involving the discovered amino acids. Mathematical models based on amino acid combinations with 100% sensitivity and specificity have been developed. Features of immune system cell metabolism in BC have been identified and potential diagnostic biomarkers have been proposed.

Keywords: monocytes, breast cancer, metabolomics, amino acids, mass spectrometry**Funding:** The study was financially supported by the Russian Federation represented by the Ministry of Science and Higher Education of the Russian Federation (agreement dated 29 September 2021 № 075-15-2021-1073 on the topic "Genetic and epigenetic editing of tumor cells and the microenvironment in order to block metastasis").**Author contribution:** Novoselova AV — material processing, monocyte amino acid profile analysis, statistical data processing, text editing; Yushina MN — material processing, text writing and editing; Patysheva MR — study concept and design, monocyte isolation; Prostakishina EA — monocyte isolation; Bragina OD, Garbukov EY — patient selection, collection of biological material; Kzhyshkowska JG — study concept and design.**Compliance with ethical standards:** the study is approved by the ethics committee of the Research Institute of Oncology under Tomsk National Research Medical Center (record No.10 dated 05 December 2019), was conducted in accordance with the standards of the ethics committee of V.I. Kulakov National Medical Research Center for Obstetrics, Gynecology and Perinatology, federal laws of the Russian Federation (Nos. 152, 323, etc.) and the 1964 Declaration of Helsinki with all subsequent additions and amendments regulating scientific research on biomaterials obtained from humans. All participants signed an informed consent to participate in the study.✉ **Correspondence should be addressed:** Anastasia V. Novoselova
Academik Oparin street, 4, Moscow, 117198, Russia; vfrankevich@gmail.com**Received:** 08.12.2022 **Accepted:** 22.12.2022 **Published online:** 28.12.2022**DOI:** 10.24075/brsmu.2022.064

ОСОБЕННОСТИ ПРОФИЛЯ АМИНОКИСЛОТ В МОНОЦИТАХ ПРИ РАКЕ МОЛОЧНОЙ ЖЕЛЕЗЫ

A. В. Новоселова¹, М. Н. Юшина¹, М. Р. Патышева^{2,3}, Е. А. Простакишина^{2,3}, О. Д. Брагина², Е. Ю. Гарбуков², Ю. Г. Кзышкowska^{3,4,5,6}¹ Национальный медицинский исследовательский центр акушерства, гинекологии и перинатологии имени В. И. Кулакова, Москва, Россия² Научно-исследовательский институт онкологии, Томский национальный исследовательский медицинский центр, Томск, Россия³ Национальный исследовательский Томский государственный университет, Томск, Россия⁴ Сибирский государственный медицинский университет, Томск, Россия⁵ Институт трансфузионной медицины и иммунологии, Медицинский факультет Маннгейм, Университет Гейдельберга, Гейдельберг, Германия⁶ Германский Красный крест Служба крови Баден-Вюртемберг — Гессен, Маннгейм, Германия

Моноциты — крупные циркулирующие в крови лейкоциты, которые во взрослом организме являются основными предшественниками тканевых макрофагов, а также опухоли-ассоциированных макрофагов. Различные типы моноцитов имеют разнонаправленное действие в отношении роста и метастатического распространения раковых клеток, как активируют, так и подавляют данные процессы. Опухолевая прогрессия связана с запуском целого каскада воспалительных и иммунных реакций. Данные патологические процессы ассоциированы с изменением содержания аминокислот в составе моноцитов, что может привести к нарушению их функции, в частности миграции, деления и созревания. Целью работы было профилировать аминокислоты моноцитов с последующим изучением особенностей аминокислотного состава моноцитов пациентов с раком молочной железы при помощи жидкостной хроматографии с масс-спектрометрической детекцией. Статистически значимые различия уровней метаболитов в моноцитах пациентов с раком молочной железы и моноцитов здоровых доноров обнаружены для глицина (p -value = 0,0127), аспарагина (p -value = 0,0197), пролина (p -value = 0,0159), метионина (p -value = 0,0357), триптофана (p -value = 0,0028), тирозина (p -value = 0,0127). В результате биоинформатического анализа метаболических путей с участием задействованных аминокислот были определены биологические сети, которые потенциально могут вовлекаться в изменение фенотипа моноцитов под воздействием РМЖ. Разработаны математические модели, построенные на комбинации аминокислот, обладающие 100% чувствительностью и специфичностью. Выявлены особенности метаболизма клеток иммунной системы при РМЖ и предложены потенциальные диагностические биомаркеры.

Ключевые слова: моноциты, рак молочной железы, метаболомика, аминокислоты, масс-спектрометрия**Финансирование:** исследование выполнено при финансовой поддержке Российской Федерации в лице Министерства науки и высшего образования Российской Федерации (соглашение от 29 сентября 2021 г. № 075-15-2021-1073 на тему: «Генетическое и эпигенетическое редактирование клеток опухоли и микроокружения с целью блокировки метастазирования»).**Вклад авторов:** А. В. Новоселова — обработка материала, анализ аминокислотного профиля моноцитов, статистическая обработка данных, редактирование текста; М. Н. Юшина — обработка материала, написание и редактирование текста; М. Р. Патышева — концепция и дизайн исследования, выделение моноцитов; Е. А. Простакишина — выделение моноцитов; О. В. Брагина, Е. Ю. Гарбуков — подбор пациентов, сбор биологического материала, Ю. Г. Кзышкowska — концепция и дизайн исследования.**Соблюдение этических стандартов:** исследование одобрено этическим комитетом НИИ онкологии Томского НИМЦ (протокол № 10 от 05 декабря 2019 г.), проведено в соответствии со стандартами этического комитета ФГБУ «Национальный медицинский исследовательский центр акушерства, гинекологии и перинатологии им. академика В. И. Кулакова», федеральными законами Российской Федерации (№ 152, 323 и др.) и Хельсинкской декларацией 1964 г. со всеми последующими дополнениями и изменениями, регламентирующими научные исследования на биоматериалах, полученных от людей. Все участники подписали информированное согласие об участии в исследовании.✉ **Для корреспонденции:** Анастасия Викторовна Новоселова
ул. Академика Опарина, д. 4, г. Москва, 117198, Россия; vfrankevich@gmail.com**Статья получена:** 08.12.2022 **Статья принята к печати:** 22.12.2022 **Опубликована онлайн:** 28.12.2022**DOI:** 10.24075/vrgmu.2022.064

Monocytes in the adult body are a dynamic population of the main cells of innate immunity, which are permanently formed from precursors in the bone marrow and circulate in the bloodstream for 3 to 6 days. Monocytes in the adult organism serve as major precursors of tissue macrophages, major sensors of innate immunity for exogenous and endogenous pathological factors from the blood, and key precursors of tumor-associated macrophages [1–5]. Representing a pool of effector cells of innate immunity with pattern-recognizing receptors, they can act as regulators of tumor growth. Different types of monocytes have mixed effects on the growth and metastatic spread of cancer cells, they both activate and inhibit these processes. Tumor progression is associated with the triggering of a whole cascade of inflammatory and immune reactions. These pathological processes are associated with changes in the amino acid content of monocytes, which can lead to impaired monocyte function [6–8].

Monocytes are precursors of tumor-associated macrophages (TAMs) and dendritic cells, which form the tumor microenvironment [9]. At the site of inflammation, they perform the function of phagocytosis and the production of pro-inflammatory cytokines. In a pro-inflammatory microenvironment, they differentiate into inflammatory macrophages and inflammatory dendritic cells, which subsequently migrate to lymph nodes and activate CD4⁺ and CD8⁺ T-lymphocytes. Activated immune cells are subsequently involved in metabolic pathways associated with cancer cell progression [10–13]. This commonality of metabolic processes creates a fundamental competition for the nutrient substrates required by both cancer and immune cells in the tumor microenvironment.

The development of analytical techniques, primarily liquid chromatography with mass spectrometric detection (LC-MS), has led to the formation of metabolomics [14–16], which is actively used to identify the metabolic features of cancer processes, to clarify the mechanisms of pathogenesis and search for new drug targets [14, 17]. To date, the study of the amino acid profile deserves special attention. Changes in amino acid levels may be important for the formation of a proper immune response [13, 18–20] and may lead to disruption of immune cell migration, division and maturation. Amino acids are involved in the control of a number of pathways that regulate immune cell responses, including mTOR signaling and NO production [19, 21]. Competition for metabolites and signaling interaction between host immune cells and pathogens can affect the development of disease, including tumor genesis [18].

Breast cancer (BC) remains the leading malignant neoplasm in women by prevalence [22]. This is the first type of cancer, for which the role of immune cells in tumor growth maintenance was demonstrated in experiments on animals [23]. Further

studies allowed to accumulate information on mutual influence of cancer cells and immune system cells [7, 9, 17, 24–29].

The study of monocyte heterogeneity and its role at different stages of cancer process progression is crucial to investigate the ability of cancer cells to obstruct immunological surveillance and hide from the aggression of immunocompetent cells. Work in this direction will make it possible in the future to identify new biomarkers of the cancer process and develop personalized cancer immunotherapy pathways [30].

The aim of this work was to determine the amino acid profile of monocytes isolated from the blood of BC patients.

METHODS

The study group included 13 patients aged 36–69 years with stage IIA-IIIa T1-2N0-1M0 breast cancer. All patients had Her2⁺ molecular tumor subtype (Ki-67 score of at least 30%). The control group included 10 healthy volunteers aged 50–67 years. Inclusion criteria for the control group: no acute chronic diseases, no history of cancer, no history of allergies or autoimmune diseases, signed informed consent to participate in the study.

The object of the study was peripheral venous blood taken on an empty stomach in test tubes with K3EDTA. Researchers obtained mononuclear cell fraction from blood by enrichment on a Ficoll density gradient (1.077 g/cm³). CD14⁺ monocytes were isolated from the obtained mononuclear cell fraction according to the Myltenyi Biotec positive magnetic separation protocol using a MidiMACS magnetic separator (Myltenyi Biotec; Germany). The purity of the obtained fraction was determined by flow cytometry on a Cytoflex (Beckman Coulter; USA) and was more than 92% CD14⁺ cells. Cell counts were based on flow cytometry data. Researchers separated an aliquot containing 4–5 million monocytes and washed it 3 times by centrifugation at 311 g for 5 min with cold 0.3% ammonium acetate. The resulting cell precipitate was dried in a nitrogen atmosphere and stored at –80 °C until extraction for not more than 6 months.

Sample preparation for LC-MS analysis

The study used acetonitrile, methanol, butanol, and chloroform (purification grades for liquid chromatography) purchased from Merck (Darmstadt; Germany), and a 37% aqueous hydrochloric acid solution (Acros Organics; USA). Deionized water was prepared using the Milli-Q Reference Water Purification System (Molesem; France).

We prepared samples according to the following procedure: add 480 µL of chloroform/methanol (2:1 vol./vol.) solution

Table 1. Composition of mobile phase for LC-MS analysis of amino acids

Time, minutes	%A	%B
0	95	5
0.1	95	5
0.2	75	25
5	70	30
15	45	55
20	30	70
20.5	5	95
25	5	95
25.5	95	5
40	95	5

Table 2. Transition parameters for mass spectrometric detection of amino acids

Amino acid	Ion precursor, m/z	Ion product, m/z	Accelerating potential of the impact cell, V	Collision energy, V
Methylhistidine	226.2	42.2	122	72
Amino butyric acid	160.1	143.1	83	4
5-Hydroxylysine	219.2	128.0	83	12
Alanine	146.1	39.2	83	20
Arginine	231.18	172.1	83	12
Asparagine	189.1	144.1	83	8
Aspartic acid	246.2	144.1	83	8
Citrulline	232.2	215.1	83	4
Cystine	353.16	130.1	122	20
Glutamic_acid	260.19	186.1	83	8
Glutamine	203.1	186.1	83	4
Glycine	132.1	76.2	44	4
Histidine	212.14	110.1	83	12
Leucine	188.17	30.3	83	20
Lysine	203.2	186.2	83	4
Methionine	206.1	104.1	83	8
Ornithine	189.2	172.2	83	8
Phenylalanine	222.1	103.1	83	40
Proline	172.1	116.1	83	12
Sarcosine	146.1	44.3	83	12
Serine	162.12	106.1	83	8
Threonine	176.13	158.1	83	4
Trans-4-hydroxyproline	188.1	86.2	83	12
Tryptophan	261.16	244.1	83	4
Tyrosine	238.1	136.1	83	12
Valine	174.15	72.2	83	12

to the monocyte sample; sonicate the sample for 10 min at room temperature, add 150 μ L of water, stir sample for 5 min; centrifuge the resulting solution at 13,000 g for 5 min at room temperature; sample 150 μ L of the upper aqueous-methanol layer; dry it in a nitrogen flow for 30 min at 60 $^{\circ}$ C; add 200 μ L of hydrochloric acid solution in butanol (0.1 mol/L); stir it for 3 minutes; centrifuge it at 13,000 g for 15 s at room temperature; then incubate at 60 $^{\circ}$ C for 15 min for the derivatization reaction; centrifuge at 13,000 g for 15 s at room temperature; dry it in a nitrogen flow for 30 min at 60 $^{\circ}$ C; stir for 5 min; centrifuge at 13,000 g for 15 s at room temperature; transfer 200 μ L of the resulting sample to a vial with an insert for further analysis.

LC-MS analysis and data processing

We analyzed the samples by high-performance liquid chromatography using a 1260 Infinity II chromatograph (Agilent; USA) with detection by a 6460 Triple Quad mass spectrometer (Agilent; USA). Samples were separated by liquid chromatography using an Agilent Zorbax Eclipse XDB-C18 2.1 \times 100 mm column with a sorbent diameter of 1.8 μ m (Agilent; USA).

For the analysis of amino acids, we injected 3 μ L of the sample and as the mobile phase, we used two eluents, fed at a flow rate of 150 μ L/min and maintained a column temperature

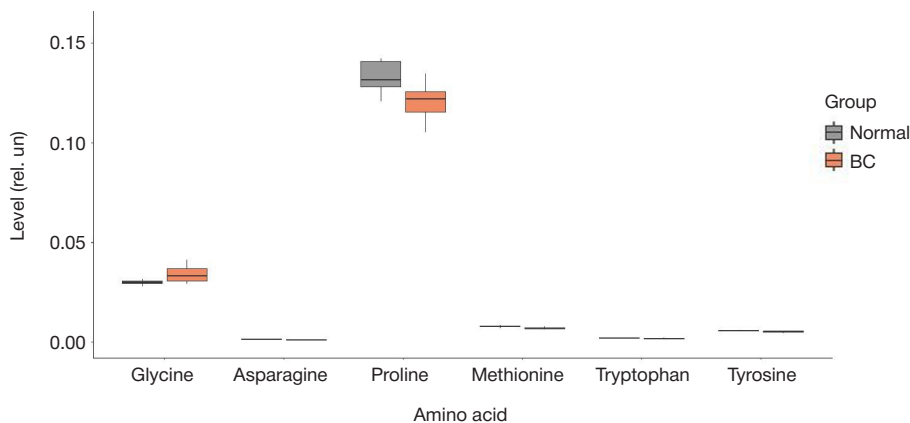


Fig. 1. Box plot of amino acids whose levels in monocytes differ significantly between the 'normal' and BC groups. The box boundaries are the first and third quartiles, the line in the middle of the box is the median; the error bars are the difference of the first quartile and the interquartile range, the sum of the third quartile and the interquartile range

Table 3. Metabolic pathways involving amino acids with significant differences in levels in monocytes from "normal" patients and breast cancer using the KEGG database

Metabolic pathway	Total number of metabolites involved	Number of metabolites that matched the experimental data	<i>P</i>	–Log (<i>P</i>)	Impact on the pathway
Biosynthesis of phenylalanine, tyrosine and tryptophan	4	1	0.015	1.812	0.5
Glycine, serine and threonine metabolism	33	1	0.121	0.916	0.246
Tryptophan metabolism	41	1	0.149	0.827	0.143
Tyrosine metabolism	42	1	0.152	0.818	0.14
Glyoxylate and dicarboxylate metabolism	32	1	0.118	0.929	0.106
Cysteine and methionine metabolism	33	1	0.121	0.916	0.104
Glutathione metabolism	28	1	0.104	0.984	0.089
Arginine and Proline Metabolism	38	1	0.139	0.858	0.078
Primary bile acid biosynthesis	46	1	0.166	0.781	0.008

at 20 °C. Eluent A was 10 mM ammonium acetate solution in water, eluent B was acetonitrile. We changed the composition of the mobile phase during the analysis according to Table 1.

Transitions between precursor ions and product ions for the analyzed amino acids are shown in Table 2. Parameters of the ion source were as follows: drying gas temperature — 150 °C, drying gas flow rate — 10 L/min, spray gas pressure — 2.76 bar, curtain gas temperature — 400 °C, curtain gas flow rate — 10 L/min, capillary voltage — 2000 V.

We determined metabolite levels using QuantAnalysis software (Agilent; USA).

Statistical analysis of the data

All data were analyzed in the R software environment (<http://www.r-project.org/>, versions R 4.1.1, 4.1.2). For initial processing of data tables we used the packages tidyverse (version 1.3.1) and readxl (1.3.1). The results were visualized using ggplot2 (version 3.3.5) and ggforestplot (version 0.1.0).

Amino acid levels were compared using the nonparametric Wilcoxon-Mann-Whitney test. Medians (Me) and quartiles Q_1 and Q_3 were used to describe quantitative data. The value of the threshold level of significance *p* was taken to be 0.05.

The team of researchers developed logistic regression models to assess the possibility of classifying patients into groups on the basis of the parameters under study. Levels of individual amino acids were considered as independent variables in the models. The dependent variable was whether the sample belonged to the 'normal' or BC group. Of all the models developed, we selected the four with the highest area under the ROC curve (AUC). The quality of the models developed was assessed by plotting the ROC curve, determining the area under the ROC curve, and calculating sensitivity and specificity.

Table 4. Metabolic pathways involving amino acids with significant differences in levels in monocytes from "normal" patients and breast cancer using the SMPDB database

Metabolic pathway	Total number of metabolites involved	Number of metabolites that matched the experimental data	<i>P</i>	–Log (<i>P</i>)	Impact on the pathway
Aspartate metabolism	34	1	0.158	0.802	0.25
Phenylalanine and tyrosine metabolism	25	1	0.118	0.928	0.221
Glutathione metabolism	19	1	0.091	1.042	0.061
Glycine and serine metabolism	50	2	0.022	1.66	0.048
Ammonia recycling	25	2	0.006	2.249	0.033
Methionine metabolism	39	1	0.179	0.747	0.009

If amino acid levels differed in monocytes from those in BC patients, we analyzed the involvement in metabolic pathways using the MetaboAnalyst 5.0 resource (<https://www.metaboanalyst.ca/home.xhtml>)

RESULTS

Semi-quantitative data on the content of 26 amino acids in monocytes of healthy donors and in monocytes of BC patients were obtained in the analysis. The list of amino acids included methyl-histidine, aminobutyric acid, 5-hydroxylysine, alanine, arginine, asparagine, aspartic acid, citrulline, cystine, glutamic acid, glutamine, glycine, histidine, leucine, lysine, methionine, ornithine, phenylalanine, proline, sarcosine, serine, threonine, trans-4-hydroxy-proline, tryptophan, tyrosine, valine. We obtained amino acid profile by dividing the chromatographic peak area of each amino acid by the total peak area of all amino acids in the corresponding sample. To search for differences in amino acid profiles in monocytes obtained from "normal" and BC patients, we compared the data obtained by LC-MS using the Wilcoxon-Mann-Whitney method. Significant differences in metabolite levels were found for glycine (*p*-value = 0.0127), asparagine (*p*-value = 0.0197), proline (*p*-value = 0.0159), methionine (*p*-value = 0.0357), tryptophan (*p*-value = 0.0028), tyrosine (*p*-value = 0.0127) (Fig. 1).

Where the levels of amino acids differed significantly between monocytes of the "normal" and BC groups, we carried out a bioinformatic analysis of metabolic pathways involving these acids. The analysis was performed using the MetaboAnalyst resource. As a result, biological networks have been identified that could potentially be involved in altering the phenotype of monocytes under the influence of BC. As we analyzed the data presented in the KEGG database and SMPDB (Tables 3, 4), we

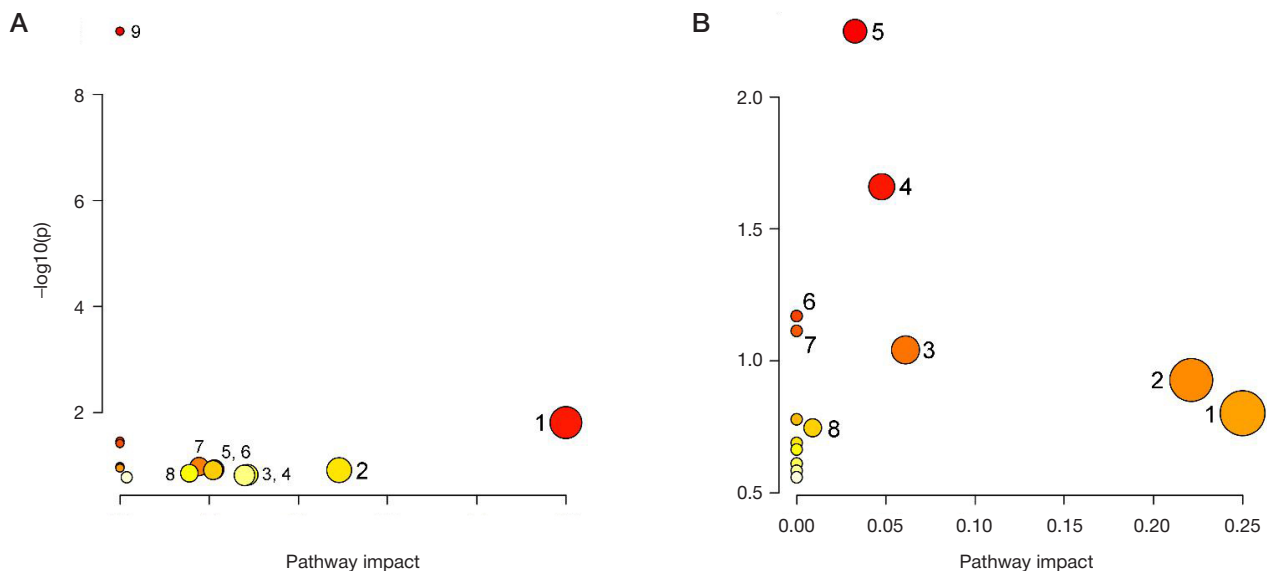


Fig. 2. Result of an analysis of the metabolic pathways involving amino acids with significant differences in levels in monocytes from patients in the "normal" group and from those in the BC group. **A.** Analysis using the KEGG database: 1 — phenylalanine, tyrosine and tryptophan biosynthesis; 2 — glycine, serine and threonine metabolism; 3 — tryptophan metabolism; 4 — tyrosine metabolism; 5 — glyoxylate and dicarboxylate metabolism; 6 — cysteine and methionine metabolism; 7 — glutathione metabolism; 8 — arginine and proline metabolism; 9 — aminoacyl-tRNA biosynthesis. **B.** Analysis using the SMPDB database: 1 — aspartate metabolism; 2 — phenylalanine and tyrosine metabolism; 3 — glutathione metabolism; 4 — glycine and serine metabolism; 5 — ammonia recycling; 6 — alanine metabolism; 7 — carnitine synthesis; 8 — methionine metabolism

were able to identify pathways ordered by levels of significance (pathway enrichment analysis — *y*-axis in Fig. 2) and the values of the influence of the metabolites in question on the pathway (pathway topology analysis — *x*-axis in Fig. 2). The color of the node corresponds to the level of significance, and the radius of the node correlates with the amount of influence on the path. The effect on the pathway was calculated as the sum of the significance values of the corresponding metabolites divided by the sum of the significance values of all metabolites in each pathway. Metabolic pathway enrichment was assessed by Over representation analysis (ORA) using a hypergeometric test.

To test the feasibility of diagnosing RBCs by amino acid levels in monocytes, we developed logistic regression models for each of the significant amino acids (Fig. 3A). We also considered models using a combination of amino acids and selected the four with the highest area under the operating curve (AUC) by ROC analysis (Fig. 3B). Table 5 shows the

results of the quality assessment of the single amino acid models. Models built on a combination of amino acids had AUC = 1 and 100% sensitivity and specificity (Fig. 3B).

DISCUSSION

Of the 26 amino acids analyzed, only six amino acids had significant differences in monocyte levels between healthy donors and BC patients. Of these six amino acids, glycine, tryptophan and asparagine are of particular interest because disturbances in the metabolic pathways associated with them are associated with tumor-induced changes [11, 13, 14, 18, 27, 31].

The availability over time of the essential amino acid tryptophan is an important determinant of the strength and quality of the immune response. Proliferation and activation of human T cells were strongly inhibited in tryptophan-free media compared to conventional nutrient media [32, 33]. Cancer cells, TAM and

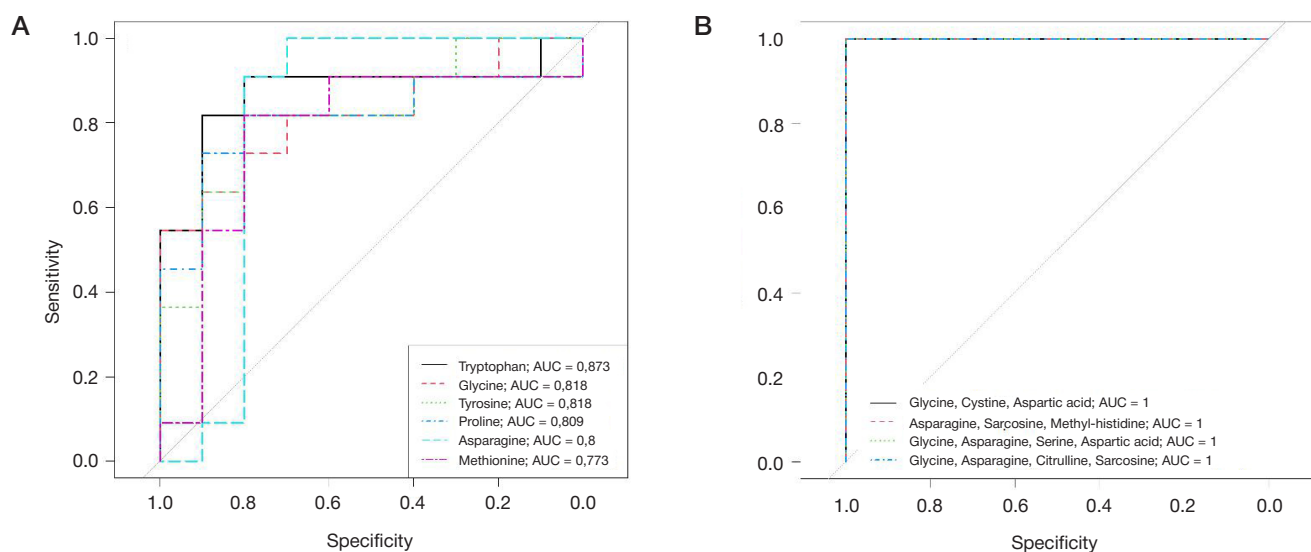


Fig. 3. ROC-curves of logistic regression models with monocyte amino acid levels as the independent variable and whether the sample belongs to the 'normal' or BC group as the dependent variable. The insets show the amino acids whose levels are taken as the independent variable, as well as the area under the operating curve for the corresponding logistic regression model. ROC curves are plotted for each of the statistically significantly different amino acids (**A**) as well as a combination of amino acids (**B**)

Table 5. Characteristics of logistic regression models predicting BC according to the content of selected amino acids whose levels in monocytes differ significantly between the "normal" group and BC

Amino acids	AUC	Threshold value	Sensitivity	Specificity	Positive predictive value
Tryptophan	0.87	0.53	0.91 (0.55; 1)	0.9 (0.7; 1)	0.92 (0.77; 1)
Glycine	0.82	0.74	0.73 (0.36; 1)	1 (0.6; 1)	1 (0.71; 1)
Tyrosine	0.82	0.46	0.82 (0.45; 1)	0.9 (0.5; 1)	0.9 (0.67; 1)
Proline	0.81	0.57	0.82 (0.45; 1)	0.9 (0.7; 1)	0.91 (0.73; 1)
Asparagine	0.8	0.45	1 (0.82; 1)	0.8 (0.5; 1)	0.85 (0.69; 1)
Methionine	0.77	0.51	0.82 (0.55; 1)	0.8 (0.5; 1)	0.83 (0.67; 1)

cancer-associated fibroblasts can reduce tryptophan levels through the enzymatic activity of indoleamine-2,3-dioxygenase (IDO) [13]. TAM, and sometimes tumor cells themselves, increase IDO levels and create an immunosuppressive microenvironment via at least two mechanisms: tryptophan depletion and accumulation of tryptophan catabolites such as kynurenine, 3-hydroxyanthranilate and quinolinate [34, 35]. Tryptophan depletion inhibits the proliferation of activated T cells, and tryptophan-derived catabolites act as ligands for aromatic hydrocarbon receptors [36]. Kinurenine is a suppressor of T-cell immunity. By stimulating aromatic hydrocarbon receptors, it directs naïve T cell differentiation towards regulatory T cells and inhibits Th17 cell differentiation [22, 37].

Biosynthesis of serine, glycine and one-carbon metabolism are crucial for maintaining cancer cell survival and proliferation and are of high clinical relevance. Excessive activation of serine and glycine biosynthesis leads to oncogenesis, providing a substrate for one-carbon metabolism. One-carbon metabolism, which is a cyclic metabolic network based on the chemical reaction of folic acid compounds, provides essential proteins, nucleic acids, lipids and other biological macromolecules to support tumor growth [31].

It was found that asparagine can affect cancer cell growth [38], leading to the use of the bacterial enzyme L-asparaginase to limit the availability of asparagine [14, 39]. Significant

efforts are being made to develop agents to deplete other amino acids and to act on central metabolic pathways that are dysregulated in cancer cells, including glycolysis, the tricarboxylic acid cycle and lipogenesis. Many of these drugs are still in preclinical stages, but some are currently being evaluated in clinical trials [14].

CONCLUSIONS

This study identified six amino acids whose levels differed significantly in the monocytes of breast cancer patients from those of healthy donors. Significant differences in metabolite levels were found for glycine (p -value = 0.0127), asparagine (p -value = 0.0197), proline (p -value = 0.0159), methionine (p -value = 0.0357), tryptophan (p -value = 0.0028), tyrosine (p -value = 0.0127). Bioinformatic analysis of metabolic pathways involving the discovered amino acids revealed biological networks that could potentially be involved in altering the phenotype of monocytes exposed to BC. The observed changes in the amino acid content of monocytes may indicate the influence of tumor processes not only on the microenvironment, but also indirectly on distant immune system participants. Based on the differences found, a model with 100% specificity and sensitivity has been proposed to diagnose BC according to the amino acid profile of monocytes.

References

- Kzhyshkowska J, Gudima A, Moganti K, Gratchev A, Orekhov A. Perspectives for Monocyte/Macrophage-Based Diagnostics of Chronic Inflammation. *Transfus Med Hemotherapy*. 2016; 43 (2): 66–77.
- Nikitina E, Larionova I, Choinzonov E, Kzhyshkowska J. Monocytes and macrophages as viral targets and reservoirs. *Int J Mol Sci*. 2018; 19 (9). DOI: 10.3390/ijms19092821.
- Patysheva M, Larionova I, Stakheyeva M, Grigoryeva E, Iamshchikov P, Tarabanovskaya N, et al. Effect of Early-Stage Human Breast Carcinoma on Monocyte Programming. *Front Oncol*. 2022; 11 (February): 1–12.
- Matuschik L, Riabov V, Schmuttermaier C, Sevastyanova T, Weiss C, Klüter H, et al. Hyperglycemia Induces Inflammatory Response of Human Macrophages to CD163-Mediated Scavenging of Hemoglobin-Haptoglobin Complexes. *Int J Mol Sci*. 2022; 23 (3): 1–19.
- Patysheva M, Frolova A, Larionova I, Afanas'ev S, Tarasova A, Cherdyn'tseva N, et al. Monocyte programming by cancer therapy. *Front Immunol*. 2022; 13 (October): 1–21.
- Qian BZ, Li J, Zhang H, Kitamura T, Zhang J, Campion LR, et al. CCL2 recruits inflammatory monocytes to facilitate breast-tumour metastasis. *Nature*. 2011; 475 (7355): 222–5.
- Hanna RN, Cekic C, Sag D, Tacke R, Thomas GD, Nowyhed H, et al. Patrolling monocytes control tumor metastasis to the lung. *Science* (80-). 2015; 350 (6263): 985–90.
- Shi C, Pamer EG. Monocyte recruitment during infection and inflammation. *Nat Rev Immunol*. 2011; 11 (11): 762–74.
- Engblom C, Pfirschke C, Pittet MJ. The role of myeloid cells in cancer therapies. *Nat Rev Cancer*. 2016; 16 (7): 447–62.
- Fox CJ, Hammerman PS, Thompson CB. Fuel feeds function: Energy metabolism and the T-cell response. *Nat Rev Immunol*. 2005; 5 (11): 844–52.
- Andrejeva G, Rathmell JC. Similarities and Distinctions of Cancer and Immune Metabolism in Inflammation and Tumors. *Cell Metab*. 2017; 26 (1): 49–70.
- Bauer DE, Harris MH, Plas DR, Lum JJ, Hammerman PS, Rathmell JC, et al. Cytokine stimulation of aerobic glycolysis in hematopoietic cells exceeds proliferative demand. *FASEB J*. 2004; 18 (11): 1303–5.
- Leone RD, Powell JD. Metabolism of immune cells in cancer. *Nat Rev Cancer*. 2020; 20 (9): 516–31.
- Schmidt DR, Patel3 R, Kirsch DG, Lewis5 CA, Heiden MG Vander, Locasale4 JW. Metabolomics in Cancer Research and Emerging Applications in Clinical Oncology. *CA Cancer J Clin*. 2021; 71 (4): 333–58.
- Odom JD, Sutton VR. Metabolomics in Clinical Practice: Improving Diagnosis and Informing Management. *Clin Chem*. 2021; 67 (12): 1606–17.
- Clish CB. Metabolomics: an emerging but powerful tool for precision medicine. *Mol Case Stud*. 2015; 1 (1): a000588.
- Wishart DS. Emerging applications of metabolomics in drug

- discovery and precision medicine. *Nat Rev Drug Discov.* 2016; 15 (7): 473–84.
18. Viola A, Munari F, Sánchez-Rodríguez R, Scolaro T, Castegna A. The metabolic signature of macrophage responses. *Front Immunol.* 2019; 10 (JULY): 1–16.
 19. Schairer DO, Chouake JS, Nosanchuk JD, Friedman AJ. The potential of nitric oxide releasing therapies as antimicrobial agents. *Virulence.* 2012; 3 (3): 271–9.
 20. Van den Bossche J, Baardman J, Otto NA, van der Velden S, Neele AE, van den Berg SM, et al. Mitochondrial Dysfunction Prevents Repolarization of Inflammatory Macrophages. *Cell Rep.* 2016; 17 (3): 684–96.
 21. Qualls JE, Subramanian C, Rafi W, Smith AM, Defreitas AA, Shirey KA, et al. Sustained generation of nitric oxide and control of mycobacterial infection requires argininosuccinate synthase 1. *Cell Host Microbe.* 2012; 12 (3): 313–23.
 22. Kaprin AD, Starinskij VV, Petrova GV, redaktory. *Zlokachestvennye novoobrazovaniya v Rossii v 2017 godu (zabolevaemost' i smertnost')*. M.: MNIIO im. P. A. Gercena — filial FGBU «NMIC radiologii» Minzdrava Rossii, 2018; 250 s. Russian.
 23. Cassetta L, Pollard JW. Repolarizing macrophages improves breast cancer therapy. *Cell Res.* 2017; 27 (8): 963–4.
 24. Kuang DM, Zhao Q, Peng C, Xu J, Zhang JP, Wu C, et al. Activated monocytes in peritumoral stroma of hepatocellular carcinoma foster immune privilege and disease progression through PD-L1. *J Exp Med.* 2009; 206 (6): 1327–37.
 25. De Sanctis F, Adamo A, Canè S, Ugel S. Targeting tumour-reprogrammed myeloid cells: the new battleground in cancer immunotherapy. *Semin Immunopathol.* 2022; (0123456789). DOI: 10.1007/s00281-022-00965-1.
 26. Nguyen PHD, Wasser M, Tan CT, Lim CJ, Lai HLH, Seow JJW, et al. Trajectory of immune evasion and cancer progression in hepatocellular carcinoma. *Nat Commun.* 2022; 13 (1): 1–13.
 27. Zhu Y, Li X, Wang L, Hong X, Yang J. Metabolic reprogramming and crosstalk of cancer-related fibroblasts and immune cells in the tumor microenvironment. *Front Endocrinol (Lausanne).* 2022; 13 (August): 1–26.
 28. Larionova I, Tuguzbaeva G, Ponomaryova A, Stakheyeva M, Cherdyntseva N, Pavlov V, et al. Tumor-Associated Macrophages in Human Breast, Colorectal, Lung, Ovarian and Prostate Cancers. *Front Oncol.* 2020; 10 (October): 1–34.
 29. Larionova I, Cherdyntseva N, Liu T, Patysheva M, Rakina M, Kzhyshkowska J. Interaction of tumor-associated macrophages and cancer chemotherapy. *Oncoimmunology.* 2019; 8 (7): 1–15.
 30. Olingy CE, Dinh HQ, Hedrick CC. Monocyte heterogeneity and functions in cancer. *J Leukoc Biol.* 2019; 106 (2): 309–22.
 31. Pan S, Fan M, Liu Z, Li X, Wang H. Serine, glycine and one-carbon metabolism in cancer (Review). *Int J Oncol.* 2021; 58 (2): 158–70.
 32. Munn DH, Sharma MD, Baban B, Harding HP, Zhang Y, Ron D, et al. GCN2 kinase in T cells mediates proliferative arrest and anergy induction in response to indoleamine 2,3-dioxygenase. *Immunity.* 2005; 22 (5): 633–42.
 33. Munn BDH, Shafizadeh E, Attwood JT, Bondarev I, Pashine A, Mellor AL. Inhibition of T Cell Proliferation by Macrophage. 1999; 189 (9): 1363–72.
 34. Platten M, Wick W, Van Den Eynde BJ. Tryptophan catabolism in cancer: Beyond IDO and tryptophan depletion. *Cancer Res.* 2012; 72 (21): 5435–40.
 35. Moffett JR, Namboodiri MA. Tryptophan and the immune response. *Immunol Cell Biol.* 2003; 81 (4): 247–65.
 36. Opitz CA, Litzenburger UM, Sahm F, Ott M, Tritschler I, Trump S, et al. An endogenous tumour-promoting ligand of the human aryl hydrocarbon receptor. *Nature.* 2011; 478 (7368): 197–203.
 37. Stephens GL, Wang Q, Swerdlow B, Bhat G, Kolbeck R, Fung M. Kynurenine 3-monooxygenase mediates inhibition of Th17 differentiation via catabolism of endogenous aryl hydrocarbon receptor ligands. *Eur J Immunol.* 2013. 43 (7): 1727–34. DOI: 10.1002/eji.201242779.
 38. RE N, TAM M. Dual Requirement of Walker Carcinosarcoma 256 in vitro for Asparagine and Glutamine. *Science.* 1956; 124 (3212): 124–5.
 39. Clavell LA, Gelber RD, Cohen HJ, Suzanne Hitchcock-Bryan RN, Cassady JR, Tarbel NJ, et al. Four-agent induction and intensive asparaginase therapy for treatment of childhood acute lymphoblastic leukemia. *N Engl J Med.* 1986; 315: 657–63.

Литература

1. Kzhyshkowska J, Gudima A, Moganti K, Gratchev A, Orekhov A. Perspectives for Monocyte/Macrophage-Based Diagnostics of Chronic Inflammation. *Transfus Med Hemotherapy.* 2016; 43 (2): 66–77.
2. Nikitina E, Larionova I, Choinzonov E, Kzhyshkowska J. Monocytes and macrophages as viral targets and reservoirs. *Int J Mol Sci.* 2018; 19 (9). DOI: 10.3390/ijms19092821.
3. Patysheva M, Larionova I, Stakheyeva M, Grigoryeva E, Iamshchikov P, Tarabanovskaya N, et al. Effect of Early-Stage Human Breast Carcinoma on Monocyte Programming. *Front Oncol.* 2022; 11 (February): 1–12.
4. Matuschik L, Riabov V, Schmuttermayer C, Sevastyanova T, Weiss C, Klüter H, et al. Hyperglycemia Induces Inflammatory Response of Human Macrophages to CD163-Mediated Scavenging of Hemoglobin-Haptoglobin Complexes. *Int J Mol Sci.* 2022; 23 (3): 1–19.
5. Patysheva M, Frolova A, Larionova I, Afanas'ev S, Tarasova A, Cherdyntseva N, et al. Monocyte programming by cancer therapy. *Front Immunol.* 2022; 13 (October): 1–21.
6. Qian BZ, Li J, Zhang H, Kitamura T, Zhang J, Campion LR, et al. CCL2 recruits inflammatory monocytes to facilitate breast-tumour metastasis. *Nature.* 2011; 475 (7355): 222–5.
7. Hanna RN, Cekic C, Sag D, Tacke R, Thomas GD, Nowyhed H, et al. Patrolling monocytes control tumor metastasis to the lung. *Science (80-).* 2015; 350 (6263): 985–90.
8. Shi C, Pamer EG. Monocyte recruitment during infection and inflammation. *Nat Rev Immunol.* 2011; 11 (11): 762–74.
9. Engblom C, Pfirsche C, Pittet MJ. The role of myeloid cells in cancer therapies. *Nat Rev Cancer.* 2016; 16 (7): 447–62.
10. Fox CJ, Hammerman PS, Thompson CB. Fuel feeds function: Energy metabolism and the T-cell response. *Nat Rev Immunol.* 2005; 5 (11): 844–52.
11. Andrejeva G, Rathmell JC. Similarities and Distinctions of Cancer and Immune Metabolism in Inflammation and Tumors. *Cell Metab.* 2017; 26 (1): 49–70.
12. Bauer DE, Harris MH, Plas DR, Lum JJ, Hammerman PS, Rathmell JC, et al. Cytokine stimulation of aerobic glycolysis in hematopoietic cells exceeds proliferative demand. *FASEB J.* 2004; 18 (11): 1303–5.
13. Leone RD, Powell JD. Metabolism of immune cells in cancer. *Nat Rev Cancer.* 2020; 20 (9): 516–31.
14. Schmidt DR, Patel R, Kirsch DG, Lewis CA, Heiden MG Vander, Locasale JW. Metabolomics in Cancer Research and Emerging Applications in Clinical Oncology. *CA Cancer J Clin.* 2021; 71 (4): 333–58.
15. Odom JD, Sutton VR. Metabolomics in Clinical Practice: Improving Diagnosis and Informing Management. *Clin Chem.* 2021; 67 (12): 1606–17.
16. Clish CB. Metabolomics: an emerging but powerful tool for precision medicine. *Mol Case Stud.* 2015; 1 (1): a000588.
17. Wishart DS. Emerging applications of metabolomics in drug discovery and precision medicine. *Nat Rev Drug Discov.* 2016; 15 (7): 473–84.
18. Viola A, Munari F, Sánchez-Rodríguez R, Scolaro T, Castegna A. The metabolic signature of macrophage responses. *Front Immunol.* 2019; 10 (JULY): 1–16.
19. Schairer DO, Chouake JS, Nosanchuk JD, Friedman AJ. The potential of nitric oxide releasing therapies as antimicrobial agents. *Virulence.* 2012; 3 (3): 271–9.
20. Van den Bossche J, Baardman J, Otto NA, van der Velden S, Neele AE, van den Berg SM, et al. Mitochondrial Dysfunction Prevents Repolarization of Inflammatory Macrophages. *Cell Rep.*

- 2016; 17 (3): 684–96.
21. Qualls JE, Subramanian C, Rafi W, Smith AM, Defreitas AA, Shirey KA, et al. Sustained generation of nitric oxide and control of mycobacterial infection requires argininosuccinate synthase 1. *Cell Host Microbe*. 2012; 12 (3): 313–23.
 22. Каприн А. Д., Старинский В. В., Петрова Г. В., редакторы. Злокачественные новообразования в России в 2017 году (заболеваемость и смертность). М.: МНИОИ им. П.А. Герцена — филиал ФГБУ «НМИЦ радиологии» Минздрава России, 2018; 250 с.
 23. Cassetta L, Pollard JW. Repolarizing macrophages improves breast cancer therapy. *Cell Res*. 2017; 27 (8): 963–4.
 24. Kuang DM, Zhao Q, Peng C, Xu J, Zhang JP, Wu C, et al. Activated monocytes in peritumoral stroma of hepatocellular carcinoma foster immune privilege and disease progression through PD-L1. *J Exp Med*. 2009; 206 (6): 1327–37.
 25. De Sanctis F, Adamo A, Canè S, Ugel S. Targeting tumour-reprogrammed myeloid cells: the new battleground in cancer immunotherapy. *Semin Immunopathol*. 2022; (0123456789). DOI: 10.1007/s00281-022-00965-1.
 26. Nguyen PHD, Wasser M, Tan CT, Lim CJ, Lai HLH, Seow JJW, et al. Trajectory of immune evasion and cancer progression in hepatocellular carcinoma. *Nat Commun*. 2022; 13 (1): 1–13.
 27. Zhu Y, Li X, Wang L, Hong X, Yang J. Metabolic reprogramming and crosstalk of cancer-related fibroblasts and immune cells in the tumor microenvironment. *Front Endocrinol (Lausanne)*. 2022; 13 (August): 1–26.
 28. Larionova I, Tuguzbaeva G, Ponomaryova A, Stakheyeva M, Cherdyntseva N, Pavlov V, et al. Tumor-Associated Macrophages in Human Breast, Colorectal, Lung, Ovarian and Prostate Cancers. *Front Oncol*. 2020; 10 (October): 1–34.
 29. Larionova I, Cherdyntseva N, Liu T, Patysheva M, Rakina M, Kzhyshkowska J. Interaction of tumor-associated macrophages and cancer chemotherapy. *Oncoimmunology*. 2019; 8 (7): 1–15.
 30. Olingy CE, Dinh HQ, Hedrick CC. Monocyte heterogeneity and functions in cancer. *J Leukoc Biol*. 2019; 106 (2): 309–22.
 31. Pan S, Fan M, Liu Z, Li X, Wang H. Serine, glycine and one-carbon metabolism in cancer (Review). *Int J Oncol*. 2021; 58 (2): 158–70.
 32. Munn DH, Sharma MD, Baban B, Harding HP, Zhang Y, Ron D, et al. GCN2 kinase in T cells mediates proliferative arrest and anergy induction in response to indoleamine 2,3-dioxygenase. *Immunity*. 2005; 22 (5): 633–42.
 33. Munn BDH, Shafizadeh E, Attwood JT, Bondarev I, Pashine A, Mellor AL. Inhibition of T Cell Proliferation by Macrophage. 1999; 189 (9): 1363–72.
 34. Platten M, Wick W, Van Den Eynde BJ. Tryptophan catabolism in cancer: Beyond IDO and tryptophan depletion. *Cancer Res*. 2012; 72 (21): 5435–40.
 35. Moffett JR, Namboodiri MA. Tryptophan and the immune response. *Immunol Cell Biol*. 2003; 81 (4): 247–65.
 36. Opitz CA, Litzemberger UM, Sahm F, Ott M, Tritschler I, Trump S, et al. An endogenous tumour-promoting ligand of the human aryl hydrocarbon receptor. *Nature*. 2011; 478 (7368): 197–203.
 37. Stephens GL, Wang Q, Swerdlow B, Bhat G, Kolbeck R, Fung M. Kynurenine 3-monooxygenase mediates inhibition of Th17 differentiation via catabolism of endogenous aryl hydrocarbon receptor ligands. *Eur J Immunol*. 2013. 43 (7): 1727–34. DOI: 10.1002/eji.201242779.
 38. RE N, TA M. Dual Requirement of Walker Carcinosarcoma 256 in vitro for Asparagine and Glutamine. *Science*. 1956; 124 (3212): 124–5.
 39. Clavell LA, Gelber RD, Cohen HJ, Suzanne Hitchcock-Bryan RN, Cassady JR, Tarbel NJ, et al. Four-agent induction and intensive asparaginase therapy for treatment of childhood acute lymphoblastic leukemia. *N Engl J Med*. 1986; 315: 657–63.

ROLE OF CLUSTERIN IN PREDICTING DEVELOPMENT OF EARLY- AND LATE-ONSET PREECLAMPSIA IN THE FIRST TRIMESTER OF PREGNANCY

Timofeeva AV[✉], Fedorov IS, Tarasova AM, Gorina KA, Suhova YuV, Gusar VA, Ivanets TYu

Kulakov National Medical Research Center for Obstetrics, Gynecology and Perinatology, Moscow, Russia

Preeclampsia (PE) occurs in 2–8% of pregnancies. It is one of the leading causes of maternal and perinatal morbidity and mortality. Today, there are no tests adopted by the practitioners that enable accurate prediction of early (weeks 20 through 34) or late (after week 34) onset of PE when the pregnancy is in its 11th to 14th week. This study aimed to evaluate the feasibility of using secretory clusterin quantification to predict early or late PE during the first trimester of pregnancy. The choice of this protein is determined, on the one hand, by the specificity of its expression for cytotrophoblast, syncytiotrophoblast, and extravascular trophoblast cells, and, on the other hand, by the proven negative effect of clusterin on the invasive properties of trophoblastic cells and gestational transformations of uterine vessels, which play a key role in the pathogenesis of PE. The study included 40 pregnant women aged 27–40 years who underwent a comprehensive screening examination in the first trimester of pregnancy. Western blotting revealed a significant increase in the level of secretory clusterin (40 kDa) in the blood serum of pregnant women in the case of PE compared to physiological pregnancy: in early-onset PE, a twofold increase in the level of clusterin in the vesicular and extravascular fractions of blood serum ($p = 0.03$ and $p = 0.004$, respectively), with late-onset PE — a threefold increase only in the extravascular fraction of blood serum ($p = 0.002$). According to logistic regression models, the level of secretory clusterin in the extravascular fraction of blood serum of pregnant women in the first trimester has prognostic significance in assessing the likelihood of developing early-onset PE (AUC = 0.97, Se = 1, Sp = 0.875, cutoff = 0.3877) and late-onset PE (AUC = 1, Se = 1, Sp = 1, cutoff = 0.5).

Keywords: peripheral blood serum, vesicles, placenta, clusterin, preeclampsia, Western blotting, miRNA, quantitative real-time PCR

Funding: the work was financially supported by the Russian Science Foundation under grant #22-15-00363 "Epigenetic and biochemical aspects of the pathology of pregnancy in violations of the invasive properties of the trophoblast: from early diagnosis to the prevention of maternal and perinatal morbidity", under the Agreement #22-15-00363 of May 13, 2022 for provision of a grant to support fundamental and basic research, made between the Russian Science Foundation, Angelika Vladimirovna Timofeeva (principal researcher/manager for the study) and V. I. Kulakov National Medical Research Center for Obstetrics, Gynecology and Perinatology.

Author contribution: Timofeeva AV — study planning, quantitative real-time PCR, Western blotting, manuscript authoring and editing; Fedorov IS — preparation of samples, Western blotting, statistical processing of the data; Tarasova AM — preparation of samples and Western blotting; Gorina KA — clinical profiling of the patients; Suhova YuV — formation of groups of patients for the study, Gusar VA — analysis of the data obtained; Ivanets TYu — screening in the 1st trimester of pregnancy.

Compliance with ethical standards: the study was approved by the Ethics Committee of V.I. Kulakov National Medical Research Center for Obstetrics, Gynecology and Perinatology (Minutes #13 of December 10, 2020), conducted in accordance with the requirements of the Declaration of Helsinki of 1964, Federal Law "On the Fundamentals of Protecting the Health of Citizens in the Russian Federation" #323-FZ of November 21, 2011 All patients signed a voluntary informed consent form to participate in the study.

✉ **Correspondence should be addressed:** Angelika V. Timofeeva
Akademika Oparina, 4, Moscow, 117997, Russia; v_timofeeva@oparina4.ru, avtimofeeva28@gmail.com

Received: 23.11.2022 **Accepted:** 17.12.2022 **Published online:** 28.12.2022

DOI: 10.24075/brsmu.2022.061

РОЛЬ КЛАСТЕРИНА В ПРОГНОЗИРОВАНИИ РАЗВИТИЯ РАННЕЙ И ПОЗДНЕЙ ПРЕЭКЛАМПСИИ В ПЕРВОМ ТРИМЕСТРЕ БЕРЕМЕННОСТИ

А. В. Тимофеева[✉], И. С. Федоров, А. М. Тарасова, К. А. Горина, Ю. В. Сухова, В. А. Гусар, Т. Ю. Иванец

Национальный медицинский исследовательский центр акушерства, гинекологии и перинатологии имени В. И. Кулакова, Москва, Россия

Преэклампсия (ПЭ) встречается в 2–8% беременностей, является одной из важнейших причин материнской и перинатальной заболеваемости и смертности. На сегодняшний день нет используемых в клинической практике тест-систем, позволяющих с высокой точностью прогнозировать на 11–14-й неделе беременности ранний дебют ПЭ (с 20-й по 34-ю неделю) или поздний дебют ПЭ (после 34-й недели). Целью исследования было оценить возможности использования количественного определения секреторной формы кластерина в прогнозировании развития ранней и поздней ПЭ в первом триместре беременности. Выбор данного белка обусловлен специфичностью его экспрессии для клеток цитотрофобласта, синцитиотрофобласта и внеклеточного трофобласта, а также доказанным негативным влиянием кластерина на инвазивные свойства трофобластных клеток и гестационные преобразования сосудов матки, играющих ключевую роль в патогенезе ПЭ. В исследование включены 40 беременных в возрасте от 27–40 лет, проходивших комплексное скрининговое обследование в первом триместре беременности. Методом Вестерн-блоттинга обнаружено значимое повышение уровня секреторного кластерина (40 кДа) в сыворотке крови беременных в случае развития ПЭ относительно физиологической беременности: при ранней ПЭ — двукратное увеличение уровня кластерина в везикулярной и вневезикулярной фракции сыворотки крови ($p = 0,03$ и $p = 0,004$ соответственно), при поздней ПЭ — трехкратное увеличение только во вневезикулярной фракции сыворотки крови ($p = 0,002$). Согласно моделям логистической регрессии уровень секреторного кластерина во вневезикулярной фракции сыворотки крови беременных в первом триместре обладает прогностической значимостью при оценке вероятности развития ранней ПЭ (AUC = 0,97, Se = 1, Sp = 0,875, cutoff = 0,3877) и поздней ПЭ (AUC = 1, Se = 1, Sp = 1, cutoff = 0,5).

Ключевые слова: сыворотка периферической крови, везикулы, плацента, кластерин, преэклампсия, Вестерн-блоттинг, мкРНК, количественная ПЦР в реальном времени

Финансирование: работа выполнена при финансовой поддержке Российского научного фонда в рамках гранта № 22-15-00363 «Эпигенетические и биохимические аспекты патологии беременности при нарушениях инвазивных свойств трофобласта: от ранней диагностики к профилактике материнской и перинатальной заболеваемости» в соответствии с соглашением № 22-15-00363 между Российским научным фондом, руководителем проекта Тимофеевой А. В. и НМИЦ АГП им. В. И. Кулакова о предоставлении гранта на проведение фундаментальных научных исследований и поисковых научных исследований от 13.05.2022 г.

Вклад авторов: А. В. Тимофеева — планирование исследования, проведение количественной ПЦР в реальном времени, проведение Вестерн-блоттинга, написание и редактирование рукописи; И. С. Федоров — пробоподготовка, проведение Вестерн-блоттинга, статистическая обработка данных; А. М. Тарасова — пробоподготовка и проведение Вестерн-блоттинга; К. А. Горина — клиническая характеристика пациенток; Ю. В. Сухова — формирование групп пациенток для исследования, В. А. Гусар — анализ полученных данных; Т. Ю. Иванец — скрининг в 1-м триместре беременности.

Соблюдение этических стандартов: исследование одобрено этическим комитетом НМИЦ АГП им. В. И. Кулакова (протокол № 13 от 10 декабря 2020 г.), проведено в соответствии с требованиями Хельсинкской декларации 1964 г. ФЗ «Об основах охраны здоровья граждан в Российской Федерации» № 323-ФЗ от 21 ноября 2011 г. Все пациентки подписали добровольное информированное согласие на участие в исследовании.

✉ **Для корреспонденции:** Анжелика Владимировна Тимофеева
ул. Академика Опарина, д. 4, г. Москва, 117997, Россия; v_timofeeva@oparina4.ru, avtimofeeva28@gmail.com

Статья получена: 23.11.2022 **Статья принята к печати:** 17.12.2022 **Опубликована онлайн:** 28.12.2022

DOI: 10.24075/vrgmu.2022.061

Preeclampsia (PE) is a multisystem complicating disease that develops in 3 to 8% of all pregnant women [1] and causes 16–18% of all maternal deaths and 40% of fetal and neonatal deaths [2]. International Society for the Study of Hypertension in Pregnancy (ISSHP) defines PE as hypertension (blood pressure above 140/90 mm Hg) developing after 20 weeks of pregnancy, combined with proteinuria (at least 0.3 g/l per day) or signs of acute renal failure, liver dysfunction, neurological disorders, hemolysis or thrombocytopenia, or intrauterine growth retardation. PE may be early and late, depending on the time of onset of clinical symptoms (before or after the 34th week of pregnancy, respectively) [3] [https://cr.minzdrav.gov.ru/schema/637_1]. Early-onset PE is characterized by the most severe course and accounts for 5–20% of all types of PE. For the fetus, the detrimental effect associated with PE comes from chronic hypoxia, intrauterine growth retardation (a highly frequent consequence); the subsequent complications are linked to prematurity and include respiratory distress syndrome, infectious and inflammatory diseases, intraventricular hemorrhages, cerebral palsy, cognitive retardation, autism, psychomotor, behavioral disorders and/or learning disabilities [4, 5].

Maternal and/or placental factors play a fundamental role in the pathogenesis of PE, which determines the time of onset of clinical manifestations of the condition and their severity. Placental factors include impaired proliferation and differentiation of trophoblast cells at the pre-implantation stage in case the embryonic program runs with errors, and at subsequent stages of implantation if there are inflammation-driven changes in the decidual layer that affect interactions between trophoblast and endometrial cells [6–8]. Impaired cell differentiation of the extravillous trophoblast leads to insufficient remodeling of the spiral uterine arteries: first, in the decidual segment before the 10th week of pregnancy in the form of reduced arterial obstruction by endovascular trophoblast cells, which translates into damage to the placental villi by reactive oxygen and nitrogen species [9], and then in the segments of the myometrium from the 16th to the 18th week of pregnancy [10]. The result of abnormal restructuring of the uterine arteries is increased resistance of the uterine arteries, mechanical damage to the placental villi due to increased pressure of blood entering the intervillous space [11–14], and, as a result, hypoxic/ischemic changes in the placental tissue due to the impaired uteroplacental blood flow [1, 15]. Placenta suffering ischemia releases various biological factors that damage vascular endothelium and trigger acute multiple organ failure in the mother. PE is linked to such changes in the level of placental factors circulating in the blood as decreased concentrations of pregnancy-associated plasma protein A (PAPP-A) and placental growth factor (PIGF), as well as to the increase of formation of soluble fms-like tyrosine kinase-1, level of vascular endothelial growth factor A (VEGF-A), inhibin A, activin A, procoagulant P-selectin, pro-inflammatory interleukin 2 and tumor necrosis factor alpha, etc. [1, 16–18]. Maternal pathogenetic factors include genetic predisposition, immunological factors, chronic diseases in the mother (metabolic syndrome, diabetes mellitus, chronic arterial hypertension), which can contribute to the regulation of the placentation process, as well as aggravate the maternal susceptibility to the factors secreted by ischemic placental tissue, which accelerates the onset of clinical symptoms in the mother [19].

Looking for reasons behind temporal differences in manifestation of the clinical symptoms of PE, researchers have compared the profiles of DNA methylome of trophoblast cells, placental transcriptome and maternal proteome peculiar

to early and late PE cases [20]. Other studies revealed that in women with PE, blood serum secretome may trigger stress of trophoblast's endoplasmic reticulum (ER), i.e., functional overload of the protein secretion apparatus resulting from faults in the folding of protein molecules [21]. Moreover, the degree of activation of the misfolded proteins utilization system differs in early and late PE cases [22, 23].

Thus, a thorough analysis of changes in the placental secretome will allow understanding the differences in the pathogenesis of early- and late-onset PE. In our previous study [24], we found a decrease in the level of the secretory form of clusterin in blood plasma of women with placenta accreta, a pregnancy complication characterized by excessive invasion of trophoblast cells and an increased level of angiogenic factors, i.e., processes radically opposite to those observed in PE. Clusterin is an intra- and extracellular chaperone. It plays an important role in stress-induced protein homeostasis (proteostasis); its activity depends on the degree of glycosylation in the ER [25, 26]. Clusterin is expressed in many tissues of a human body, including cells of cytotrophoblast, syncytiotrophoblast, and extravillous trophoblast [27]. Clusterin is known to inhibit the epithelial-mesenchymal transition during phenotypic transformation of trophoblast cells, which lowers their migration and invasion by suppressing the expression of matrix metalloproteinase 9 and vimentin and increasing the expression of E-cadherin [27]. Under physiological conditions, clusterin is mainly secreted into the extracellular space after post-translational modification in the ER and Golgi apparatus, then it binds with misfolded proteins into aggregates that are internalized by receptor-mediated endocytosis and then sent to autophagosomes for degradation. When ER is under stress (e.g., as a consequence of oxidative stress), clusterin is released therefrom into cytosol to create aggregates with misfolded proteins, which are transported directly to proteasomes for degradation [28]. The pronounced expression of ER stress markers leads to activation of signaling pathways involved in inflammation and apoptosis, which support the accumulation of misfolded protein molecules and exacerbate the pathological process.

Since clusterin participates in the processes induced by stress of the ER, which manifests vividly in PE, and because of the specifics of clusterin expression in trophoblast cells and it having a secretory form, we designed and conducted this study, which aimed to evaluate the significance of secretory clusterin found in different fractions of blood serum of women (vesicular and extravesicular) for prediction of development of early or late PE during the first trimester of pregnancy.

METHODS

All patients that participated in this study applied to the V. I. Kulakov National Medical Research Center for Obstetrics, Gynecology and Perinatology for pregnancy follow-up.

The first cohort of patients included 40 pregnant women aged 27–40 years who underwent a set of examinations as part of the first trimester screening routine. They formed four groups (Table 1): 1) 10 women at low risk of developing PE (according to the Astraia screening done in the first trimester) whose pregnancy was normal and who gave birth to full-term babies; 2) 9 women at high risk of developing PE whose pregnancy was normal and who gave birth to full-term babies; 3) 10 women at high risk of developing PE, with condition manifestations at pregnancy weeks 34–37; 4) 11 women at high risk of developing PE, with condition manifestations at pregnancy weeks 25–33.

Table 1. Clinical characteristics of the first cohort patients, all groups, screened in the first trimester of pregnancy

	Normal, N (n = 10)	Normal, at high risk of developing PE, Nhr (n = 9)	Late-onset preeclampsia, IPE (n = 10)	Early-onset preeclampsia, ePE (n = 11)
First pregnancy trimester screening				
Gestational age	12.5 (12.0; 13.4)	12.1 (11.2; 13.1)	12.2 (11.6; 12.5)	12.0 (11.2; 12.4)
Crown rump length, CRL (43.0–84.0 mm)	62.5 (54.0; 74.7)	59.1 (50.0; 69.0)	59.6 (55.1; 64.0)	57.4 (50.0; 62.0)
Nuchal translucency thickness, NT (1.6–1.7 mm)	1.4 (1.1; 2.2)	1.5 (1.0; 2.0)	1.6 (1.3; 2.0)	1.7 (1.1; 2.9)
Uterine artery pulsatility index, UA (PI), 0.9–2.6 (5 th and 95 th percentiles)	1.6 (0.4; 2.2)	1.8 (1.2; 2.5)	1.7 (0.7; 2.4)	2.1 (1.3; 3.5)
UA (PI) MoM	0.9 (0.3; 1.3)	1.1 (0.8; 1.4)	1.0 (0.4; 1.5)	1.1 (0.3; 2.1)
b-hCG (50.0–55.0 IU/ml)	68.7 (52.3; 89.8)	47.1 (23.1; 114.6)	36.4 (27.8; 53.6)	43.4 (15.6; 94.3)
b-hCG (0.5–2.0 MoM)	1.5 (1.1; 2.3)	1.1 (0.4; 2.5)	0.8 (0.5; 1.6)	0.9 (0.3; 1.7)
PAPP-A (0.7–6.0 IU/L)	3.1 (1.6; 6.9)	2.4 (1.1; 4.2)	2.7 (0.6; 5.0)	2.4 (0.8; 6.2)
PAPP-A (0.5–2.0 MoM)	1.2 (0.5; 3.2)	1.2 (0.4; 2.4)	0.9 (0.4; 2.7)	1.1 (0.5; 2.9)
Delivery				
Gestational age	38.6 (36.0; 40.6)	37.7 (31.0; 40.2)	37.3 (35.4; 38.5)	31.9 (28.2; 35.6)
Alanine-aminotransferase, ALT (up to 31.0 U/l)	31.8 (8.8; 95.0)	24.1 (11.8; 46.1)	34.2 (12.4; 165.1)	78.2 (11.8; 352.2)
Aspartate aminotransferase, AST (up to 31.0 U/l)	19.7 (11.1; 25.5)	24.3 (13.0; 40.5)	48.9 (10.9; 262.3)	68.7 (13.6; 282.4)
Alkaline phosphatase (up to 239.0 U/l)	182.3 (130.8; 292.6)	130.2 (94.2; 183.0)	208.8 (154.3; 319.6)	119.8 (87.1; 169.2)
Lactate dehydrogenase, LDH (130.0–220.0 U/l)	345.6 (271.0; 408.2)	362.2 (296.8; 422.2)	435.8 (36.4; 743.1)	598.7 (351.4; 1680.0)
BP systolic (20 to 40 years: 120–127 mm Hg)	118 (90; 140)	135 (105; 170)	140 (127; 160)	152 (140; 170)
BP diastolic (75–80 mm Hg)	77 (60; 90)	86 (70; 110)	91 (80; 105)	98 (90; 110)
Protein level in urine (0.0–0.2, g/l)	0.1 (0.1; 0.1)	0.1 (0.0; 0.1)	0.4 (0.2; 0.9)	2.1 (0.2; 3.4)
Peripheral blood leukocytes (4.0–9.0 thou/mm ³)	9.5 (5.2; 15.6)	8.8 (7.8; 10.5)	10.8 (7.7; 24.4)	11.5 (3.3; 23.2)
Platelets of peripheral blood (150–390 thou/mm ³)	261.8 (201.0; 390.0)	209.9 (146.0; 287.0)	210.1 (93.0; 300.0)	203.5 (82.0; 359.0)
PLGF (250–1200 pg/ml)	115.3 (94.4; 143.8)	74.9 (43.2; 113.4)	83.6 (34.2; 152.0)	56.8 (22.2; 109.7)
sFLT-1 (950–2800 pg/ml)	6271.0 (5168.0; 7763.0)	11895.6 (5190.0; 19418.0)	9651.7 (4027.0; 14131.0)	10722.8 (5216.0; 19738.0)
sFLT-1/ PLGF	54.4 (53.9; 54.8)	173.4 (107.3; 430.1)	129.4 (66.8; 233.6)	285.4 (48.8; 636.2)
Edema of legs and feet (number of patients)	3	1	4	5
Full-term fetus weight, 3200–3500 g	3396.5 (2880.0; 3952.0)	2764.4 (780.0; 3550.0)	2744.9 (2132.0; 3518.0)	1424.2 (900.0; 2582.0)
Placenta weight at full-term pregnancy, 390–415 g	463.1 (303.0; 650.0)	324.4 (106.0; 449.0)	370.3 (257.0; 465.0)	230.2 (119.0; 371.0)
Mean uterine artery PI (39 th week, 5 th and 95 th percentiles: 0.47–0.91)	0.6 (0.5; 0.7)	0.8 (0.5; 1.7)	0.9 (0.6; 1.1)	1.2 (1.0; 1.5)
Umbilical artery PI (39 th week, 5 th and 95 th percentiles: 0.76–1.03)	0.8 (0.6; 1.4)	1.1 (0.7; 2.3)	0.9 (0.7; 1.0)	1.4 (0.8; 1.8)
Middle cerebral artery PI (39 th week, 5 th and 95 th percentiles: 0.93–1.73)	1.4 (1.2; 1.7)	1.4 (1.2; 1.6)	1.3 (0.6; 1.7)	1.6 (1.1; 2.4)
Cerebro-placental ratio, > 1	1.8 (1.1; 2.5)	1.4 (0.6; 2.0)	1.5 (1.1; 2.3)	1.3 (0.8; 1.9)

Note: all data except for "edema of legs and feet" are given as means (minimum; maximum).

The second cohort included 27 pregnant women aged 25–38 years who delivered by caesarean section. They formed four groups (Table 2): 1) 6 women with full-term normal pregnancy (37–39 weeks); 2) 7 women with placenta previa and premature rupture of membranes at 25–31 weeks of gestation without clinical manifestations of preeclampsia; 3) 7 women with early-onset preeclampsia (pregnancy weeks 25–30); 4) 7 women with late-onset preeclampsia (weeks 36–38).

The exclusion criteria for both cohorts were as follows: pregnancy through assisted reproductive technology application, multiple pregnancy, aggravated somatic history of the woman, fetal aneuploidy. The participants underwent the following examinations/tests: blood examination (clinical and biochemical), ultrasonography of pelvic organs and the fetus, Doppler imaging of fetoplacental circulation, cardiotocography, blood pressure measurement, urine protein test, determination of the concentration of PLGF, sFlt-1, PAPP, β -hCG in serum blood.

Blood serum (800 μ l) of each patient from the first cohort was centrifuged for 10 minutes at 300 g at 4 °C, and the supernatant was re-centrifuged for 10 min at 3000 g at

4 °C to remove impurities from blood cells. Purified serum (200 out of 700 μ l) was used for RNA isolation with the help of the miRNeasy Serum/Plasma kit (Qiagen; Germany) with preliminary addition of 5.6×10^8 copies of synthetic cel-miR-39 RNA (Qiagen; Germany) after serum incubation with phenol mixture Qiazol to control the efficiency of RNA extraction and cDNA synthesis as recommended by the manufacturer. Seven μ l of the RNA eluate were used for reverse transcription done with the miScript II RT Kit (Qiagen; Germany) as recommended by the manufacturer. The synthesized cDNA (2 μ l) served as a template for real-time PCR analysis that employed a sense primer specific to the studied miRNA (miR-320a-3p, MIMAT0000510, 5'-aaaagctgggttgagagggcga, annealing temperature with template 59.5°C; miR-17-5p, MIMAT0000070, 5'-caaagtgctacagtcaggtag, 55°C; miR-25-3p, MIMAT0000081, 5'-cattgcactgtctcggctga, 56°C; miR-92a-3p, MIMAT0000092, tattgcactgt, °Cgg06tcc), cel-miR-39 (miScript Primer Assay, Ce_miR-39_1, 55°C; Qiagen; Germany), and miScript SYBR Green PCR Kit (Qiagen; Germany) containing miScript Universal Primer (antisense) and PCR mix SYBR Green PCR MasterMix. The PCR reaction conditions were as

Table 2. Clinical characteristics of the second cohort patients, normal and complicated pregnancy groups

	Normal pregnancy		Complicated pregnancy	
	Planned caesarean section	Emergency caesarean section because of the risk of early pregnancy failure	Caesarean section because of early preeclampsia	Planned caesarean section because of late preeclampsia
Group of pregnant women (number of patients)	I (6). <i>n</i> > 34	II (7). <i>n</i> < 34	III (7). ePE	IV (7). IPE
Preeclampsia manifestation time (weeks)	No	No	24.5 (22.0; 28.0)*	36.1 (36.0; 37.0)*
Delivery time (weeks)	38.0 (37.0; 39.0)*	29.0 (25.0; 32.0)*	28.2 (25.0; 30.0)*	36.9 (36.0; 38.0)*
Severe preeclampsia (number of people)	0	0	7	1
Mild preeclampsia (number of people)	0	0	0	6
Edema of legs and feet (number of people)	0	0	1	5
Urine protein level (0.0–0.2 g/l)	Normal	Normal	2.3 (0.2; 4.6)*	1.4 (0.1; 4.1)*
Blood pressure – systolic – diastolic	112 (107; 119)* 68 (65; 71)*	116 (112; 120)* 77 (74; 81)*	155 (125; 180)* 100 (80; 120)*	144 (120; 175)* 93 (70; 100)*
ALT (up to 31.0 U/l)	No data	No data	74 (11; 215)*	23 (12; 32)*
AST (up to 31.0 U/l)	No data	No data	55 (11; 194)*	29 (16; 48)*
Alkaline phosphatase (up to 239.0 U/l)	No data	No data	110 (54; 179)*	165 (79; 252)*
Platelets of peripheral blood (150–390 thou/mm ³)	228 (166; 290)*	238 (183; 293)*	145 (68; 243)*	238 (181; 308)*
PLGF (250–1200 pg/ml)	No data	No data	30 (14; 47)*	101 (54; 216)*
sFLT-1 (950–2800 pg/ml)	No data	No data	11957 (5615; 23226)*	14657 (7489; 24990)*
sFLT-1/ PLGF	No data	No data	444 (126; 847)*	193 (42; 348)*

Note: * — the data are given as means (minimum; maximum) registered at admission to the hospital.

follows: 15 min at 95 °C, subsequent 40 cycles (15 s at 94 °C, 30 s at the primer annealing temperature, and 30 s at 70 °C) in a StepOnePlus™ amplifier (Applied Biosystems; USA). The relative level of cDNA expression was estimated by the ΔCt method, where $\Delta Ct = (Ct)_{si} - (Ct)_{ri}$, where $(Ct)_{si}$ is the value of the threshold amplification cycle for cDNA of miRNA analyzed in the sample; $(Ct)_{ri}$ is the value of the threshold amplification cycle for cDNA of the reference cel-miR-39 RNA in the sample.

The remaining 500 μ l of purified blood serum from the first cohort patients were used to isolate microvesicles using the miRCURY Exosome Kits (Qiagen; Germany), the process involving addition of 200 μ l of a precipitating solution and 14-hour incubation at 4 °C, followed by centrifugation at 1500 g for 30 min at 20 °C. The supernatant was collected in a clean tube, diluted 100-fold with addition of Laemmli Sample Buffer (#1610737, BioRad; USA) with 5% (v/v) 2-mercaptoethanol (Am-O482-0.1, VWR Life Science AMRESCO; USA) and used for Western blotting. Two hundred and seventy μ l of resuspension buffer were added to the precipitate containing the vesicles; the final 1000-fold dilution of the vesicles supplemented with Laemmli Sample Buffer (#1610737, BioRad; USA) with 5% (v/v) 2-mercaptoethanol (Am-O482-0.1, VWR Life Science AMRESCO; USA) was used for Western blotting.

Samples of the placental tissue collected from the second cohort patients no later than 10 minutes after delivery were tissue sections 5 mm thick that presented all layers of the placenta and included both the fetal and maternal parts thereof from the chorionic plate to the decidua. The collected placental tissue samples were washed in 0.9% NaCl and instantly frozen in liquid nitrogen for subsequent storage at –80 °C. The tissue was ground to a powder in liquid nitrogen vapor; 10 mg of the tissue were lysed in RIPA

Lysis Buffer System (sc-24948, Santa Cruz; USA). After incubation on ice for 30 min and centrifugation of the lysate at 10,000 g, we measured the concentration of soluble protein fraction with the help of the biuret method and a NanoDrop One spectrophotometer (ThermoScientific; USA). For subsequent Western blotting analysis, we took 40 μ g of protein from each sample.

Western blotting was used to quantify the level of the secretory clusterin's alpha subunit in peripheral blood serum (first cohort) and placenta (second cohort). Before fractionation in a 10% polyacrylamide gel in hydroxymethylaminomethanetricine buffer (100 mM hydroxymethylaminomethane, 100 mM tricine, 0.1% sodium dodecyl sulfate), the samples were denatured at 70 °C for 10 min in Laemmli Sample Buffer (#1610737, BioRad; USA) containing 5% (v/v) 2-mercaptoethanol (Am-O482-0.1, VWR Life Science AMRESCO; USA). To determine molecular weight of the analyzed protein we introduced a PageRuler protein molecular weight marker, 10–250 kDa (#26619, Thermo Fisher Scientific; USA), into each PAAG well. When electrophoresis was over, the proteins were moved to a nitrocellulose membrane (0.45 μ m, BioRad; USA), the transfer done semi-dry with 10 mM 3-cyclohexylamino-1-propanesulfonic acid (SW18805, Sigma-Aldrich; USA), pH 10.5, 10% ethanol. After membrane blocking in 5% skimmed milk (Blotting-Grade Blocker, #1706404, BioRad; USA), 0.1% Tween20 (#1706531, BioRad; USA), 50 mM Tris (T4661, Sigma; USA), pH 7.5, 150 mM NaCl (A1371, AppliChem Panreac ITW Companies; Germany) for 2 h, we incubated it for 1 h with primary antibodies to the clusterin's alpha subunit at a dilution of 1 : 400 (B-5, sc-5289, Santa Cruz Biotechnology; USA), or to actin at a dilution of 1 : 400 (H-6, sc-376421, Santa Cruz Biotechnology; USA), in 5% skim milk, 0.1% Tween20, 50 mM Tris, pH 7.5, 150 mM NaCl, washing the membrane three

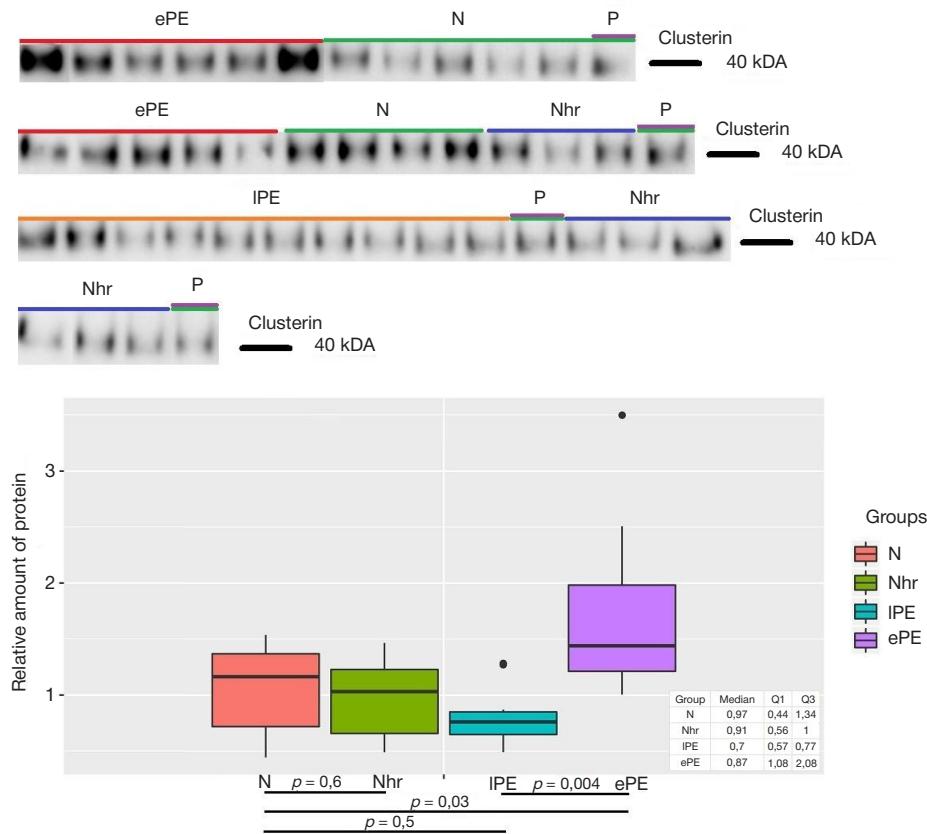


Fig. 1. Western blotting of clusterin in the vesicular fraction of blood serum of patients from the first cohort, 12th week of pregnancy

times for 5 min in 0.05% Tween20, 50 mM Tris, pH 7.5, 150 mM NaCl, and then incubated for 1 hour with secondary polyclonal antibodies conjugated to horseradish peroxidase at a dilution of 1 : 2000 (HAF007, R&D Systems; USA) in 1% skim milk, 0.1% Tween20, 50 mM Tris, pH 7.5, 150 mM NaCl. After washing the membrane three times for 5 min in 0.05% Tween20, 50 mM Tris, pH 7.5, 150 mM NaCl, peroxidase activity was measured by adding Clarity Max™ Western ECL Substrate (#1705062, BioRad; USA) and detecting chemiluminescence in the ChemiDoc MP gel documentation system (#12003154, BioRad; USA).

Statistical analysis of the data

Microsoft Excel and RStudio (Posit; USA) software were used for the purposes of statistical processing of the data. When the distribution did not obey the normal distribution law, we used the pairwise Mann–Whitney tests to do the statistical analysis. When the distribution of attributes differed from normal, they were described as a median (Me) and quartiles Q_1 and Q_3 in the Me (Q_1 ; Q_3) format. The significance threshold value was adopted at $p = 0.05$. The differences were considered significant at $p < 0.05$. To assess the possibility of classifying patients into groups based on the data obtained, we developed logistic regression models and verified their quality with the help of a ROC curve and sensitivity and specificity calculations.

RESULTS

Analysis of the content of secretory clusterin in the blood serum of patients of the first cohort

At the first stage of the study, we applied Western blotting with primary antibodies to the alpha subunit of the protein to retrospectively quantify secretory clusterin in the blood serum

of the patients. At that time, on average, they were at the 12th week of pregnancy. Depending on the outcome of pregnancy, patients of the first cohort (Table 1) were divided into four groups (see "Patients and methods"). The miRCURY Exosome Kit (Qiagen; Germany), the action of which relies on precipitation in the presence of polyethylene glycol, allowed obtaining two fractions of blood serum: vesicular fraction, which included microvesicles, exosomes, apoptotic bodies, and a vesicle-free fraction (supernatant). Fig. 1 shows the results of the blood serum's vesicular fraction analysis. Top part of the figure contains blots with chemiluminescent bands representing 40 kDa clusterin alpha subunit as registered in samples collected in the N (normal), Nhr (normal, high risk of PE) groups (according to the Astraia screening results), and ePE and IPE groups. In order to register the efficiency of protein transfer from gel to membrane and record differences in exposure during imaging in the gel-documenting system, we applied a reference sample (P) from the N group to one of the wells of each gel (same sample in all cases), thus enabling comparison of the chemiluminescence values in every sample. Compared to the N group, ePE group exhibited a significant ($p = 0.03$) two-fold increase in the level of secretory clusterin in the vesicular fraction of blood serum of patients in the first trimester of pregnancy, as indicated in the diagram of Figure 1. As for the IPE group, it did not differ significantly from the N group in terms of the level of secretory clusterin in blood serum's vesicular fraction.

Using the Spearman's rank correlation coefficient, we revealed an inverse correlation between the level of secretory clusterin in the blood serum's vesicular fraction and CRL ($r = -0.31$; $p = 0.052$), as well as a direct correlation between the level of this clusterin and the value of β -hCG in the blood serum ($r = 0.28$; $p = 0.082$) of women at the 12th week of pregnancy.

Fig. 2 presents the results of Western blotting aimed at establishing the level of secretory clusterin's alpha subunit in the

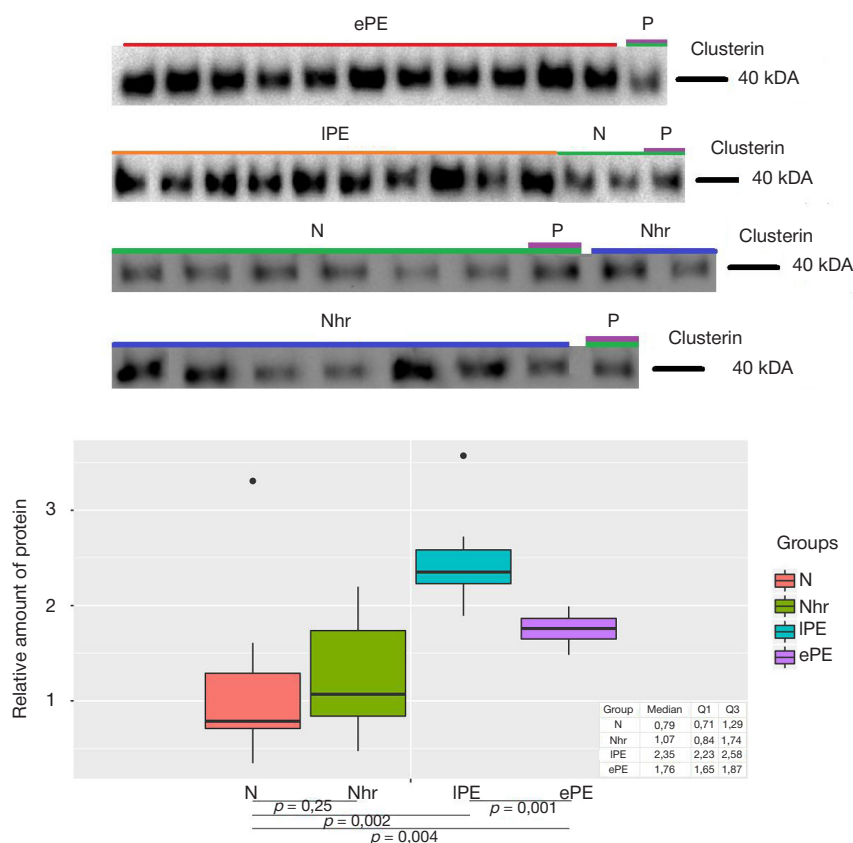


Fig. 2. Western blotting of clusterin in the vesicle-free fraction of blood serum of patients from the first cohort, 12th week of pregnancy

vesicle-free fraction of blood serum. As the diagram of Fig. 2 shows, compared to the N group, ePE and IPE groups ($p = 0.004$ and $p = 0.002$, respectively) exhibited a significant increase of the level of secretory clusterin (40 kDa) in the blood serum's extravascular fraction (samples collected during the 1st trimester of pregnancy), this increase being 2.2-fold and 3-fold, respectively. Moreover, for IPE the level of clusterin in the extravascular fraction was 1.5 times higher than for ePE ($p < 0.001$). As for the comparison of N and Nhr groups, we found no significant differences in the level of secretory clusterin in vesicular and extravascular fractions of the blood serum (Fig. 1 and 2).

Using the Spearman's rank correlation coefficient, we revealed an inverse correlation between the level of secretory clusterin in the blood serum's vesicle-free fraction and β -hCG MoM ($r = -0.3$; $p = 0.0627$).

Quantification of miR-25-3p, miR-92a-3p, miR-320a and miR-17-5p in the blood serum of the first cohort patients

According to data from miRWalk, miRanda, RNA22, and Targetscan databases, the potential regulators of the clusterin expression level are miR-320a, miR-30a-5p, miR-17-5p, miR-21-5p, miR-30c-5p, miR-1323, miR-25-3p, miR-138-5p, miR-34a-5p, miR-92a-3p. In a study investigating the relationship between the levels of clusterin and miRNAs regulating it in placenta accreta cases [24], we found significant inverse correlations between the content of secretory clusterin in the peripheral blood plasma of pregnant women, with the values being " $-\Delta Ct$ " miR-25-3p, miR-92a-3p, miR-320a, miR-17-5p at the time of delivery. Due to the fact that trophoblastic cells in placenta accreta and preeclampsia cases have directly opposite invasive properties, it seemed interesting to us to trace the possible relationships between miRNA data and clusterin in the blood serum of patients from the first cohort at 11–14 weeks

of pregnancy. The values of the relative content of miR-25-3p, miR-92a-3p, miR-320a, miR-17-5p in the serum of pregnant women were obtained using the method of quantitative real-time RT-PCR as " $-\Delta Ct$ " values (see "Patients and methods"). Spearman's rank correlation method revealed a statistically significant positive correlation between the content of secretory clusterin in the extravascular fraction of blood serum of pregnant women and the miR-17-5p " $-\Delta Ct$ " value ($r = 0.34$; $p = 0.0356$) of blood serum. It should be noted that, according to the miRTargetLink 2.0 database (<https://ccb-compute.cs.uni-saarland.de/mirtargetlink2/network/a7aa6e41-7676-4e3b-875c-43c926dedae5>), clusterin is an experimentally proven target for miR-17-5p.

Spearman's rank correlation method revealed statistically significant positive correlations between blood serum " $-\Delta Ct$ " miR-16-5p and uterine artery pulsation index (UA (PI): $r = 0.37$, $p = 0.021$; UA (PI) MoM: $r = 0.32$, $p = 0.046$). In turn, inverse relationships were found between the uterine artery pulsation index and pregnancy-associated plasma protein A (UA (PI) and PAPP-A: $r = -0.41$; $p = 0.01$; UA (PI) MoM and PAPP-A MoM: $r = -0.35$, $p = 0.0296$).

Evaluation of the probability of development of early- and late-onset PE by the level of secretory clusterin in two fractions (vesicular and extravascular) of the blood serum of women in the first trimester of pregnancy

Based on the values of the content of secretory clusterin in the blood serum of women in the first cohort (Table 1), who underwent screening in the first trimester of pregnancy, we built logistic regression models to calculate the probability of development of early and late PE (Fig. 3).

It was found that the best prognostic accuracy (with high specificity and sensitivity) is provided by the models built to

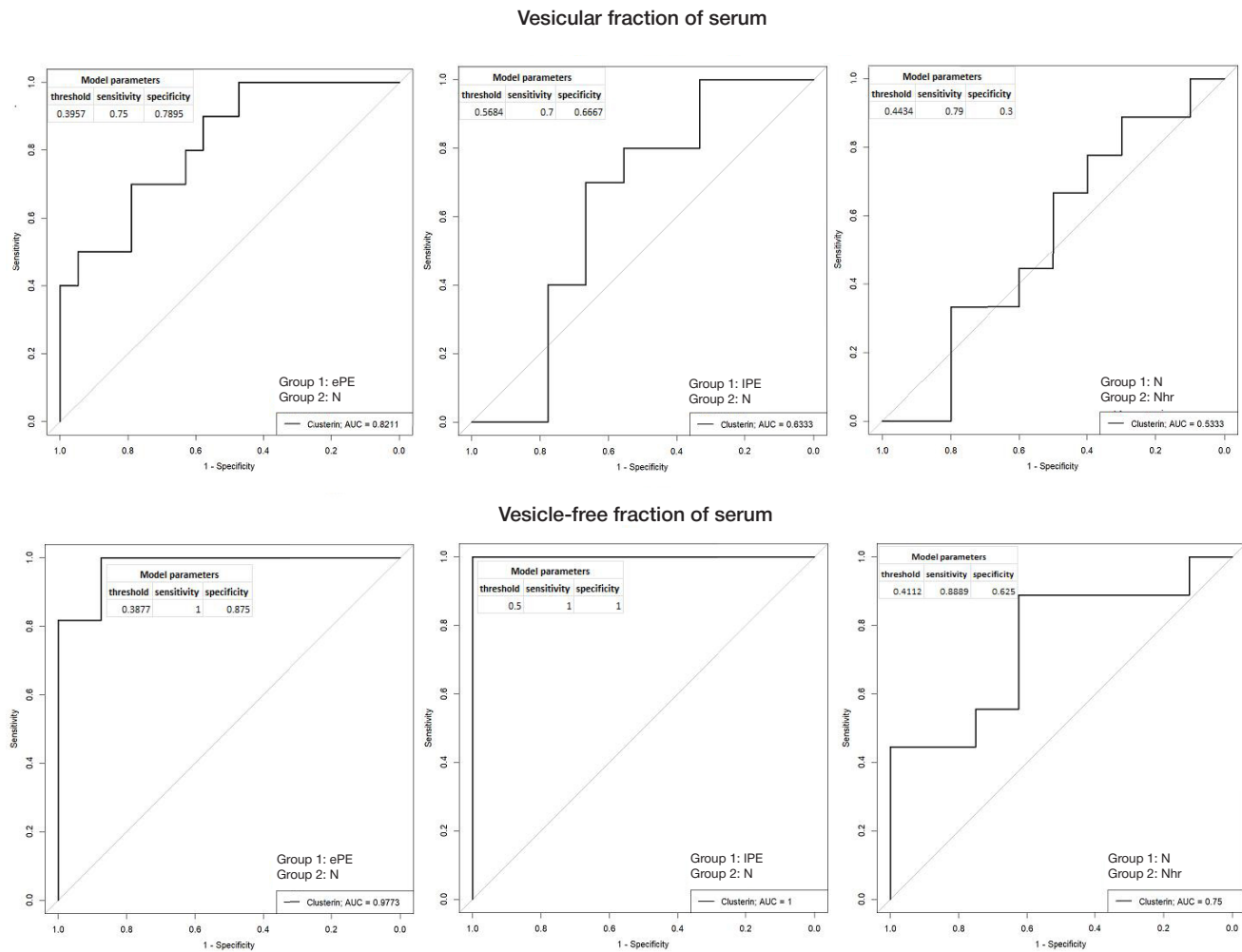


Fig. 3. Logistic regression models predicting development of ePE and IPE by the level of secretory clusterin in the vesicular and vesicle-free fractions of serum collected from the patients at 12th week of pregnancy

assess probability of occurrence of clinical manifestations of ePE and IPE after the 20th week of pregnancy, three assessment based on the level of secretory clusterin in the vesicle-free fraction of the blood serum of patients (but not in the vesicular fraction) by 11–14 weeks of pregnancy. The formulas for calculating the probability of development of early PE (formula 1) and late PE (formula 2) are given below:

$$\frac{1}{1 + e^{15.71 - 10.9x}} \quad (1)$$

$$\frac{1}{1 + e^{267.11 - 152.58x}} \quad (2)$$

Analysis of the content of secretory clusterin in placental tissue collected from the second cohort patients at the time of delivery

The second cohort of patients was analyzed to identify secretory clusterin in placental tissue collected from women suffering ePE and IPE, the analysis including comparison with groups of the corresponding gestational age (N < 34 weeks, N > 34 weeks) without signs of PE (Table 2). The chemiluminescence data obtained for clusterin were correlated with the chemiluminescent signal from actin registered in the same sample. Comparing to the N group, we found a significant decrease in the level of secretory clusterin with a molecular weight of 40 kDa in the placenta from women that had PE, the decrease being 2.3-fold for ePE (p = 0.001) and 2.6-fold for IPE (p = 0.013), as shown on the diagram in Fig. 4.

DISCUSSION

In the present study, we decided to focus on quantification of the secretory clusterin in blood serum collected from women at the 11–14th weeks of pregnancy; the goal was to identify possible differences in the pathogenesis of ePE and IPE, which could form the basis of mathematical models enabling prediction of these complications in the first trimester before PE starts to clinically manifest itself.

We established that, compared to normal pregnancy, both ePE and IPE cause a significant increase in the level of secretory clusterin (40 kDa) in the extravascular fraction of the blood serum of patients in the first trimester of pregnancy (two-fold and three-fold increase, respectively). Despite a more pronounced increase in the level of clusterin secretion in case of IPE (compared to ePE), the total amount of secretory clusterin circulating in the blood serum in ePE cases is much greater than that in IPE patients because of the vesicular fraction, where the level of clusterin is 2.7 times higher in ePE in compared to IPE. Moreover, since there were 10 times more vesicular fraction of blood serum than extravascular fraction taken for Western blotting, it can be concluded that clusterin is more functionally important in the composition of extracellular vesicles circulating in the blood in ePE cases compared to IPE cases.

The data obtained in the present work on the increase of the level of clusterin in the peripheral blood of pregnant women with PE are consistent with the results of a study that used semi-quantitative nano LC/MS and found a statistically

significant increase in the level of clusterin in the blood serum of women at the 10–20th week of pregnancy, followed by the development of hypertensive disorders after the 20th gestational week [29]. However, in that work, pregnant women with ePE were not analyzed: it only included two groups of patients, with IPE and with hypertensive disorders without proteinuria. In other studies, analysis of blood plasma of pregnant women at the time of delivery revealed a statistically significant increase in the level of clusterin in the group of women with PE relative to the group of women with normal pregnancy [30, 31]; moreover, pregnant women with PE in combination with fetal growth retardation had a more significant increase in clusterin levels than pregnant women with PE with normal fetometric parameters [31]. The induction of clusterin synthesis during PE may be caused by the promoter region holding the gene encoding it in the binding sites for such factors as SP1, NF1, AP-1, HSF1, YB-1, p53, B-MYB, the level of which under conditions of oxidative stress, hypoxia and apoptosis rises sharply [32–35]. In turn, clusterin regulates the activity of the transcription factor NF- κ B, which plays an important role in cell viability, their motility, proliferation, phenotypic transformation and inflammation [36]. Besides, the expression of clusterin, like any other protein, can be regulated at the post-transcriptional level by miRNA. In this work, quantification of potential regulators of clusterin expression (miR-25-3p, miR-92a-3p, miR-320a-3p and miR-17-5p) in the blood serum of women in the first trimester of pregnancy revealed a significant correlation between the secretory clusterin content in blood serum's extravesicular fraction and the miR-17-5p " $-\Delta$ Ct" value. One of the articles describes in detail the involvement of miR-25-3p, miR-92a-3p, miR-320a-3p, and miR-17-5p in the induction of the epithelial-mesenchymal transition [37]. It is possible that the participation of these miRNAs in the phenotypic transformation of extravillous trophoblast cells and subsequent remodeling of the uterine artery wall is reflected in the positive correlation we found between " $-\Delta$ Ct" miR-16-5p blood serum of pregnant women and the uterine artery pulsation index (UA (PI): $r = 0,37$, $p = 0.021$; UA (PI) MoM: $r = 0.32$, $p = 0.046$), the values of which were inversely correlated with the level of plasma pregnancy-associated protein A (UA (PI) and PAPP-A: $r = -0,41$, $p = 0.01$; UA (PI) MoM and PAPP-A MoM: $r = -0.35$, $p = 0.0296$).

Since there are three forms of clusterin in eukaryotic cells (nuclear, secretory, and cytosolic) [25], we deemed it interesting to analyze the possible differences between ePE and IPE cases in terms of the level of secretory clusterin (40 kDa) in placental tissue at the time of delivery as compared with placental samples from patients (similar pregnancy term) without signs of PE. We discovered a significant two-fold decrease of clusterin expression in the placental tissue of pregnant women with ePE and IPE. It is possible that the expression of secretory clusterin in the placenta of women with PE is reduced because of the excessive level of its secretion, which we observed in the participants of this study as early as in the first trimester of pregnancy (the participants that subsequently developed PE). Another possible reason is the increased transition of secretory clusterin from the placenta into the maternal blood in case of PE, which is caused by the oxidative stress and hypoxic/ischemic processes in the placental tissue peculiar to this pregnancy complication. First, clusterin enters cytosol from the ER [38–40], then transitions to the maternal bloodstream as part of microvesicles and exosomes, or as part of apoptotic bodies in case of severe syncytiotrophoblast and cytotrophoblast ER stress [1]. It was found that oxidative stress and activation of ER stress markers, as well as the release of placental microvesicles into the bloodstream, are more pronounced in case of ePE than

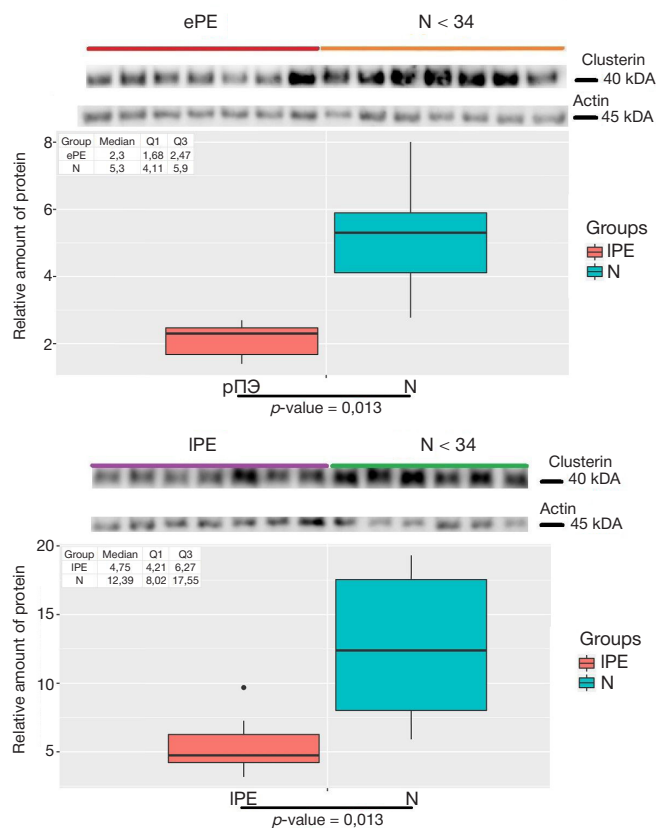


Fig. 4. Western blotting of clusterin in placental tissue at the time of delivery, ePE and IPE groups. The diagrams show the clusterin to actin content ratio

in IPE cases [22, 41]. Moreover, the concentration of exosomes in the woman's blood serum increases only when she suffers ePE but not IPE [42]. In our study, we established that the level of clusterin as part of the vesicles grows significantly in patients with ePE, while there no significant changes in clusterin content in the vesicular fraction of serum in patient with IPE. It was also proven that secretory clusterin in the blood serum of pregnant women can have a negative effect on proliferation, invasion, and survival of the trophoblast cells [27, 29], forming a positive feedback: "ER stress of syncytiotrophoblast cells — an increase in extratrophoblastic clusterin — aggravation of ER stress of syncytiotrophoblast cells and apoptotic/necrotic processes in them — replenishment of the extratrophoblastic clusterin fraction in the maternal circulation".

Since for the two types of PE (early and late) statistically significant changes in the level of secretory clusterin were found in the extra-vesicular fraction of the blood serum of women in the first trimester of pregnancy compared with normal pregnancy, it is advisable to use this fraction to predict the development of PE at the stage of the first pregnancy screening, applying the logistic regression models developed in this study.

CONCLUSIONS

In the context of this study, we developed logistic regression models based on the level of secretory clusterin that allow predicting early and late PE long before the onset of clinical manifestations of any of them. However, before practical application of these models it is necessary to verify the obtained data on a larger sample. New pathogenetic mechanisms of the development of early- and late-onset PE were clarified based on the quantitative analysis of secretory clusterin in two fractions (vesicular and extravascular) of the blood serum of women in the first trimester of pregnancy and in the placental tissue at the time of delivery (Fig. 5).

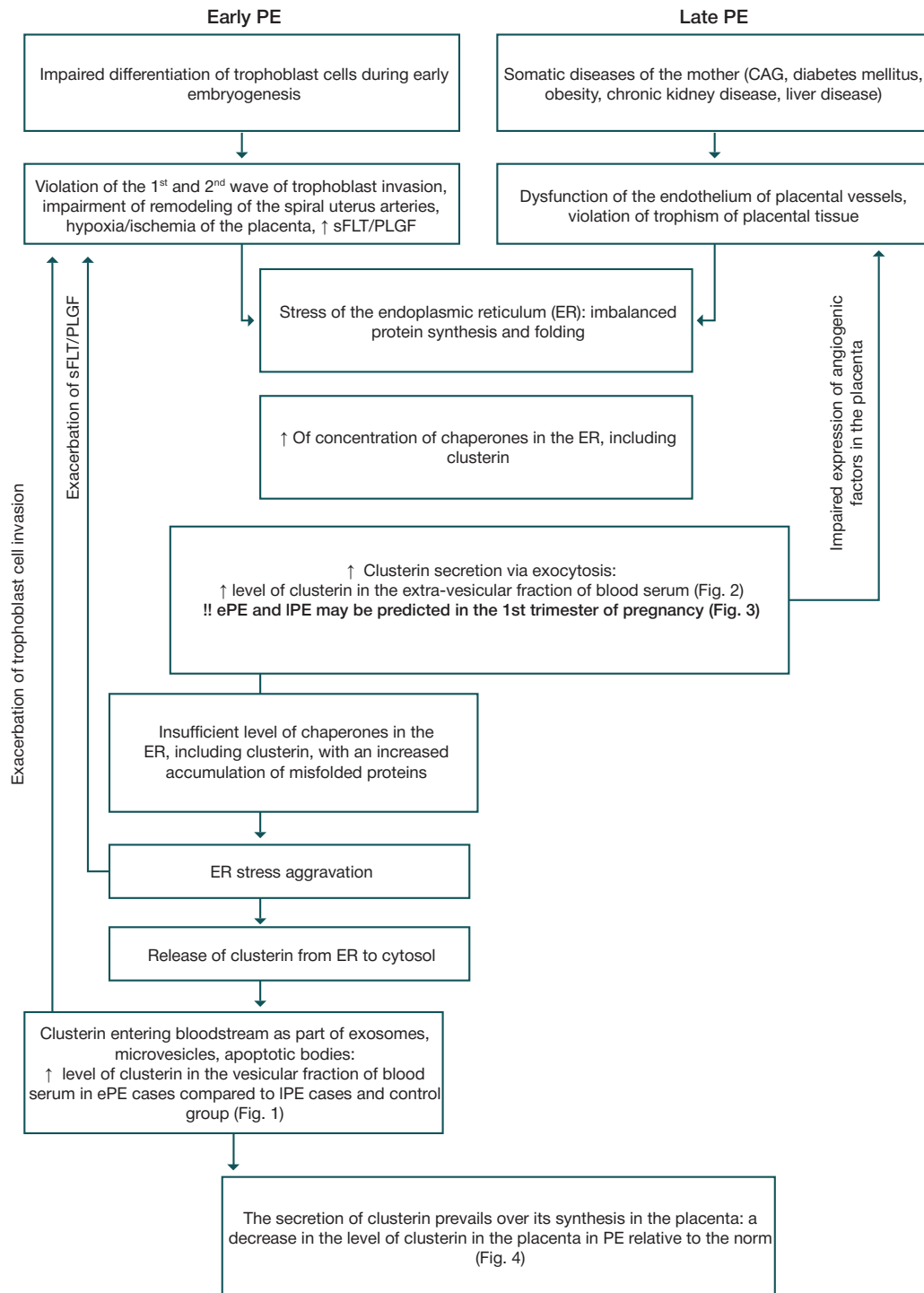


Fig. 5. Schematic representation of the role of secretory clusterin in the pathogenesis of early- and late-onset PE

References

- Burton GJ, Redman CW, Roberts JM, Moffett A. Pre-eclampsia: pathophysiology and clinical implications. *BMJ*, 2019; 366: l2381. DOI: 10.1136/bmj.l2381.
- Ananth CV, Lavery JA, Friedman AM, Wapner RJ, Wright JD. Serious maternal complications in relation to severe pre-eclampsia: a retrospective cohort study of the impact of hospital volume. *BJOG*. 2017; 124: 1246–53. DOI: 10.1111/1471-0528.14384.
- Brown MA, Magee LA, Kenny LC, Karumanchi SA, McCarthy FP, Saito S, et al. The hypertensive disorders of pregnancy: ISSHP classification, diagnosis & management recommendations for international practice. *Pregnancy Hypertens*. 2018; 13: 291–310. DOI: 10.1016/j.preghy.2018.05.004.
- Pierrat V, Marchand-Martin L, Arnaud C, Kaminski M, Resche-Rigon M, Lebeaux C, et al. Neurodevelopmental outcome at 2 years for preterm children born at 22 to 34 weeks' gestation in France in 2011: EPIPAGE-2 cohort study. *BMJ*. 2017; 358: j3448. DOI: 10.1136/bmj.j3448.
- Van Beek PE, Rijken M, Broeders L, Ter Horst HJ, Koopman-

- Esseboom C, de Kort E, et al. Two-year neurodevelopmental outcome in children born extremely preterm: the EPI-DAF study. *Arch Dis Child Fetal Neonatal Ed.* 2022; 107: 467–74. DOI: 10.1136/archdischild-2021-323124.
6. Huppertz B. Placental origins of preeclampsia: challenging the current hypothesis. *Hypertens. (Dallas, Tex. 1979).* 2008; 51: 970–75. DOI: 10.1161/HYPERTENSIONAHA.107.107607.
 7. Garrido-Gomez T, Dominguez F, Quiñonero A, Diaz-Gimeno P, Kapidzic M, Gormley M, et al. Defective decidualization during and after severe preeclampsia reveals a possible maternal contribution to the etiology. *Proc Natl Acad Sci USA.* 2017; 114: E8468–E8477. DOI: 10.1073/pnas.1706546114.
 8. Ruane PT, Berneau SC, Koeck R, Watts J, Kimber SJ, Brison DR, et al. Apposition to endometrial epithelial cells activates mouse blastocysts for implantation. *Mol Hum Reprod.* 2017; 23: 617–27. DOI: 10.1093/molehr/gax043.
 9. Myatt L. Review: Reactive oxygen and nitrogen species and functional adaptation of the placenta. *Placenta.* 2010; 31 Suppl: S66–9. DOI: 10.1016/j.placenta.2009.12.021.
 10. Pijnenborg R, Bland JM, Robertson WB, Brosens I. Uteroplacental arterial changes related to interstitial trophoblast migration in early human pregnancy. *Placenta.* 1983; 4: 397–413. DOI: 10.1016/s0143-4004(83)80043-5.
 11. Burton GJ, Woods AW, Jauniaux E, Kingdom JCP. Rheological and physiological consequences of conversion of the maternal spiral arteries for uteroplacental blood flow during human pregnancy. *Placenta.* 2009; 30: 473–82. DOI: 10.1016/j.placenta.2009.02.009.
 12. James JL, Saghian R, Perwick R, Clark AR. Trophoblast plugs: impact on utero-placental haemodynamics and spiral artery remodelling. *Hum Reprod.* 2018; 33: 1430–41. DOI: 10.1093/humrep/dey225.
 13. Allerkamp HH, Clark AR, Lee TC, Morgan TK, Burton GJ, James JL. Something old, something new: digital quantification of uterine vascular remodelling and trophoblast plugging in historical collections provides new insight into adaptation of the uteroplacental circulation. *Hum Reprod.* 2021; 36: 571–86. DOI: 10.1093/humrep/deaa303.
 14. Staff AC, Fjeldstad HE, Fosheim IK, Moe K, Turowski G, Johnsen GM, et al. Failure of physiological transformation and spiral artery atherosclerosis: their roles in preeclampsia. *Am J Obstet Gynecol.* 2022; 226: S895–S906. DOI: 10.1016/j.ajog.2020.09.026.
 15. Sidorova IS. Solved and unsolved problems of preeclampsia in Russia (Editorial). *Russ Bull Obstet.* 2015; 15: 4–9. DOI: 10.17116/rosakush20151524-9.
 16. Rana S, Burke SD, Karumanchi SA. Imbalances in circulating angiogenic factors in the pathophysiology of preeclampsia and related disorders. *Am J Obstet Gynecol.* 2022; 226: S1019–S1034. DOI: 10.1016/j.ajog.2020.10.022.
 17. Haram K, Mortensen JH, Myking O, Magann EF, Morrison JC. The role of oxidative stress, adhesion molecules and antioxidants in preeclampsia. *Curr Hypertens Rev.* 2019; 15: 105–12. DOI: 10.2174/1573402115666190119163942.
 18. Tomimatsu T, Mimura K, Matsuzaki S, Endo M, Kumasawa K, Kimura T. Preeclampsia: maternal systemic vascular disorder caused by generalized endothelial dysfunction due to placental antiangiogenic factors. *Int J Mol Sci.* 2019; 20. DOI: 10.3390/ijms20174246.
 19. Staff AC. The two-stage placental model of preeclampsia: An update. *J Reprod Immunol.* 2019; 134–135: 1–10. DOI: 10.1016/j.jri.2019.07.004.
 20. Than NG, Romero R, Tarca AL, Kekesi KA, Xu Y, Xu Z, et al. Integrated systems biology approach identifies novel maternal and placental pathways of preeclampsia. *Front Immunol.* 2018; 9: 1661. DOI: 10.3389/fimmu.2018.01661.
 21. Castro KR, Prado KM, Lorenzon AR, Hoshida MS, Alves EA, Francisco RP, et al. Serum from preeclamptic women triggers endoplasmic reticulum stress pathway and expression of angiogenic factors in trophoblast cells. *Front Physiol.* 2021; 12: 799653. DOI: 10.3389/fphys.2021.799653.
 22. Yung HW, Atkinson D, Campion-Smith T, Olovsson M, Charnock-Jones DS, Burton GJ. Differential activation of placental unfolded protein response pathways implies heterogeneity in causation of early- and late-onset pre-eclampsia. *J Pathol.* 2014; 234: 262–76. DOI: 10.1002/path.4394.
 23. Burton GJ, Yung H-W. Endoplasmic reticulum stress in the pathogenesis of early-onset pre-eclampsia. *Pregnancy Hypertens.* 2011; 1: 72–78. DOI: 10.1016/j.preghy.2010.12.002.
 24. Timofeeva AV, Fedorov IS, Pirogova MM, Vasilenko ON, Chagovets VV, Ezhova LS, et al. Clusterin and its potential regulatory microRNAs as a part of secretome for the diagnosis of abnormally invasive placenta: Accreta, Increta, and Percreta Cases. *Life (Basel, Switzerland).* 2021; 11. DOI: 10.3390/life11040270.
 25. Janiszewska E, Kmiecik A, Kacperczyk M, Witkowska A, Kratz EM. The influence of clusterin glycosylation variability on selected pathophysiological processes in the human body. *Oxid Med Cell Longev.* 2022; 2022: 7657876. DOI: 10.1155/2022/7657876.
 26. Zoubeidi A, Gleave M. Small heat shock proteins in cancer therapy and prognosis. *Int J Biochem Cell Biol.* 2012; 44: 1646–56. DOI: 10.1016/j.biocel.2012.04.010.
 27. Zeng S, Pan Y, Liu F, Yin J, Jiang M, Long Y, et al. Role of clusterin in the regulation of trophoblast development and preeclampsia. *Biochem Biophys Res Commun.* 2021; 583: 128–34. DOI: 10.1016/j.bbrc.2021.10.064.
 28. Satapathy S, Wilson MR. The dual roles of clusterin in extracellular and intracellular proteostasis. *Trends Biochem Sci.* 2021; DOI: <https://doi.org/10.1016/j.tibs.2021.01.005>.
 29. Zeng S, Han M, Jiang M, Liu F, Hu Y, Long Y, et al. Serum complement proteomics reveal biomarkers for hypertension disorder of pregnancy and the potential role of Clusterin. *Reprod Biol Endocrinol.* 2021; 19: 56. DOI: 10.1186/s12958-021-00742-z.
 30. Watanabe H, Hamada H, Yamada N, Sohda S, Yamakawa-Kobayashi K, Yoshikawa H, et al. Proteome analysis reveals elevated serum levels of clusterin in patients with preeclampsia. *Proteomics.* 2004; 4: 537–43. DOI: 10.1002/pmic.200300565.
 31. Oztas E, Ozler S, Ersoy AO, Iskender CT, Sucak A, Ergin M, et al. Increased levels of serum clusterin is associated with intrauterine growth restriction and adverse pregnancy outcomes in preeclampsia. *J Perinat Med.* 2016; 44: 269–75. DOI: 10.1515/jpm-2015-0120.
 32. Trougakos IP. The molecular chaperone apolipoprotein J/clusterin as a sensor of oxidative stress: implications in therapeutic approaches — a mini-review. *Gerontology.* 2013; 59: 514–23. DOI: 10.1159/000351207.
 33. Shiota M, Zoubeidi A, Kumano M, Beraldi E, Naito S, Nelson CC, et al. Clusterin is a critical downstream mediator of stress-induced YB-1 transactivation in prostate cancer. *Mol Cancer Res.* 2011; 9: 1755–66. DOI: 10.1158/1541-7786.MCR-11-0379.
 34. Criswell T, Klokov D, Beman M, Lavik JP, Boothman DA. Repression of IR-inducible clusterin expression by the p53 tumor suppressor protein. *Cancer Biol Ther.* 2003; 2: 372–80. DOI: 10.4161/cbt.2.4.430.
 35. Cervellera M, Raschella G, Santilli G, Tanno B, Ventura A, Mancini C, et al. Direct transactivation of the anti-apoptotic gene apolipoprotein J (clusterin) by B-MYB. *J Biol Chem.* 2000; 275: 21055–60. DOI: 10.1074/jbc.M002055200.
 36. Santilli G, Aronow BJ, Sala A. Essential requirement of apolipoprotein J (clusterin) signaling for I κ B α expression and regulation of NF- κ B activity. *J Biol Chem.* 2003; 278: 38214–9. DOI: 10.1074/jbc.C300252200.
 37. Garg M. Targeting microRNAs in epithelial-to-mesenchymal transition-induced cancer stem cells: therapeutic approaches in cancer. *Expert Opin Ther Targets.* 2015; 19: 285–97. DOI: 10.1517/14728222.2014.975794.
 38. Nizard P, Tetley S, Le Dréan Y, Watrin T, Le Goff P, Wilson MR, et al. Stress-induced retrotranslocation of clusterin/ApoJ into the cytosol. *Traffic.* 2007; 8: 554–65. DOI: 10.1111/j.1600-0854.2007.00549.x.
 39. Wilson MR, Zoubeidi A. Clusterin as a therapeutic target. *Expert Opin Ther Targets.* 2017; 21: 201–13. DOI: 10.1080/14728222.2017.1267142.
 40. Rohne P, Prochnow H, Wolf S, Renner B, Koch-Brandt C. The chaperone activity of clusterin is dependent on glycosylation and redox environment. *Cell Physiol Biochem Int J. Exp Cell Physiol Biochem Pharmacol.* 2014; 34: 1626–39. DOI: 10.1159/000366365.

41. Chen Y, Huang Y, Jiang R, Teng Y. Syncytiotrophoblast-derived microparticle shedding in early-onset and late-onset severe preeclampsia. *Int J Gynaecol Obstet Off Organ Int Fed Gynaecol Obstet*. 2012; 119: 234–38. DOI: 10.1016/j.ijgo.2012.07.010.
42. Pillay P, Maharaj N, Moodley J, Mackraj I. Placental exosomes and pre-eclampsia: Maternal circulating levels in normal pregnancies and, early and late onset pre-eclamptic pregnancies. *Placenta*. 2016; 46: 18–25. DOI: 10.1016/j.placenta.2016.08.078.

Литература

- Burton GJ, Redman CW, Roberts JM, Moffett A. Pre-eclampsia: pathophysiology and clinical implications. *BMJ*. 2019; 366: l2381. DOI: 10.1136/bmj.l2381.
- Ananth CV, Lavery JA, Friedman AM, Wapner RJ, Wright JD. Serious maternal complications in relation to severe pre-eclampsia: a retrospective cohort study of the impact of hospital volume. *BJOG*. 2017; 124: 1246–53. DOI: 10.1111/1471-0528.14384.
- Brown MA, Magee LA, Kenny LC, Karumanchi SA, McCarthy FP, Saito S, et al. The hypertensive disorders of pregnancy: ISSHP classification, diagnosis & management recommendations for international practice. *Pregnancy Hypertens*. 2018; 13: 291–310. DOI: 10.1016/j.preghy.2018.05.004.
- Pierrat V, Marchand-Martin L, Arnaud C, Kaminski M, Resche-Rigon M, Lebeaux C, et al. Neurodevelopmental outcome at 2 years for preterm children born at 22 to 34 weeks' gestation in France in 2011: EPIPAGE-2 cohort study. *BMJ*. 2017; 358: j3448. DOI: 10.1136/bmj.j3448.
- Van Beek PE, Rijken M, Broeders L, Ter Horst HJ, Koopman-Esseboom C, de Kort E, et al. Two-year neurodevelopmental outcome in children born extremely preterm: the EPI-DAF study. *Arch Dis Child Fetal Neonatal Ed*. 2022; 107: 467–74. DOI: 10.1136/archdischild-2021-323124.
- Huppertz B. Placental origins of preeclampsia: challenging the current hypothesis. *Hypertens*. (Dallas, Tex. 1979). 2008; 51: 970–75. DOI: 10.1161/HYPERTENSIONAHA.107.107607.
- Garrido-Gomez T, Dominguez F, Quiñero A, Diaz-Gimeno P, Kapidzic M, Gormley M, et al. Defective decidualization during and after severe preeclampsia reveals a possible maternal contribution to the etiology. *Proc Natl Acad Sci USA*. 2017; 114: E8468–E8477. DOI: 10.1073/pnas.1706546114.
- Ruane PT, Berneau SC, Koeck R, Watts J, Kimber SJ, Brison DR, et al. Apposition to endometrial epithelial cells activates mouse blastocysts for implantation. *Mol Hum Reprod*. 2017; 23: 617–27. DOI: 10.1093/molehr/gax043.
- Myatt L. Review: Reactive oxygen and nitrogen species and functional adaptation of the placenta. *Placenta*. 2010; 31 Suppl: S66–9. DOI: 10.1016/j.placenta.2009.12.021.
- Pijnenborg R, Bland JM, Robertson WB, Brosens I. Uteroplacental arterial changes related to interstitial trophoblast migration in early human pregnancy. *Placenta*. 1983; 4: 397–413. DOI: 10.1016/s0143-4004(83)80043-5.
- Burton GJ, Woods AW, Jauniaux E, Kingdom JCP. Rheological and physiological consequences of conversion of the maternal spiral arteries for uteroplacental blood flow during human pregnancy. *Placenta*. 2009; 30: 473–82. DOI: 10.1016/j.placenta.2009.02.009.
- James JL, Saghian R, Perwick R, Clark AR. Trophoblast plugs: impact on utero-placental haemodynamics and spiral artery remodelling. *Hum Reprod*. 2018; 33: 1430–41. DOI: 10.1093/humrep/dey225.
- Allerkamp HH, Clark AR, Lee TC, Morgan TK, Burton GJ, James JL. Something old, something new: digital quantification of uterine vascular remodelling and trophoblast plugging in historical collections provides new insight into adaptation of the uteroplacental circulation. *Hum Reprod*. 2021; 36: 571–86. DOI: 10.1093/humrep/deaa303.
- Staff AC, Fjeldstad HE, Fosheim IK, Moe K, Turowski G, Johnsen GM, et al. Failure of physiological transformation and spiral artery atherosclerosis: their roles in preeclampsia. *Am J Obstet Gynecol*. 2022; 226: S895–S906. DOI: 10.1016/j.ajog.2020.09.026.
- Sidorova IS. Solved and unsolved problems of preeclampsia in Russia (Editorial). *Russ Bull Obstet*. 2015; 15: 4–9. DOI: 10.17116/rosakush20151524-9.
- Rana S, Burke SD, Karumanchi SA. Imbalances in circulating angiogenic factors in the pathophysiology of preeclampsia and related disorders. *Am J Obstet Gynecol*. 2022; 226: S1019–S1034. DOI: 10.1016/j.ajog.2020.10.022.
- Haram K, Mortensen JH, Myking O, Magann EF, Morrison JC. The role of oxidative stress, adhesion molecules and antioxidants in preeclampsia. *Curr Hypertens Rev*. 2019; 15: 105–12. DOI: 10.2174/1573402115666190119163942.
- Tomimatsu T, Mimura K, Matsuzaki S, Endo M, Kumasawa K, Kimura T. Preeclampsia: maternal systemic vascular disorder caused by generalized endothelial dysfunction due to placental antiangiogenic factors. *Int J Mol Sci*. 2019; 20. DOI: 10.3390/ijms20174246.
- Staff AC. The two-stage placental model of preeclampsia: An update. *J Reprod Immunol*. 2019; 134–135: 1–10. DOI: 10.1016/j.jri.2019.07.004.
- Than NG, Romero R, Tarca AL, Kekesi KA, Xu Y, Xu Z, et al. Integrated systems biology approach identifies novel maternal and placental pathways of preeclampsia. *Front Immunol*. 2018; 9: 1661. DOI: 10.3389/fimmu.2018.01661.
- Castro KR, Prado KM, Lorenzon AR, Hoshida MS, Alves EA, Francisco RP, et al. Serum from preeclamptic women triggers endoplasmic reticulum stress pathway and expression of angiogenic factors in trophoblast cells. *Front Physiol*. 2021; 12: 799653. DOI: 10.3389/fphys.2021.799653.
- Yung HW, Atkinson D, Champion-Smith T, Olovsson M, Charnock-Jones DS, Burton GJ. Differential activation of placental unfolded protein response pathways implies heterogeneity in causation of early- and late-onset pre-eclampsia. *J Pathol*. 2014; 234: 262–76. DOI: 10.1002/path.4394.
- Burton GJ, Yung H-W. Endoplasmic reticulum stress in the pathogenesis of early-onset pre-eclampsia. *Pregnancy Hypertens*. 2011; 1: 72–78. DOI: 10.1016/j.preghy.2010.12.002.
- Timofeeva AV, Fedorov IS, Pirogova MM, Vasilchenko ON, Chagovets VV, Ezhova LS, et al. Clusterin and its potential regulatory microRNAs as a part of secretome for the diagnosis of normally invasive placenta: Accreta, Increta, and Percreta Cases. *Life (Basel, Switzerland)*. 2021; 11. DOI: 10.3390/life11040270.
- Janiszewska E, Kmiecik A, Kacperczyk M, Witkowska A, Kratz EM. The influence of clusterin glycosylation variability on selected pathophysiological processes in the human body. *Oxid Med Cell Longev*. 2022; 2022: 7657876. DOI: 10.1155/2022/7657876.
- Zoubeidi A, Gleave M. Small heat shock proteins in cancer therapy and prognosis. *Int J Biochem Cell Biol*. 2012; 44: 1646–56. DOI: 10.1016/j.biocel.2012.04.010.
- Zeng S, Pan Y, Liu F, Yin J, Jiang M, Long Y, et al. Role of clusterin in the regulation of trophoblast development and preeclampsia. *Biochem Biophys Res Commun*. 2021; 583: 128–34. DOI: 10.1016/j.bbrc.2021.10.064.
- Satapathy S, Wilson MR. The dual roles of clusterin in extracellular and intracellular proteostasis. *Trends Biochem Sci*. 2021; DOI: <https://doi.org/10.1016/j.tibs.2021.01.005>.
- Zeng S, Han M, Jiang M, Liu F, Hu Y, Long Y, et al. Serum complement proteomics reveal biomarkers for hypertension disorder of pregnancy and the potential role of Clusterin. *Reprod Biol Endocrinol*. 2021; 19: 56. DOI: 10.1186/s12958-021-00742-z.
- Watanabe H, Hamada H, Yamada N, Sohda S, Yamakawa-Kobayashi K, Yoshikawa H, et al. Proteome analysis reveals elevated serum levels of clusterin in patients with preeclampsia. *Proteomics*. 2004; 4: 537–43. DOI: 10.1002/pmic.200300565.
- Oztas E, Ozler S, Ersoy AO, Iskender CT, Sucak A, Ergin M, et al. Increased levels of serum clusterin is associated with intrauterine growth restriction and adverse pregnancy outcomes in preeclampsia. *J Perinat Med*. 2016; 44: 269–75. DOI: 10.1515/jpm-2015-0120.
- Trougakos IP. The molecular chaperone apolipoprotein J/clusterin as a sensor of oxidative stress: implications in therapeutic

- approaches — a mini-review. *Gerontology*. 2013; 59: 514–23. DOI: 10.1159/000351207.
33. Shiota M, Zoubeidi A, Kumano M, Beraldi E, Naito S, Nelson CC, et al. Clusterin is a critical downstream mediator of stress-induced YB-1 transactivation in prostate cancer. *Mol Cancer Res*. 2011; 9: 1755–66. DOI: 10.1158/1541-7786.MCR-11-0379.
 34. Criswell T, Klokov D, Beman M, Lavik JP, Boothman DA. Repression of IR-inducible clusterin expression by the p53 tumor suppressor protein. *Cancer Biol Ther*. 2003; 2: 372–80. DOI: 10.4161/cbt.2.4.430.
 35. Cervellera M, Raschella G, Santilli G, Tanno B, Ventura A, Mancini C, et al. Direct transactivation of the anti-apoptotic gene apolipoprotein J (clusterin) by β -MYB. *J Biol Chem*. 2000; 275: 21055–60. DOI: 10.1074/jbc.M002055200.
 36. Santilli G, Aronow BJ, Sala A. Essential requirement of apolipoprotein J (clusterin) signaling for I κ B expression and regulation of NF- κ B activity. *J Biol Chem*. 2003; 278: 38214–9. DOI: 10.1074/jbc.C300252200.
 37. Garg M. Targeting microRNAs in epithelial-to-mesenchymal transition-induced cancer stem cells: therapeutic approaches in cancer. *Expert Opin Ther Targets*. 2015; 19: 285–97. DOI: 10.1517/14728222.2014.975794.
 38. Nizard P, Tetley S, Le Dréan Y, Watrin T, Le Goff P, Wilson MR, et al. Stress-induced retrotranslocation of clusterin/ApoJ into the cytosol. *Traffic*. 2007; 8: 554–65. DOI: 10.1111/j.1600-0854.2007.00549.x.
 39. Wilson MR, Zoubeidi A. Clusterin as a therapeutic target. *Expert Opin Ther Targets*. 2017; 21: 201–13. DOI: 10.1080/14728222.2017.1267142.
 40. Rohne P, Prochnow H, Wolf S, Renner B, Koch-Brandt C. The chaperone activity of clusterin is dependent on glycosylation and redox environment. *Cell Physiol Biochem Int J. Exp Cell Physiol Biochem Pharmacol*. 2014; 34: 1626–39. DOI: 10.1159/000366365.
 41. Chen Y, Huang Y, Jiang R, Teng Y. Syncytiotrophoblast-derived microparticle shedding in early-onset and late-onset severe pre-eclampsia. *Int J. Gynaecol Obstet Off Organ Int Fed Gynaecol Obstet*. 2012; 119: 234–38. DOI: 10.1016/j.ijgo.2012.07.010.
 42. Pillay P, Maharaj N, Moodley J, Mackraj I. Placental exosomes and pre-eclampsia: Maternal circulating levels in normal pregnancies and, early and late onset pre-eclamptic pregnancies. *Placenta*. 2016; 46: 18–25. DOI: 10.1016/j.placenta.2016.08.078.

CORRELATION OF MICROEMBOLISM RISK FACTORS WITH AGE IN THE ISCHEMIC STROKE RECOVERY PERIOD

Orlova EV , Beraldin AB, Lelyuk VG

Federal Center of Brain and Neurotechnologies of the Federal Medical Biological Agency, Moscow, Russia

Identification of the age-related features of interaction between the risk factors of microembolism can improve understanding of the mechanisms underlying the development of ischemic stroke (IS). The study was aimed to assess the effects of age and other risk factors of stroke on the biophysical characteristics of microembolic signals (MES) recorded during the ischemic stroke recovery period. Transcranial Doppler ultrasound (TCD) involving microembolus detection (MED) was performed in 515 people, the data of 28 patients having a history of ischemic stroke, among them 9 women (32%) and 19 men (68%) aged 33–78 (average age 58 ± 13 years), were included in the study. Using the mixed-effects linear model it was found that age and interaction between age and atrial fibrillation affected the power of MES. The increase in the power of the recorded MES with age is observed, that is especially evident in patients with atrial fibrillation ($p < 0.0005$). As for cardioembolic IS variant, the power and duration of MES turn out to be significantly higher in elderly patients ($p < 0.0005$). The power of MES gradually increases with age in patients with no atherosclerosis and gradually decreases in patients with atherosclerosis, while MES power in patients with atherosclerosis in general (all age groups) is significantly higher ($p < 0.0005$) than that observed in patients with no atherosclerosis.

Keywords: ischemic stroke, age, atrial fibrillation, atherosclerosis, microembolism

Funding: State Assignment No. 388-00083-22-00 of 30.12.2021, research project No. 122022100113-7 of 21 February 2022

Author contribution: Orlova EV — literature review, manuscript writing, working with the database, analysis of the results; Beraldin AB — working with the dataset, statistical processing of the results, part in writing the results and the discussion; Lelyuk VG — study planning and management, search for sources of funding, manuscript editing.

Compliance with ethical standards: the study was approved by the Ethics Committee of the Federal Center of Brain and Neurotechnologies of FMBA of Russia (protocol № 01/24-10-22 of 24 October 2022); the informed consent was submitted by all study participants.

 **Correspondence should be addressed:** Ekaterina V. Orlova
Ostrovityanova, 1/10, k. A8-008, Moscow, 117513, Russia; ekaterina.shlyk@gmail.com

Received: 28.10.2022 **Accepted:** 29.11.2022 **Published online:** 12.12.2022

DOI: 10.24075/brsmu.2022.058

ВЗАИМОСВЯЗЬ ФАКТОРОВ РИСКА МИКРОЭМБОЛИИ С ВОЗРАСТОМ В ВОССТАНОВИТЕЛЬНОМ ПЕРИОДЕ ИШЕМИЧЕСКОГО ИНСУЛЬТА

Е. В. Орлова , А. Б. Бердалин, В. Г. Лелюк

Федеральный центр мозга и нейротехнологий Федерального медико-биологического агентства, Москва, Россия

Выявление сопряженных с возрастом особенностей взаимодействия факторов риска развития микроэмболии может расширить представления о механизмах развития ишемического инсульта (ИИ). Целью исследования было изучить влияние возраста и других факторов риска инсульта на биофизические характеристики микроэмболических сигналов (МЭС), регистрируемых в восстановительном периоде ишемического инсульта. Транскраниальное доплеровское мониторирование с микроэмболдетекцией провели 515 лицам, в исследование были включены сведения о 28 пациентах, перенесших ишемический инсульт, из которых 9 (32%) женщин и 19 (68%) мужчин в возрасте 33–78 лет (средний возраст — 58 ± 13 лет). При помощи смешанной линейной модели выявлено, что возраст и взаимодействие возраста с наличием фибрилляции предсердий оказывали влияние на мощность МЭС. С возрастом наблюдается увеличение мощности регистрируемых МЭС, особенно заметное у пациентов с фибрилляцией предсердий ($p < 0,0005$). При кардиоэмболическом варианте ИИ мощность и длительность МЭС оказалась значимо больше у более пожилых лиц ($p < 0,0005$). При отсутствии атеросклероза мощность МЭС с возрастом постепенно увеличивалась, а при его наличии — постепенно уменьшалась, при этом мощность МЭС у пациентов с атеросклерозом в целом (во всех возрастных группах) была достоверно выше ($p < 0,0005$), чем при его отсутствии.

Ключевые слова: ишемический инсульт, возраст, фибрилляция предсердий, атеросклероз, микроэмболия

Финансирование: Государственное задание № 388-00083-22-00 от 30.12.2021, регистрационный номер НИР 122022100113-7 от 21 февраля 2022 г.

Вклад авторов: Е. В. Орлова — работа с источниками литературы, написание статьи, работа с базой данных, анализ полученных результатов; А. Б. Бердалин — работа с массивом данных, статистическая обработка результатов, участие в написании результатов исследования и их обсуждения; В. Г. Лелюк — планирование и руководство исследованием, поиск источников финансирования, редактирование статьи.

Соблюдение этических стандартов: исследование одобрено этическим комитетом ФЦМН ФМБА России (протокол № 01/24-10-22 от 24 октября 2022 г.); все участники исследования подписали добровольное информированное согласие.

 **Для корреспонденции:** Екатерина Владимировна Орлова
ул. Островитянова, д. 1/10, к. А8-008, г. Москва, 117513, Россия; ekaterina.shlyk@gmail.com

Статья получена: 28.10.2022 **Статья принята к печати:** 29.11.2022 **Опубликована онлайн:** 12.12.2022

DOI: 10.24075/vrgmu.2022.058

Brain embolism is one of the most common causes of ischemic stroke (IS) [1–4]. However, the sources of embolism and embolic material are extremely heterogeneous [5]. Thus, atrial fibrillation (AF), atherosclerosis of the brain-supplying arteries, and a number of less frequent conditions, such as inferior vena cava thrombosis, heart valve disease, etc., are considered as the sources of emboli [2, 6–8].

It is known that AF results in the five-fold increased risk of stroke and two-fold increased stroke mortality [9]. AF is one of the most common types of arrhythmia [10–12], the prevalence of AF in the entire population reaches 2–4%. AF increases the risk of ischemic stroke by 0.2–20% on average annually [13, 14]. Arterial hypertension is considered the main cause of AF. In the middle and senior age groups, AF is recognized as the most

Table 1. Basic information about the subjects enrolled

Characteristics	Number, abs.		Share, %
Gender	Male	19	67.90
	Female	9	32.10
	Total	28	100
Age	≤ 50 years	9	32.10
	>50 years	19	67.90
	Total	28	100
Pathogenetic variant of IS	Atherothrombotic	7	25
	Cardioembolic	6	21.40
	Cryptogenic	14	50
	Lacunar	1	3.60
	Total	28	100
Affected system	Vertebrobasilar	7	25
	Carotid	21	75
	Total	28	100
Affected side	Bilateral	4	14.30
	Left	9	32.10
	Right	15	53.60
	Total	28	100
Arterial hypertension	Present	5	17.90
	Absent	23	82.10
	Total	28	100
Diabetes mellitus	Present	18	64.30
	Absent	10	35.70
	Total	28	100
AF	Present	23	82.10
	Absent	5	17.90
	Total	28	100

common cause of cardiogenic brain embolism [10–12]. There is evidence that the risk of stroke increases as a function of AF duration and, accordingly, of age [10, 15].

Atherosclerosis, being the cause of IS, fulfils its potential in different ways: through atherothrombosis, hypoperfusion or arterio-arterial embolism [1, 2]. The frequency of these mechanisms is uncertain, however, we know that hypoperfusion is the least common mechanism of all [5, 6].

Information on the nature and prevalence of brain embolism available from other sources is even more limited [8, 16].

This is largely due to the high rate of situations, in which there is more than one cause of stroke, among stroke survivors, as well as to difficulties in verifying the fact of embolism [1]. Microembolus detection (MED) by transcranial Doppler ultrasound (TCD) is the only option for in vivo detection of emboli and assessment of the embolic signal intensity and type (based on indirect characteristics) by extraction of appropriate signals from the Doppler spectral blood flow waveforms of cerebral arteries [17]. Microembolic signals (MES) recorded by the specified method are regarded as an independent risk factor of IS and transient ischemic attack (TIA) [2–4]. The use of the method is limited by the lack of the temporal acoustic access.

Despite the fact that the results of studies focused on assessing MES and their intensity in patients with various conditions have been broadly published, there is a few data about the factors affecting embolism and its intensity, as well as the biophysical characteristics of MES and their interaction [2–5, 16].

Thus, it has been determined that asymptomatic paroxysmal AF with lower MES intensity is more favorable compared to chronic symptomatic AF, in which a significantly larger number of MES is detected. Further studies are required to confirm, whether MES have some predictive value in patients with chronic AF predisposed to ischemic stroke [16].

The presence of MES that is associated with the greatly increased risk of IS could be considered a predictor of early IS relapse [1].

Due to the fact that IS and TIA in younger patients and patients of the older age groups have different etiology and pathogenesis [6, 18, 19], identification of the age-related features of interaction between the risk factors of microembolism can have practical significance and can also expand understanding of the mechanisms underlying stroke development.

Inability to fully take into account interaction between factors affecting the event (characteristic, parameter) is a well-known limitation of all observational studies. In particular, it is unclear whether AF (or any other risk factor of IS) is associated with the registered MES, or this relationship is questionable and is due to the fact that individuals with AF are older, and microembolism is in fact associated with age. Thus, the use of statistical methods (see Methods) allowing for at least partial separation of interacting factors (for example, AF and age) is promising since it allows us to get closer to understanding of the cause and effect relationships that contribute to the MES occurrence.

The study was aimed to assess the effects of age and other risk factors of stroke on the biophysical characteristics of MES

Table 2. Information about the carotid artery stenosis severity in the patients enrolled

	Median	1 st quartile	3 rd quartile	Maximum	Minimum
Severity of the right CCA stenosis (%)	33	30	40	50	20
Severity of the left CCA stenosis (%)	35	30	48	50	25
Severity of the right ICA stenosis (%)	35	30	40	100	25
Severity of the left ICA stenosis (%)	35	30	50	70	20

recorded in patients with ischemic stroke during the recovery period.

METHODS

After the peer reviewing the data of the multimodal instrumental study of 1600 clinical cases of IS during the recovery period, the group of experts that included ultrasound and functional diagnostics doctors, radiologists, neurologists, senior researchers and Head of the Department of Ultrasound and Functional Diagnostics selected 515 people, who underwent TCD involving MED in 2019–2021. In terms of design, we performed the cross-sectional observational study as part of the prospective cohort study.

Inclusion criteria: the history of IS, the presence of potential sources of embolism based on the comprehensive ultrasound examination.

Exclusion criteria: no temporal acoustic access for TCD involving MED.

Post-processing of the recordings revealed the signs of MES in 46 patients out of 515 observations (8.9%). After analyzing the MES acquired, we failed to obtain the values of the MES biophysical characteristics in all patients due to accidental technical difficulties. Thus, the data of 28 patients having a history of IS were included in the study. Among them 9 (32%) were women and 19 (68%) were men aged 33–78 years (the average age was 58 ± 13 years).

The patients enrolled underwent inpatient treatment at the departments of medical rehabilitation of the Federal Center of Brain and Neurotechnologies of FMBA of Russia. The following tests were performed in all patients.

1. Duplex scanning of the brachiocephalic arteries (DS BCA), transcranial duplex scanning (TCD), and transthoracic echocardiography (TTE) were performed using the Epiq 7 scanners (Philips; USA); extracranial sections of the BCA were examined using the 3–12 MHz broadband multi-frequency linear transducers, while TCD and TTE were performed using the 1–5 MHz broadband multi-frequency sector transducers.

2. TCD involving MED was performed with the Angiodin-Universal scanner (NPF BLOSS; Russia) equipped with the 2 MHz pulse wave sensors fixed in the Spencer's helmet. Blood flows in the middle cerebral artery (MCA) and posterior cerebral artery (PCA) were detected simultaneously from two sides using the temporal acoustic access; scanning was performed for 60 min when lying down or sitting [17]. To minimize artifacts during the study, the lowest possible amplification and power values that ensured preservation of Doppler spectrum

were used. Automatic MES recording was performed during monitoring using the Bionita Cabinet software (Biosoft-M; Russia), while the subsequent analysis of the results and differentiation between MES and artifacts were performed in the manual mode. The size of the sample volume mark was 20 mm, detection was performed at a depth of 50–60 mm.

In case the signs of embolism were revealed, the embolism intensity was assessed (number of MES/hour). The duration (ms; an indirect characteristic of the embolus size), frequency (Hz; an indirect characteristic of the embolus structure), and power (dB; integral characteristic of the embolus) were defined for each MES.

3. Electrocardiography (ECG) was performed using the Neurosoft ECG monitoring system with the Poly-Spectrum software (Neurosoft; Russia) in accordance with the standard method.

Statistical processing of the results was performed in the SPSS Statistics ver. 26.0 software package (IBM; USA) and R software ver. 4.0.2. (R Core Team; Austria). The null hypothesis was rejected at a significance level of $p \leq 0.05$. The quantitative variables were described using mean and standard deviation or median and quartiles (in case of non-normal distribution), while qualitative variables were described using frequency and share (percentage). The distribution of quantitative variables was tested for normality using the Shapiro–Wilk test. The mixed-effects linear model with nested data was used to assess the effects of AF and intraluminal carotid artery buildup on the biophysical characteristics of MES adjusted for age taking into account every single MES.

RESULTS

The main data of the patients enrolled are provided in Table 1.

No cases of myocardial infarction, coronary stenting, carotid endarterectomy, brachiocephalic artery dissection were reported.

The data on the extracranial BCA stenosis severity are provided in Table 2.

TCD involving MED revealed MES in all the people enrolled. A total of 938 MES were extracted. General information about the number and characteristics of MES is provided in Table 3.

The differences in the MES biophysical characteristics between patients having and not having AF were significant ($p < 0.05$).

The analysis of the AF impact on the MES characteristics adjusted for age performed using the mixed-effects linear model showed that the impact of the patient's age and

Table 3. Biophysical characteristics and the number of MES

	Mean	Standard deviation	Median	25 th percentile	75 th percentile	Maximum	Minimum
Total number of MES per patient	34	105	3	1	10	532	1
Average MES power (dB)	11.06	3.32	10.22	8.31	14.2	17.75	7.28
Average MES duration (ms)	9.06	4.86	7.09	6	11.33	23.66	4.67
Average MES frequency (Hz)	528.19	241.8	475.92	328	750	968	230.5

Table 4. Biophysical characteristics of MES in patients having or not having AF

		AF	
		Absent	Present
Adjusted number of MES per patient	Mean	8.8333	149
	Standard deviation	13.2588	219.7476
Average MES power	Mean	10.0763	14.7022
	Standard deviation	2.4233	4.1322
Average MES duration	Mean	7.5597	15.4918
	Standard deviation	2.5796	6.955
Average MES frequency	Mean	500.7776	612.8418
	Standard deviation	237.8698	223.7408
Average MES Energy Index (EI)	Mean	0.0803	0.2784
	Standard deviation	0.0449	0.1675

interaction between age and AF on the recorded MES power was significant ($p < 0.0005$), thus indicating the modifying effect of one parameter on the effect of another one (Fig. 1). However, the isolated effect of AF (adjusted for age) was non-significant ($p = 0.109$). Thus, the recorded MES power increased with age, and this was particularly evident in patients with AF. In other words, AF resulted in the higher MES power only in elderly people, while young people with AF showed no significant differences in the MES power.

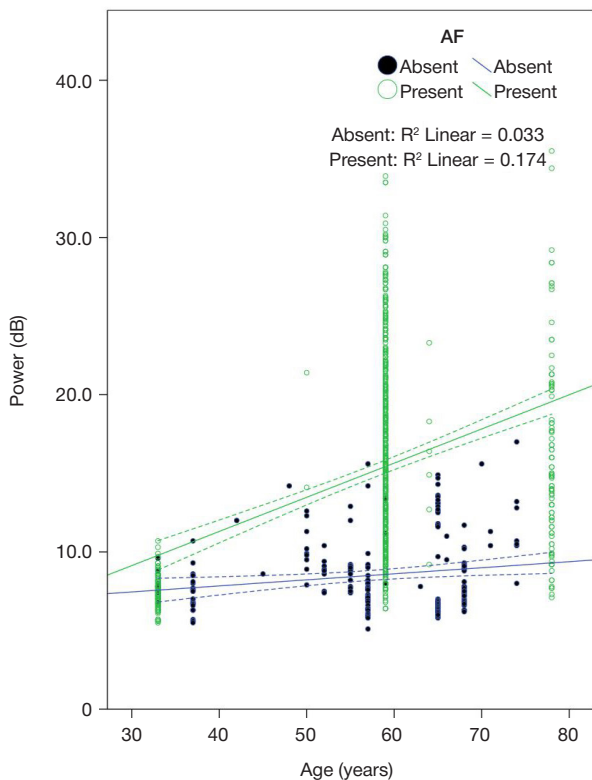
The mixed-effects linear model for assessment of the impact of the stroke type (cardioembolic/not cardioembolic) adjusted for age on the power and duration of the recorded

MES showed that such parameters as age ($p < 0.0005$) and interaction between age and IS variant ($p < 0.001$) were significant (Fig. 2). The pattern was broadly similar to the model for AF, i.e. the differences between cardioembolic stroke and stroke of another etiology were significant only in elderly patients with IS.

The constructed mixed-effects linear model of the impact of atherosclerotic plaques (ASPs) in the carotid arteries on the biophysical characteristics of the recorded MES constructed based on age showed that the presence of ASPs in the right and left common carotid artery (CCA) and interaction between these factors and age ($p < 0.0005$) were the significant factors (Fig. 3).

According to the findings, the very fact of the presence of ASPs in the carotid arteries was associated with the higher MES power, while the power-age trends correlated with the presence of ASPs. In other words, when no ASPs were found in the carotid arteries, the power of MES gradually increased with age. In contrast, when ASPs were present, the power of MES gradually decreased.

The mixed-effects linear model taking into account the effects of such risk factors as AF and ASPs in the carotid arteries together with age on the power and duration of MES was constructed in order to assess the competing causes of IS. However, interaction between the aforementioned parameters turned out to be non-significant ($p > 0.05$), i.e. in our study the effects of ASPs and AF on the biophysical characteristics of MES turned out to be unrelated.



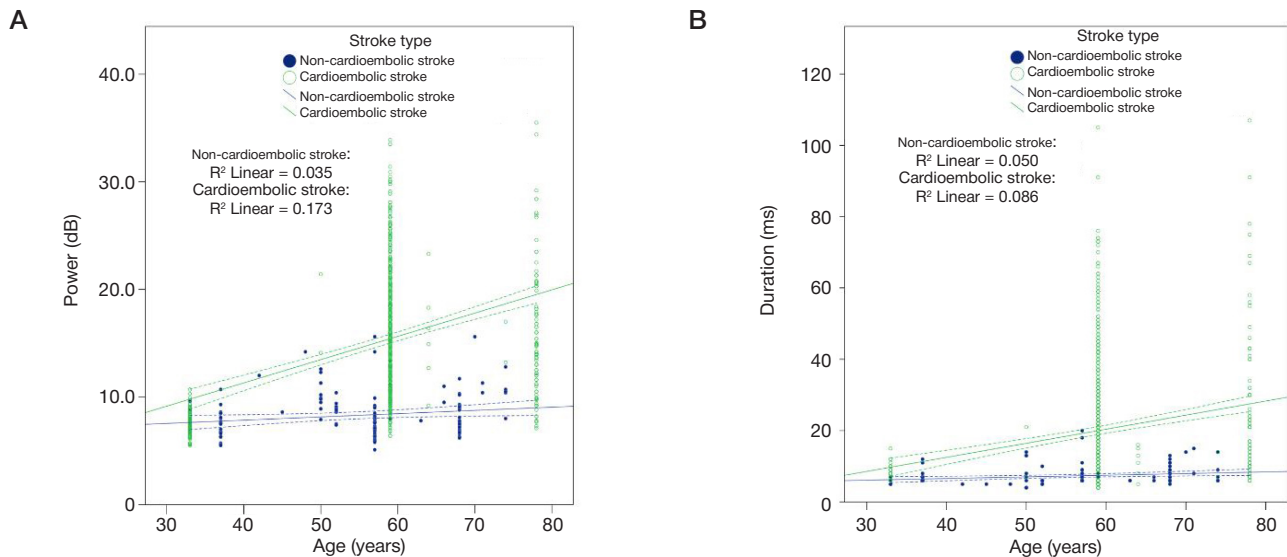
Source	F-test	Significance, p
Adjusted model	374,728	$< 0,0005$
Age	24,978	$< 0,0005$
AF	2,571	0,109
Interaction between age and AF	13,718	$< 0,0005$

Fig. 1. Mixed-effects linear model of the impact of age and AF on the MES power

DISCUSSION

The study has a number of limitations. The first one is related to the embolic event, the embolic material intensity and type, while the second one is related to the method of TCD involving MED. Brain embolism is most often discrete, and its intensity is variable [4, 17]. Furthermore, emboli can be represented by the fragments of blood clots of various age, as well as by the fragments of atherosclerotic plaques, valves, components of vascular wall, etc. [1, 5, 16]. Therefore, biophysical parameters of MES may vary significantly in the same case. Methodological determinants result mainly from the flaws of software used for MES extraction from noise [17]. The reported facts show that the results obtained by the applied method cannot be considered as the data giving a comprehensive picture, however, this approach is currently the only available method for in vivo assessment of cerebral embolism.

Given the above limitations, it can be stated that the findings of our study that reflect the correlation of the biophysical



Source	F-test for the model of impact on the MES intensity	p	F-test for the model of impact on the MES duration	p
Adjusted model	240.572	< 0.0005	1518.162	< 0.0005
Age	19.922	< 0.0005	16.181	< 0.0005
Stroke type (binary)	2.226	0.136	1.913	0.167
Interaction between age and stroke type	11.58	< 0.001	10.801	< 0.001

Fig. 2. Mixed-effects linear model of the impact of age and stroke type on the power and duration of MES. **A.** Mixed-effects linear model of the impact of age and stroke type on the power of MES. **B.** Mixed-effects linear model of the impact of age and stroke type on the duration of MES

characteristics of MES with the patient's age and interaction between age and other risk factors of IS require further analysis.

A number of researchers question whether AF itself can be the main cause of cardioembolic complications. They assume that AF is a kind of marker of atrial cardiopathy that can be considered as the proximate cause of cardioembolism [7, 20, 21]. There is also evidence of the relationship between the markers of atrial cardiopathy and IS, regardless of the presence of AF [22, 23].

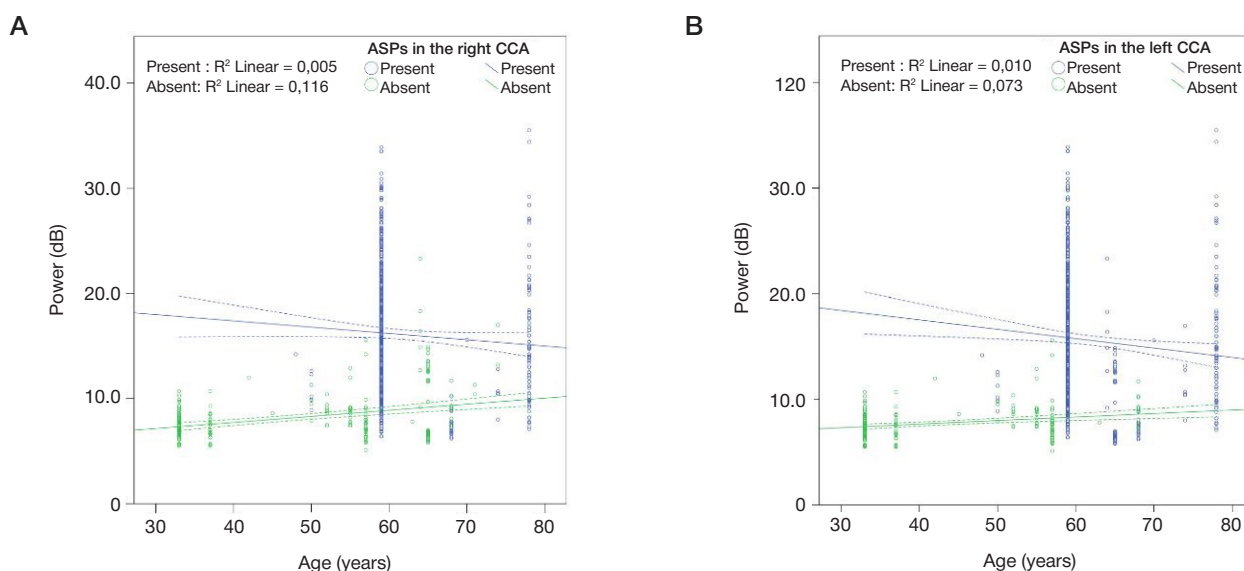
To date, the literature reports no studies focused on the analysis of the IS risk factor impact on the biophysical characteristics of MES. The results of our study involving creation of the mixed-effects linear model for the impact of age and AF on the biophysical characteristics of MES show that age and interaction between age and AF are significant. MES power, being an integral biophysical characteristic that indirectly reflects both the size and the structure of microemboli, depends on age adjusted for the presence of AF. The data obtained also show that MES power (if any MES recorded) observed in young patients is independent of AF. However, AF affects MES power during ageing, i.e. in older patients. This is probably because of the fact that the pronounced slowing of blood flow, especially in the left atrial appendages of patients with AF, occurs only in elderly patients. Such slowing of blood flow combined with other possible factors results in thrombogenesis and cardioembolism of the brain blood vessels. This is partially confirmed by the literature data showing that the risk of stroke increases with the age-related increase in the atrial ectopic activity. However, the risk could be partially due to prothrombotic endothelial dysfunction developing in patients who develop atrial cardiopathy in addition to arrhythmia [10, 21]. The impact of other unidentifiable factors that simulate such an effect also cannot be excluded. The development of AF resulting from atrial remodeling takes time, and the prevalence of such AF is higher in older people. In younger people, AF can be associated with other factors (genetic predisposition), not with the alterations in atrial

wall. This indirectly confirms the increasingly popular viewpoint that cardioembolism is associated not with AF itself, but with alterations in atrial wall, such as inflammation [11, 21, 24]. AF itself is caused by the same remodeling processes. In younger patients, AF that is not associated with atrial remodeling never causes the emergence of MES.

The analysis of similar model taking into account the variant of stroke (in binary mode: cardioembolic/non-cardioembolic) instead of the presence of AF makes it possible to trace the relationship between two MES characteristics (power and duration) associated with ageing and stroke type. Furthermore, in cases of cardioembolic stroke, the values of these two characteristics are significantly higher in elderly patients. Perhaps, the discovered pattern reflects the occurrence of larger microemboli during realization of factors promoting age-related thrombogenesis. We also should take into account the fact that this could be partially due to almost mandatory assignment of IS to cardioembolic variant based on the TOAST criteria [25] in cases of AF.

The mixed-effects model taking into account both ASPs in the carotid arteries and age allows us to state that the impact of atherosclerosis on MES intensity gradually decreases with age. However, it is obvious that the presence of ASPs in the carotid arteries is associated with the significantly increased MES power compared to patients with no ASPs in both young and elderly patients. It can be assumed that atherosclerosis and arterio-arterial embolism is a major pathogenetic mechanism of acute focal cerebral ischemia, irrespective of age. We also cannot rule out that the cardiac sources may occupy a significant place in the structure of embolic events together with atherosclerosis and age. This explains the gradual increase in MES power with age in patients with no ASPs in the carotid arteries.

There is evidence of the impact of concomitant atherosclerotic vascular disease on the outcomes of ischemic events in patients with AF. Thus, it has been found that burden in the form of the combination of the cerebral artery



Source	F-test (right CCA)	<i>p</i>	F-test (left CCA)	<i>p</i>
Adjusted model	63 017.362	< 0,0005	16 882.306	< 0,0005
Age	5.723	0.017	3.851	0,05
Presence of ASPs in the CCA	129.205	< 0,0005	53.639	< 0,0005
Interaction between age and the presence of ASPs in the CCA	24.601	< 0,0005	18.659	< 0,0005

Fig. 3. Mixed-effects linear model of the impact of age and ASPs in the right and left CCA on the MES power. **A.** Mixed-effects linear model of the impact of age and ASPs in the right CCA on the MES power. **B.** Mixed-effects linear model of the impact of age and ASPs in the left CCA on the MES power

atherosclerosis and AF can be a cumulative marker of the high risk of adverse cardiovascular outcomes [26]. In our study we assessed the impact of AF and atherosclerotic alterations in the carotid arteries on the power and duration of MES taking into account the patients' age. The impact turned out to be non-significant, i.e. the earlier statement [26] was not confirmed.

Thus, the results of using TCD involving MED may be used for implementation of the personalized approach to secondary prevention of IS in the groups of patients with various combinations of risk factors.

CONCLUSIONS

Age and the association of age with AF affect MES power in patients having a history of IS during the recovery period. The

correlation can be traced of the age-related MES power and duration with the stroke variant. Moreover, in cardioembolic variant the values of these characteristics are higher in older patients. Our findings show that MES power gradually decreases with age in patients with ASPs in the carotid arteries, in contrast to patients with no atherosclerosis, while the power of MES in patients with atherosclerosis in general (all age groups) is higher. The impact of AF and ASPs in the carotid arteries, assessed taking into account the patients' age, on the power and duration of MES is non-significant. The findings will make it possible to expand the range of diagnostic information obtained by TCD involving MED in the groups of patients with various combinations of risk factors during the IS recovery period, thus contributing to the strategy of secondary prevention.

References

1. Bazan R, Luvizutto GJ, Braga GP, et al. Relationship of spontaneous microembolic signals to risk stratification, recurrence, severity, and mortality of ischemic stroke: a prospective study. *Ultrasound J.* 2020; 12 (1): 6.
2. Liu WS, Zhu SF, Liu WF, Li GL, Jiang HQ. Relationship between microemboli in the internal carotid artery and the occurrence of ischemic stroke after transient ischemic attack. *J Clin Neurosci.* 2013; 20 (10): 1366–70.
3. Yan J, Li Z, Wills M, Rajah G, Wang X, Bai Y, Dong P, Zhao X. Intracranial microembolic signals might be a potential risk factor for cognitive impairment. *Neurol Res.* 2021; 43 (11): 867–73. DOI: 10.1080/01616412.2021.1939488. Epub 2021 Aug 19. PMID: 34409926.
4. Das AS, Regenhardt RW, LaRose S, Monk AD, Castro PM, Sheriff FG, et al. Microembolic Signals Detected by Transcranial Doppler Predict Future Stroke and Poor Outcomes. *J Neuroimaging.* 2020; 30 (6): 882–9. DOI: 10.1111/jon.12749. Epub 2020 Jul 10. PMID: 32648610; PMCID: PMC7721963.
5. Best LM, Webb AC, Gurusamy KS, Cheng SF, Richards T. Transcranial Doppler Ultrasound Detection of Microemboli as a Predictor of Cerebral Events in Patients with Symptomatic and Asymptomatic Carotid Disease: A Systematic Review and Meta-Analysis. *Eur J Vasc Endovasc Surg.* 2016; 52 (5): 565–80. DOI: 10.1016/j.ejvs.2016.05.019.
6. Skvorcova VI, Kolcova EA, Kimelfeld EI. Sravnitel'nyj analiz faktorov riska i patogeneticheskix variantov ishemičeskogo insulta v molodom i pozhilom vozraste. *Chelovek i ego zdorov'e.* 2012; 3: 81–87. Russian.
7. Brambatti M, Connolly SJ, Gold MR, Morillo CA, Capucci A, Muto C, et al. Temporal relationship between subclinical atrial fibrillation and embolic events. *Circulation.* 2014; 129 (21): 2094–9.
8. Cho H, Kim T, Song IU, Chung SW. The Prevalence of Microembolic

- Signals in Transcranial Doppler Sonography with Bubble Test in Acute Ischemic Stroke. *J Ultrasound Med.* 2022; 41 (2): 439–46.
9. Migdady I, Russman A, Buletko AB. Atrial Fibrillation and Ischemic Stroke: A Clinical Review. *Semin Neurol.* 2021; 41 (4): 348–64.
 10. Healey JS, Amit G, Field TS. Atrial fibrillation and stroke: how much atrial fibrillation is enough to cause a stroke? *Curr Opin Neurol.* 2020; 33 (1): 17–23.
 11. Maida CD, Norrito RL, Daidone M, Tuttolomondo A, Pinto A. Neuroinflammatory Mechanisms in Ischemic Stroke: Focus on Cardioembolic Stroke, Background, and Therapeutic Approaches. *Int J Mol Sci.* 2020; 21 (18): 6454. Published 2020 Sep 4. DOI: 10.3390/ijms21186454.
 12. Pistoia F, Sacco S, Tiseo C, Degan D, Ornello R, Carolei A. The Epidemiology of Atrial Fibrillation and Stroke. *Cardiol Clin.* 2016; 34 (2): 255–68.
 13. Haeusler KG, Tütüncü S, Schnabel RB. Detection of Atrial Fibrillation in Cryptogenic Stroke. *Curr Neurol Neurosci Rep.* 2018; 18 (10): 66.
 14. Kirchhof P, Benussi S, Kotecha D, et al. ESC Guidelines for the management of atrial fibrillation developed in collaboration with EACTS. *Eur Heart J.* 2016; 37: 2893–962.
 15. Spence JD. Stroke: Atrial fibrillation, stroke prevention therapy and aging. *Nat Rev Cardiol.* 2009; 6 (7): 448–50. DOI: 10.1038/nrcardio.2009.98. PMID: 19554003.
 16. Kumral E, Balkir K, Uzuner N, Evyapan D, Nalbantgil S. Microembolic signal detection in patients with symptomatic and asymptomatic lone atrial fibrillation. *Cerebrovasc Dis.* 2001; 12 (3): 192–6.
 17. Ringelstein EB, Droste DW, Babikian VL, Evans DH, Grosset DG, Kaps M, et al. Consensus on microembolus detection by TCD. International Consensus Group on Microembolus Detection. *Stroke.* 1998; 29 (3): 725–9. DOI: 10.1161/01.str.29.3.725. PMID: 9506619.
 18. Dmytriw AA, Dibas M, Schirmer CM, et al. North American Neurovascular COVID–19 (NAN–C) Consortium. Age and Acute Ischemic Stroke Outcome in North American Patients With COVID–19. *J Am Heart Assoc.* 2021; 10 (14): 021046.
 19. George MG. Risk Factors for Ischemic Stroke in Younger Adults: A Focused Update. *Stroke.* 2020; 51 (3): 729–35. DOI: 10.1161/STROKEAHA.119.024156. Epub 2020 Feb 12. PMID: 32078487; PMCID: PMC7112557.
 20. Shaik TA, Haseeb M, Faisal S, et al. Impact of Catheter Ablation on Long-Term Outcomes in Patients With Atrial Fibrillation: A Meta-Analysis. *Cureus.* 2022; 14 (9): e29202. Published 2022 Sep 15. DOI: 10.7759/cureus.29202.
 21. Sajeev JK, Kalman JM, Dewey H, Cooke JC, Teh AW. The Atrium and Embolic Stroke: Myopathy Not Atrial Fibrillation as the Requisite Determinant? *JACC Clin Electrophysiol.* 2020; 6 (3): 251–61. DOI: 10.1016/j.jacep.2019.12.013.
 22. Kamel H, Soliman EZ, Heckbert SR, Kronmal RA, Longstreth WT Jr, Nazarian S, et al. P-wave morphology and the risk of incident ischemic stroke in the Multi-Ethnic Study of Atherosclerosis. *Stroke.* 2014; 45 (9): 2786–8.
 23. Keach JW, Bradley SM, Turakhia MP, Maddox TM. Early detection of occult atrial fibrillation and stroke prevention. *Heart.* 2015; 101 (14): 1097–102.
 24. Ronsoni RM, Saffi MAL, Gonçalves MVM, Nakayama IH, Luz Leiria TL. A New Vision at the Interface of Atrial Fibrillation and Stroke. *Front Cardiovasc Med.* 2021; 8: 689313. Published 2021 Aug 9. DOI: 10.3389/fcvm.2021.689313.
 25. Adams HP Jr, Bendixen BH, Kappelle LJ, Biller J, Love BB, Gordon DL, et al. Classification of subtype of acute ischemic stroke. Definitions for use in a multicenter clinical trial. TOAST. Trial of Org 10172 in Acute Stroke Treatment. *Stroke.* 1993; 24 (1): 35–41. DOI: 10.1161/01.str.24.1.35. PMID: 7678184.
 26. Park JH, Chung JW, Bang OY, et al. Atherosclerotic Burden and Vascular Risk in Stroke Patients With Atrial Fibrillation. *Stroke.* 2021; 52 (5): 1662–72.

Литература

1. Bazan R, Luvizutto GJ, Braga GP, et al. Relationship of spontaneous microembolic signals to risk stratification, recurrence, severity, and mortality of ischemic stroke: a prospective study. *Ultrasound J.* 2020; 12 (1): 6.
2. Liu WS, Zhu SF, Liu WF, Li GL, Jiang HQ. Relationship between microemboli in the internal carotid artery and the occurrence of ischemic stroke after transient ischemic attack. *J Clin Neurosci.* 2013; 20 (10): 1366–70.
3. Yan J, Li Z, Wills M, Rajah G, Wang X, Bai Y, Dong P, Zhao X. Intracranial microembolic signals might be a potential risk factor for cognitive impairment. *Neurol Res.* 2021; 43 (11): 867–73. DOI: 10.1080/01616412.2021.1939488. Epub 2021 Aug 19. PMID: 34409926.
4. Das AS, Regenhardt RW, LaRose S, Monk AD, Castro PM, Sheriff FG, et al. Microembolic Signals Detected by Transcranial Doppler Predict Future Stroke and Poor Outcomes. *J Neuroimaging.* 2020; 30 (6): 882–9. DOI: 10.1111/jon.12749. Epub 2020 Jul 10. PMID: 32648610; PMCID: PMC7721963.
5. Best LM, Webb AC, Gurusamy KS, Cheng SF, Richards T. Transcranial Doppler Ultrasound Detection of Microemboli as a Predictor of Cerebral Events in Patients with Symptomatic and Asymptomatic Carotid Disease: A Systematic Review and Meta-Analysis. *Eur J Vasc Endovasc Surg.* 2016; 52 (5): 565–80. DOI: 10.1016/j.ejvs.2016.05.019.
6. Скворцова В. И., Кольцова Е. А., Кимельфельд Е. И. Сравнительный анализ факторов риска и патогенетических вариантов ишемического инсульта в молодом и пожилом возрасте. *Человек и его здоровье.* 2012; 3: 81–87.
7. Brambatti M, Connolly SJ, Gold MR, Morillo CA, Capucci A, Muto C, et al. Temporal relationship between subclinical atrial fibrillation and embolic events. *Circulation.* 2014; 129 (21): 2094–9.
8. Cho H, Kim T, Song IU, Chung SW. The Prevalence of Microembolic Signals in Transcranial Doppler Sonography with Bubble Test in Acute Ischemic Stroke. *J Ultrasound Med.* 2022; 41 (2): 439–46.
9. Migdady I, Russman A, Buletko AB. Atrial Fibrillation and Ischemic Stroke: A Clinical Review. *Semin Neurol.* 2021; 41 (4): 348–64.
10. Healey JS, Amit G, Field TS. Atrial fibrillation and stroke: how much atrial fibrillation is enough to cause a stroke? *Curr Opin Neurol.* 2020; 33 (1): 17–23.
11. Maida CD, Norrito RL, Daidone M, Tuttolomondo A, Pinto A. Neuroinflammatory Mechanisms in Ischemic Stroke: Focus on Cardioembolic Stroke, Background, and Therapeutic Approaches. *Int J Mol Sci.* 2020; 21 (18): 6454. Published 2020 Sep 4. DOI: 10.3390/ijms21186454.
12. Pistoia F, Sacco S, Tiseo C, Degan D, Ornello R, Carolei A. The Epidemiology of Atrial Fibrillation and Stroke. *Cardiol Clin.* 2016; 34 (2): 255–68.
13. Haeusler KG, Tütüncü S, Schnabel RB. Detection of Atrial Fibrillation in Cryptogenic Stroke. *Curr Neurol Neurosci Rep.* 2018; 18 (10): 66.
14. Kirchhof P, Benussi S, Kotecha D, et al. ESC Guidelines for the management of atrial fibrillation developed in collaboration with EACTS. *Eur Heart J.* 2016; 37: 2893–962.
15. Spence JD. Stroke: Atrial fibrillation, stroke prevention therapy and aging. *Nat Rev Cardiol.* 2009; 6 (7): 448–50. DOI: 10.1038/nrcardio.2009.98. PMID: 19554003.
16. Kumral E, Balkir K, Uzuner N, Evyapan D, Nalbantgil S. Microembolic signal detection in patients with symptomatic and asymptomatic lone atrial fibrillation. *Cerebrovasc Dis.* 2001; 12 (3): 192–6.
17. Ringelstein EB, Droste DW, Babikian VL, Evans DH, Grosset DG, Kaps M, et al. Consensus on microembolus detection by TCD. International Consensus Group on Microembolus Detection. *Stroke.* 1998; 29 (3): 725–9. DOI: 10.1161/01.str.29.3.725. PMID: 9506619.
18. Dmytriw AA, Dibas M, Schirmer CM, et al. North American Neurovascular COVID–19 (NAN–C) Consortium. Age and Acute Ischemic Stroke Outcome in North American Patients With

- COVID-19. *J Am Heart Assoc.* 2021; 10 (14): 021046.
19. George MG. Risk Factors for Ischemic Stroke in Younger Adults: A Focused Update. *Stroke.* 2020; 51 (3): 729–35. DOI: 10.1161/STROKEAHA.119.024156. Epub 2020 Feb 12. PMID: 32078487; PMCID: PMC7112557.
 20. Shaik TA, Haseeb M, Faisal S, et al. Impact of Catheter Ablation on Long-Term Outcomes in Patients With Atrial Fibrillation: A Meta-Analysis. *Cureus.* 2022; 14 (9): e29202. Published 2022 Sep 15. DOI: 10.7759/cureus.29202.
 21. Sajeev JK, Kalman JM, Dewey H, Cooke JC, Teh AW. The Atrium and Embolic Stroke: Myopathy Not Atrial Fibrillation as the Requisite Determinant? *JACC Clin Electrophysiol.* 2020; 6 (3): 251–61. DOI: 10.1016/j.jacep.2019.12.013.
 22. Kamel H, Soliman EZ, Heckbert SR, Kronmal RA, Longstreth WT Jr, Nazarian S, et al. P-wave morphology and the risk of incident ischemic stroke in the Multi-Ethnic Study of Atherosclerosis. *Stroke.* 2014; 45 (9): 2786–8.
 23. Keach JW, Bradley SM, Turakhia MP, Maddox TM. Early detection of occult atrial fibrillation and stroke prevention. *Heart.* 2015; 101 (14): 1097–102.
 24. Ronsoni RM, Saffi MAL, Gonçalves MVM, Nakayama IH, Luz Leiria TL. A New Vision at the Interface of Atrial Fibrillation and Stroke. *Front Cardiovasc Med.* 2021; 8: 689313. Published 2021 Aug 9. DOI: 10.3389/fcvm.2021.689313.
 25. Adams HP Jr, Bendixen BH, Kappelle LJ, Biller J, Love BB, Gordon DL, et al. Classification of subtype of acute ischemic stroke. Definitions for use in a multicenter clinical trial. TOAST. Trial of Org 10172 in Acute Stroke Treatment. *Stroke.* 1993; 24 (1): 35–41. DOI: 10.1161/01.str.24.1.35. PMID: 7678184.
 26. Park JH, Chung JW, Bang OY, et al. Atherosclerotic Burden and Vascular Risk in Stroke Patients With Atrial Fibrillation. *Stroke.* 2021; 52 (5): 1662–72.

NEUTROPHIL AND MONOCYTE EXTRACELLULAR TRAPS IN THE DIAGNOSIS OF POST-COVID SYNDROME

Salmasi JM, Poryadin GV, Panina MI, Larina VN, Ryzhikh AA, Stodelova EA, Kazimirskii AN [✉]

Pirogov Russian National Research Medical University, Moscow, Russia

Post-COVID syndrome (long covid, post COVID-19 condition) is characterized by cognitive and mental disorders, chest and joint pain, impaired sense of smell and taste, as well as by gastrointestinal and cardiac disorders. The diagnosis of post-COVID syndrome is based mainly on the patients' complaints. To date, no optimal diagnostic method has been proposed. The study was aimed to compare the informative value of the indicators obtained during conventional assessment of patients with post-COVID syndrome and the blood levels of neutrophil (NETs) and monocyte (METs) extracellular traps. The study involved neutrophils and monocytes collected from 21 patients with post-COVID syndrome aged 18–59. Fluorescence microscopy and the SYBR Green (Evrogen) fluorescent dye for double-stranded DNA were used for enumeration and imaging of extracellular traps. Clinical and laboratory indicators make it impossible to identify the changes specific for post-COVID syndrome. At the same time, post-COVID syndrome is characterized by inflammation in the vascular endothelium. The filamentous forms of NETs found in blood are a laboratory feature of such aseptic inflammation. The filamentous forms of NETs have been detected only in those patients who have a history of mild to severe COVID-19, while the filamentous forms of METs have been found in patients having a history of severe infection. The findings show that the detection of the filamentous forms of NETs and METs in blood is the most informative diagnostic feature of post-COVID syndrome.

Keywords: post-COVID syndrome, diagnosis, neutrophil extracellular traps, monocyte extracellular traps, filamentous forms

Acknowledgements: the authors express their gratitude to all the patients enrolled for their active cooperation and thank the physicians and nurses at the Diagnostic Clinical Center No. 1 of the Moscow Department of Health.

Author contribution: Poryadin GV, Larina VN — study concept and design; Ryzhikh AA, Stodelova EA — data acquisition and processing; Stodelova EA, Kazimirskii AN — experimental studies, preparation of illustrations; Panina MI — statistical data processing; Kazimirskii AN — manuscript writing; Salmasi JM, Panina MI — editing.

Compliance with ethical standards: the study was approved by the Ethics Committee at the Pirogov Russian National Research Medical University (protocol № 203 of 21 December 2021); all patients submitted the informed consent to study participation.

✉ **Correspondence should be addressed:** Alexander N. Kazimirskii
Ostrovityanova, 1, Moscow, 117997, Russia; alnica10@mail.ru

Received: 29.10.2022 **Accepted:** 25.11.2022 **Published online:** 09.12.2022

DOI: 10.24075/brsmu.2022.057

НЕЙТРОФИЛЬНЫЕ И МОНОЦИТАРНЫЕ ЭКСТРАКЛЕТОЧНЫЕ ЛОВУШКИ В ДИАГНОСТИКЕ ПОСТКОВИДНОГО СИНДРОМА

Ж. М. Салмаси, Г. В. Порядин, М. И. Панина, В. Н. Ларина, А. А. Рыжих, Е. А. Стоделова, А. Н. Казимирский [✉]

Российский национальный исследовательский медицинский университет имени Н. И. Пирогова, Москва, Россия

Постковидный синдром характеризуется когнитивными и психическими нарушениями, болями в груди и суставах, нарушениями обоняния и вкуса, а также желудочно-кишечными и сердечными расстройствами. Диагностика постковидного синдрома основывается преимущественно на жалобах больных. В настоящее время оптимального метода диагностики не предложено. Целью исследования было сравнить информативность показателей, полученных при традиционном обследовании больных с постковидным синдромом, с уровнем в крови нейтрофильных (НЭЛ) и моноцитарных (МЭЛ) экстраклеточных ловушек. Исследовали нейтрофилы и моноциты, полученные от 21 больного в возрасте 18–59 лет с диагнозом постковидный синдром. Для визуализации и подсчета экстраклеточных ловушек использовали метод флуоресцентной микроскопии с применением флуоресцентного красителя для двухцепочечной ДНК SYBR Green (Evrogen). Клинико-лабораторные показатели не позволяют выявить специфичные для постковидного синдрома изменения. Вместе с тем, постковидный синдром характеризуется воспалительным процессом в сосудистом эндотелии. Лабораторным признаком такого асептического воспаления служат найденные нами в крови НЭЛ в нитевидной форме. Нитевидные структуры НЭЛ обнаружены только у тех больных, которые перенесли COVID-19 в легкой и среднетяжелой форме. А у больных, перенесших эту инфекцию в тяжелой форме, найдены нитевидные МЭЛ. Результаты исследования демонстрируют, что наиболее информативным диагностическим признаком постковидного синдрома является обнаружение в крови НЭЛ и МЭЛ в нитевидной форме.

Ключевые слова: постковидный синдром, диагностика, нейтрофильные экстраклеточные ловушки, моноцитарные экстраклеточные ловушки, нитевидные формы

Благодарности: авторы благодарят за активное сотрудничество всех участвовавших в исследовании пациентов и выражают признательность врачам и медицинским сестрам Диагностического клинического центра № 1 Департамента здравоохранения г. Москвы.

Вклад авторов: Г. В. Порядин, В. Н. Ларина — концепция и дизайн исследования; А. А. Рыжих, Е. А. Стоделова — сбор и обработка материала; Е. А. Стоделова, А. Н. Казимирский — экспериментальные исследования, подготовка иллюстративного материала; М. И. Панина — статистическая обработка материала; А. Н. Казимирский — написание текста; Ж. М. Салмаси, М. И. Панина — редактирование.

Соблюдение этических стандартов: исследование одобрено этическим комитетом РНИМУ им. Н. И. Пирогова (протокол № 203 от 21 декабря 2021 г.); все пациенты подписали добровольное информированное согласие на участие в исследовании.

✉ **Для корреспонденции:** Александр Николаевич Казимирский
ул. Островитянова, д. 1, г. Москва, 117997, Россия; alnica10@mail.ru

Статья получена: 29.10.2022 **Статья принята к печати:** 25.11.2022 **Опубликована онлайн:** 09.12.2022

DOI: 10.24075/vrgmu.2022.057

Post-COVID syndrome (long COVID, post-COVID-19 condition) is a novel poorly understood disorder. Despite the fact that there is no precise definition of post-COVID syndrome, many studies have shown that fatigue and dyspnoea are the most common symptoms that persist several months after the acute COVID-19 [1]. Other chronic manifestations of post-COVID-19 condition include cognitive and mental disorders, chest and joint pain, palpitations, myalgia, impaired sense of smell and taste, cough, headache, as well as gastrointestinal and cardiovascular disorders [2]. The post-COVID syndrome pathogenesis is associated with damage to the large number of different cells and organs resulting in a whole range of symptoms. The long-term symptoms emerge in patients having a history of both mild and severe COVID-19. The symptoms of previous COVID-19 are diverse, however, they are not systematized.

Post-COVID syndrome most often gradually regress within half a year, however, multi-organ disorders persist over a long time and complications develop in some patients. The diagnosis of post-COVID syndrome is subjective, it is based on the patients' complaints.

Blood coagulation disturbances can be observed in the majority of patients showing a variety of symptoms. A D-dimer test for determination of the fibrin degradation product formed during enzymatic hydrolysis of the blood clot protein network is used for laboratory confirmation of hemostatic disorders associated with post-COVID condition [3, 4]. However, high D-dimer concentrations are not observed in all patients, that is why D-dimer cannot be considered the full-fledged and unique marker of post-COVID syndrome. Currently, there is no optimal diagnosis method allowing one to identify the informative pathogenetically significant diagnostic criteria of post-COVID syndrome.

Given the fact that the post-COVID syndrome pathogenesis is associated with cell damage resulting in inflammation, it has been suggested that the functional activity of the major inflammatory cells, neutrophils and monocytes, could be changed. Extracellular trap formation is a manifestation of the involvement of these cells in inflammatory response.

The study was aimed to compare the informative value of the indicators obtained during conventional clinical and laboratory assessment of patients with post-COVID syndrome and the results of blood testing for neutrophil and monocyte extracellular traps.

METHODS

A total of 21 outpatients aged 18–59 (36 [27÷50]) were enrolled. Inclusion criteria: the diagnosis of post-COVID syndrome. The comparison group (control group) included 20 healthy donors aged 18–59 (38.5 [29÷51.5]) who had no history of coronavirus infection.

Biochemical parameters of blood collected from patients and healthy donors were defined using the Olympus 5800 biochemical analyzer (JP, Olympus Corporation; USA) in the diagnostic laboratory of the Diagnostic Clinical Center № 1 of the Moscow Department of Health. The study was carried out in the laboratory of the Department of Physiology and Clinical Pathophysiology at the Faculty of General Medicine, Pirogov Russian National Research Medical University. All the procedures were performed in accordance with the adopted ethical standards. The new laboratory tests, i.e. determination of neutrophil and monocyte extracellular traps, were used during the study along with conventional clinical and laboratory tests.

Determining the levels of neutrophil and monocyte extracellular traps. Cell fractionation

Isolation of neutrophils and monocytes

The patients' venous blood was collected in the siliconized EDTA tubes for prevention of blood clotting. To isolate neutrophils and monocytes from venous blood treated with EDTA, blood was two-fold diluted with sodium phosphate buffer (pH 7.4) and layered on top of the Ficoll-verografin double density gradient medium. The top layer density was 1.077 g/cm³, and the density of bottom layer was 1.190 g/cm³. After centrifugation (1600 rpm, 30 min) neutrophils accumulated in the interface between the gradients (98–100% purity), and the monocyte ring appeared on the surface of the gradient medium top layer (1.077).

Neutrophils and monocytes were twice washed with sodium phosphate buffer (50 mmol, pH 7.4) to remove the Ficoll impurities. Sedimentation of blood cells was performed by centrifugation (1200 rpm, 15 min). The isolated neutrophils and monocytes in the RPMI-1640 medium were used for cell culture experiments. The viability of the isolated neutrophils and monocytes was 95 and 99%, respectively.

Immunofluorescence detection of neutrophil and monocyte extracellular traps

Fluorescence microscopy was used for detection and enumeration of neutrophil and monocyte extracellular traps. The method is explored in detail in the patent application RF No. 2021104936/14 (010852).

The results were presented as percentage, the ratio of the number of extracellular traps against the total number of cells in the field of view.

The neutrophil and monocyte extracellular traps were detected using the SYBR Green fluorescent dye (Evrogen; Russia) capable of specific interaction with double-stranded DNA. The cells and extracellular structures were enumerated and photographed at ×700 magnification.

Statistical processing

The STATISTICA 12.0 software package (StatSoft Ink.; USA) was used for statistical data processing. The results were reported as mean (M) and standard error of the mean or, when the distribution was non-normal, these were reported as median (Me) and the 25th and 75th percentile values of the distribution of indicator values (interquartile range). The quantitative characteristics were compared using the Mann–Whitney U test and the Kruskal–Wallis analysis of variance. The differences were considered significant at $p < 0.05$.

RESULTS

Initial assessment of the patients in the index group was performed between days 60 and 119 since the disease onset, i.e. after 95 [89–109] days or 13.6 weeks. The age of patients with post-COVID syndrome was 36.0 [27.0–50.0] years, while the age of healthy donors was 38.5 [29.0–51.5] years ($p = 0.818$). The patients and healthy donors had almost the same body mass index: 25.0 [22.0–28.7] kg/m² and 24.6 [23.3–29.5] kg/m² ($p = 0.783$), respectively.

A total of 11 patients (52.4%) had a history of mild disease, 7 patients (33.3%) had a history of moderate disease, and 3 patients (14.3%) had a history of severe disease. The COVID-19

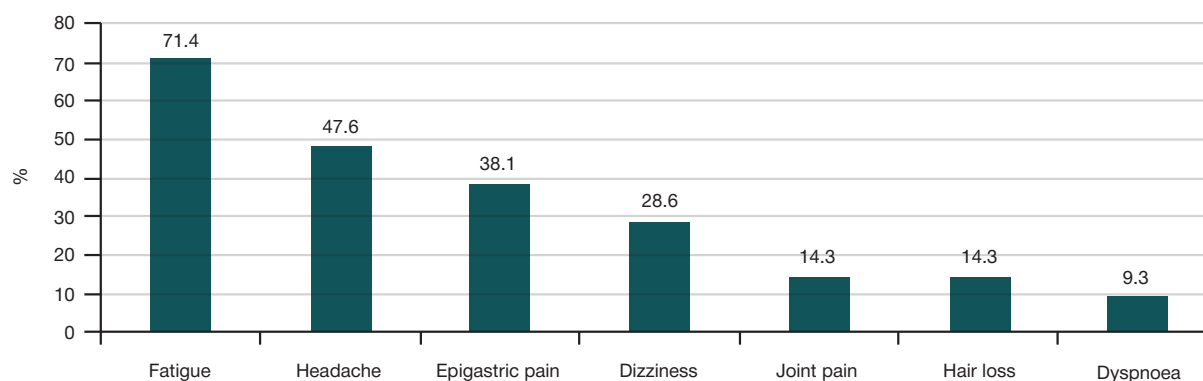


Fig. 1. Symptom occurrence in patients with post-COVID syndrome by day 95 [89–109] after the disease onset

symptom occurrence by day 95 [89–109] of the disease is provided in Fig. 1. On average, one patient had 1–6 symptoms (2.4 ± 1.1).

Fatigue, headache, epigastric pain, and dizziness were most often observed in the surveyed patients (Fig. 1). The patients less often complained of hair loss and dyspnoea. The other papers on the research of symptoms observed in patients with post-COVID syndrome most often report fatigue, myalgia,

headache, and the symptoms of autonomic disorders. It can be assumed that such clinical features are most typical for post-COVID syndrome. The symptom cluster that does not require specific treatment possibly results from microangiopathy and vascular endothelial damage.

Laboratory parameters of patients with post-COVID syndrome compared to that of healthy donors are provided in Table.

Table. Laboratory parameters of patients with post-COVID syndrome and healthy donors

Parameters	Patients with post-COVID syndrome ($n = 21$)	Healthy donors (controls) ($n = 20$)	Probability P
	Me [25–75]	Me [25–75]	
Hemoglobin (g/L)	136,0 [127,0–157,0]	133,5 [130,0–147,5]	0,725
Mean corpuscular hemoglobin (pg)	29,6 [29,0–30,4]	30,7 [30,1–32,0]	0,005
Red blood cell distribution width (%)	13,5 [12,7–14,1]	12,4 [12,1–12,9]	0,015
Red blood cell count ($10^{12}/L$)	4,7 [4,5–5,1]	4,3 [4,1–4,7]	0,005
White blood cell count ($10^9/L$)	6,2 [5,7–8,1]	5,5 [4,6–6,8]	0,059
Neutrophils ($10^9/L$)	3,1 [2,5–4,8]	3,3 [2,2–4,4]	0,583
Lymphocytes ($10^9/L$)	2,2 [2,0–2,9]	1,8 [1,3–2,1]	0,001
Eosinophils ($10^9/L$)	0,2 [0,1–0,2]	0,1 [0,1–0,2]	0,0007
Platelet count ($10^9/L$)	264,0 [228,0–316,0]	261,0 [221,0–292,0]	0,464
Leukopenia, n (%)	0	3 (15)	0,179
Neutropenia, n (%)	2 (9,5)	1 (5)	0,965
Vitamin D deficiency, n (%)	7 (33,3)	8 (40)	0,658
Elevated D-dimer levels, n (%)	1 (4,8)	2 (10)	0,706
Erythrocyte sedimentation rate (mm/h)	5,0 [2,0–10,0]	7,5 [3,5–9,5]	0,57
Vitamin D (ng/mL)	17,3 [14,1–23,3]	23,0 [16,9–36,8]	0,211
Iron ($\mu\text{mol}/L$)	14,4 [9,4–22,9]	18,5 [14,5–24,6]	0,25
Ferritin (ng/mL)	35,4 [17,1–105,4]	97,3 [43,5–191,5]	0,229
Alanine transaminase (U/L)	25,8 [16,0–43,0]	15,5 [13,0–21,0]	0,007
Aspartate transaminase (U/L)	22,0 [20,5–27,4]	19,0 [16,0–22,0]	0,028
Gamma-glutamyltransferase (U/L)	33,0 [33,0–51,8]	15,5 [11,5–30,5]	0,031
Alkaline phosphatase (U/L)	213,5 [128,9–834,0]	58,0 [53,0–76,5]	0,018
Cholesterol (mmol/L)	5,3 [4,6–5,9]	5,4 [5,1–5,9]	0,612
Low-density lipoprotein (mmol/L)	3,4 [2,3–3,5]	3,1 [2,6–3,8]	0,719
Potassium (mmol/L)	4,7 [4,4–4,9]	5,0 [4,6–5,1]	0,328
Uric acid ($\mu\text{mol}/L$)	332,0 [277,0–465,0]	285,0 [213,5–345,5]	0,114
Urea (mmol/L)	4,7 [3,9–6,6]	4,0 [3,5–5,1]	0,116
Creatinine (mmol/L)	75,5 [64,5–80,5]	70,0 [54,0–82,5]	0,292
Thyroid-stimulating hormone (mIU/L)	1,5 [1,1–1,8]	2,0 [1,2–2,7]	0,177
Glucose (mmol/L)	5,2 [5,1–5,8]	4,6 [4,4–4,8]	0,0007
D-dimer ($\mu\text{g}/L$)	235,0 [190,0–300,0]	247,5 [192,0–361,5]	0,831

Note: Me — median value; [25–75] — interquartile range.

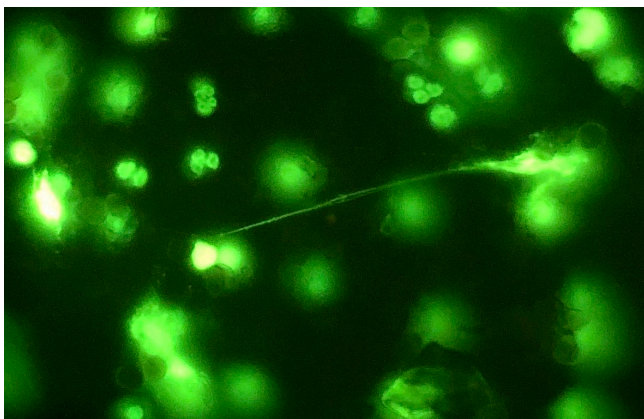


Fig. 2. Neutrophil extracellular traps in the form of single DNA filaments emerging from the neutrophil nuclei in patients with post-COVID syndrome

Thus, the patients with post-COVID syndrome showed some relative increase in the red blood cell, lymphocyte, and eosinophil counts in peripheral blood compared to controls, along with elevated liver enzyme levels and blood glucose concentrations. Despite the fact that the changes in blood parameters observed in patients were within the reference ranges, these were clearly not accidental. In our opinion, the relative increase in red blood cell counts observed in patients having a history of COVID-19 was associated with concomitant hypoxia.

The increase in transaminase activity and blood glucose levels could be due to moderate hepatocyte damage.

This assumption is confirmed by the increase in the gamma-glutamyltransferase and alkaline phosphatase enzyme activity. In our opinion, the observed moderate increase in the eosinophil and lymphocyte counts reflects the hypothalamo-pituitary-adrenal axis fatigue during COVID-19 resulting in certain reduction of the surveyed patients' blood cortisol levels. The D-dimer levels in these patients remain virtually unchanged, which can be explained by no thrombogenesis or bland thrombogenesis.

DISCUSSION

The clinical and laboratory indicators provided in Table make it generally impossible to reveal specific changes characteristic of post-COVID syndrome. However, it is known that post-COVID syndrome is characterized by severe inflammation in the vascular endothelium [5]. The filamentous forms of neutrophil extracellular traps (NETs) detected in blood are considered a laboratory feature of such aseptic inflammation [6]. It is noteworthy that these filamentous structures are found only in those patients who have a history of mild to moderate disease (Fig. 2). The amount of NETs in those who experienced mild illness was $6.55 \pm 0.94\%$ ($p < 0.05$), while in moderate cases the amount of NETs was $0.86 \pm 0.51\%$ ($p < 0.05$). No NETs were found in patients of these groups.

No NETs were revealed in patients having a history of severe COVID-19. However, DNA degradation products, the extracellular purine nitrogenous bases, were found in severe disease survivors [7]. We suggested the presence of the filamentous forms of METs and then detected those in such patients (Fig. 3). The levels of METs in these patients were low: $1.01 \pm 0.71\%$ ($p < 0.05$).

Enzymatic degradation of DNA filaments results in the emergence of factors of secondary alteration, the extracellular purine nitrogenous bases capable of damaging cells in the central nervous system (CNS) and internal organs, thus



Fig. 3. Monocyte extracellular traps in the form of single DNA filaments emerging from the cell nuclei in patients with post-COVID syndrome

maintaining aseptic inflammation. Moreover, filamentous forms of extracellular traps and elevated levels of extracellular purine nitrogenous bases have been reported in patients with post-COVID syndrome for a long time (three months or more). We believe that elevated levels of extracellular purine nitrogenous bases are the most significant factor of the post-COVID syndrome pathogenesis that should be restricted in order to prevent damage to the endothelium, cells of the CNS and internal organs. The filamentous structures originating from neutrophils and monocytes constitute the source of these damaging molecules (factors of secondary alteration). Thus, effective therapy should be aimed at restriction of the neutrophil and monocyte extracellular trap formation in patients with post-COVID syndrome.

Currently, the majority of researchers define the extracellular structures produced by neutrophils (NETs) as the net-like structures and believe that neutrophils produce these net-like structures only. However, this is not true. We have for the first time revealed the relationship between the neutrophil extracellular trap morphology and the type of inflammation, we have also found that filamentous forms of NETs are unique to aseptic inflammation [6]. The net-like NETs are formed only in cases of the favorable course of inflammation caused by infection [6]. The net-like structure of NET is of special physiological significance, since it is functionally active. The filaments of such net capture pathogens and dying cells of the body, and then perform retraction [8]. Monocytes/macrophages absorb and hydrolyze the net together with the pathogens and the remains of dead cells. Filamentous forms of NETs are not capable of such responses and serve as a source of the factors of secondary alteration, the extracellular purine nitrogenous bases. Furthermore, adenin, that is increasingly released during the enzymatic hydrolysis of DNA filaments, inhibits T cells and can cause secondary immunodeficiency. Our findings make it possible to conclude that detection of filamentous forms of neutrophil and monocyte extracellular traps in blood is the most typical diagnostic feature of post-COVID syndrome.

CONCLUSIONS

Filamentous forms of neutrophil and monocyte extracellular traps are the diagnostic feature of post-COVID syndrome. Filamentous forms of neutrophil extracellular traps were found in patients with post-COVID syndrome who had a history of mild to moderate COVID-19. No neutrophil extracellular traps were found in patients with post-COVID syndrome who had a history of severe disease, however, filamentous forms of monocyte extracellular traps were detected in blood of these patients.

References

1. Yong SJ. Long COVID or post-COVID-19 syndrome: putative pathophysiology, risk factors, and treatments. *Infect Dis (Lond)*. 2021; 53 (10): 737–54. DOI: 10.1080/23744235.2021.1924397.
2. Tirelli U, Taibi R, Chirumbolo S. Post COVID syndrome: a new challenge for medicine. *Eur Rev Med Pharmacol Sci*. 2021; 25 (12): 4422–5. DOI: 10.26355/eurrev_202106_26154.
3. Song X, Ji J, Reva B, Joshi H, Calinawan AP, Mazumdar M, Wisnivesky JP, et al. Post-anticoagulant D-dimer is a highly prognostic biomarker of COVID-19 mortality. *ERJ open research*. 2021; 7 (3): 18. DOI: 10.1183/23120541.00018-2021.
4. Townsend L, Fogarty H, Dyer A, Martin-Loeches I, Bannan C, Nadarajan P, et al. Prolonged elevation of D-dimer levels in convalescent COVID-19 patients is independent of the acute phase response. *J Thromb Haemost*. 2021; 19 (4): 1064–70. DOI: 10.1111/jth.15267.
5. Ostergaard L. SARS CoV-2 related microvascular damage and symptoms during and after COVID-19: Consequences of capillary transit-time changes, tissue hypoxia and inflammation. *Physiol Rep*. 2021; 9 (3): e14726. DOI: 10.14814/phy2.14726.
6. Kazimirskii AN, Salmasi JM, Poryadin GV, Panina MI. Novye vozmozhnosti diagnostiki i issledovaniya patogeneza razlichnykh vidov vospaleniya. *Patologicheskaya fiziologiya i ehksperimental'naya terapiya*. 2022; 66 (2): 34–42. DOI: 10.25557/0031-2991.2022.02.34-42. Russian.
7. Kazimirskii AN, Salmasi JM, Poryadin GV, Panina MI, Larina VN, Ryzhikh AA. Postkovidnyj sindrom associirovan s povysheniem vnekletochnykh purinovyx osnovanij i nejtrofil'nykh ehkstrakletochnykh lovushek v plazme krovi. *Byulleten' sibirskoj mediciny*. 2022; 21 (2): 41–47. DOI: 10.20538/1682-0363-2022-2-41-47. Russian.
8. Kukes IV, Salmasi JM, Ternovoy KS, Kazimirskii AN, Obodzinskaya TE, Lim VG, i dr. Predposylki k sozdaniyu atlasa postkovidnogo vospaleniya kak sposoba personalizirovannoj farmakoterapii, a takzhe prognozirovaniya i preduprezhdeniya organnykh i sistemnykh disfunkcij. *Medicinskij Sovet*. 2021; (12): 72–88. DOI: 10.21518/2079-701X-2021-12-72-88. Russian.

Литература

1. Yong SJ. Long COVID or post-COVID-19 syndrome: putative pathophysiology, risk factors, and treatments. *Infect Dis (Lond)*. 2021; 53 (10): 737–54. DOI: 10.1080/23744235.2021.1924397.
2. Tirelli U, Taibi R, Chirumbolo S. Post COVID syndrome: a new challenge for medicine. *Eur Rev Med Pharmacol Sci*. 2021; 25 (12): 4422–5. DOI: 10.26355/eurrev_202106_26154.
3. Song X, Ji J, Reva B, Joshi H, Calinawan AP, Mazumdar M, Wisnivesky JP, et al. Post-anticoagulant D-dimer is a highly prognostic biomarker of COVID-19 mortality. *ERJ open research*. 2021; 7 (3): 18. DOI: 10.1183/23120541.00018-2021.
4. Townsend L, Fogarty H, Dyer A, Martin-Loeches I, Bannan C, Nadarajan P, et al. Prolonged elevation of D-dimer levels in convalescent COVID-19 patients is independent of the acute phase response. *J Thromb Haemost*. 2021; 19 (4): 1064–70. DOI: 10.1111/jth.15267.
5. Ostergaard L. SARS CoV-2 related microvascular damage and symptoms during and after COVID-19: Consequences of capillary transit-time changes, tissue hypoxia and inflammation. *Physiol Rep*. 2021; 9 (3): e14726. DOI: 10.14814/phy2.14726.
6. Казимирский А. Н., Салмаси Ж. М., Порядин Г. В., Панина М. И. Новые возможности диагностики и исследования патогенеза различных видов воспаления. *Патологическая физиология и экспериментальная терапия*. 2022; 66 (2): 34–42. DOI: 10.25557/0031-2991.2022.02.34-42.
7. Казимирский А. Н., Салмаси Ж. М., Порядин Г. В., Панина М. И., Ларина В. Н., Рыжих А. А. Постковидный синдром ассоциирован с повышением внеклеточных пуриновых оснований и нейтрофильных экстраклеточных ловушек в плазме крови. *Бюллетень сибирской медицины*. 2022; 21 (2): 41–47. DOI: 10.20538/1682-0363-2022-2-41-47.
8. Кукес И. В., Салмаси Ж. М., Терновой К. С., Казимирский А. Н., Ободзинская Т. Е., Лим В. Г., и др. Предпосылки к созданию атласа постковидного воспаления как способа персонализированной фармакотерапии, а также прогнозирования и предупреждения органных и системных дисфункций. *Медицинский Совет*. 2021; (12): 72–88. DOI: 10.21518/2079-701X-2021-12-72-88.

ALGORITHM OF SEGMENTATION OF OCT MACULAR IMAGES TO ANALYZE THE RESULTS IN PATIENTS WITH AGE-RELATED MACULAR DEGENERATION

Ibragimova RR¹✉, Gilmanov II², Lopukhova EA², Lakman IA^{1,2}, Bilyalov AR¹, Mukhamadeev TR^{1,3}, Kutluyarov RV², Idrisova GM^{1,3}

¹ Bashkir State Medical University, Ufa, Russia

² Ufa State Aviation Technical University, Ufa, Russia

³ Optimedservice, Ufa, Russia

Age-related macular degeneration (AMD) is one of the main causes of loss of sight and hypovision in people over working age. Results of optical coherence tomography (OCT) are essential for diagnostics of the disease. Developing the recommendation system to analyze OCT images will reduce the time to process visual data and decrease the probability of errors while working as a doctor. The purpose of the study was to develop an algorithm of segmentation to analyze the results of macular OCT in patients with AMD. It allows to provide a correct prediction of an AMD stage based on the form of discovered pathologies. A program has been developed in the Python programming language using the PyTorch and TensorFlow libraries. Its quality was estimated using OCT macular images of 51 patients with early, intermediate, late AMD. A segmentation algorithm of OCT images was developed based on convolutional neural network. UNet network was selected as architecture of high-accuracy neural net. The neural net is trained on macular OCT images of 125 patients (197 eyes). The author algorithm displayed 98.1% of properly segmented areas on OCT images, which are the most essential for diagnostics and determination of an AMD stage. Weighted sensitivity and specificity of AMD stage classifier amounted to 83.8% and 84.9% respectively. The developed algorithm is promising as a recommendation system that implements the AMD classification based on data that promote taking decisions regarding the treatment strategy.

Keywords: artificial intelligence, neural network, age-related macular degeneration, optical coherent tomography, machine learning algorithm

Financing: the study was partially conducted as part of the State Assignment of the Ministry of Education and Science of the Russian Federation for the Ufa State Aviation Technical University (code of scientific assignment #FEUE-2021-0013, agreement № 075-03-2021-014) at the scientific research laboratory named 'Sensor systems based on appliances of integrated photonics' (sections 'Materials and methods', 'Study results', 'Discussion of results') and as part of the project backed by subsidies in the area of science taken from the budget of the Republic of Bashkortostan to ensure state support of scientific research conducted under the guidance of the leading scientists (НОЦ-ПМГ-2021, agreement with the Ufa State Aviation Technical University) (Introduction section).

Author contribution: Ibragimova RR — review of literature, data acquisition and analysis, writing an article; Gilmanov II — development of software, searching a database, testing the existing code components; Lopukhova EA — development of software, writing an article, data acquisition and analysis; Lakman IA, Mukhamadeev TR, Kutluyarov RV — study concept and design, scientific editing; Bilyalov AR — scientific editing; Idrisova GM — data analysis, scientific editing.

Compliance with ethical standards: the study was performed in accordance with the principles of Declaration of Helsinki; all patients signed voluntary informed consent to OCT.

✉ **Correspondence should be addressed:** Rada R. Ibragimova
Lenina, d. 3, Ufa, 450008, Russia; ibragimova.rada2016@yandex.ru

Received: 03.11.2022 **Accepted:** 03.12.2022 **Published online:** 27.12.2022

DOI: 10.24075/brsmu.2022.062

АЛГОРИТМ СЕГМЕНТАЦИИ ОКТ-ИЗОБРАЖЕНИЙ МАКУЛЫ ДЛЯ АНАЛИЗА ПАЦИЕНТОВ С ВОЗРАСТНОЙ МАКУЛЯРНОЙ ДЕГЕНЕРАЦИЕЙ

Р. Р. Ибрагимова¹✉, И. И. Гильманов², Е. А. Лопухова², И. А. Лакман^{1,2}, А. Р. Билялов¹, Т. Р. Мухамадеев^{1,3}, Р. В. Кутлугаров², Г. М. Идрисова^{1,3}

¹ Башкирский государственный медицинский университет, Уфа, Россия

² Уфимский государственный авиационный технический университет, Уфа, Россия

³ Закрытое акционерное общество «Оптимедсервис», Уфа, Россия

Одной из основных причин слепоты и слабовидения у лиц старшего трудоспособного возраста является возрастная макулярная дегенерация (ВМД), для диагностики которой крайне важны результаты оптической когерентной томографии (ОКТ). Создание рекомендательной системы для анализа ОКТ-снимков позволит сократить время на обработку визуальной информации и снизить вероятность ошибок в процессе работы врача. Целью исследования было разработать алгоритм сегментации для анализа данных ОКТ макулы пациентов с ВМД, позволяющий, основываясь на форме выделенных патологий, корректно предсказывать стадию развития ВМД. Разработана программа на языке программирования Python с использованием библиотеки PyTorch и TensorFlow. Качество работы программы оценили на ОКТ-изображениях макулы 51 пациента с ВМД ранней, промежуточной и поздней стадией. Разработанный алгоритм сегментации ОКТ-снимков, основанный на сверточной нейронной сети. В качестве архитектуры сверточной нейронной сети была выбрана сеть UNet. Нейронная сеть обучена на ОКТ-снимках макулы 125 пациентов (197 глаз). Авторский алгоритм продемонстрировал 98,1% верно сегментированных областей на ОКТ-снимках, наиболее важных для диагностики и определения стадии ВМД. Взвешенная чувствительность и специфичность классификатора стадий ВМД составили соответственно 83,8% и 84,9%. Разработанный алгоритм перспективен в качестве рекомендательной системы, реализующей классификацию ВМД на основе данных, способствующей принятию решений о тактике лечения пациентов.

Ключевые слова: искусственный интеллект, нейронная сеть, возрастная макулярная дегенерация, оптическая когерентная томография, алгоритм машинного обучения

Финансирование: исследование частично выполнено в рамках работ по государственному заданию Минобрнауки России для ФГБОУ ВО «УГАТУ» (код научной темы #FEUE-2021-0013, соглашение № 075-03-2021-014) в молодежной научно-исследовательской лаборатории НОЦ «Сенсорные системы на основе устройств интегральной фотоники» (разделы «Материалы и методы», «Результаты исследования», «Обсуждение результатов»), а также в рамках проекта, поддержанного субсидией в области науки из бюджета Республики Башкортостан для государственной поддержки научных исследований, проводимых под руководством ведущих ученых (НОЦ-ПМГ-2021, соглашение с ФГБОУ ВО «УГАТУ») (раздел «Введение»).

Вклад авторов: Р. Р. Ибрагимова — обзор литературы, получение и анализ данных, написание статьи; И. И. Гильманов — разработка программного обеспечения, поиск базы данных, тестирование существующих компонентов кода; Е. А. Лопухова — разработка программного обеспечения, написание статьи, получение и анализ данных; И. А. Лакман, Т. Р. Мухамадеев, Р. В. Кутлугаров — концепция и дизайн исследования, научное редактирование; А. Р. Билялов — научное редактирование; Г. М. Идрисова — анализ данных, научное редактирование.

Соблюдение этических стандартов: исследование проведено в соответствии с принципами Хельсинкской декларации; все пациенты подписали добровольное информированное согласие на проведение ОКТ.

✉ **Для корреспонденции:** Рада Радиковна Ибрагимова
ул. Ленина, д. 3, г. Уфа, 450008, Россия; ibragimova.rada2016@yandex.ru

Статья получена: 03.11.2022 **Статья принята к печати:** 03.12.2022 **Опубликована онлайн:** 27.12.2022

DOI: 10.24075/vrgmu.2022.062

Age-related macular degeneration (AMD) is one of the main causes of loss of sight and hypovision in people aged 50 and over [1–3]. An annual growth of patients with this pathology is noted due to an increased expectation of life and upgrading the methods of diagnostics [4, 5]. Thus, based on prognosis of the World Health Organization, a number of people with AMD will be increased by 1.2 times from 2020 to 2030 (from 195.6 to 243.3 million of people) [6].

There exist various classifications of AMD: we differentiate between dry (non-exudative and atrophic in the late stage) and wet (exudative or neovascular) forms of AMD [7, 8]. According to the Age-Related Eye Disease Study (AREDS), an early, intermediate and late stages of age-related macular degeneration have been identified [9]. Based on literature data, in 10–20% of cases the non-exudative form of disease is transformed into the exudative one; in other cases, the course is slowly progressing and results in a geographic atrophy [10–12]. Specific treatment of dry AMD is currently lacking, and the emphasis is on prevention measures [13]. Wet AMD leads to rapid and irreversible loss of central vision. Intravitreal injections of vascular endothelial growth factor (VEGF) inhibitors improve vision and reduce the possibility of blindness in wet AMD [14]. However, treatment success depends on many factors, one of which being modern diagnostics of the disease [3]. Optical coherence tomography (OCT) acquired the most widespread use both in clinical trials, and in real practice as a means of diagnostics and monitoring of patients with AMD [15–16]. It is highly informative, contactless and allows to estimate the architecture of eye structures and retina, in particular, in real time [17]. A growing number of patients with this pathology is accompanied by an increased need in OCT studies, improved capacity of medical institutions and improved quality of the method.

Analysis and interpretation of large amounts of data is one of the issues [18, 19]. It can be solved using artificial intelligence (AI). AI intelligence becomes a perspective trend in diagnostics of ophthalmological diseases [20]. Thus, machine learning can be used to detect peculiarities of retinal tissue structure to evaluate the changes in it [21], detect vascular plexuses [22] and such retinal lesions as intraretinal cysts or subretinal fluid [23]. Methods of deep learning have recently become popular in the sphere of computer vision and are now included into the area of retinal image analysis. The methods of detecting retinal disease based on isolated biomarkers have gained special recognition; it enables close imitation of visual analysis by an expert and makes verification of a classifier easier [24–30]. Latest studies in the area of integration of recommendation systems in ophthalmology reveal brilliant results regarding less time spent on diagnostics and influence of a human factor on the process of doctors' working [31, 32]. These systems were operated based on the intellectual algorithms similar to previously available ones, which proves relevance of the search and development of new algorithms that could be used to determine the signs of AMD of various stages on OCT images with high sensitivity and specificity.

The purpose of the research is to develop an algorithm of segmentation to analyze macular OCT data in patients with AMD, that enables proper prediction of an AMD stage based on the form of extracted pathologies.

METHODS

To solve the set task, supervised learning was used. During this training, the intellectual algorithm compares incoming and expert-labeled data increasing the generalization ability

for unknown examples. At the stage of formation of three samples (training, validation and test ones), it was decided to use the database obtained during a standard ophthalmological examination and macular OCT using Avanti XR (Optovue; USA) and REVO NX (Optopol; Poland) at Optimed Center for Laser Eye Surgery (Ufa, Russia). Direct formation of a data set made it possible to regulate the parameters of the ratio of classes (stages) of the disease, gender and age-related distribution of patients and concomitant diseases, and a number of produced biomarkers, resulting in analysis of working algorithm outcomes in the presence of formerly known peculiarities of a set of OCT images. Incoming data included OCT macular images of 125 patients (197 eyes) with 89 women and 36 men having a mean age of 74.88 years (40–97). Inclusion criteria: patients with early (32%), intermediate (26%) and late (42%) stages AMD with sufficient transparency of optical media. Exclusion criteria: presence of diabetic retinopathy, retinal vessel occlusion; pachichoroid diseases; pathology of vitreomacular interface; and myopic choroidal neovascularization. The obtained set of OCT images consisted of training, validation and testing samples that account for 80, 10 and 10% respectively. Python programming language was a tool to develop an algorithm of image classification and formatting using TensorFlow and Pytorch libraries. Predictors of AMD stages were searched using the convolutional neural network segmenting the eye pathology. The operation principle of this neural networks was based on multi-layered successive convolution of an image with filters, whereas weight coefficients are selected while training an algorithm. These filters are intended to mark various image-located forms and textures in accordance with the principle of cerebral cortex operation having small parts of cells sensitive to certain areas of the field of vision. UNet initially created for segmentation of biomedical images was selected as architecture of a convolutional neural network. This architecture implements not only a slow increase of numerous signs (a tensor) that characterize the incoming image using four layers of convolution with filters and compression in encoder. It also preserves data related to their localization on the image by adhesion to parallel layers of convolution and use of operations reverse to file compression in a decoder.

ReLU was used as a function of activation. It provided qualitative training of a model using a relatively low amount of incoming data. OpenCV library was selected to ensure the best indicators of image processing and noise clearance.

To solve the issue of overfitting, several approaches were reviewed. Transfer learning, when the applied network is previously educated using a large set of data, is a popular method in this context [33–35]. However, it should be taken into account that the biomarkers marked on an OCT image will have little correlation with entities produced by networks trained using common databases such as ImageNet. This can make the method less effective [36, 37]. Using methods of attention concentration is another approach that reduces the probability of network overfitting. For this, a block of attention was added to the neural network structure following every convolution layer. This block included searching of key points of the outcome of the layer process and increase of nearby values of network-processed tensor elements, on one hand, and a method of searching the adaptive limit value of tensor elements, on the other hand.

Classification based on segmented data was done by calculating the area of the largest pathologies of the same nature. The limit values were determined taking into consideration clinical signs of AMD by the size of concomitant pathologies [9].

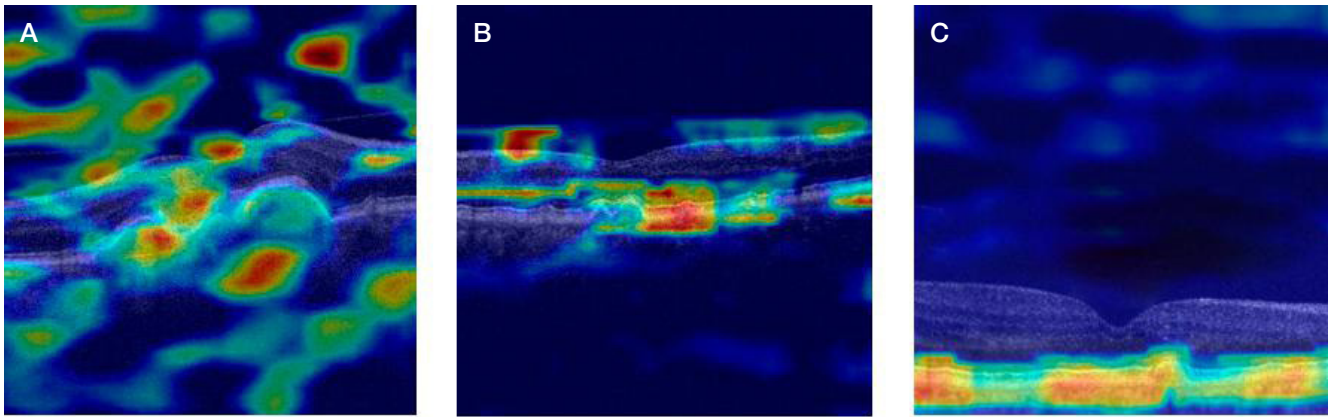


Fig. 1. Class activation cards: with no use of attention concentration module (A); while using the SIFT method (B); while using the SALV method (C)

It was estimated whether an AMD stage was classified properly based on the automatic recognition of OCT images and analysis of the nine-field coupling matrix, which is a matrix that provides correspondence between the actual and predicted AMD stages (early, intermediate, late). Three four-field coupling matrices developed using the principle of prediction of one AMD stages only were obtained. Thus, values of specificity and sensitivity for every AMD stages were calculated for every matrix. Sensitivity means a percentage of properly predicted cases of a certain stages of AMD, whereas specificity is a percentage of properly predicted cases not related to the AMD stages.

Weighted sensitivity (Se_w) and specificity (Sp_w) of the entire classification algorithm were calculated using definite values

$$Se_w = \frac{Se_1 n_1 + Se_2 n_2 + Se_3 n_3}{n},$$

$$Sp_w = \frac{Sp_1 n_1 + Sp_2 n_2 + Sp_3 n_3}{n},$$

where Se_1 , Sp_1 mean sensitivity and specificity of early AMD recognition; Se_2 , Sp_2 denote sensitivity and specificity of late AMD recognition; Se_3 , Sp_3 mean sensitivity and specificity of intermediate AMD recognition; n_1 means a number of cases with early AMD; n_2 means a number of cases with late AMD; n_3 means a number of cases with intermediate AMD, where $n = n_1 + n_2 + n_3$.

RESULTS

To develop a recommendation system determining AMD stages, an approach imitating a visual analysis made by an expert was selected. When it is used, position and form of disease pathologies can be found on an OCT image and they can be compared with a previous diagnostic experience. At the stage of detecting pathologies, the key issue consists in transfer of an expert's experience in its differentiation with an intellectual algorithm. As use of methods of deep learning displays its effectiveness and immunity to the variety of incoming information only in the presence of a sufficient scope

of the training samples, which is proportional to the algorithm complexity [38], a set of marked OCT images is required. Its generation is a resource-intensive task.

To avoid the limitation in the structure of UNet segmenting neural network, it was decided to include a block of additional treatment of a set of signs from an output of the convolution layer. This is how data about pathology contours were preserved, which could be reduced to the neural network attention concentration. The presented approach enables to decrease the complexity of the applied neural network algorithm by reducing a number of educated values while preserving exactness in a training sample. Effectiveness of the attention concentration approach was estimated by comparing the exact determination of segmented abnormal area borders using test data and analysis of class activation maps of abnormal retinal parts of UNet coder that visualizes the key areas of the images used for segmentation of this predictor.

During training of the neural network with a set of data formed by the authors with no involvement of the attention concentration block into UNet, the segmentation results amounted to 58.7% of properly segmented abnormal areas. The class activation maps presented in Fig. 1A, display little concentration of attention on AMD signs. This is how low accuracy of pathology borderlines can be explained.

When selecting an algorithm of the attention concentration block it has been taken into account that retinal layers on OCT images have a properly marked difference in shades of gray. Deformation of pigmented epithelium and neuroepithelial edema are clearly seen. These shades, considering their difference in size during different stages of the disease, can be revealed by finding scale-invariant key points with Scale-Invariant Feature Transform (SIFT) [39]. They denote edges and angles and deformity margins on the image using the method of searching the adaptive limit value (SALV). The method proved to be effective while detecting pathologies [40].

The SIFT approach with a fixed lower threshold of key point scope, equal to the minimal sizes of drusen found in early stages of AMD [9] enabled to improve exactness of abnormal

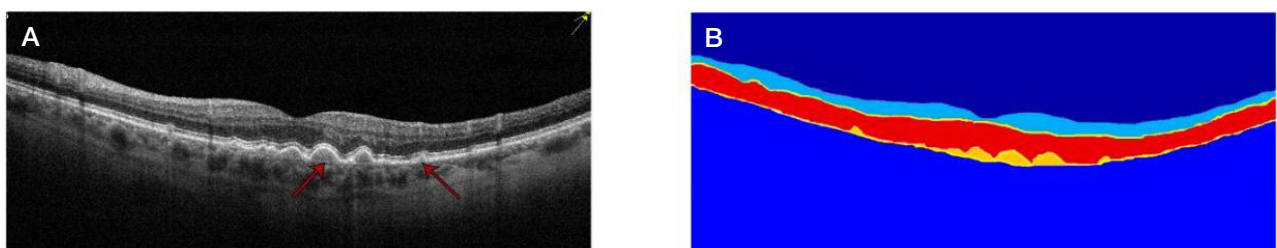


Fig. 2. OCT macular images in early and intermediate AMD. A. Hard and soft Bruch's membrane drusen (red arrows) marked by the doctor. B. Algorithm segmented image

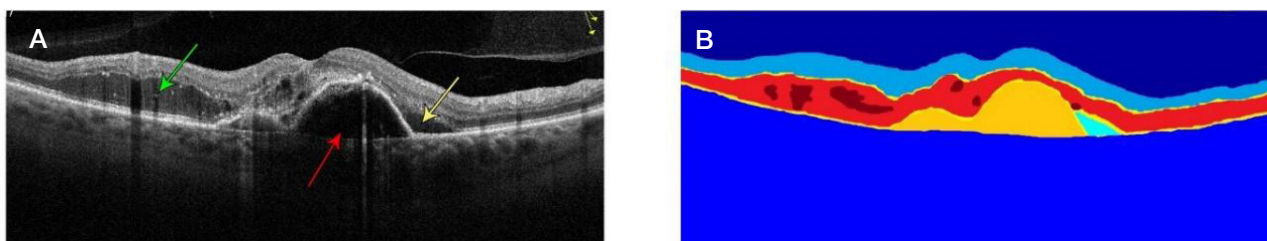


Fig. 3. OCT image late macular OCT image in AMD. **A.** Signs of AMD recorded by the physician (described in the text). **B.** Algorithm segmented data

segmentation to 76.7%. However, the attention concentration block helps find key areas not related to pathologies (Fig. 1B), decreasing the concentration of the neural network.

While using the attention concentration block based on the SALV method, accuracy of properly segmented abnormal areas was achieved in 98.1% of cases. Owing to the method, the entire attention of the neural network was concentrated on drusen (Fig. 1C). When the rate of occurred pathologies was changed from equally likely to statistical [10, 11], exact detection of neuroepithelial edema was reduced by 15%. Thus, to increase effectiveness, a conclusion was made that distribution of all pathologies on the training sample should be regular.

Segmentation results for predictors of dry intermediate AMD using the latest version of attention concentration block are well shown on Fig. 2. Hard and soft drusen of Bruch's membrane that deform the pigmented epithelium (displayed in arrows) are visualized on OCT macular images (Fig. 2A). The layers that correspond to structural elements of photoreceptors are above the drusen. The internal layers of neuroepithelium are clear and not deformed. Foveolar deepening has a proper configuration. In Fig. 2B these areas are segmented using the algorithm where the deformed pigmented epithelium is shown in yellow, just like the orange layers above the drusen.

Retinal thickness is increased due to cystic edema of neuroepithelium (green arrow), local elevation of pigmented epithelium probably occurring due to the hidden neovascular membrane (red arrow) with accumulation of hyporeflexive content found under the neuroepithelium (yellow arrow). The fovea is concave. On Fig. 3B neuroepithelial edema is highlighted in dark red, elevation of pigmented epithelium in orange, and fluid accumulation under the neuroepithelium in blue. Predictors of late AMD are shown on Fig. 3A.

Automatic classification of AMD stages was done based on the obtained results, and values of specificity and sensitivity for each stage were calculated as well (Table). Based on the acquired values, the weighted values of sensitivity and specificity of a stage classifier ($Se_w = 0.838$ and $Sp_w = 0.849$) were calculated.

DISCUSSION

The presented results were obtained while using OCT images from tomography scanners of several manufacturers. This produced a significant effect on accurate operation of segmentation algorithm due to differences in data visualization. Owing to specific block attention concentration methods when various labeling of OCT images is provided along with predictors, it is necessary to implement additional training of the recommendation system using new examples or remove

the mentioned data. In this case, preliminary treatment of images can be required.

It should also be noted that the obtained forms of segmented areas will differ depending on the disease presence and stage. The data contain predictors needed for detection and determination of an AMD stage by the recommendation system. However, in some cases the limits of the ratio of abnormal area shape and proper diagnosis in an expert opinion can be rather blurred due to individual features of the disease course in a patient and in a different selection of eye radial scanning images.

Thus, a fully connected layer, which is the most frequently applied in computer vision tasks with neural networks, as a classifier of AMD stages will also require an extensive training sample to provide the indistinct borders. Considering statistics about an irregular frequency of AMD stage determination [10, 11], the task can't be solved easily. Same conclusions will be just for the limit values of AMD stage determination by the area of pathologies. It means that their hard task can involve additional errors. It is advisable to use methods of imprecise logics that effectively display a doctor's heuristic experience to analyze the signs resulting from the segmentation algorithm.

The obtained composite indices of specificity and sensitivity of the classification algorithm display proper quality of recognition of AMD stages (> 83%). Their values were mainly determined by a classification of OCT images from several tomography scanners with various imaging techniques. This occurs due to a wish to improve the generalizing capability of the algorithm for appliances from different manufacturers. It should also be noted that the average result of sensitivity is obtained for the intermediate AMD (58% only). It occurs because the stage of AMD is the most complicated one for recognition due to very similar forms of pathologies. It is suggested that methods of fuzzy logic should be applied to improve sensitivity while determining the stage of AMD during subsequent studies.

CONCLUSIONS

The machine learning algorithm was developed to segment the AMD pathologies based on OCT-images with attention concentration. A physician can apply the obtained results to focus on the most important for diagnostics areas or as part of the recommendation system of detection and determination of an AMD stage that has to be developed in subsequent studies. The algorithm displayed its perspectives regarding organizational issues associated with AMD diagnostics, less load on ophthalmologists, and effective recognition of AMD on OCT images with 98.1% of properly segmented abnormal areas.

Table. Values of specificity and sensitivity for every stage

Quality metrics	Late	Early	Intermediate
Sensitivity Se	0.929	0.921	0.58
Specificity Sp	0.823	0.769	0.993

References

- Zapata MA, Royo-Fibla D, Font O, Vela JI, Marcantonio I, Moya-Sánchez EU, et al. Artificial intelligence to identify retinal fundus images, quality validation, laterality evaluation, macular degeneration, and suspected glaucoma. *Clinical Ophthalmology (Auckland, NZ)*. 2020; 14: 419. Available from: <https://www.ncbi.nlm.nih.gov/pmc/articles/PMC7025650/>.
- Stark K, Olden M, Brandt C, Dietl A, Zimmermann ME, Schelker SC, et al. The German AugUR study: study protocol of a prospective study to investigate chronic diseases in the elderly. *BMC geriatrics*. 2015; 15 (1): 1–8. Available from: <https://link.springer.com/article/10.1186/s12877-015-0122-0>.
- Mehta S. Age-related macular degeneration. *Primary Care: Clinics in Office Practice*. 2015; 42 (3): 377–91. Available from: [https://www.primarycare.theclinics.com/article/S0095-4543\(15\)00042-1/fulltext](https://www.primarycare.theclinics.com/article/S0095-4543(15)00042-1/fulltext).
- Lawrenson JG, Evans JR, Downie LE. A critical appraisal of national and international clinical practice guidelines reporting nutritional recommendations for age-related macular degeneration: are recommendations evidence-based? *Nutrients*. 2019; 11 (4): 823. Available from: <https://www.mdpi.com/2072-6643/11/4/823>.
- Li JQ, Welchowski T, Schmid M, Mauschitz M M, Holz FG, Finger RP. Prevalence and incidence of age-related macular degeneration in Europe: a systematic review and meta-analysis. *British Journal of Ophthalmology*. 2020; 104 (8): 1077–84. Available from: <https://bj.o.bmj.com/content/104/8/1077.abstract>.
- Vsemirnyj doklad o probleme zreniya [World report on vision]. Zheneva: Vsemirnaya organizaciya zdravooxraneniya, 2020. Licenziya: CC BY-NC-SA 3.0 IGO.
- Balashovich LI, Izmajlov AS, Ulitina AY. Modificirovannaya klinicheskaya klassifikaciya vozrastnoj makulyarnoy degeneracii. *Oftal'mologicheskie vedomosti*. 2011; 4 (4): 41–47. Available from: <https://cyberleninka.ru/article/n/modifitsirovannaya-klinicheskaya-klassifikatsiya-vozrastnoy-makulyarnoy-degeneratsii>. Russian.
- Avdeeva ON, Avetisov SEh, Aklaeva NA, Akopov EL, Alekseev VN, Astaxov SYu, i dr. redaktory. *Oftal'mologiya: nacional'noe rukovodstvo*. M.: GEHOTAR-Media, 2018; 625 s. Russian.
- Ferris III FL, Wilkinson CP, Bird A, Chakravarthy U, Chew E, Csaky K, et al. Beckman Initiative for Macular Research Classification Committee. Clinical classification of age-related macular degeneration. *Ophthalmology*. 2013; 120 (4): 844–51. Available from: <https://www.sciencedirect.com/science/article/abs/pii/S016164201201055X>.
- Hyttinen JM, Kannan R, Felszeghy S, Niittykoski M, Salminen A, Kaarniranta K. The regulation of NFE2L2 (NRF2) signalling and epithelial-to-mesenchymal transition in age-related macular degeneration pathology. *International journal of molecular sciences*. 2019; 20 (22): 5800. Available from: <https://www.mdpi.com/1422-0067/20/22/5800>.
- Friedman DS, O'Colmain BJ, Munoz B, Tomany SC, McCarty C, De Jong Pt, et al. Prevalence of age-related macular degeneration in the United States. *Arch ophthalmol*. 2004; 122 (4): 564–72. Available from: <https://jamanetwork.com/journals/jamaophthalmology/article-abstract/416232>.
- Schultz NM, Bhardwaj S, Barclay C, Gaspar L, Schwartz J. Global Burden of Dry Age-Related Macular Degeneration: A Targeted Literature Review. *Clin Ther*. 2021; 43 (10): 1792–818. DOI: 10.1016/J.CLINTHERA.2021.08.011.
- The Age-Related Eye Disease Study Research Group. A randomized, placebo-controlled, clinical trial of supplementation with vitamins C and E and beta-carotene for age related cataract and vision loss: AREDS report number 9. *Arch. Ophthalmol*. 2001; 119: 1439–52.
- Varma R, Bressler NM, Doan QV, Danese M, Dolan CM, Lee A, et al. Visual impairment and blindness avoided with ranibizumab in Hispanic and non-Hispanic whites with diabetic macular edema in the United States. *Ophthalmology*. 2015; 122 (5): 982–89. Available from: <https://www.sciencedirect.com/science/article/pii/S0161642014011476>.
- Aznabaev BM, Muxamadeev TR, Dibaev TI. Opticheskaya kogerentnaya tomografiya + angiografiya glaza v diagnostike, terapii i xirurgii glaznyx boleznej. M.: Avgust Borg, 2019; 57 s. Russian.
- Drexler W, Fujimoto JG, editors. *Optical coherence tomography: technology and applications*. Berlin: Springer, 2015; 2.
- Victor AA. *The Role of Imaging in Age-Related Macular Degeneration*. In *Visual Impairment and Blindness-What We Know and What We Have to Know*. London, UK: IntechOpen, 2019.
- Schmidt-Erfurth U, Sadeghipour A, Gerendas BS, Waldstein SM, Bogunović H. Artificial intelligence in retina. *Progress in retinal and eye research*. 2018; 67: 1–29. Available from: <https://www.sciencedirect.com/science/article/pii/S1350946218300119>.
- Venhuizen FG, van Ginneken B, van Asten F, van Grinsven MJ, Fauser S, Hoyng CB, et al. Automated staging of age-related macular degeneration using optical coherence tomography. *Investigative ophthalmology & visual science*. 2017; 58 (4): 2318–28. Available from: <https://iovs.arvojournals.org/article.aspx?articleid=2623584>.
- Shlyapnikova OA, Kamenskix TG, Roshhepkin VV, Reshnikova LB. Perspektivnye napravleniya razvitiya oftal'mologii (obzor). *Saratovskij nauchno-medicinskij zhurnal*. 2021; 17 (3): 675–8. Available from: <https://cyberleninka.ru/article/n/perspektivnye-napravleniya-razvitiya-oftal'mologii-obzor>. Russian.
- Quelleg G, Lee K, Dolejsi M, Garvin MK, Abramoff MD, Sonka M. Three-dimensional analysis of retinal layer texture: identification of fluid-filled regions in SD-OCT of the macula. *IEEE transactions on medical imaging*. 2010; 29 (6): 1321–30. Available from: <https://ieeexplore.ieee.org/abstract/document/5440910>.
- Hu Z, Niemeijer M, Abramoff MD, Garvin MK. Multimodal retinal vessel segmentation from spectral-domain optical coherence tomography and fundus photography. *IEEE transactions on medical imaging*. 2012; 31 (10): 1900–11. Available from: <https://ieeexplore.ieee.org/abstract/document/6228540>.
- Esmaili M, Dehnavi AM, Rabbani H, Hajizadeh F. Three-dimensional segmentation of retinal cysts from spectral-domain optical coherence tomography images by the use of three-dimensional curvelet based K-SVD. *Journal of medical signals and sensors*. 2016; 6 (3): 166. Available from: <https://www.ncbi.nlm.nih.gov/pmc/articles/PMC4973460/>.
- Chakravarty A, Sivaswamy J. A supervised joint multi-layer segmentation framework for retinal optical coherence tomography images using conditional random field. *Comput. Methods Programs Biomed*. 2018; 165: 235–50. DOI: 10.1016/J.CMPB.2018.09.004.
- Bogunović H, et al. Machine Learning of the Progression of Intermediate Age-Related Macular Degeneration Based on OCT Imaging. *Investigative ophthalmology & visual science*. 2017; 58 (6): BIO141–BIO150.
- Tvenning AO, Hanssen SR, Austeng D, Morken TS. Deep learning identify retinal nerve fibre and choroid layers as markers of age-related macular degeneration in the classification of macular spectral-domain optical coherence tomography volumes. *Acta Ophthalmologica*. 2022. DOI: 10.1111/AOS.15126.
- Rim TH, et al. Detection of features associated with neovascular age-related macular degeneration in ethnically distinct data sets by an optical coherence tomography: trained deep learning algorithm. *British Journal of Ophthalmology*. 2020; 105 (8): 1133–9. DOI: 10.1136/BJOPHTHALMOL-2020-316984.
- Zhang G, et al. Clinically relevant deep learning for detection and quantification of geographic atrophy from optical coherence tomography: a model development and external validation study. *Lancet Digit Heal*. 2021; 3 (10): e665–e675. DOI: 10.1016/S2589-7500(21)00134-5.
- Sousa JA, Paiva A, Silva A, Almeida JD, Braz Junior G, Diniz JO, et al. Automatic segmentation of retinal layers in OCT images with intermediate age-related macular degeneration using U-Net and DexiNed. *Plos one*. 2021; 16 (5): e0251591.
- Alsaih Khaled, et al. Deep learning architectures analysis for age-related macular degeneration segmentation on optical coherence tomography scans. *Computer methods and programs*

- in biomedicine. 2020; 195: 105566.
31. Lee B, D'Souza M, Singman EL, Wang J, Woreta FA, Boland MV, et al. Integration of a physician assistant into an ophthalmology consult service in an academic setting. *American journal of ophthalmology*. 2018; 190: 125–33. Available from: <https://www.sciencedirect.com/science/article/abs/pii/S0002939418301387>.
 32. Pandey SK, Sharma V. Robotics and ophthalmology: Are we there yet? *Indian Journal of Ophthalmology*. 2019; 67 (7): 988. Available from: <https://www.ncbi.nlm.nih.gov/pmc/articles/PMC6611303/>.
 33. Yan Y, Jin K, Gao Z, Huang X, Wang F, Wang Y, et al. Attention — based deep learning system for automated diagnoses of age-related macular degeneration in optical coherence tomography images. *Medical Physics*. 2021; 48 (9): 4926–34. DOI: 10.1002/MP.15002.
 34. Treder M, Laueremann JL, Eter N. Automated detection of exudative age-related macular degeneration in spectral domain optical coherence tomography using deep learning. *Graefes Archive for Clinical and Experimental Ophthalmology*. 2017; 256 (2): 259–65. DOI: 10.1007/S00417-017-3850-3.
 35. Bhatia KK, Graham MS, Terry L, Wood A, Tranos P, Trikha S, et al. Disease classification of macular optical coherence tomography scans using deep learning software: validation on independent, multicenter data. *Retina*. 2020; 40 (8): 1549–57. DOI: 10.1097/IAE.0000000000002640.
 36. Tvenning AO, Hanssen SR, Austeng D, Morken TS. Deep learning identify retinal nerve fibre and choroid layers as markers of age-related macular degeneration in the classification of macular spectral-domain optical coherence tomography volumes. *Acta Ophthalmologica*. 2022. DOI: 10.1111/AOS.15126.
 37. Sunija AP, Kar S, Gayathri S, Gopi VP, Palanisamy P. Octnet: A lightweight cnn for retinal disease classification from optical coherence tomography images. *Computer methods and programs in biomedicine*. 2021; 200: 105877. DOI: 10.1016/J.CMPB.2020.105877.
 38. Juba B, Le HS. Precision-recall versus accuracy and the role of large data sets. In *Proceedings of the AAAI conference on artificial intelligence*. 2019; 33 (01): 4039–48. DOI: 10.1609/AAAI.V33I01.33014039.
 39. Lowe DG. Distinctive image features from scale-invariant keypoints. *International journal of computer vision*. 2004; 60 (2): 91–110. Available from: <https://link.springer.com/article/10.1023/B:VISI.0000029664.99615.94>
 40. Shahedi MB, Amirfattahi R, Azar FT, Sadri S. Accurate breast region detection in digital mammograms using a local adaptive thresholding method. In *Eighth International Workshop on Image Analysis for Multimedia Interactive Services (WIAMIS'07)*. IEEE. 2007; 26–26. Available from: <https://ieeexplore.ieee.org/abstract/document/4279134>.

Литература

1. Zapata MA, Royo-Fibla D, Font O, Vela JI, Marcantonio I, Moya-Sánchez EU, et al. Artificial intelligence to identify retinal fundus images, quality validation, laterality evaluation, macular degeneration, and suspected glaucoma. *Clinical Ophthalmology (Auckland, NZ)*. 2020; 14: 419. Available from: <https://www.ncbi.nlm.nih.gov/pmc/articles/PMC7025650/>.
2. Stark K, Olden M, Brandl C, Dietl A, Zimmermann ME, Schelker SC, et al. The German AugUR study: study protocol of a prospective study to investigate chronic diseases in the elderly. *BMC geriatrics*. 2015; 15 (1): 1–8. Available from: <https://link.springer.com/article/10.1186/s12877-015-0122-0>.
3. Mehta S. Age-related macular degeneration. *Primary Care: Clinics in Office Practice*. 2015; 42 (3): 377–91. Available from: [https://www.primarycare.theclinics.com/article/S0095-4543\(15\)00042-1/fulltext](https://www.primarycare.theclinics.com/article/S0095-4543(15)00042-1/fulltext).
4. Lawrenson JG, Evans JR, Downie LE. A critical appraisal of national and international clinical practice guidelines reporting nutritional recommendations for age-related macular degeneration: are recommendations evidence-based? *Nutrients*. 2019; 11 (4): 823. Available from: <https://www.mdpi.com/2072-6643/11/4/823>.
5. Li JQ, Welchowski T, Schmid M, Mauschwitz M M, Holz FG, Finger RP. Prevalence and incidence of age-related macular degeneration in Europe: a systematic review and meta-analysis. *British Journal of Ophthalmology*. 2020; 104 (8): 1077–84. Available from: <https://bjo.bmj.com/content/104/8/1077.abstract>.
6. Всемирный доклад о проблемах зрения [World report on vision]. Женева: Всемирная организация здравоохранения, 2020. Лицензия: CC BY-NC-SA 3.0 IGO.
7. Балашевич Л. И., Измайлов А. С., Улитина А. Ю. Модифицированная клиническая классификация возрастной макулярной дегенерации. *Офтальмологические ведомости*. 2011; 4 (4): 41–47. Available from: <https://cyberleninka.ru/article/n/modifitsirovannaya-klinicheskaya-klassifikatsiya-vozzrastnoy-makulyarnoy-degeneratsii>.
8. Авдеева О. Н., Аветисов С. Э., Аклаева Н. А., Акопов Е. Л., Алексеев В. Н., Астахов С. Ю., и др. редакторы. *Офтальмология: национальное руководство*. М.: ГЭОТАР-Медиа, 2018; 625 с.
9. Ferris III FL, Wilkinson CP, Bird A, Chakravarthy U, Chew E, Csaky K, et al. Beckman Initiative for Macular Research Classification Committee. Clinical classification of age-related macular degeneration. *Ophthalmology*. 2013; 120 (4): 844–51. Available from: <https://www.sciencedirect.com/science/article/abs/pii/S016164201201055X>.
10. Hyttinen JM, Kannan R, Felszeghy S, Niittykoski M, Salminen A, Kaarniranta K. The regulation of NFE2L2 (NRF2) signalling and epithelial-to-mesenchymal transition in age-related macular degeneration pathology. *International journal of molecular sciences*. 2019; 20 (22): 5800. Available from: <https://www.mdpi.com/1422-0067/20/22/5800>.
11. Friedman DS, O'Colmain BJ, Munoz B, Tomany SC, McCarty C, De Jong Pt, et al. Prevalence of age-related macular degeneration in the United States. *Arch ophthalmol*. 2004; 122 (4): 564–72. Available from: <https://jamanetwork.com/journals/jamaophthalmology/article-abstract/416232>.
12. Schultz NM, Bhardwaj S, Barclay C, Gaspar L, Schwartz J. Global Burden of Dry Age-Related Macular Degeneration: A Targeted Literature Review. *Clin Ther*. 2021; 43 (10): 1792–818. DOI: 10.1016/J.CLINTHERA.2021.08.011.
13. The Age-Related Eye Disease Study Research Group. A randomized, placebocontrolled, clinical trial of supplementation with vitamins C and E and beta-carotene for age related cataract and vision loss: AREDS report number 9. *Arch. Ophthalmol*. 2001; 119: 1439–52.
14. Varma R, Bressler NM, Doan QV, Danese M, Dolan CM, Lee A, et al. Visual impairment and blindness avoided with ranibizumab in Hispanic and non-Hispanic whites with diabetic macular edema in the United States. *Ophthalmology*. 2015; 122 (5): 982–89. Available from: <https://www.sciencedirect.com/science/article/pii/S0161642014011476>.
15. Азнабаев Б. М., Мухамадеев Т. Р., Дибаяев Т. И. Оптическая когерентная томография + ангиография глаза в диагностике, терапии и хирургии глазных болезней. М.: Август Борг, 2019; 57 с.
16. Drexler W, Fujimoto JG, editors. *Optical coherence tomography: technology and applications*. Berlin: Springer, 2015; 2.
17. Victor AA. The Role of Imaging in Age-Related Macular Degeneration. In *Visual Impairment and Blindness-What We Know and What We Have to Know*. London, UK: IntechOpen, 2019.
18. Schmidt-Erfurth U, Sadeghipour A, Gerendas BS, Waldstein SM, Bogunović H. Artificial intelligence in retina. *Progress in retinal and eye research*. 2018; 67: 1–29. Available from: <https://www.sciencedirect.com/science/article/pii/S1350946218300119>.
19. Venhuizen FG, van Ginneken B, van Asten F, van Grinsven MJ, Fauser S, Hoyng CB, et al. Automated staging of age-related macular degeneration using optical coherence tomography. *Investigative ophthalmology & visual science*. 2017; 58 (4):

- 2318–28. Available from: <https://iovs.arvojournals.org/article.aspx?articleid=2623584>.
20. Шляпникова О. А., Каменных Т. Г., Рощепкин В. В., Решникова Л. Б. Перспективные направления развития офтальмологии (обзор). Саратовский научно-медицинский журнал. 2021; 17 (3): 675–8. Available from: <https://cyberleninka.ru/article/n/perspektivnye-napravleniya-razvitiya-oftalmologii-obzor>.
 21. Quellec G, Lee K, Dolejsi M, Garvin MK, Abramoff MD, Sonka M. Three-dimensional analysis of retinal layer texture: identification of fluid-filled regions in SD-OCT of the macula. *IEEE transactions on medical imaging*. 2010; 29 (6): 1321–30. Available from: <https://ieeexplore.ieee.org/abstract/document/5440910>.
 22. Hu Z, Niemeijer M, Abramoff MD, Garvin MK. Multimodal retinal vessel segmentation from spectral-domain optical coherence tomography and fundus photography. *IEEE transactions on medical imaging*. 2012; 31 (10): 1900–11. Available from: <https://ieeexplore.ieee.org/abstract/document/6228540>.
 23. Esmaeili M, Dehnavi AM, Rabbani H, Hajizadeh F. Three-dimensional segmentation of retinal cysts from spectral-domain optical coherence tomography images by the use of three-dimensional curvelet based K-SVD. *Journal of medical signals and sensors*. 2016; 6 (3): 166. Available from: <https://www.ncbi.nlm.nih.gov/pmc/articles/PMC4973460/>.
 24. Chakravarty A, Sivaswamy J. A supervised joint multi-layer segmentation framework for retinal optical coherence tomography images using conditional random field. *Comput. Methods Programs Biomed*. 2018; 165: 235–50. DOI: 10.1016/J.CMPB.2018.09.004.
 25. Bogunović H, et al. Machine Learning of the Progression of Intermediate Age-Related Macular Degeneration Based on OCT Imaging. *Investigative ophthalmology & visual science*. 2017; 58 (6): BIO141–BIO150.
 26. Tvenning AO, Hanssen SR, Austeng D, Morken TS. Deep learning identify retinal nerve fibre and choroid layers as markers of age-related macular degeneration in the classification of macular spectral-domain optical coherence tomography volumes. *Acta Ophthalmologica*. 2022. DOI: 10.1111/AOS.15126.
 27. Rim TH, et al. Detection of features associated with neovascular age-related macular degeneration in ethnically distinct data sets by an optical coherence tomography: trained deep learning algorithm. *British Journal of Ophthalmology*. 2020; 105 (8): 1133–9. DOI: 10.1136/BJOPHTHALMOL-2020-316984.
 28. Zhang G, et al. Clinically relevant deep learning for detection and quantification of geographic atrophy from optical coherence tomography: a model development and external validation study. *Lancet Digit Heal*. 2021; 3 (10): e665–e675. DOI: 10.1016/S2589-7500(21)00134-5.
 29. Sousa JA, Paiva A, Silva A, Almeida JD, Braz Junior G, Diniz JO, et al. Automatic segmentation of retinal layers in OCT images with intermediate age-related macular degeneration using U-Net and DexiNed. *Plos one*. 2021; 16 (5): e0251591.
 30. Alsaih Khaled, et al. Deep learning architectures analysis for age-related macular degeneration segmentation on optical coherence tomography scans. *Computer methods and programs in biomedicine*. 2020; 195: 105566.
 31. Lee B, D'Souza M, Singman EL, Wang J, Woreta FA, Boland MV, et al. Integration of a physician assistant into an ophthalmology consult service in an academic setting. *American journal of ophthalmology*. 2018; 190: 125–33. Available from: <https://www.sciencedirect.com/science/article/abs/pii/S0002939418301387>.
 32. Pandey SK, Sharma V. Robotics and ophthalmology: Are we there yet? *Indian Journal of Ophthalmology*. 2019; 67 (7): 988. Available from: <https://www.ncbi.nlm.nih.gov/pmc/articles/PMC6611303/>.
 33. Yan Y, Jin K, Gao Z, Huang X, Wang F, Wang Y, et al. Attention — based deep learning system for automated diagnoses of age-related macular degeneration in optical coherence tomography images. *Medical Physics*. 2021; 48 (9): 4926–34. DOI: 10.1002/MP.15002.
 34. Treder M, Lauermaun JL, Eter N. Automated detection of exudative age-related macular degeneration in spectral domain optical coherence tomography using deep learning. *Graefe's Archive for Clinical and Experimental Ophthalmology*. 2017; 256 (2): 259–65. DOI: 10.1007/S00417-017-3850-3.
 35. Bhatia KK, Graham MS, Terry L, Wood A, Tranos P, Trikha S, et al. Disease classification of macular optical coherence tomography scans using deep learning software: validation on independent, multicenter data. *Retina*. 2020; 40 (8): 1549–57. DOI: 10.1097/IAE.0000000000002640.
 36. Tvenning AO, Hanssen SR, Austeng D, Morken TS. Deep learning identify retinal nerve fibre and choroid layers as markers of age-related macular degeneration in the classification of macular spectral-domain optical coherence tomography volumes. *Acta Ophthalmologica*. 2022. DOI: 10.1111/AOS.15126.
 37. Sunija AP, Kar S, Gayathri S, Gopi VP, Palanisamy P. Octnet: A lightweight cnn for retinal disease classification from optical coherence tomography images. *Computer methods and programs in biomedicine*. 2021; 200: 105877. DOI: 10.1016/J.CMPB.2020.105877.
 38. Juba B, Le HS. Precision-recall versus accuracy and the role of large data sets. In *Proceedings of the AAAI conference on artificial intelligence*. 2019; 33 (01): 4039–48. DOI: 10.1609/AAAI.V33I01.33014039.
 39. Lowe DG. Distinctive image features from scale-invariant keypoints. *International journal of computer vision*. 2004; 60 (2): 91–110. Available from: <https://link.springer.com/article/10.1023/B:VISI.0000029664.99615.94>
 40. Shahedi MB, Amirfatahi R, Azar FT, Sadri S. Accurate breast region detection in digital mammograms using a local adaptive thresholding method. In *Eighth International Workshop on Image Analysis for Multimedia Interactive Services (WIAMIS'07)*. IEEE. 2007; 26–26. Available from: <https://ieeexplore.ieee.org/abstract/document/4279134>.

JUSTIFICATION OF USE OF FIXED RETAINERS BASED ON THE ANALYSIS OF SIZE OF THE INCISOR AND CANINE CROWNS

Postnikov MA¹, Butvilovsky AV²✉, Alsharifi AAM², Madatyan AV³, Kopetskiy IS⁴, Eremin DA⁴

¹ Samara State Medical University, Samara, Russia

² Belarusian State Medical University, Minsk, Republic of Belarus

³ Sechenov University, Moscow, Russia

⁴ Pirogov Russian National Research Medical University, Moscow, Russia

Anatomical features of the teeth should be accounted for dental treatment plans. The need for constant monitoring of changes in the dentition system determines the relevance of this research. The study aimed to establish the size of anterior teeth with the help of odontometry. We made bi-layer single stage impressions and cast diagnostic models of the anterior teeth of 50 male and 50 female participants aged 18–24 years. The absolute sizes of crowns of incisors and canines were established. To assess the reduction of lateral incisors, we calculated the interincisor index (II) of teeth 22 and 21; sexual dimorphism was determined using the Garn–Lewis formula. It was discovered that there are no differences in the mesiodistal widths of crowns of contralateral teeth on the right and left sides ($p > 0.05$). The mesiodistal width of crowns of anterior teeth decreases (significant changes) in the following order: maxillary central incisors → maxillary canines → mandibular canines and maxillary lateral incisors → mandibular lateral incisors → mandibular central incisors. The degree of reduction of lateral incisors is low ($li = 74.9$) and more prominent in males than in females. In the examined patients, the greatest mean length of crowns of anterior teeth is that of upper central incisors and lower canines, while upper canines are shorter in length and upper lateral incisors, lower central and lateral incisors have the shortest mean crown length. Males have longer (mean length) crowns of lower canines, upper incisors and canines than females, the difference being significant ($p < 0.001$). The parameters of the crowns determined in this study showed that they have sufficient height and mesiodistal width, which, together with the low degree of reduction of the lateral incisors, justifies the possibility of direct fabrication of orthodontic fixed retainers. The data can also be used at the stage of dental treatment planning.

Keywords: teeth anatomy, odontometry, teeth crowns mesiodistal dimensions, teeth crowns height, dental treatment planning, orthodontic retainer

Author contribution: Postnikov MA — literature analysis; Butvilovsky AV — research planning; Alsharifi AAM — data collection and interpretation; Madatyan AV — manuscript drafting; Kopetskiy IS — data collection; Eremin DA — data analysis.

Compliance with ethical standards: the study was approved by the Ethical Committee of the Belarusian State Medical University (Minutes #15 of June 23, 2022).

✉ **Correspondence should be addressed:** Alexander V. Butvilovsky
pr. Dzerzhinskogo, 83, 220083, Minsk, Republic of Belarus; alexbutv@rambler.ru

Received: 11.11.2022 **Accepted:** 08.12.2022 **Published online:** 31.12.2022

DOI: 10.24075/brsmu.2022.069

ОБОСНОВАНИЕ ИСПОЛЬЗОВАНИЯ НЕСЪЕМНЫХ РЕТЕЙНЕРОВ НА ОСНОВАНИИ АНАЛИЗА РАЗМЕРОВ КОРОНОК РЕЗЦОВ И КЛЫКОВ

М. А. Постников¹, А. В. Бутвиловский² ✉, А. А. М. Алшарифи², А. В. Мадатян³, И. С. Копецкий⁴, Д. А. Еремин⁴

¹ Самарский государственный медицинский университет, Самара, Россия

² Белорусский государственный медицинский университет, Минск, Республика Беларусь

³ Сеченовский университет, Москва, Россия

⁴ Российский национальный исследовательский медицинский университет имени Н. И. Пирогова, Москва, Россия

При планировании стоматологического лечения необходимо учитывать анатомические особенности зубов. Необходимость постоянного мониторинга изменчивости зубочелюстной системы определяет актуальность данной работы. Целью работы было оценить размеры коронок фронтальной группы зубов с помощью одонтометрии. Получены двухслойные одноэтапные оттиски и отлиты диагностические модели переднего участка челюстей у 50 мужчин и 50 женщин в возрасте 18–24 лет. Определены абсолютные значения размеров коронок резцов и клыков. Для оценки редукции латеральных резцов вычислен межрезцовый индекс (II) по зубам 22 и 21, половой диморфизм определен по формуле Garn–Lewis. Установлено, что различия мезиодистальных размеров коронок одноименных зубов правой и левой стороны отсутствуют ($p > 0,05$). Мезиодистальные размеры коронок статистически значимо убывают в ряду: верхние центральные резцы → верхние клыки → нижние клыки и верхние латеральные резцы → нижние латеральные резцы → нижние центральные резцы. Степень выраженности редукции латеральных резцов низка ($li = 74,9$) и более выражена у мужчин, чем у женщин. У обследованных пациентов среди передних зубов наибольшая высота коронки свойственна верхним центральным резцам и нижним клыкам, меньшая — верхним клыкам, а наименьшая — верхним латеральным резцам, нижним центральным и латеральным резцам. У мужчин высота коронок нижних клыков, верхних резцов и клыков статистически значимо ($p < 0,001$) больше, чем у женщин. Полученные параметры коронок свидетельствуют об их достаточной высоте и мезиодистальных размерах, что в совокупности с низкой степенью выраженности редукции латеральных резцов обосновывает возможность изготовления несъемных ретейнеров прямым методом. Данные могут быть использованы и на этапе планирования стоматологического лечения.

Ключевые слова: анатомия зубов, одонтометрия, мезиодистальные размеры коронок зубов, высота коронок зубов, планирование стоматологического лечения, ретейнер

Вклад авторов: М. А. Постников — анализ литературы; А. В. Бутвиловский — планирование исследования; А. А. М. Алшарифи — сбор и интерпретация данных; А. В. Мадатян — подготовка черновика рукописи; И. С. Копецкий — сбор данных; Д. А. Еремин — анализ данных.

Соблюдение этических стандартов: исследование одобрено этическим комитетом Белорусского государственного медицинского университета (протокол № 15 от 23 июня 2022 г.).

✉ **Для корреспонденции:** Александр Валерьевич Бутвиловский
пр. Дзержинского, д. 83, 220083, г. Минск, Республика Беларусь; alexbutv@rambler.ru

Статья получена: 11.11.2022 **Статья принята к печати:** 08.12.2022 **Опубликована онлайн:** 31.12.2022

DOI: 10.24075/vrgmu.2022.069

Retention is an integral stage of orthodontic treatment. It is defined as preservation of the optimal aesthetic and functional position of teeth once the active phase of orthodontic treatment is over [1].

After active orthodontic treatment, teeth do not become stable, they situation should be considered as dynamic and constantly changing. Therefore, there arises a need for permanent retention to ensure stability of the position of teeth post-treatment. There is a number of biological goals that should be considered when choosing a retainer, such as maintenance of the good condition of periodontal tissues, ensuring optimal oral hygiene, maintaining optimal functional loads on teeth [2, 3].

The reasons behind a potential recurrence of problems addressed with orthodontic treatment may be associated with prolonged remodeling of periodontal tissues, muscle imbalance, changes caused by growth and aging [4]. Long-term studies reveal that in 90% of cases the said problems reappear within 10 to 20 years after the end of the retention phase of treatment [5]. Since only a certain part of dentition needs retention, a term "differential retention" was introduced to stress the special attention paid to the section most prone to recurrence in each orthodontic case [3].

Retainers can be fixed and removable. As the name implies, removable retainers can be removed, which simplifies oral hygiene procedures and allows patients to wear them only through a part of the day, if necessary. However, in some situations retainers should remain in the oral cavity 24 hours a day in order to reduce the chance of recurrence; typically, such conditions call for a fixed retainer [6, 7].

Removable retainers were the retention appliances of choice for many years. In the 1970s, fixed retainers were suggested as a solution preventing recurrence of the treated orthodontic problems around mandibular incisors [8]. A study published in 2002 reported that a third of orthodontists prefer fixed lingual retainers for the mandible and 5% choose fixed retainers for the maxilla [9]. A 2011 publication has shown a shift in opinions: fixed retainers were selected by 42% of orthodontists for the lower jaw and by 11% for the upper jaw [10].

There ways of retaining treatment results preferred by the orthodontists vary greatly region to region. For example, in Norway and the Netherlands, both fixed and removable retainers are often prescribed for the maxilla and fixed retainers for the mandible. In Switzerland, a combination of two types of retainers is often used in cases of maxillary extractions and jaw expansions. Orthodontists practicing in the US, Saudi Arabia and Australia usually opt for removable retainers for the

upper jaw and fixed retainers for the lower jaw. In most studies, vacuum formed retainers are the preferred type of a removable retainer [11, 12].

In terms of retainer wear duration, less than 20% of orthodontists in Norway, 52% in Saudi Arabia, approximately 80% in Australia, the US and the UK and 90% in Germany prescribe permanent retention. These differences in the approaches practiced by the orthodontists underscore the importance of having a clear understanding of the relative advantages of each type of retention [11].

In recent years, the list of situation when fixed retainers are prescribed has expanded significantly [13]:

- diastema closure;
- tremas between anterior teeth;
- potential post-orthodontic tooth migration in adult patients;
- loss of teeth or large tremas in maxillary dentition before orthodontic treatment;
- treatment involving extraction of mandibular incisors;
- severe tortoanomaly of maxillary incisors before orthodontic treatment;
- corrected palatal impaction of the canines.

The advantages of fixed retainers are: easy adaptation (usually the adaptation period lasts no more than a week); no active involvement of the patient in the retention process; constant action on the teeth, which reduces both the retention period and the risk of recurrence; virtual invisibility during conversations; minimal effect on articulation [14].

There are direct and indirect methods of fixed retainer fabrication. The choice of the splinting method depends on the anatomy of anterior teeth [15, 16].

Odontometry and odontoscopy provide a scientific basis for selection of the splinting method. The features of dentition and jaws system tend to change in the population, therefore, these studies must be carried out dynamically [17–19]. Odontometry yields results for the following criteria.

1. *Crown anatomy.* Anatomy of the crown drives selection of a tooth to be extracted for orthodontic reasons. This choice is the subject of ongoing debate among orthodontic schools. Some of the schools recommend extraction of a specific (not any) tooth in each case when there is a need for extra space; this approach is largely justified by the anatomy of crowns of teeth. For example, in the upper jaw it is common to extract the second premolar and not the first one. The idea behind this concept is that extraction of the first premolar can cause imbalance as well as aesthetic and functional mismatch of the dental arches. Odontometry is also an integral part of the dental treatment planning process (aesthetic restorations, dental

Table 1. Mesiodistal widths of crowns of incisors and canines

Tooth	Mesiodistal width, mm	<i>U</i> value	<i>p</i> value
13	7.30 (6.86–7.77)	835	0.903
23	7.27 (6.93–7.63)		
12	6.10 (5.72–6.65)	4753	0.547
22	6.07 (5.71–6.52)		
11	8.08 (7.77–8.43)	4931	0.964
21	8.07 (7.75–8.48)		
31	5.12 (4.84–5.42)	4802	0.807
41	5.12 (4.85–5.38)		
32	5.51 (5.27–5.81)	4694	0.455
42	5.51 (5.20–5.73)		
33	6.31 (6.07–6.72)	4935	0.874
43	6.39 (6.03–6.70)		

Table 2. Z value (lower left corner) and *p* error, pairwise comparisons of the groups of teeth formed by mesiodistal distance of the crown

Teeth	z and p values					
	13 + 23	12 + 22	11 + 21	31 + 41	32 + 42	33 + 43
13 + 23	–	< 0.001	0.002	< 0.001	< 0.001	< 0.001
12 + 22	10.31	–	< 0.001	< 0.001	< 0.001	0.012
11 + 21	4.64	14.94	–	< 0.001	< 0.001	< 0.001
31 + 41	20.71	10.42	25.31	–	< 0.001	< 0.001
32 + 42	16.96	6.65	21.58	3.79	–	< 0.001
33 + 43	7.79	2.53	12.42	12.94	9.18	–

Note: here and hereafter, the cells where $p < p_{crit}$ are highlighted in gray.

prosthetics) and a feasible study in the context of diagnosing increased tooth wear and their subsequent restoration [20, 21].

2. Root anatomy. In the orthodontic literature, the importance of root anatomy in orthodontic treatment is conveyed via the concept of anchorage. Anchorage is resistance to undesirable displacement of teeth [22].

A specific anchorage value is selected for each tooth based on various criteria: root surface; capability of periodontal ligament to resist displacement regardless of its direction; root length, i.e. a longer root is considered to be fixed deeper. The most preferred method of anchorage calculation involves assessment of the root volume, which represents the three-dimensional integrity of root and alveolar bone [20].

3. Anatomy of the entire tooth. In some clinical situations, the anatomy of the entire tooth shapes the treatment plan. One of such cases, for example, is transposition of the lateral incisor and maxillary canine. Currently, the advancements of restorative and orthopedic dentistry allow changing the shape of the tooth crown (coronoplasty), a popular solution for a lateral incisor implying shaping it as a canine [20].

It should be noted that the last odontometric studies in the Republic of Belarus were conducted over 10 years ago, which, together with the need for constant monitoring of the variability of the dentition [23], establishes the relevance of this work.

This study aimed to establish the size of crowns of incisors and canines in the population of the Republic of Belarus and substantiate the possibility of using fixed retainers.

METHODS

Using disposable plastic spoons and C-silicone from the Zetaplus L TrialKit (Zhermack Spa; Italy), two-layer one-stage impressions of the anterior teeth of 100 volunteering participants (50 male, 50 female) were made and studied. The inclusion criteria were: age from 18 to 24; permanent residence in the Republic of Belarus. The exclusion criteria were: refusal to participate in the study, restorations or prosthetics on the upper and lower incisors and canines.

We cast diagnostic models EliteModel (Zhermack SpA) superegypsum and, using them, established mesiodistal dimensions (distance between the protruding points of the mesial and distal edges of a crown) and height of crowns of incisors and canines with an electronic caliper DR6003 (Dr.Iron; China) with resolution of 0.01 mm and accuracy of ± 0.01 mm. The results of sizing 797 incisors (including 199 upper central, 200 upper lateral, 200 lower central, 198 lower lateral) and 400 canines (including 200 upper, 200 lower canines) were recorded in the study card.

To assess the reduction of lateral incisors, we calculated the interincisor index (Ii) for teeth 22 and 21 [24, 25]; sexual dimorphism was determined using the Garn–Lewis formula, median values [26].

Statistical processing of the obtained results was enabled by the Past 3.0 software [27]. The quantitative variables as a median, lower and upper quantiles $Me (Q_1-Q_3)$ were described.

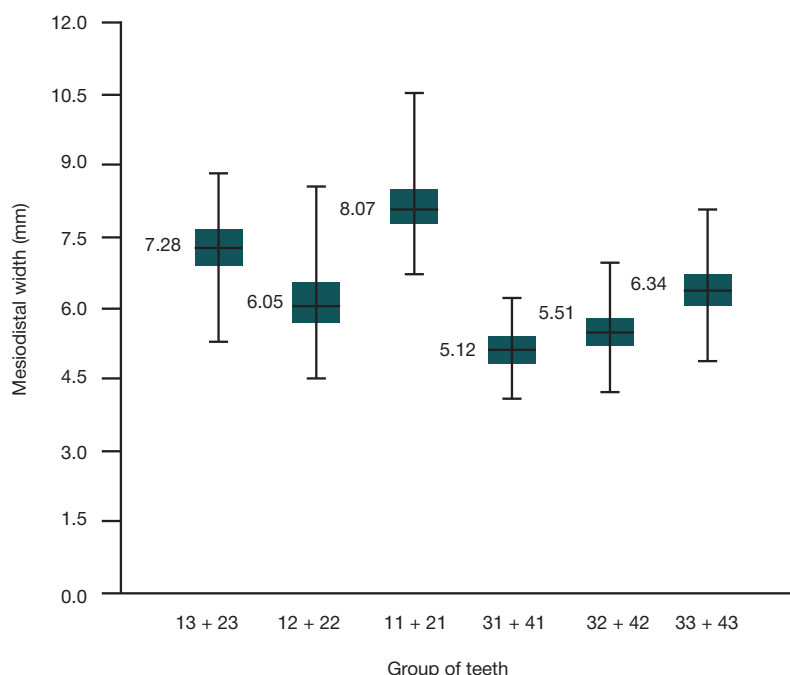
**Fig. 1.** Comparison of mesiodistal widths of crowns, individual groups of teeth

Table 3. Mesiodistal widths of anterior teeth crowns in men and women

Teeth	Sex	Mesiodistal width, mm	<i>U</i> value	<i>p</i> value	Sexual dimorphism
Maxillary canines	male	7.26 (6.92–7.63)	4371	0.125	–1.6
	female	7.38 (6.95–7.80)			
Maxillary lateral incisors	male	5.92 (5.38–6.35)	3161	<0.001	–6.3
	female	6.32 (5.94–6.66)			
Maxillary central incisors	male	7.99 (7.59–8.40)	4256	0.088	–1.8
	female	8.14 (7.81–8.51)			
Mandibular central incisors	male	5.09 (4.81–5.37)	4455	0.27	–1.5
	female	5.17 (4.89–5.42)			
Mandibular lateral incisors	male	5.45 (5.10–5.69)	3907	0.008	–1.4
	female	5.53 (5.33–5.86)			
Mandibular canines	male	6.37 (6.03–6.72)	4852	0.718	1
	female	6.31 (6.06–6.68)			

The degree of variation intensity was determined with the coefficient of variation (*V*).

The significance of differences between two independent groups was determined by the *U* (Mann-Whitney) and χ^2 (Pearson) tests with a critical level of significance for statistical hypotheses at 0.05. The significance of differences in multiple comparisons was determined by the *H* test (Kruskal–Wallis, with a critical significance level of 0.05), in post hoc comparisons - by the Dunn's test (*z* value) with the Bonferroni correction (with a critical significance level of 0.0034 (six compared groups)) [28, 29].

RESULTS

The median age of the examined patients was 21.0 (20.0–22.0); we did not discover significant differences in the age of men (21.0 (20.0–22.3)) and women (21.0 (21.0–21.3)) (*U* = 1116; *p* > 0.05). Table 1 presents the mesiodistal width of the anterior teeth crowns.

It was noticed that there are no differences in the mesiodistal widths of crowns of contralateral teeth on the right and left sides, which allowed grouping them. Multiple comparisons of the formed groups of teeth revealed significant differences between them (*H* = 937.0; *p* < 0.001), post hoc comparisons (Table 2) showed significant differences between all groups (except for the comparison of lower canines and upper lateral incisors).

Table 4. Height of crowns of incisors and canines

Tooth	Crown height, mm	<i>U</i> value	<i>p</i> value
13	9.29 (8.59–9.99)	4701	0.247
23	9.18 (8.54–9.84)		
12	8.14 (7.47–8.77)	4695	0.456
22	8.25 (7.65–8.69)		
11	9.60 (8.91–10.27)	4917	0.936
21	9.58 (9.01–10.26)		
31	7.91 (7.30–8.70)	4645	0.526
41	7.88 (7.22–8.60)		
32	8.28 (7.62–8.94)	4867	0.746
42	8.19 (7.61–8.91)		
33	9.53 (8.81–10.24)	4953	0.906
43	9.51 (8.78–10.24)		

The mesiodistal widths of crowns (Fig. 1) decrease in the following order: upper central incisors (8.07 (7.77–8.46 mm)) → upper canines (7.28 (6.93–7.69) mm) → lower canines (6.34 (6.05–6.70) mm) and upper lateral incisors (6.05 (5.71–6.58) mm) → lower lateral incisors (5.51 (5.23–5.77) mm) → lower central incisors (5.12 (4.85–5.39) mm). It should be noted that these data are consistent with the results reported in previous studies [23].

Comparing the mesiodistal widths of the anterior teeth crowns of male and female participants (Table 3), we discovered significant differences in cases of maxilla lateral incisors (5.92 (5.38–6.35) mm and 6.32 (5.94–6.66) mm, respectively) and mandible lateral incisors (5.45 (5.10–5.69) mm and 5.53 (5.33–5.86) mm, respectively). A noteworthy observation is that the highest degree of sexual dimorphism was characteristic of the upper lateral incisors (the value of the Gang–Lewis index was –6.3).

The *li* value for all examined patients was 74.9 (70.8–80.8), which indicates a low degree of lateral incisor reduction. It was found that the degree of intensity of variation of *li* is low (*V* = 9.62), and only in 21% of cases its value was below 70.

Females had the interincisal index value at 76.3 (73.1–82.0), which is significantly (*U* = 855; *p* < 0.01), by 4.0% greater than registered in men (73.4 (67, 8–78.1)). Males (*n* = 17; 34.0%) had the value of this index below 70 4.3 times more often ($\chi^2 = 10.2$; *p* < 0.01) than females (*n* = 4; 8.0%), which suggests a conclusion that, in the population of the Republic of Belarus,

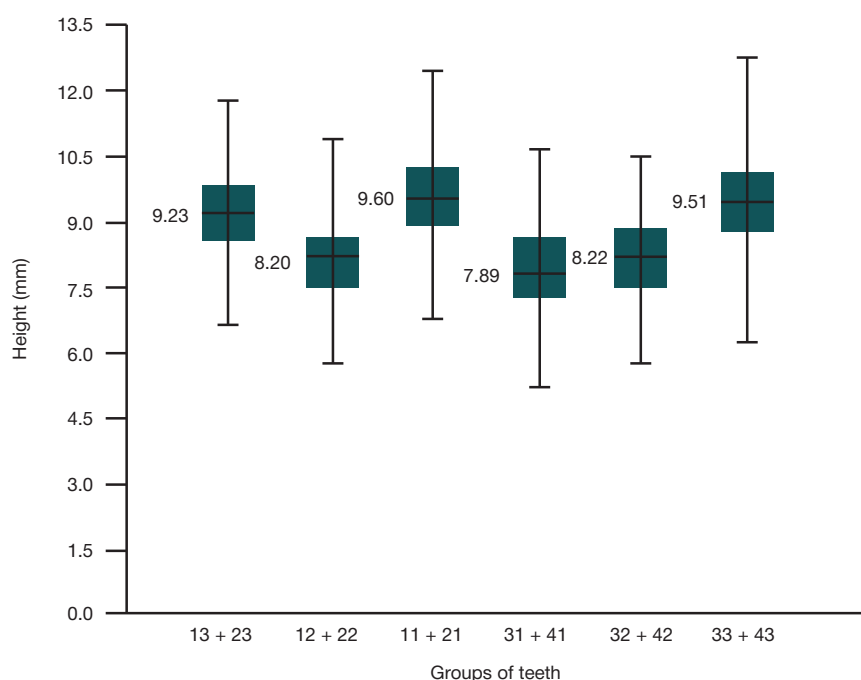


Fig. 2. Comparison of the crown height of individual groups of teeth

there is a more pronounced reduction of lateral incisors in males.

Table 4 presents data on the height of anterior teeth crowns.

It was discovered that there are no differences in height of crowns of contralateral teeth on the right and left sides ($p > 0.05$), which allowed grouping them (Fig. 2). Multiple comparison of the formed groups of teeth yielded the Kruskal–Wallis test value of 371.2, which indicates significant differences between them ($p < 0.001$).

The longest crowns were those of the upper central incisors (9.60 (8.96–10.27) mm), lower canines (9.51 (8.81–10.24) mm) and upper canines (9.23 (8.96–10.24) mm). .55–9.90) mm), and the smallest — of the upper lateral incisors (8.20 (7.54–8.72) mm), lower central and lateral incisors (7.89 (7.23–8.63) and 8.22 (7.62 – 8.91) mm, respectively).

The results of post hoc comparisons are given in Table 5. We found significant differences between all groups (with the exception of comparisons of upper canines and lower canines, upper lateral incisors and lower incisors, upper central incisors and The mesiodistal width of crowns of anterior teeth decrease (significant changes) in the following order: maxillary central incisors — maxillary canines — mandibular canines and maxillary lateral incisors — mandibular lateral incisors — mandibular central incisors, lower canines).

It was established that males have longer crowns of the lower canines, upper central and lateral incisors and canines (Table 6), the difference with females being significant (the values of the Gang–Lewis index for this attribute were 8.4, 6.8, 7.3, and 4.7).

Table 5. Z value (lower left corner) and p error, pairwise comparisons of the groups of teeth formed by crown height

Teeth	z and p values					
	13 + 23	12 + 22	11 + 21	31 + 41	32 + 42	33 + 43
13 + 23	–	< 0.001	0.002	< 0.001	< 0.001	0.037
12 + 22	8.89	–	< 0.001	0.109	0.438	< 0.001
11 + 21	3.13	12	–	< 0.001	< 0.001	0.295
31 + 41	10.47	1.61	13.57	–	0.017	< 0.001
32 + 42	8.11	0.78	11.23	2.38	–	< 0.001
33 + 43	2.08	10.97	1.05	12.54	10.19	–

DISCUSSION

The study established that the mesiodistal widths of crowns (Fig. 1) in the population of the Republic of Belarus decrease in the following order: upper central incisors (8.07 (7.77–8.46) mm) → upper canines (7.28 (6.93–7.69) mm) → lower canines (6.34 (6.05–6.70) mm) and upper lateral incisors (6.05 (5.71–6.58) mm) → lower lateral incisors (5.51 (5.23–5.77) mm) → lower central incisors (5.12 (4.85–5.39) mm). These data are consistent with the results of a study completed in 2009 [23]. The crowns of the maxillary and mandibular lateral incisors of females are larger in mesiodistal width than those in males.

The severity of reduction of lateral incisors was found to be low ($li = 74.9$ (70.8 – 80.8)). Males in the Republic of Belarus have more pronounced reduction of lateral incisors ($li = 73.4$ (67.8–78.1)) than females ($li = 76.3$ (73.1–82.0)). This conclusion is consistent with the results of a study that found the prevalence of reduction of lateral incisors in men [30].

In the examined patients, the longest crowns in the anterior segment were those of upper central incisors (9.60 (8.96–10.27) mm) and lower canines (9.51 (8.81–10.24) mm), while upper canines were smaller in length (9.23 (8.55–9.90) mm) and upper lateral incisors (8.20 (7.54–8.72) mm), lower central and lateral incisors (7.89 (7.23–8.63) and 8.22 (7.62–8.91) mm, respectively) the smallest. It was demonstrated that males have longer crowns of the lower canines, upper incisors and canines than females, the difference being significant ($p < 0.001$).

Table 6. Crown height of anterior teeth crowns in men and women

Teeth	Sex	Height, mm	U value	p value	Sexual dimorphism
Maxillary canines	male	9.52 (9.09–10.23)	3094	< 0.001	4.7
	female	8.90 (7.87–9.52)			
Maxillary lateral incisors	male	8.42 (8.02–9.02)	3061	< 0.001	7.3
	female	7.85 (7.10–8.45)			
Maxillary central incisors	male	9.99 (9.21–10.40)	3029	< 0.001	6.8
	female	9.35 (8.43–9.90)			
Mandibular central incisors	male	7.94 (7.43–8.66)	4414	0.228	0.8
	female	7.88 (7.13–8.60)			
Mandibular lateral incisors	male	8.33 (7.66–9.07)	4315	0.094	2.8
	female	8.10 (7.56–8.79)			
Mandibular canines	male	9.93 (9.18–10.74)	2845	< 0.001	8.4
	female	9.16 (8.44–9.88)			

CONCLUSIONS

Thus, the size parameters of incisors and canines determined in this study show that these teeth have sufficient crown length and mesiodistal width, which, together with the low

degree of reduction of lateral incisors, justifies the possibility of direct fabrication of orthodontic fixed retainers. The data from this study can also be used at the stage of dental treatment planning (aesthetic restorations, orthopedics and orthodontics).

References

- Bearn DR. Bonded orthodontic retainers: a review. *Am J Orthod Dentofac Orthop.* 1995; 108 (2): 207–13. Available from: [https://doi.org/10.1016/S0889-5406\(95\)70085-4](https://doi.org/10.1016/S0889-5406(95)70085-4).
- Zachrisson BU. Long-term experience with direct-bonded retainers: update and clinical advice. *J Clin Orthod.* 2007; 12 (2): 728–37.
- Eapen JC, Prakash A. Enigma of Fixed Retainers. *Orthodontic Journal of Nepal.* 2017; 7 (2): 52–55. Available from: <https://doi.org/10.3126/ojn.v7i2.20168>.
- Bondemark L, et al. Long-term stability of orthodontic treatment and patient satisfaction. A systematic review. *Angle Orthod.* 2007; 77 (1): 181–91. Available from: <https://doi.org/10.2319/011006-16R.1>.
- Little RM, Riedel RA, Artun J. An evaluation of changes in mandibular anterior alignment from 10 to 20 years postretention. *Am J Orthod Dentofac Orthop.* 1988; 93 (5): 423–8. Available from: [https://doi.org/10.1016/0889-5406\(88\)90102-3](https://doi.org/10.1016/0889-5406(88)90102-3).
- Karpov AN, Postnikov MA, Stepanov GV. *Ortodontiya: uchebnik.* Samara: Pravo, 2022; 319 s. Russian.
- Johnston CD, Littlewood SJ. Retention in orthodontics. *Br Dent J.* 2015; 218 (3): 119–22. Available from: <https://doi.org/10.1038/sj.bdj.2015.47>.
- Pandis N, et al. Long-term periodontal status of patients with mandibular lingual fixed retention. *Eur J Orthod.* 2007; 29 (5): 471–6. Available from: <https://doi.org/10.1093/ejo/cjm042>.
- Keim RG, et al. JCO study of orthodontic diagnosis and treatment procedures. Part 1. Results and trends. *J Clin Orthod.* 2002; 36 (10): 553–68.
- Pratt MC, et al. Evaluation of retention protocols among members of the American Association of Orthodontists in the United States. *Am J Orthod Dentofac Orthop.* 2011; 140 (4): 520–6. Available from: <https://doi.org/10.1016/j.ajodo.2010.10.023>.
- Al-Moghrbi S, Littlewood J, Fleming PS. Orthodontic retention protocols: an evidence-based overview. *Br Dent J.* 2021; 230 (11): 770–6. Available from: <https://doi.org/10.1038/s41415-021-2954-7>.
- Padmos JAD, Fudalej PS, Renkema AM. Epidemiologic study of orthodontic retention procedures. *Am J Orthod Dentofac Orthop.* 2018; 153 (4): 496–504. Available from: <https://doi.org/10.1016/j.ajodo.2017.08.013>.
- Zachrisson BU. The bonded lingual retainer and multiple spacing of anterior teeth. *Swed Dent J Suppl.* 1982; 15: 247–55.
- Xotajt AX, Butvilovsky AV. Sposob izgotovleniya nes'emnogo individual'nogo retejnera. *Ortodontiya. Gnatologiya.* 2020; 3 (2): 22–26. Russian.
- Karton EA. *Lendengolc ZhA, Persin LS. Retenciya i recidyv: ucheb. M.: MGMSU, 2006; 46 s. Russian.*
- Butvilovsky AV, Xotajt AX. Opyt primeneniya High-Q-Bond light cure retainer (BJM LAB) dlya vremennogo shinirovaniya zubov. *Stomatologicheskij zhurnal.* 2017; 1: 69–71. Russian.
- Gatalsky VV. *Mezhpokolennaya i ehpoخال'naya izmenchivost' osobennostej zubochehlyustnoj sistemy v populyacijax Belorussii (dissertaciya).* Minsk, 2000; 19 s. Russian.
- Postnikov MA, redaktor. *Ortodontiya. Ehtiologiya, patogenez, diagnostika i profilaktika zubochehlyustnyx anomalij i deformacij: uchebnik — chast' 1.* Samara: Pravo, 2022; 348 s. Russian.
- Postnikov MA, i dr. *Kliniko-rentgenologicheskie metody diagnostiki v stomatologii: uchebnoe posobie.* Samara: Pravo, 2021; 141 s. Russian.
- Nabbout F, Baron P. *Orthodontics and Dental Anatomy: Three-dimensional Scanner Contribution.* *J Int Soc Prev Community Dent.* 2017; 7 (6): 321–8. Available from: https://doi.org/10.4103/jispcd.JISPCD_394_17.
- Feldmann I, Bondemark L. Orthodontic anchorage: a systematic review. *Angle Orthod.* 2006; 76 (3): 493–501.
- Postnikov MA, i dr. *Osobennosti diagnostiki i lecheniya pacientov s povyshennoj stiraemost'yu zubov (obzor literatury).* 2021; 93 (4): 40–42. Russian.
- Tegako OV. *Morfologicheskaya izmenchivost' koronki i kornevoj sistemy zubov u naseleniya g. Minska (discertaciya).* Minsk, 2009; 18 s. Russian.
- Zubov AA. *Odontologiya. Metodika antropologicheskix issledovanij.* M.: Nauka, 1968; 199 s. Russian.
- Luckaya IK. *Terapevticheskaya stomatologiya: ucheb. posobie.* Minsk: Vyshehshaya shkola, 2014; c. 258–9. Russian.
- Garn SM, Lewis AB, Kerewsky RS. The relationship between sexual dimorphism in tooth size and body size as studied within families. *Arch Oral Biol.* 1967; 12 (2): 299–301. Available from: [https://doi.org/10.1016/0003-9969\(67\)90050-7](https://doi.org/10.1016/0003-9969(67)90050-7).

27. Hammer O, Harper DAT, Ryan PD. PAST: Paleontological statistics software package for education and data analysis. *Palaeontologia Electronica*. 2001; 4 (1): 1–9.
28. Grzhibovsky AM. Analiz trex i bolee nezavisimyx grupp dannyx. *Ehkologiya*. 2008; 3: 50–58. Russian.
29. Rebrova OYu. Statisticheskij analiz medicinskix dannyx. *Primenenie*

paketa prikladnyx programm STATISTICA. M.: Mediasfera, 2002; 312 s. Russian.

30. Zyuul'kina LA. Polovoj dimorfizm odontometricheskix karakteristik u zhitelej Penzenskogo regiona 21–36 let v zavisimosti ot parametrov kraniio-facial'nogo kompleksa (dissertaciya). Volgograd, 2011; 23 s. Russian.

Литература

1. Bearn DR. Bonded orthodontic retainers: a review. *Am J Orthod Dentofac Orthop*. 1995; 108 (2): 207–13. Available from: [https://doi.org/10.1016/S0889-5406\(95\)70085-4](https://doi.org/10.1016/S0889-5406(95)70085-4).
2. Zachrisson BU. Long-term experience with direct-bonded retainers: update and clinical advice. *J Clin Orthod*. 2007; 12 (2): 728–37.
3. Eapen JC, Prakash A. Enigma of Fixed Retainers. *Orthodontic Journal of Nepal*. 2017; 7 (2): 52–55. Available from: <https://doi.org/10.3126/ojn.v7i2.20168>.
4. Bondemark L, et al. Long-term stability of orthodontic treatment and patient satisfaction. A systematic review. *Angle Orthod*. 2007; 77 (1): 181–91. Available from: <https://doi.org/10.2319/011006-16R.1>.
5. Little RM, Riedel RA, Artun J. An evaluation of changes in mandibular anterior alignment from 10 to 20 years postretention. *Am J Orthod Dentofac Orthop*. 1988; 93 (5): 423–8. Available from: [https://doi.org/10.1016/0889-5406\(88\)90102-3](https://doi.org/10.1016/0889-5406(88)90102-3).
6. Карпов А. Н., Постников М. А., Степанов Г. В. Ортодонтия: учебник. Самара: Право, 2022; 319 с.
7. Johnston CD, Littlewood SJ. Retention in orthodontics. *Br Dent J*. 2015; 218 (3): 119–22. Available from: <https://doi.org/10.1038/sj.bdj.2015.47>.
8. Pandis N, et al. Long-term periodontal status of patients with mandibular lingual fixed retention. *Eur J Orthod*. 2007; 29 (5): 471–6. Available from: <https://doi.org/10.1093/ejo/cjm042>.
9. Keim RG, et al. JCO study of orthodontic diagnosis and treatment procedures. Part 1. Results and trends. *J Clin Orthod*. 2002; 36 (10): 553–68.
10. Pratt MC, et al. Evaluation of retention protocols among members of the American Association of Orthodontists in the United States. *Am J Orthod Dentofac Orthop*. 2011; 140 (4): 520–6. Available from: <https://doi.org/10.1016/j.ajodo.2010.10.023>.
11. Al-Moghrbi S, Littlewood J, Fleming PS. Orthodontic retention protocols: an evidence-based overview. *Br Dent J*. 2021; 230 (11): 770–6. Available from: <https://doi.org/10.1038/s41415-021-2954-7>.
12. Padmos JAD, Fudalej PS, Renkema AM. Epidemiologic study of orthodontic retention procedures. *Am J Orthod Dentofac Orthop*. 2018; 153 (4): 496–504. Available from: <https://doi.org/10.1016/j.ajodo.2017.08.013>.
13. Zachrisson BU. The bonded lingual retainer and multiple spacing of anterior teeth. *Swed Dent J Suppl*. 1982; 15: 247–55.
14. Хотайт А. Х., Бутвиловский А. В. Способ изготовления несъемного индивидуального ретейнера. *Ортодонтия. Гнатология*. 2020; 3 (2): 22–26.
15. Картон Е. А. Ленденгольц Ж. А., Персин Л. С. Ретенция и рецидивы: учеб. М.: МГМСУ, 2006; 46 с.
16. Бутвиловский А. В., Хотайт А. Х. Опыт применения High-Q-Bond light cure retainer (BJM LAB) для временного шинирования зубов. *Стоматологический журнал*. 2017; 1: 69–71.
17. Гатальский В. В. Межпоколенная и эпохальная изменчивость особенностей зубочелюстной системы в популяциях Белоруссии. (диссертация). Минск, 2000; 19 с.
18. Постников М. А., редактор. Ортодонтия. Этиология, патогенез, диагностика и профилактика зубочелюстных аномалий и деформаций: учебник — часть 1. Самара: Право, 2022; 348 с.
19. Постников М. А. и др. Клинико-рентгенологические методы диагностики в стоматологии: учебное пособие. Самара: Право, 2021; 141 с.
20. Nabbout F, Baron P. Orthodontics and Dental Anatomy: Three-dimensional Scanner Contribution. *J Int Soc Prev Community Dent*. 2017; 7 (6): 321–8. Available from: https://doi.org/10.4103/jispcd.JISPCD_394_17.
21. Feldmann I, Bondemark L. Orthodontic anchorage: a systematic review. *Angle Orthod*. 2006; 76 (3): 493–501.
22. Постников М. А., и др. Особенности диагностики и лечения пациентов с повышенной стираемостью зубов (обзор литературы). 2021; 93 (4): 40–42.
23. Тегакко О. В. Морфологическая изменчивость коронки и корневой системы зубов у населения г. Минска (диссертация). Минск, 2009; 18 с.
24. Зубов А. А. Ортодонтия. Методика антропологических исследований. М.: Наука, 1968; 199 с.
25. Луцкая И. К. Терапевтическая стоматология: учеб. пособие. Минск: Вышэйшая школа, 2014; с. 258–9.
26. Garn SM, Lewis AB, Kerewsky RS. The relationship between sexual dimorphism in tooth size and body size as studied within families. *Arch Oral Biol*. 1967; 12 (2): 299–301. Available from: [https://doi.org/10.1016/0003-9969\(67\)90050-7](https://doi.org/10.1016/0003-9969(67)90050-7).
27. Hammer O, Harper DAT, Ryan PD. PAST: Paleontological statistics software package for education and data analysis. *Palaeontologia Electronica*. 2001; 4 (1): 1–9.
28. Гржибовский А. М. Анализ трех и более независимых групп данных. *Экология*. 2008; 3: 50–58.
29. Реброва О. Ю. Статистический анализ медицинских данных. Применение пакета прикладных программ STATISTICA. М.: Медиафера, 2002; 312 с.
30. Зюлькина Л. А. Половой диморфизм одонтометрических характеристик у жителей Пензенского региона 21–36 лет в зависимости от параметров кранио-фациального комплекса (диссертация). Волгоград, 2011; 23 с.

AMICOUMACIN-BASED PRODRUG DEVELOPMENT APPROACH

Shmygarev VI¹, Prokopenko YuA¹, Terekhov SS¹, Zakharova MYu¹, Dubinnyi MA¹, Smirnov IV¹, Yampolsky IV^{1,2}, Tsarkova AS^{1,2}✉¹ Shemyakin–Ovchinnikov Institute of Bioorganic Chemistry RAS, Moscow, Russia² Pirogov Russian National Research Medical University, Moscow, Russia

Coronavirus disease COVID-19, caused by the SARS-CoV-2 virus, is highly contagious and has a severe morbidity. Providing care to patients with COVID-19 requires the development of new types of antiviral drugs. The aim of this work is to develop a prodrug for the treatment of coronavirus disease using the antibiotic Amicoumacin A (Ami), the mechanism of action of which is based on translation inhibition. Enzymatic hydrolysis of an inactivated prodrug by the SARS-CoV-2 main protease can lead to the release of the active Ami molecule and, as a consequence, the suppression of protein biosynthesis in infected cells. To test the proposed hypothesis, a five-stage synthesis of an inactivated analogue of Amicoumacin A was carried out. Its *in vitro* testing with the SARS-CoV-2 recombinant protease M^{Pro} showed a low percentage of hydrolysis. Further optimization of the peptide fragment of the inactivated analog recognized by the SARS-CoV-2 M^{Pro} protease may lead to an increase in proteolysis and the release of Amicoumacin A.

Keywords: translation, translation inhibitor, antiviral agents, prodrugs, inactivated amicoumacin derivatives**Funding:** the work was supported by the grant № 075-15-2021-1049 from the Ministry of Science and Higher Education of the Russian Federation.**Author contribution:** Prokopenko YuA — production and isolation of Amikomacin; Shmygarev VI — complete synthesis of an inactivated analog of Amicoumacin A; Terekhov SS, Zakharova MYu — *in vitro* experiments with M^{Pro} protease; Dubinnyi MA — NMR spectroscopy and data analysis; Tsarkova AS — literature analysis, data processing, article writing; Yampolsky IV, Smirnov IV — general project management.**Compliance with ethical standards:** the work was carried out in compliance with the principles of the Helsinki Declaration of the World Medical Association.✉ **Correspondence should be addressed:** Aleksandra S. Tsarkova
Miklukho-Maklaya, 16/10, Moscow, 117997, Russia; altsarkova@gmail.com**Received:** 15.11.2022 **Accepted:** 20.12.2022 **Published online:** 30.12.2022**DOI:** 10.24075/brsmu.2022.073

ПОДХОД К РАЗРАБОТКЕ ПРОЛЕКАРСТВА НА ОСНОВЕ АМИКУМАЦИНА А

В. И. Шмыгарев¹, Ю. А. Прокопенко¹, С. С. Терехов¹, М. Ю. Захарова¹, М. А. Дубинный¹, И. В. Смирнов¹, И. В. Ямпольский^{1,2}, А. С. Царькова^{1,2}✉¹ Институт биоорганической химии имени М. М. Шемякина и Ю. А. Овчинникова РАН, Москва, Россия² Российский национальный исследовательский медицинский университет имени Н. И. Пирогова, Москва, Россия

Современная коронавирусная болезнь COVID-19, вызываемая вирусом SARS-CoV-2, характеризуется высокой контагиозностью и тяжелым течением. Оказание помощи пациентам с COVID-19 требует разработки новых видов противовирусных препаратов. Цель работы — разработать пролекарство для лечения коронавирусной болезни с применением антибиотика Амикумацин А (Ами), механизм действия которого основан на ингибировании трансляции. Ферментативный гидролиз инактивированного пролекарства основной протеазой SARS-CoV-2 может привести к высвобождению активной молекулы Ами и как следствие к подавлению биосинтеза белка в инфицированных клетках. Для проверки предложенной гипотезы был осуществлен пятистадийный синтез инактивированного аналога Амикумацина А, *in vitro* тестирование которого с рекомбинантной протеазой M^{Pro} SARS-CoV-2 показало низкий процент гидролиза. Дальнейшая оптимизация пептидного фрагмента инактивированного аналога, распознаваемого протеазой M^{Pro} SARS-CoV-2, возможно, приведет к повышению протеолиза и высвобождению Амикумацина А.

Ключевые слова: трансляция, ингибитор трансляции, противовирусные препараты, пролекарства, инактивированные производные Амикумацина**Финансирование:** работа выполнена при поддержке гранта Министерства науки и высшего образования Российской Федерации № 075-15-2021-1049.**Вклад авторов:** Ю. А. Прокопенко — наработка и выделение Амикумацина; В. И. Шмыгарев — полный синтез инактивированного аналога Амикумацина А; С. С. Терехов, М. Ю. Захарова — проведение *in vitro* экспериментов с протеазой M^{Pro}; М. А. Дубинный — ЯМР-спектроскопия и анализ данных; А. С. Царькова — анализ литературы, обработка данных, написание статьи; И. В. Ямпольский, И. В. Смирнов — общее руководство проектом.**Соблюдение этических стандартов:** работа проведена с соблюдением принципов Хельсинкской декларации Всемирной медицинской ассоциации.✉ **Для корреспонденции:** Александра Сергеевна Царькова
ул. Миклухо-Маклая, д. 16/10, г. Москва, 117997, Россия; altsarkova@gmail.com**Статья получена:** 15.11.2022 **Статья принята к печати:** 20.12.2022 **Опубликована онлайн:** 30.12.2022**DOI:** 10.24075/vrgmu.2022.073

The 2019 coronavirus disease (COVID-19) has caused catastrophic healthcare and economic crises in many countries around the world [1]. Although several vaccines have been effective in slowing the spread of the SARS-CoV-2 virus, their long-term protection and effectiveness against variants of the virus is still unclear [2–5]. Outbreaks of epidemics caused by coronaviruses in 2002 and 2012 served as a powerful impetus for pharmaceutical and biotechnological research, but only in 2021 did the first drug candidates appear that successfully passed clinical trials [6, 7]. Despite the fact that mass vaccination greatly reduces the spread efficiency and lethality of a viral infection, the remaining high levels of morbidity and

mortality [8, 9] require the development of new antiviral drugs for the treatment of COVID-19.

An attractive molecular target for new antiviral drugs is the translational machinery of the infected cell. In this study, the highly potent translational inhibitor Amicoumacin A (Ami), first isolated from Gram-positive bacteria *Bacillus pumilus* [10], was used to develop a prodrug against SARS-CoV-2. One approach to targeted therapy for coronavirus infection may be proteolytic activation of an Ami-based prodrug. The recognition sequence of the main protease M^{Pro} allows for the targeted release of the active Ami molecule and subsequent translation inhibition. The aim of the study was the synthesis of

Amicoumacin A inactivated analog, which is a promising tool for the development of drugs aimed at specific translational suppression.

METHODS

NMR spectra (δ , ppm; J, Hz) were recorded on a Bruker Fourier 300 (300 MHz; USA) and Bruker Avance I (700 MHz, USA) instruments at 303 K in CDCl_3 and DMSO-d_6 , internal reference TMS. Mass spectra were recorded on a Waters ACQUITY UPLC H-Class LC/MS System (Waters; USA) by electrospray ionization (ESI). Melting points were determined on an SMP30 apparatus and were not corrected. Analytical and preparative thin layer chromatography was performed on Merck plates (Germany) with a UV-254 fluorescent indicator. Silica gel from Merck (Kieselgel 60, 70–230 mesh) was used for column chromatography. Acros Organics (Thermo Fisher Scientific; Belgium) and SigmaAldrich (Merck; Germany) reagents were used without additional purification. The reactions were carried out using freshly distilled solvents from Khimmed (Russia).

Synthesis of an inactivated derivative of Amicoumacin A

N-tert-butoxycarbonyl-L-glutamic acid dimethyl ester (1)

14.7 g (0.10 mol) of L-glutamic acid were suspended in 75 ml of methanol and 25 ml (0.20 mol) of trimethylsilyl chloride were added dropwise at room temperature. The precipitate gradually dissolved. The reaction mixture was left overnight at room temperature. The next day the solvent was evaporated. To the residue were added 75 ml of methanol, 40 ml (0.3 mol) of triethylamine and 22 g (0.1 mol) of di-tert-butyl carbonate. The reaction mixture was left at room temperature for a day. Control by thin layer chromatography (TLC) ethyl acetate : hexane — 1 : 1 ($R_f = 0.36$). Then the solvent was evaporated, the mixture was diluted with 200 ml of water and extracted with 3×50 ml of ethyl acetate. The organic layer was washed with water, 5% hydrochloric acid, 5% potassium carbonate and again with water. After drying over sodium sulfate, the solvent was evaporated producing 23 g of product 1 in the form of a colorless viscous oil, with 85% yield.

$^1\text{H NMR}$ (300 MHz, CDCl_3) δ 5.09(s, br, 1H), 4.32(s, br, 1H), 3.73(s, 3H), 3.67(s, 3H), 2.47–2.31(m, 2H), 2.24–2.10(m, 1H), 2.03–1.85(m, 1H), 1.43(s, 9H).

$^{13}\text{C NMR}$ (75 MHz, CDCl_3) δ 173.2, 172.6, 155.3, 80.0, 52.9, 52.4, 51.8, 30.0, 28.3, 27.8

MS (EI): m/z , 276.2 [$\text{M}+\text{H}^+$].

Dimethyl(2S,4R)-2-[(tert-butoxycarbonyl)-amino]-cyanomethylpentanedioate (2)

To a solution of 7.5 g (27.3 mmol) of *N*-tert-butoxycarbonyl-L-glutamic acid dimethyl ester (1) in 50 ml of dry tetrahydrofuran (THF) 60 ml (60 mmol) of 1M solution of LiHMDS in THF was added at -80°C . The reaction mixture was kept at this temperature for 1 h, and then a solution of 1.9 ml (27.3 mmol) of bromoacetonitrile in 10 ml of dry THF was slowly added so that the temperature did not rise above -70°C . TLC control ethyl acetate : hexane — 1 : 1 ($R_f = 0.48$). After 40 min, a 1M HCl solution was added to the mixture at -70°C until the pH was neutral, then the organic layer was evaporated. The residue was dissolved in 100 ml of a water-benzene mixture (1 : 1). The organic layer was evaporated and the residue was chromatographed on silica gel, eluent petroleum ether : ethyl acetate (3 : 1), producing 5 g of product 2 with 58% yield.

$^1\text{H NMR}$ (300 MHz, CDCl_3) δ 5.10(s, br, 1H), 4.38(s, br, 1H), 3.75(s, 3H), 3.74(s, 3H), 2.9–2.7(m, 3H), 2.25–2.05(m, 2H), 1.43(s, 9H).

$^{13}\text{C NMR}$ (75 MHz, CDCl_3) δ 172.4, 172.0, 155.5, 117.1, 80.6, 52.7, 52.6, 51.0, 38.3, 33.9, 28.3, 19.0

MS (EI): m/z , 287.2 [$\text{M}+\text{H}^+$].

Methyl (2S)-2-[(tert-butoxycarbonyl)amino]-3-[(3S)-2-hydroxypyrrolidin-3-yl]propanoate (3)

2 g (6.4 mmol) of cyanomethyl derivative 2 and 0.83 g (6.4 mmol) of cobalt chloride were dissolved in 40 ml of methanol. Upon cooling to -10°C , 2.2 g (57 mmol) of dry sodium borohydride was added portionwise. After each portion, the mixture turned black and then brightened again. After 24 hours at room temperature the reaction was complete, according to LC/MS mass spectrometry data. The organic solvent was evaporated, the residue was suspended in ethyl acetate and passed through a thin layer of silica gel, the solvent was evaporated, and the residue was chromatographed on silica gel, eluent ethyl acetate ($R_f = 0.16$), producing 1.0 g of crystalline substance 3 with 55% yield; melt. point 114°C

$^1\text{H NMR}$ (300 MHz, CDCl_3) δ 6.42(s, br, 1H), 5.54(d, 8.4 Hz, 1H), 4.30(m, 1H), 3.72(s, 3H), 3.37–3.27(m, 2H), 2.50–2.35(m, 2H), 2.15–2.05(m, 1H), 1.90–1.75(m, 2H), 1.42(s, 9H).

$^{13}\text{C NMR}$ (75 MHz, CDCl_3) δ 179.7, 172.9, 155.7, 79.9, 52.4, 52.3, 40.3, 38.1, 34.1, 28.3, 28.1

MS (EI): m/z , 315.3 [$\text{M}+\text{H}^+$].

Methyl (2S)-2-[[2-(benzyloxycarbonylamino)-4-methylpentanoyl]amino]-3-[(3S)-2-hydroxypyrrolidin-3-yl]propanoate (4)

30 mg (0.104 mmol) of ester 3 was dissolved in 0.3 ml of methylene chloride and 0.2 ml of trifluoroacetic acid was added. After 30 min at room temperature, the starting material disappeared according to TLC data. Trifluoroacetic acid was evaporated on a rotary evaporator. The obtained trifluoroacetate salt was dissolved in 1 ml of methylene chloride, 33 mg (0.13 mmol) of Cbz-L-leucine, 40 mg (0.13 mmol) of TBTU, 15 mg (0.13 mmol) of *N*-hydroxybenzotriazole were added and cooled to 0°C . 0.11 ml (0.62 mmol) of diisopropylethylamine was added to the reaction mixture. The mixture was kept in the refrigerator overnight. The reaction mixture was treated with a mixture of potassium carbonate solution and ethyl acetate, the organic layer was washed with water and evaporated. The residue was chromatographed on silica gel, eluent chloroform:methanol 95/5 ($R_f = 0.14$). 30 mg of product 4 was obtained as a yellowish viscous oil with 66% yield.

$^1\text{H NMR}$ (300 MHz, CDCl_3) δ 7.96(d, 7.0 Hz, 1H), 7.40–7.21(m, 5H), 6.64(s, 1H), 5.56(d, 9.0, 1H), 5.07(s, 2H), 4.54–4.30(m, 2H), 3.70(s, 3H), 3.36–3.18(m, 2H), 2.47–2.27(m, 2H), 2.26–2.11(m, 1H), 1.82–1.59(m, 4H), 1.57–1.43(m, 1H), 0.95(d, 6.1 Hz, 6H)

$^{13}\text{C NMR}$ (75 MHz, CDCl_3) δ 179.9, 173.0, 172.2, 156.1, 136.3, 128.5, 128.1, 127.9, 66.8, 53.3, 52.4, 51.4, 42.4, 40.5, 398.3, 32.9, 2.2.1

MS (EI): m/z , 434.4 [$\text{M}+\text{H}^+$].

Benzyl (1-(((S)-1-(((3S,4S,5S)-1-amino-4,5-dihydroxy-6-(((S)-1-((S)-8-hydroxy-1-hydroxychroman-3-yl)-3-methylbutyl)amino)-1,6-dioxohexan-3-yl)amino)-1-oxo-3-((S)-2-oxopyrrolidin-3-yl)propane-2-yl)amino)-4-methyl-1-oxopentan-2-yl)carbamate (5)

4 mg (9 μmol) of dipeptide 4 ester was dissolved in 0.1 ml of methanol and 0.02 ml (20 μmol) of 1M LiOH solution in water

Table 1. ¹H and ¹³C chemical shifts of target compound 5. DMSO-d₆, 700 MHz. The atom numbering is shown in Fig. 2

Res.	Atom №	¹ H, ppm	¹³ C, ppm	Res.	Atom №	¹ H, ppm	¹³ C, ppm
Ami	3	4.694	81.52	Leu	NH	7.428	–
	4	2.856	29.53		2	4.037	53.73
		3.083			3	1.449	40.96
	5	6.819	118.92		4	1.608	24.69
	6	7.478	136.71		5	0.838	21.88
	7	7.411	115.69		6	0.858	23.45
	1'	0.872	22.09	CG	NH	8.032	–
	2'	0.918	23.76		2	4.312	51.37
	3'	1.683	24.48		3	1.535	34.25
	4'	1.365	39.57			1.959	
		1.688			4	2.248	37.39
	5'	4.213	48.60		5	1.645	27.71
	6'-NH	7.782	–			2.097	
	8'	3.845	72.32		6	3.035	39.91
	9'	3.609	74.25			3.106	
	10'	4.264	48.31		7-NH	7.558	–
10'-NH	7.805	–	Cbz	1	5.023	65.80	
	11'	2.326		35.25	3,7	7.342	128.00
2.448		4,6			7.358	128.40	
				5	7.308	128.16	

was added. After 1 h at room temperature, according to LCMS data, the reaction was complete. The mixture was neutralized with 0.02 ml of a 1M hydrochloric acid solution, the solvents were evaporated on a rotary evaporator. The resulting acid was dissolved in 0.1 ml of DMF, 3 mg (6 μmol) of Amicoumacin A trifluoroacetate, 3.8 mg (11.7 μmol) of TBTU, 6.2 mg (6 μmol) of N-hydroxybenzotriazole were added and cooled to 0 °C. 0.01 ml (54 μmol) of diisopropylethylamine was added to the reaction mixture. 24 hours later, the reaction mixture was diluted with water and extracted with ethyl acetate, after evaporation of the organic solvent, the product was isolated by preparative TLC on silica gel, eluent ethyl acetate: methanol 85/15 (R_f = 0.3). 0.5 mg of product 5 was obtained as a mixture of diastereomers (3 : 1) with 10% yield.

¹H and ¹³C NMR DMSO-d₆: see Table. 1.

MS (EI): m/z, 825.6 [M+H⁺].

Amicoumacin A Production and Purification

The study used the strain *Bacillus pumilus* VKM B-3464D (Patent RU2737856C1) [11], alternative name *Bacillus pumilus* strain 124, GenBank: QENN00000000.1, isolated in 2017 [12]. *B. pumilus* (GenBank: QENN00000000.1) producing Ami was cultured at 28°C in SYC medium containing 40 g/L sucrose, 5 g/L yeast extract, 4 g/L CaCO₃, 1.5 g/L K₂HPO₄, 2 g/L glucose, 2 g/L NaCl, 1.5 g/L MgSO₄, 2 g/L (NH₄)₂SO₄, 0.01 g/L FeSO₄, 0.01 g/L MnCl₂. *B. pumilus* was inoculated from an overnight culture (using a dilution of 1 : 100) and cultured in 750 ml flasks in 100 ml of medium on a thermostatically controlled shaker with a shaking intensity of 250 rpm. Cells were centrifuged at 10,000 g for 10 min, and the supernatant was filtered using a Millistak + HC Pod Depth Filter (Millipore, Billerica; USA).

The extraction of Ami involved three chromatographic steps. At the first stage, the supernatant was purified by solid-phase extraction with the LPS-500 sorbent (Technosorbent; Russia) on an XK 26 column (GE Healthcare Life Sciences; USA) using buffer A (10 mM NH₄OAc, pH 5.0, 5% ACN), buffer

B (10 mM NH₄OAc, pH 5.0, 80% ACN), flow rate 6 ml/min, step gradient 0–10 min (0% B), 10–20 min (20% B), 20–36 min (40% B) and 36–45 min (100% B). Fractions containing Ami (40% B) were lyophilized, dissolved in dimethyl sulfoxide (DMSO), and fractionated twice on a RP-HPLC Zorbax ODS 62 × 250 mm column (Agilent; USA) using buffer A and B, flow rate 5 ml/min, gradient 0–10 min (0% B), 10–24 min (0–70% B), 24–25 min (70–100% B). Finally, Ami was purified on a Symmetry C18 5 μm 4.6 × 150 mm (Waters; USA) RP-HPLC column using buffer A and B, flow rate 1 ml/min, gradient 0–5 min (0% B), 5–20 min (0–100% B). Amicoumacin A was monitored by absorbance at 315 nm. Ami concentration was measured using εMeOH_{315nm} = 4380 M⁻¹cm⁻¹.

Protease Production and Purification

The codon-optimized sequence of the gene encoding the full-length M^{Pro} of SARS-CoV-2 fused to the 6xHis sequence at the C-terminus and to the GST protein at the N-terminus in the pGEX6p plasmid [13] was kindly provided by Prof. Rolf Hilgenfeld. The M^{Pro}-encoding gene was flanked by sequences of two protease sites for subsequent processing of full-length M^{Pro}: an M^{Pro} recognition site for autoprocessing (at the N-terminus of the sequence) and a PreScissionTM protease site just before 6xHis for its removal, as described previously [13]. The full-length M^{Pro} protein was obtained in *E. coli* BL21(DE3) cells and purified according to the procedure [13]. The GST-M^{Pro} protein was self-processing during expression. M^{Pro}-His was purified by metal chelate chromatography using TALON sorbent (Clontech; USA) and treated with PreScissionTM Pro (M^{Pro} to PreScission ratio as 100:1) for 48 h at 4°C to remove 6xHis and obtain M^{Pro} with intact C-terminus. The M^{Pro}/PreScissionTM Pro mixture was purified using GST-Sepharose (Amersham Biosciences, Germany) and TALON (Clontech; USA) IMAC sorbents. Western blot analysis using antibodies to 6xHis showed that the 6xHis sequence was completely removed. M^{Pro} was concentrated to 10 mg/ml in 50 mM Tris-HCl pH 7.5.

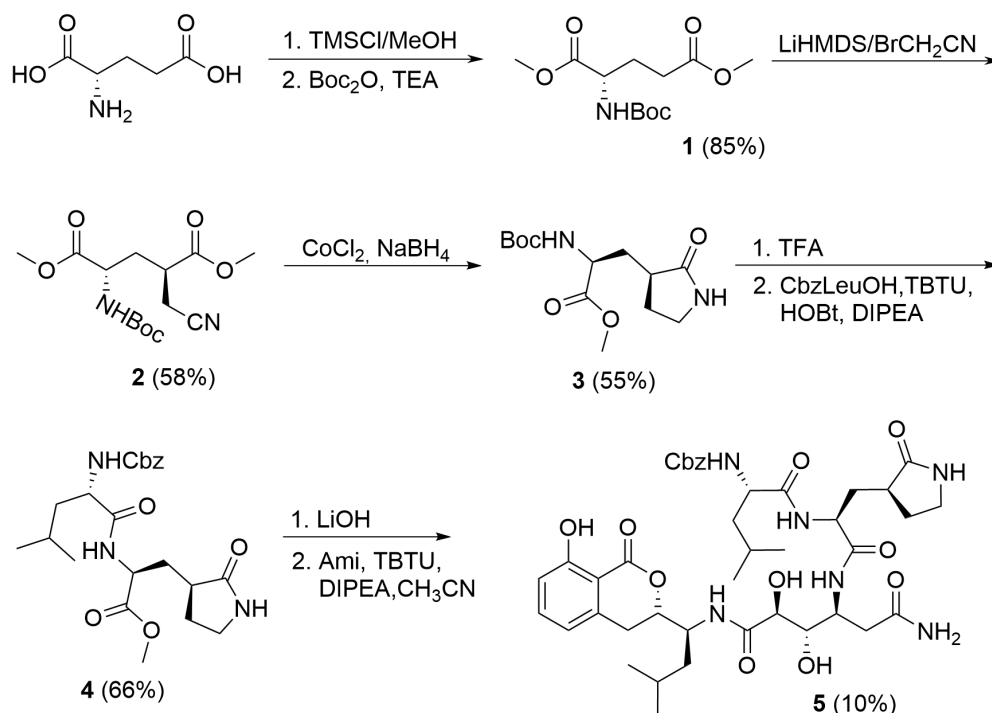


Fig. 1. Total synthesis of the inactivated Amicoumacin 5

Analysis of Cbz-Leu-CG-Ami prodrug activation by M^{Pro} protease

The specific activity of M^{Pro} was evaluated using the FRET substrate (FRET-S), Dabcyl-KTSAVLQ↓SGFRKM-E(Edans)-NH₂ (BPS Bioscience, USA) and corresponded to the pure M^{Pro} preparation [14]. Proteolysis of the prodrug was carried out in the presence of 0.1–1 μM M^{Pro} in reaction buffer (20 mM Tris-HCl pH 7.3, 100 mM NaCl, 1.0 mM EDTA, and 1.0 mM DTT) using 10 μM Cbz-Leu-CG-Ami at 30 °C. The reaction products were analyzed using reverse phase HPLC according to the previously described procedure [15]. Amicoumacin A and its derivatives were detected by absorbance at 315 nm. The concentration was evaluated using the Ami standard, $\epsilon_{\text{MeOH}}_{315\text{nm}} = 4380 \text{ M}^{-1}\text{cm}^{-1}$.

Cytotoxicity measurement

Cytotoxicity was assessed using the MTT assay using the HEK-293 cell line (ATCC; USA). A549 cells were seeded at 2×10^5 cells/well in a 96-well microplate in DMEM (Gibco, Invitrogen; USA) with 2 mM L-glutamine (Invitrogen; USA), 10% fetal bovine serum (Gibco; USA), and incubated at 37°C and 5% CO₂ for 24 h. After incubation, the medium was removed. Cells were then treated with fresh medium containing varying concentrations of Amicoumacin A and Cbz-Leu-CG-Ami analog in the range of 0.01–50 μg/ml for 48 h. After this procedure, the medium was removed and the cells were treated for 2 h with MTT reagent (concentration 2.5 mg/ml). Live cells converted MTT to formazan, which turns blue-violet when dissolved in DMSO. The solution was removed and 200 μl of DMSO was added

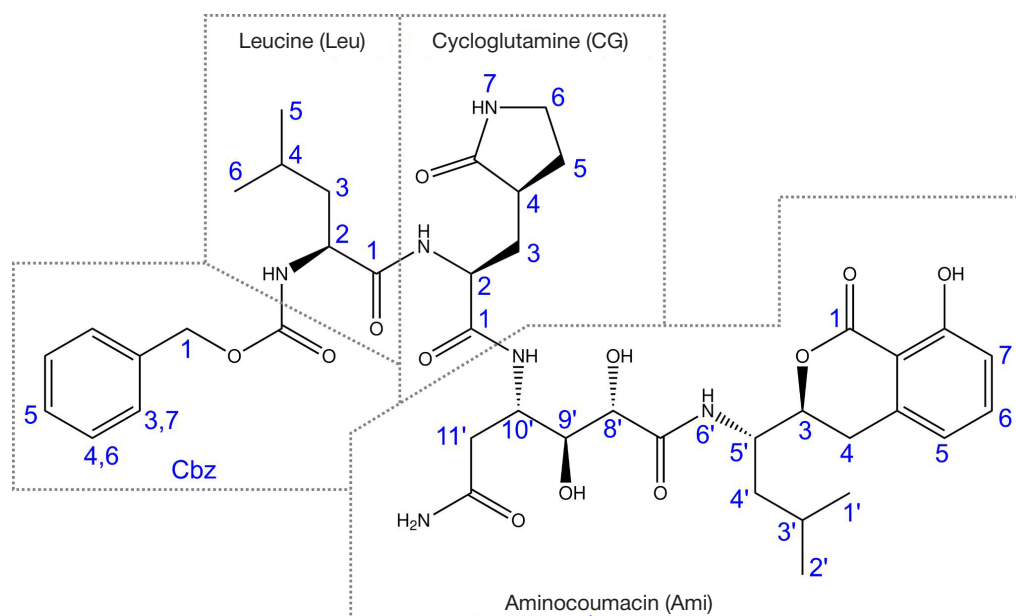


Fig. 2. Atom numbering of compound 5 in Table 1

to dissolve the formazan. Optical absorbance of treated cells and control (untreated) cells was measured at 570 nm using a Varioskan Flash plate reader (Thermo Fischer Scientific; USA). Cell viability was evaluated as the ratio of optical density of treated cells to control measured in each experiment.

RESULTS

To obtain a peptide that mimics the recognition site of the M^{Pro} protease [16], a glutamine analog (cycloglutamine) 3 was synthesized in four steps with a total yield of 27% from glutamic acid [17, 18]. Alkylation of glutamic acid diester 1 proceeds stereoselectively, however, incomplete conversion of the starting diester is observed (Fig. 1). Reaction product 2 was purified by normal-phase column chromatography. Nitrile reduction was carried out with sodium borohydride in methanol at –10 °C. In the process of reduction, as a result of a competing reaction, dimerization of compound 2 occurs with the formation of a secondary amine (~15–20%), which is easily separated during chromatographic purification.

After removal of the Boc protecting group from 3, subsequent acylation with Cbz-leucine in the presence of the condensing agent TBTU [16], and ester hydrolysis, the dipeptide 4 containing a methyl protecting group on the carboxyl fragment was obtained (Fig. 1).

Amicoumacin A is a particularly potent translation inhibitor in both pro- and eukaryotes [19, 20]. In nature, Ami is produced by probiotic strains of *Bacillus pumilus* [10, 12], which mediate their antimicrobial activity. For this study, Amicoumacin A was obtained by production in *B. pumilus* bacteria according to the method described previously [21].

At the final stage of the synthesis, after quantitative cleavage of the methyl protecting group with an alkali solution in water, dipeptide 4 was condensed with Amicoumacin A in the presence of TBTU without additional purification (Fig. 1). The target product Cbz-Leu-CG-Ami 5 purified by preparative TLC was obtained as a mixture of diastereomers (3 : 1). For target compound 5 1D ¹H, 2D multiplicity-edited ¹³C-HSQC and 2D TOCSY NMR spectra (Bruker Avance I 700 MHz) were recorded. An analysis of the NMR spectra made it possible to isolate the spin systems and, after comparison with the spectra of the two initial fragments (Amicoumacin A and dipeptide 4), unambiguously assign the chemical shifts of protons and ¹³C atoms attached to them through one chemical bond (Table 1 and Fig. 2). Modification of Amicoumacin A at 10¹-NH₂ led to a change in the chemical shifts of the carbon atom 10¹ (–2.56 ppm) and neighboring atoms 9¹ and 11¹ (+1.52 and +1.57 ppm, respectively).

As a result, an inactivated analog of Ami 5 was synthesized and used in the subsequent testing for possible activation by SARS-CoV-2 protease M^{Pro}. In contrast to the original Amicoumacin A, which has a highly effective antiproliferative effect (IC₅₀ = 0.06 ± 0.02 µg/ml) [19, 22], the modified Cbz-Leu-CG-Ami 5 derivative did not inhibit cell growth up to an

increase in the concentration of 50 µg/ml. Despite the fact that the sequence of the Cbz-Leu-CG peptide allows highly efficient targeting of M^{Pro} [16], the Cbz-Leu-CG-Ami molecule was stable in the presence of the M^{Pro} protease. It has been shown that less than 3% of free Amicoumacin A can be released in the presence of 1 µM M^{Pro} ([S]/[E] = 10–100) within 4 hours.

DISCUSSION

The emergence of COVID-19 in 2019 posed challenges for healthcare professionals to quickly diagnose and provide medical care to patients. Currently, most of the drugs used to treat COVID-19 are non-specific, have a large number of serious side effects, and are applicable only in emergency cases [23]. Only two SARS-CoV-2-specific drug candidates have successfully passed clinical trials [6, 7], one of which has now found application in the drug nirmatrelvir [23]. Currently, an intensive study of the clinical and epidemiological features of the coronavirus disease, as well as the development of new means of its prevention and treatment continues.

The results of the evaluation of the cellular cytotoxicity of the Cbz-Leu-CG-Ami 5 conjugate obtained in this study on the HEK-293 cell line show a decrease in the IC₅₀ of the inactivated Amicoumacin by several orders of magnitude compared to the initial Ami, which indicates that, despite the high efficiency of the natural Amicoumacin A in the inhibition of eukaryotic translation, inactivated analogs can be created on its basis, the subsequent specific activation of which will allow for targeted therapeutic effects. However, the rate of proteolysis of the synthetic derivative Cbz-Leu-CG-Ami is more than four orders of magnitude lower than the rate of proteolysis characteristic of natural substrates, which indicates the need for further optimization of the resulting molecule. The introduction of substituents at the P1' position is critical for the functioning of many proteases, which, apparently, is also characteristic of M^{Pro} and requires additional introduction of adapter sequences.

CONCLUSIONS

The development of drugs directed toward specific cellular targets and mechanisms underlies the successful treatment of viral diseases. The present work proposes the development of a new inactivated analog of the natural protein biosynthesis inhibitor Amicoumacin A, modified with the Cbz-Leu-CG peptide sequence recognized by the main M^{Pro} protease of the SARS-CoV-2 virus. The study of the ability of the synthetic analog of Ami to be activated by the main SARS-CoV-2 protease revealed the fundamental possibility of creating a prodrug with the indicated principle of action, however, the observed low level of hydrolysis indicates the need for further modification of the resulting molecule. Optimization of the structure and increase in activity of new analogs of Amicoumacin A represent, in our opinion, a promising approach for the development of drug candidates for the treatment of COVID-19.

References

- Kolahchi Z, De Domenico M, Uddin LQ, Cauda V, Grossmann I, Lacasa L, et al. COVID-19 and its Global Economic Impact. *Adv Exp Med Biol.* 2021; 1318: 825–37.
- Marabotti C. Efficacy and effectiveness of covid-19 vaccine — absolute vs. relative risk reduction. *Expert Rev Vaccines.* 2022; 21 (7): 873–75.
- Olliaro P, Torreele E, Vaillant M. COVID-19 vaccine efficacy and effectiveness—the elephant (not) in the room. *The Lancet Microbe.* 2021; 2 (7): e279–e280.
- Knoll MD, Wonodi C. Oxford-AstraZeneca COVID-19 vaccine efficacy. *Lancet.* 2021; 397 (10269): 72–74.
- Jones I, Roy P. Sputnik V COVID-19 vaccine candidate appears safe and effective. *Lancet.* 2021; 397 (10275): 642–3.
- Owen DR, Allerton CMN, Anderson AS, Aschenbrenner L, Avery M,

- Berritt S, et al. An oral SARS-CoV-2 Mpro inhibitor clinical candidate for the treatment of COVID-19. *Science*. 2021; 374: 1586–93.
7. de Vries M, Mohamed AS, Prescott RA, Valero-Jimenez AM, Desvignes L, O'Connor R, et al. A comparative analysis of SARS-CoV-2 antivirals characterizes 3CLpro inhibitor PF-00835231 as a potential new treatment for COVID-19. *J Virol*. 2021; 95 (10): e01819–20.
 8. Saban M, Kaim A, Myers V, Wilf-Miron R. COVID-19 Vaccination, Morbidity, and Mortality During a 12-Month Period in Israel: Can We Maintain a “Herd Immunity” State? *Popul Health Manag*. 2022; 25 (5): 684.
 9. Stepanova M, Lam B, Younossi E, Felix S, Ziyayee M, Price J, et al. The impact of variants and vaccination on the mortality and resource utilization of hospitalized patients with COVID-19. *BMC Infect Dis*. 2022; 22: 702.
 10. Itoh J, Omoto S, Shomura T, Nishizawa N, Miyado S, Yuda Y, et al. Amicoumacin-A, a new antibiotic with strong antiinflammatory and antiulcer activity. *J Antibiot (Tokyo)*. 1981; 34 (5): 611–3.
 11. Terekhov SS, Mokrushina YuA, Smirnov IV, Gabibov AG. *Bacillus pumilus* strain producing wide-spectrum antibiotic Amikumacin. RU2737856C1, 2020. <https://patents.google.com/patent/RU2737856C1/en?q=RU2737856C1>.
 12. Terekhov SS, Smirnov IV, Malakhova MV, Samoilov AE, Manolo AI, Nazarov AS, et al. Ultrahigh-throughput functional profiling of microbiota communities. *Proc Natl Acad Sci U S A*. 2018; 115 (38): 9551–6.
 13. Zhang L, Lin D, Sun X, Curth U, Drosten C, Sauerhering L, et al. Crystal structure of SARS-CoV-2 main protease provides a basis for design of improved α -ketoamide inhibitors. *Science*. 2020; 368 (6489): 409–12.
 14. Zakharova MY, Kuznetsova AA, Uvarova VI, Fomina AD, Kozlovskaya LI, Kaliberda EN, et al. Pre-Steady-State Kinetics of the SARS-CoV-2 Main Protease as a Powerful Tool for Antiviral Drug Discovery. *Front Pharmacol*. 2021; 12: 3243.
 15. Baranova MN, Kudzhaev AM, Mokrushina YA, Babenko VV, Kornienko MA, Malakhova MV, et al. Deep Functional Profiling of Wild Animal Microbiomes Reveals Probiotic *Bacillus pumilus* Strains with a Common Biosynthetic Fingerprint. *Int J Mol Sci*. 2022; 23 (3): 1168.
 16. Vuong W, Khan MB, Fischer C, Arutyunova E, Lamer T, Shields J, et al. Feline coronavirus drug inhibits the main protease of SARS-CoV-2 and blocks virus replication. *Nat Commun*. 2020; 11: 4282.
 17. Schädel N, Icik E, Martini M, Altevogt L, Ramming I, Greulich A, et al. Synthesis of Imidazole and Histidine-Derived Cross-Linkers as Analogues of GOLD and Desmosine. *Synthesis (Stuttg)*. 2021; 53 (13): 2260–8.
 18. Mou K, Xu B, Ma C, Yang X, Zou X, Lü Y, et al. Novel CADD-based peptidyl vinyl ester derivatives as potential proteasome inhibitors. *Bioorg Med Chem Lett*. 2008; 18 (6): 2198–202.
 19. Prokhorova IV, Akulich KA, Makeeva DS, Osterman IA, Skvortsov DA, Sergiev PV, et al. Amicoumacin A induces cancer cell death by targeting the eukaryotic ribosome. *Sci Rep*. 2016; 6: 27720.
 20. Maksimova EM, Vinogradova DS, Osterman IA, Kasatsky PS, Nikonov OS, Milón P, et al. Multifaceted Mechanism of Amicoumacin A Inhibition of Bacterial Translation. *Front Microbiol*. 2021; 12: 618857.
 21. Terekhov SS, Nazarov AS, Mokrushina YA, Baranova MN, Potapova NA, Malakhova MV, et al. Deep functional profiling facilitates the evaluation of the antibacterial potential of the antibiotic amicoumacin. *Antibiotics*. 2020; 9: 157.
 22. Terekhov SS, Mokrushina YA, Nazarov AS, Zlobin A, Zalevsky A, Bourenkov G, et al. A kinase bioscavenger provides antibiotic resistance by extremely tight substrate binding. *Sci Adv*. 2020; 6 (26): eaaz9861.
 23. Therapeutics and COVID-19: living guideline, Geneva: World Health Organization c2022 [cited 2022 Dec 19]. Available from: <https://app.magicapp.org/#/guideline/nBkO1E/section/nYlJyL>.

Литература

1. Kolahchi Z, De Domenico M, Uddin LQ, Cauda V, Grossmann I, Lacasa L, et al. COVID-19 and Its Global Economic Impact. *Adv Exp Med Biol*. 2021; 1318: 825–37.
2. Marabotti C. Efficacy and effectiveness of covid-19 vaccine — absolute vs. relative risk reduction. *Expert Rev Vaccines*. 2022; 21 (7): 873–75.
3. Olliaro P, Torreele E, Vaillant M. COVID-19 vaccine efficacy and effectiveness—the elephant (not) in the room. *The Lancet Microbe*. 2021; 2 (7): e279–e280.
4. Knoll MD, Wonodi C. Oxford-AstraZeneca COVID-19 vaccine efficacy. *Lancet*. 2021; 397 (10269): 72–74.
5. Jones I, Roy P. Sputnik V COVID-19 vaccine candidate appears safe and effective. *Lancet*. 2021; 397 (10275): 642–3.
6. Owen DR, Allerton CMN, Anderson AS, Aschenbrenner L, Avery M, Berritt S, et al. An oral SARS-CoV-2 Mpro inhibitor clinical candidate for the treatment of COVID-19. *Science*. 2021; 374: 1586–93.
7. de Vries M, Mohamed AS, Prescott RA, Valero-Jimenez AM, Desvignes L, O'Connor R, et al. A comparative analysis of SARS-CoV-2 antivirals characterizes 3CLpro inhibitor PF-00835231 as a potential new treatment for COVID-19. *J Virol*. 2021; 95 (10): e01819–20.
8. Saban M, Kaim A, Myers V, Wilf-Miron R. COVID-19 Vaccination, Morbidity, and Mortality During a 12-Month Period in Israel: Can We Maintain a “Herd Immunity” State? *Popul Health Manag*. 2022; 25 (5): 684.
9. Stepanova M, Lam B, Younossi E, Felix S, Ziyayee M, Price J, et al. The impact of variants and vaccination on the mortality and resource utilization of hospitalized patients with COVID-19. *BMC Infect Dis*. 2022; 22: 702.
10. Itoh J, Omoto S, Shomura T, Nishizawa N, Miyado S, Yuda Y, et al. Amicoumacin-A, a new antibiotic with strong antiinflammatory and antiulcer activity. *J Antibiot (Tokyo)*. 1981; 34 (5): 611–3.
11. Терехов С. С., Мокрушина Ю. А., Смирнов И. В., Габиев А. Г. Штамм *Bacillus pumilus*, продуцирующий антибиотик широкого спектра действия амикумацин. RU2737856C1, 2020. Доступно по ссылке: <https://patents.google.com/patent/RU2737856C1/en?q=RU2737856C1>.
12. Terekhov SS, Smirnov IV, Malakhova MV, Samoilov AE, Manolo AI, Nazarov AS, et al. Ultrahigh-throughput functional profiling of microbiota communities. *Proc Natl Acad Sci U S A*. 2018; 115 (38): 9551–6.
13. Zhang L, Lin D, Sun X, Curth U, Drosten C, Sauerhering L, et al. Crystal structure of SARS-CoV-2 main protease provides a basis for design of improved α -ketoamide inhibitors. *Science*. 2020; 368 (6489): 409–12.
14. Zakharova MY, Kuznetsova AA, Uvarova VI, Fomina AD, Kozlovskaya LI, Kaliberda EN, et al. Pre-Steady-State Kinetics of the SARS-CoV-2 Main Protease as a Powerful Tool for Antiviral Drug Discovery. *Front Pharmacol*. 2021; 12: 3243.
15. Baranova MN, Kudzhaev AM, Mokrushina YA, Babenko VV, Kornienko MA, Malakhova MV, et al. Deep Functional Profiling of Wild Animal Microbiomes Reveals Probiotic *Bacillus pumilus* Strains with a Common Biosynthetic Fingerprint. *Int J Mol Sci*. 2022; 23 (3): 1168.
16. Vuong W, Khan MB, Fischer C, Arutyunova E, Lamer T, Shields J, et al. Feline coronavirus drug inhibits the main protease of SARS-CoV-2 and blocks virus replication. *Nat Commun*. 2020; 11: 4282.
17. Schädel N, Icik E, Martini M, Altevogt L, Ramming I, Greulich A, et al. Synthesis of Imidazole and Histidine-Derived Cross-Linkers as Analogues of GOLD and Desmosine. *Synthesis (Stuttg)*. 2021; 53 (13): 2260–8.
18. Mou K, Xu B, Ma C, Yang X, Zou X, Lü Y, et al. Novel CADD-based peptidyl vinyl ester derivatives as potential proteasome inhibitors. *Bioorg Med Chem Lett*. 2008; 18 (6): 2198–202.
19. Prokhorova IV, Akulich KA, Makeeva DS, Osterman IA, Skvortsov DA, Sergiev PV, et al. Amicoumacin A induces cancer cell death by targeting the eukaryotic ribosome. *Sci Rep*. 2016; 6: 27720.
20. Maksimova EM, Vinogradova DS, Osterman IA, Kasatsky PS,

- Nikonov OS, Milón P, et al. Multifaceted Mechanism of Amicoumacin A Inhibition of Bacterial Translation. *Front Microbiol.* 2021; 12: 618857.
21. Terekhov SS, Nazarov AS, Mokrushina YA, Baranova MN, Potapova NA, Malakhova MV, et al. Deep functional profiling facilitates the evaluation of the antibacterial potential of the antibiotic amicoumacin. *Antibiotics.* 2020; 9: 157.
 22. Terekhov SS, Mokrushina YA, Nazarov AS, Zlobin A, Zalevsky A, Bourenkov G, et al. A kinase bioscavenger provides antibiotic resistance by extremely tight substrate binding. *Sci Adv.* 2020; 6 (26): eaaz9861.
 23. Therapeutics and COVID-19: living guideline, Geneva: World Health Organization c2022 [cited 2022 Dec 19]. Available from: <https://app.magicapp.org/#/guideline/nBkO1E/section/nYlJyL>.

EFFICACY OF FAVIPIRAVIR AND MOLNUPIRAVIR AGAINST NOVEL SARS-COV-2 VARIANTS *IN VITRO* AND *IN VIVO*

Siniyavin AE^{1,2} ✉, Russu LI¹, Vasina DV¹, Shidlovskaya EV¹, Kuznetsova NA¹, Gushchin VA^{1,3}, Gintsburg AL^{1,4}

¹ Gamaleya National Research Center for Epidemiology and Microbiology, Moscow, Russia

² Shemyakin and Ovchinnikov Institute of Bioorganic Chemistry, Moscow, Russia.

³ Lomonosov Moscow State University, Moscow, Russia

⁴ Sechenov University, Moscow, Russia

The COVID-19 disease pandemic remains a significant global problem, resulting in hundreds of millions of cases and millions of deaths. The search for specific inhibitors of SARS-CoV-2 for the treatment of this infection remains relevant. Drugs such as Favipiravir and Molnupiravir, which exhibit specific antiviral activity against SARS-CoV-2, are already being used to treat patients. However, there is limited evidence of their effectiveness, especially against novel genetic variants of the COVID-19 pathogen. The aim of this study was to investigate the antiviral effect of these drugs using an *in vitro* experimental model of SARS-CoV-2 infection in Vero E6 cell culture and an animal model of infection using Syrian hamsters. It has been established that Molnupiravir has an inhibitory effect against variants of the SARS-CoV-2 with IC50 values from 16.51 to 7.88 μM *in vitro*, and reduces the infectious titer of the virus in the lungs of animals by $\sim 1.5 \text{ Log}_{10}$ *in vivo*, while Favipiravir shows lower activity and severe toxicity. Dose selection and frequency of use remain unexplored.

Keywords: COVID-19, SARS-CoV-2, antiviral activity, Favipiravir, Molnupiravir, Omicron, antivirals

Funding: the study was supported by the Russian Ministry of Health, grant № 121111200070-4 (P16).

Acknowledgments: the authors would like to thank the staff of N.I. N.F. Gamaleya A. Zakharova and T. Remizov for organizing the supply of reagents for the study.

Author contribution: Siniyavin AE — design of the experiment, study of antiviral activity, data analysis, writing the text; Russu LI — work with the virus and animals; Vasina DV — work with animals; Shidlovskaya EV, Kuznetsova NA — PCR analysis, data processing; Gushchin VA — research supervision, text editing; Gintsburg AL — approval of the research concept.

Compliance with ethical standards: the study was approved by the ethics committee of the Federal State Budgetary Institution "N.N. N.F. Gamaleya" of the Ministry of Health of the Russian Federation (protocol № 27 of June 6, 2022); conducted in compliance with the principles of the Declaration of Helsinki of the World Medical Association.

✉ **Correspondence should be addressed:** Andrey E. Siniyavin
Gamalei, 16, Moscow, 123098, Russia; andreysi93@yandex.ru

Received: 05.12.2022 **Accepted:** 20.12.2022 **Published online:** 31.12.2022

DOI: 10.24075/brsmu.2022.071

ЭФФЕКТИВНОСТЬ ФАВИПИРАВИРА И МОЛНУПИРАВИРА ПРОТИВ НОВЫХ ВАРИАНТОВ SARS-COV-2 В СИСТЕМАХ *IN VITRO* И *IN VIVO*

А. Э. Синявин^{1,2} ✉, Л. И. Руссу¹, Д. В. Васина¹, Е. В. Шидловская¹, Н. А. Кузнецова¹, В. А. Гушчин^{1,3}, А. Л. Гинцбург^{1,4}

¹ Национальный исследовательский центр эпидемиологии и микробиологии имени Н. Ф. Гамалеи, Москва, Россия

² Институт биоорганической химии имени М. М. Шемякина и Ю. А. Овчинникова, Москва, Россия

³ Московский государственный университет имени М. В. Ломоносова, Москва, Россия

⁴ Первый Московский государственный медицинский университет имени И. М. Сеченова

Пандемия заболевания COVID-19 остается важной глобальной проблемой общественного здравоохранения, которая приводит к сотням миллионов случаев заболевания и миллионам летальных исходов. По всему миру активно идут разработка и исследования специфических ингибиторов SARS-CoV-2 для лечения данной инфекции. Такие препараты, как фавипиравир и молнупиравир, проявляющие специфичную противовирусную активность против SARS-CoV-2, уже применяются для лечения пациентов. Однако имеются ограниченные данные об их эффективности, особенно против новых генетических вариантов возбудителя COVID-19. Целью исследования было изучить противовирусный эффект этих препаратов с использованием экспериментальной модели инфекции SARS-CoV-2 на культуре клеток Vero E6 *in vitro* и животной модели инфекции с использованием сирийских хомячков. Установлено, что молнупиравир оказывает выраженное ингибирующее действие против различных вариантов вируса SARS-CoV-2 со значениями IC50 от 16,51 до 7,88 μM *in vitro* и снижает инфекционный титр вируса в легких животных на $\sim 1,5 \text{ Log}_{10}$ *in vivo*, в то время как фавипиравир проявляет более низкую активность и выраженную токсичность. Полученные результаты указывают на необходимость дальнейших исследований в направлении подбора дозировок и кратности применения.

Ключевые слова: COVID-19, SARS-CoV-2, противовирусная активность, фавипиравир, молнупиравир, Омикрон, противовирусные препараты

Финансирование: исследование выполнено при финансовой поддержке Минздрава России, грант № 121111200070-4 (П16).

Благодарности: авторы выражают благодарность сотрудникам НИЦЭМ им. Н.Ф. Гамалеи А. Захаровой и Т. Ремизову за организацию поставки реагентов для исследования.

Вклад авторов: А. Э. Синявин — планирование эксперимента, исследование противовирусной активности, анализ данных, написание текста; Л. И. Руссу — работа с вирусом и животными; Д. В. Васина — работа с животными; Е. В. Шидловская, Н. А. Кузнецова — ПЦР-анализ, обработка данных; В. А. Гушчин — руководство исследованием, редактирование текста; А.Л. Гинцбург — утверждение концепции исследования.

Соблюдение этических стандартов: исследование одобрено этическим комитетом ФГБУ «НИЦЭМ им. Н.Ф. Гамалеи» МЗ РФ (протокол № 27 от 6 июня 2022 г.); проведено с соблюдением принципов Хельсинкской декларации Всемирной медицинской ассоциации.

✉ **Для корреспонденции:** Андрей Эдуардович Синявин
ул. Гамалеи, д. 16, г. Москва, 123098, Россия; andreysi93@yandex.ru

Статья получена: 05.12.2022 **Статья принята к печати:** 20.12.2022 **Опубликована онлайн:** 31.12.2022

DOI: 10.24075/vrgmu.2022.071

The COVID-19 pandemic caused by severe acute respiratory syndrome coronavirus 2 (SARS-CoV-2) continues to pose a global public health threat and increase the economic burden. The spread of the virus in humans is still ongoing, and new variants of SARS-CoV-2 are constantly emerging, leading to an urgent need for drugs to treat this disease, as well as for expanded studies on the effectiveness of approved treatments for COVID-19.

For the treatment of COVID-19 in the Russian Federation, it is recommended to use several drugs with a specific antiviral effect, including Favipiravir and Molnupiravir. But the efficacy of these drugs for new variants of SARS-CoV-2 remains unknown.

The broad-spectrum antiviral drug Favipiravir [1] targets the viral RNA-dependent RNA polymerase (RdRp). It is effective against both seasonal virus and avian influenza, as well as SARS-CoV-2 in cell culture and *in vivo* in experimental animal models. In humans, Favipiravir is phosphorylated by cellular enzymes to its active form, Favipiravir-ribofuranosyl-5'-triphosphate (F-RTP). F-RTP does not greatly affect on cellular transcription. There are several hypotheses regarding how F-RTP interacts with RdRp. Some studies have shown that when F-RTP incorporated into the nascent RNA strand, it prevents RNA strand elongation and virus replication. It has also been shown, that the presence of purine analogues can reduce the antiviral activity of Favipiravir, i.e., competition between F-RTP and purine nucleosides for binding to RdRp is possible. According to the results of clinical studies, Favipiravir does not improve cure time or clinical outcomes and does not show an antiviral effect in the treatment of COVID-19 infection [2–4].

β -D-N4-hydroxycytidine (NHC, EIDD-1931) is a ribonucleoside analogue with a wide spectrum of activity against various RNA viruses [5]. Molnupiravir (MK-4482/EIDD-2801), or β -D-N4-hydroxycytidine-5'-isopropyl ether, is a biologically active NHC prodrug. It is an oral drug and is more convenient for mass administration in humans than remdesivir or other antiviral agents such as convalescent plasma and neutralizing antibodies, which require intravenous or intramuscular injection and hospital use. NHC has been shown to be effective against various RNA viruses such as influenza, Ebola virus (EBOV), Venezuelan encephalitis virus (VEEV), SARS-CoV-2, SARS-CoV, MERS-CoV and related zoonotic groups 2b or 2c Bat-CoV in *in vivo* and *in vitro* experiments [6–8]. A series of preclinical and clinical trials have proven that Molnupiravir is safe and effective for the treatment of SARS-CoV-2 infection [9, 10]. Following oral administration, Molnupiravir is rapidly converted to active NHC in plasma, distributed to various organs, and converted to the corresponding 5'-triphosphate by human kinases [11]. It is known that NHC 5'-triphosphate is a competitive substrate for viral RNA-dependent RNA polymerase, integrates into viral RNA, and leads to the accumulation of lethal mutations in the viral genome [12].

Since 2022, the new SARS-CoV-2 variant B.1.1.529 (Omicron) and its subvariants containing multiple mutations in the viral genome have dominated all over the world [13]. Mutations in the RBD domain of S-glycoprotein reduce the effectiveness of preexisting antibodies formed after infection of COVID-19 and vaccination [14]. Given the emergence of new variants of SARS-CoV-2, the aim of this study was to evaluate the efficacy of Favipiravir and Molnupiravir against different variants of SARS-CoV-2.

METHODS

Experiments were performed on the cell line Vero E6 (ATCC CRL-1586). Cells were cultured in DMEM growth medium

(Gibco; USA) supplemented with 5% fetal bovine serum (FBS; HyClone, USA), 1× antimycotic antibiotic solution (Capricorn Scientific GmbH; Germany) and 1× GlutaMAX (Gibco; USA). To study the antiviral effect, various dilutions of the test compound were added to the cell monolayer and incubated for 1 h at 37 °C and 5% CO₂. After that, cells were infected with the SARS-CoV-2 at 100 TCID₅₀ (TCID₅₀ is a tissue culture dose that causes the death of 50% of the monolayer cells). In this experiment, the following variants of the SARS-CoV-2 virus were used: Wuhan B.1.1 (PMVL-4), Omicron BA.4.6 (PMVL-55), Omicron BA.5 (PMVL-52) and Omicron BA.5.2 (PMVL-54). Inhibition of the virus-induced cytopathic effect (CPE) under the action of the compound was determined by MTT test [15].

As an animal model of infection, female Syrian hamsters were used ("Stolbovaya"; Russia). Animals were kept in individually ventilated cages (temperature 21–25 °C, humidity 20%, pressure –0.1 kPa) with free access to food and water. The light regime was 12 hours of light and 12 hours of darkness. Animals were divided into experimental groups (5–8 animals each), which were orally administered Molnupiravir (200 mg/kg), Favipiravir (200–300 mg/kg), and a control group of infected animals. Animals were infected intranasally with SARS-CoV-2 strain PMVL-4 or PMVL-52 at 10⁵ TCID₅₀. For four days, the animals were administered study drugs twice a day. On the fifth day of the experiment, the animals were euthanized by CO₂ inhalation and cervical dislocation, and lung tissues were collected at necropsy for analysis. Hamster lungs were subjected to homogenization followed by separation of the supernatant by low speed centrifugation at 12,000 rpm for 10 min. The virus titer was determined in a monolayer of Vero E6 cells. For each lung homogenate sample, the virus titer was determined after 72 hours of infection and expressed as PFU/mg lung (plaque forming units). Total RNA was isolated from lung homogenates using the ExtractRNA reagent (Evrogen; Russia) according to the manufacturer's instructions. The reverse transcription reaction was performed using a SARS-CoV-2 FRT kit for quantitative determination of SARS-CoV-2 coronavirus RNA using a panel characterized by the number of copies of the SARS-CoV-2 amplified fragment (N.F. Gamaleya National Research Center for Epidemiology and Microbiology; Russia). Results were expressed as numbers converted to log₁₀ SARS-CoV-2 viral load per mg lung tissue.

RESULTS

At the first stage of the study, the cytotoxicity of Favipiravir and Molnupiravir on Vero E6 cells was assessed. It was found that Favipiravir has a pronounced cytotoxic effect, significantly inhibiting cell proliferation at a concentration of 1000 μ M (decrease in cell viability up to 60%). At all other concentrations tested, Favipiravir showed a dose-dependent cytotoxic effect (Fig. 1). Molnupiravir had no significant effect on cell viability, inhibiting their proliferation at 200 μ M by an average of 10%.

The study of the antiviral activity of Favipiravir and Molnupiravir against SARS-CoV-2 was carried out using four variants of the virus: the reference strain of the Wuhan variant (genetic line B.1.1) and three variants of the Omicron virus currently circulating in the Russian Federation, and worldwide (BA.4.6, BA.5 and BA.5.2) (Fig. 2). It was found, that at a concentration of 1000 μ M, Favipiravir showed no activity against the reference strain from line B.1.1. Inhibition on ~50% at the same concentration (~160 mg/mL) was found for the BA.5 and BA.5.2 variants of the Omicron. Inhibition of the Omicron BA.4.6 virus variant did not exceed 20%. Molnupiravir showed a broad spectrum of antiviral activity,

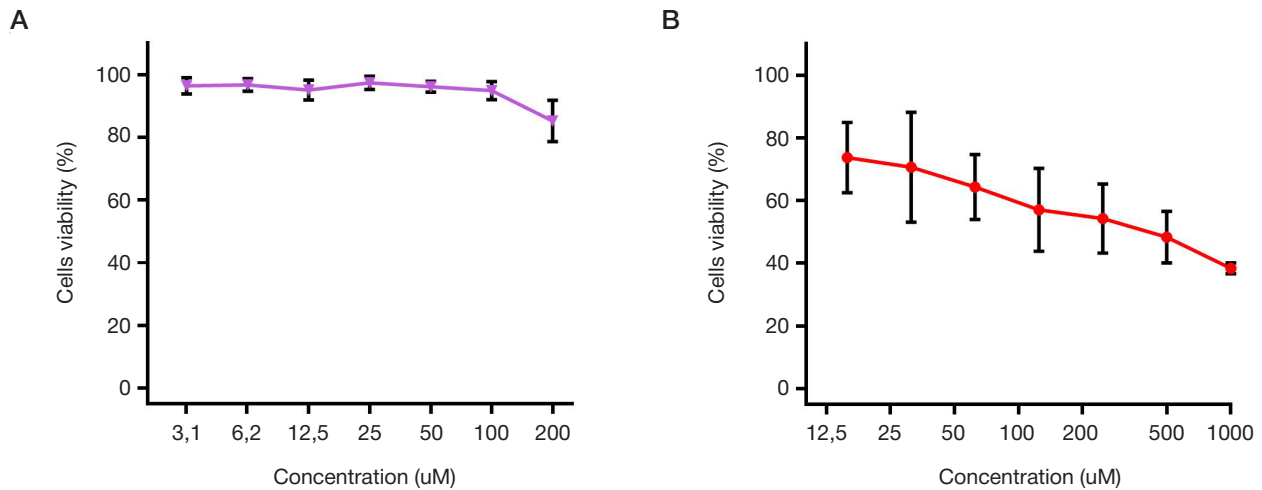


Fig. 1. Cytotoxicity study of Molnupiravir (A) and Favipiravir (B) using Vero E6 cells inhibiting all virus variants used with IC_{50} values from 16.51 to 7.88 μ M.

Further, the effectiveness of the drugs was investigated using an infectious animal model. Syrian hamsters were treated with 300 mg/kg Favipiravir or 200 mg/kg Molnupiravir via oral gavage. The animals were then infected intranasally with the SARS-CoV-2 Wuhan variant. The drugs were given to the animals twice a day for four days. During infection, animals from the infected control group lost more than 20% weight ($p < 0.01$). Animals treated with Favipiravir lost weight by 10% ($p > 0.05$), showed apathy and food refusal, which indicates the toxic effect of the drug. Animals treated with Molnupiravir gained weight during the experiment (Fig. 3). A study of SARS-CoV-2 viral load in the lungs of animals showed that both Molnupiravir and Favipiravir reduced the amount of viral RNA (1 Log₁₀). When determining the infectious titer of SARS-CoV-2 in the lungs of animals, it was found that all drugs suppress the replication of the virus. Treatment of animals with Molnupiravir and Favipiravir significantly reduced the virus titer (~1.5 Log₁₀). When studying the effectiveness of drugs in animals using the Omicron BA.5 virus variant, it was found that this variant is less pathogenic than the Wuhan variant. The drug were administrated with the same doses (200 mg/kg). During the experiment, the animals gained weight in all the studied groups. A decrease in viral load in the lungs by 1.5 Log₁₀ was found for the group of animals treated with molnupiravir (EIDD-2801), however, the data are not statistically significant ($p > 0.05$; 1.5 Log₁₀). For Favipiravir, the reduction in viral load (0.5 Log₁₀) and viable virus titer (1 Log₁₀) was less pronounced and was not statistically significant ($p > 0.05$).

DISCUSSION

Previous studies of the antiviral activity of Favipiravir against SARS-CoV-2 show that it has a low antiviral effect with EC_{50} values $> 200 \mu$ M. High doses of Favipiravir have been associated with signs of toxicity in animals in drug efficacy studies [16], since in vivo Favipiravir exhibits an antiviral effect at a double dose of 300 mg/kg, with a decrease in the infectious titer of the virus in the lungs by $\sim 1.5 \text{ Log}_{10}$ [17]. Other studies have shown that Favipiravir exhibits activity with an EC_{50} value of $\sim 62 \mu$ M [18]. The results of our study also point to the limited antiviral potential of Favipiravir. When Vero E6 cells were infected with the SARS-CoV-2 virus, it was found that this drug does not have antiviral activity in vitro, and also exhibits cytotoxicity. We have shown the efficacy of this drug at a dose of 300 mg/kg twice a day in an animal model of infection using a Wuhan variant. In an animal model using the Omicron variant, when using a dosage reduced to 200 mg/kg, the effect was not significant. However, changes in the behavior of animals and a decrease in their weight during treatment with Favipiravir at a dose of 300 mg/kg indicate its toxic effect and the need for further dose selection in order to combine the absence of toxicity and preservation of drug activity.

Studies using primary human cells and other cell lines have confirmed that NHC (the active metabolite of Molnupiravir) has potent antiviral activity against various coronaviruses such as SARS-CoV, SARS-CoV-2 and MERS-CoV. The IC_{50} values for molnupiravir against SARS-CoV-2 were 0.3–0.08 μ M [19]. We found that Molnupiravir exhibits antiviral activity for all studied variants of the SARS-CoV-2 virus, with low

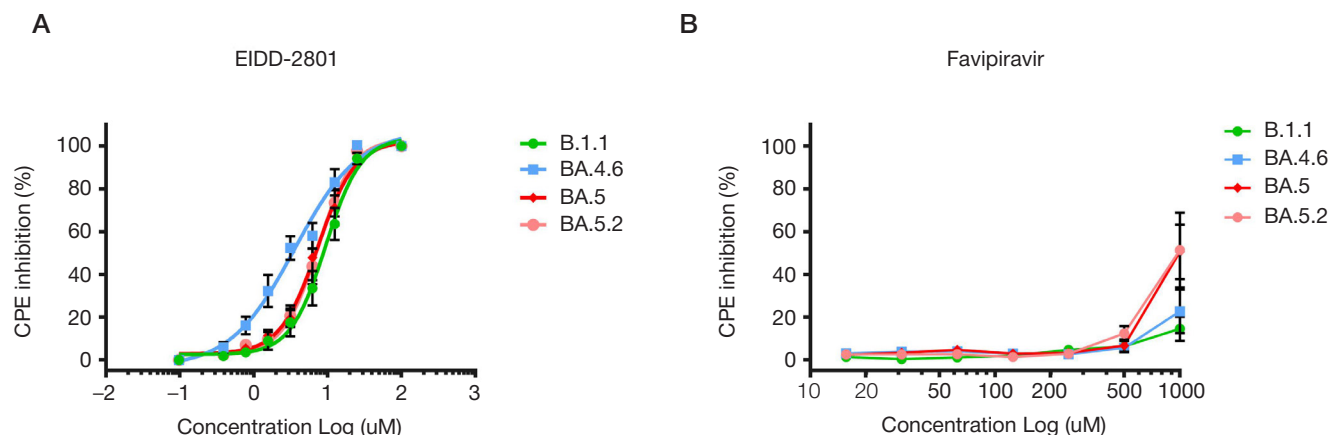


Fig. 2. Antiviral activity of Molnupiravir (EIDD-2801) (A) and Favipiravir (B) against four different variants of the SARS-CoV-2 virus

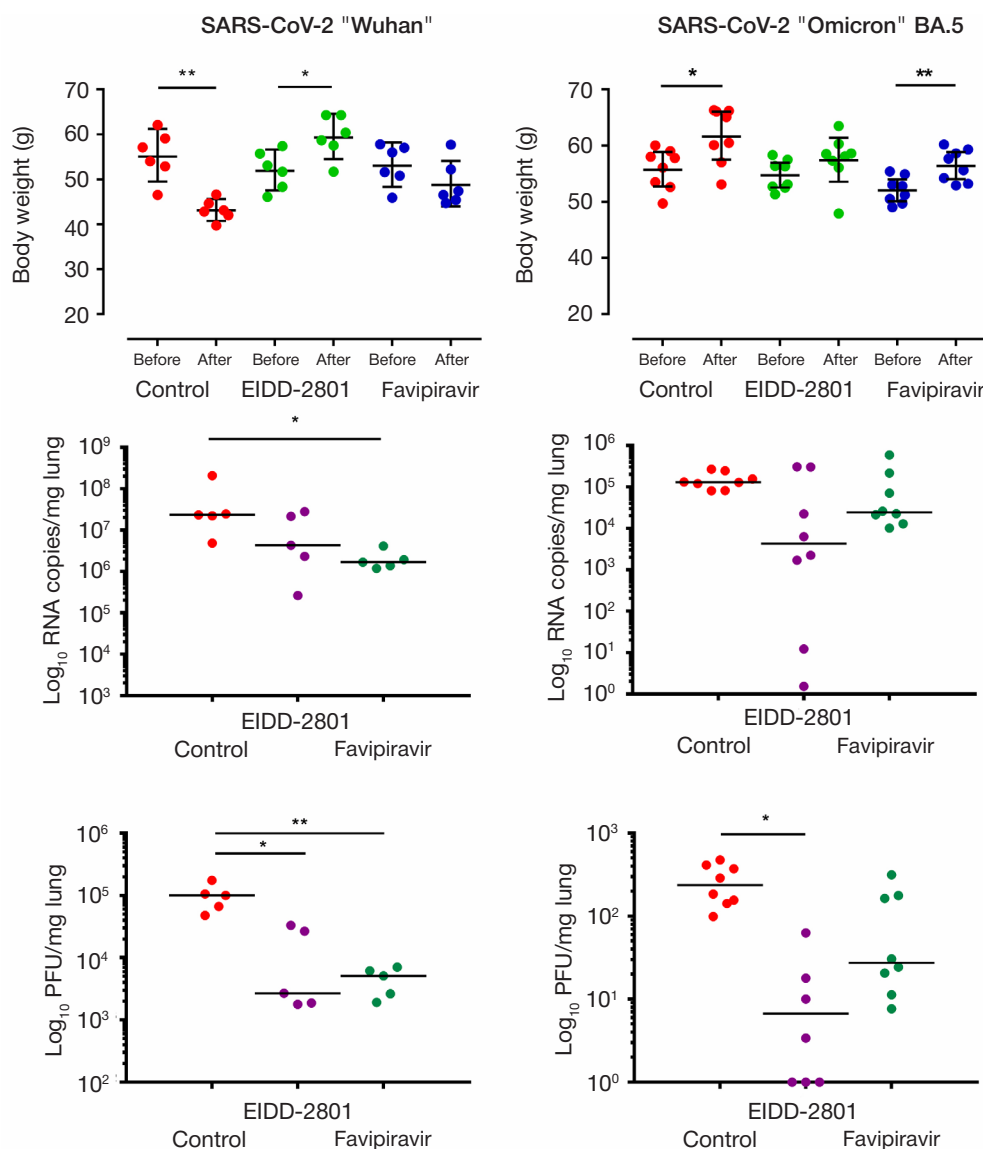


Fig. 3. The effectiveness of drugs against the Wuhan and Omicron BA.5 in animal models. Animals weight changes are presented, as well as the values of viral load and virus titer in the lungs for each animal in the corresponding group. ANOVA with Tukey's post hoc test: * — $p < 0.05$; ** — $p < 0.01$

cytotoxicity. Molnupiravir showed antiviral activity in animals infected with both Wuhan and Omicron BA.5 viruses. In a recent study, Molnupiravir also inhibited virus replication in the lungs of hamsters infected with the Omicron variant [20]. Molnupiravir significantly inhibited viral replication in the upper and lower respiratory tracts of hamsters. At the same time, the researchers found that Omicron is less pathogenic for animals compared to earlier SARS-CoV-2 genetic lines [21].

CONCLUSIONS

Favipiravir showed a rather low antiviral effect against SARS-CoV-2 at the maximum tested concentration, which had the

most pronounced cytotoxic effect. Due to the pronounced cytotoxic potential and weak antiviral activity *in vitro* and *in vivo*, additional studies of the safety and efficacy of Favipiravir, dose selection, frequency of use, and clarification of indications for use are required in order to combine efficacy with minimal toxicity to the human. Molnupiravir has shown greater efficacy and safety in *in vitro* and *in vivo* models. The results for activity against the Omicron variant expand on previous data for both drugs. Further efforts are required in the search for new inhibitors and their compositions with higher specific antiviral activity. Further research is needed on the approved drugs Favipiravir and Molnupiravir in order to select the optimal treatment regimens to achieve the maximum antiviral effect.

References

1. Yousuke F, Takashi K, Takaaki N. Favipiravir (T-705), a broad-spectrum inhibitor of viral RNA polymerase. *Proc Jpn Acad Ser B Phys Biol Sci.* 2017; 93 (7): 449–63.
2. McMahon JH, Lau JS, Coldham A, et al. Favipiravir in early symptomatic COVID-19, a randomised placebo-controlled trial. *EclinicalMedicine.* 2022; 20 (54): 101703.
3. Yanagisawa K, Takara K, Suga H, et al. The Assessment of the Efficacy and Safety of Favipiravir for Patients with SARS-CoV-2 Infection: A Multicenter Non-randomized, Uncontrolled Single-arm Prospective Study. *Intern Med.* 2022; 61 (21): 3197–204.

4. Bosaeed M, Alharbi A, Mahmoud E, et al. Efficacy of favipiravir in adults with mild COVID-19: a randomized, double-blind, multicentre, placebo-controlled clinical trial. *Clin Microbiol Infect.* 2022; 28 (4): 602–8.
5. Lee CC, Hsieh CC, Ko WC. Molnupiravir-A Novel Oral Anti-SARS-CoV-2 Agent. *Antibiotics (Basel).* 2021; 10 (11): 1294.
6. Toots M, Yoon JJ, Hart M, Natchus MG, Painter GR, Plemper RK. Quantitative efficacy paradigms of the influenza clinical drug candidate EIDD-2801 in the ferret model. *Transl Res.* 2020; 218: 16–28.
7. Yoon JJ, Toots M, Lee S, et al. Orally Efficacious Broad-Spectrum Ribonucleoside Analog Inhibitor of Influenza and Respiratory Syncytial Viruses. *Antimicrob Agents Chemother.* 2018; 62 (8): e00766–18.
8. Sheahan TP, Sims AC, Zhou S, et al. An orally bioavailable broad-spectrum antiviral inhibits SARS-CoV-2 in human airway epithelial cell cultures and multiple coronaviruses in mice. *Sci Transl Med.* 2020; 12 (541): eabb5883.
9. Wahl A, Gralinski LE, Johnson CE, et al. SARS-CoV-2 infection is effectively treated and prevented by EIDD-2801. *Nature.* 2021; 591 (7850): 451–7.
10. Painter WP, Holman W, Bush JA, Almazedi F, Malik H, Eraut NC, Morin MJ, Szewczyk LJ, Painter GR. Human Safety, Tolerability, and Pharmacokinetics of Molnupiravir, a Novel Broad-Spectrum Oral Antiviral Agent with Activity Against SARS-CoV-2. *Antimicrob Agents Chemother.* 2022; 65 (5): e02428–20.
11. Imran M, Arora MK, Asdaq SM, et al. Discovery, Development, and Patent Trends on Molnupiravir: A Prospective Oral Treatment for COVID-19. *Molecules.* 2021; 26 (19): 5795.
12. Kabinger A, Stiller C, Schmitzová J, Dienemann C, Kocic G, Hillen HS, Höbartner C, Cramer P. Mechanism of molnupiravir-induced SARS-CoV-2 mutagenesis. *Nat Struct Mol Biol.* 2021; 28 (9): 740–746.
13. Mohapatra RK, Kuppli S, Suvvari TK, et al. SARS-CoV-2 and its variants of concern including Omicron: A never ending pandemic. *Chem Biol Drug Des.* 2022; 99 (5): 769–88.
14. Gushchin VA, Pochtovyi AA, Kustova DD, et al. Dynamics of SARS-CoV-2 Major Genetic Lineages in Moscow in the Context of Vaccine Prophylaxis. *Int J Mol Sci.* 2022; 23 (23): 14670.
15. Siniavin AE, Streltsova MA, Nikiforova MA, et al. Snake venom phospholipase A2s exhibit strong virucidal activity against SARS-CoV-2 and inhibit the viral spike glycoprotein interaction with ACE2. *Cell Mol Life Sci.* 2021; 78 (23): 7777–94.
16. Driouch JS, Cochin M, Lingas G, et al. Favipiravir antiviral efficacy against SARS-CoV-2 in a hamster model. *Nat Commun.* 2021; 12 (1): 1735.
17. Abdelnabi R, Foo CS, Kaptein SJ, et al. The combined treatment of Molnupiravir and Favipiravir results in a potentiation of antiviral efficacy in a SARS-CoV-2 hamster infection model. *EBioMedicine.* 2021; 72: 103595.
18. Wang M, Cao R, Zhang L, Yang X, Liu J, Xu M, Shi Z, Hu Z, Zhong W, Xiao G. Remdesivir and chloroquine effectively inhibit the recently emerged novel coronavirus (2019-nCoV) in vitro. *Cell Res.* 2020; 30 (3): 269–71.
19. Sheahan TP, Sims AC, Zhou S, et al. An orally bioavailable broad-spectrum antiviral inhibits SARS-CoV-2 in human airway epithelial cell cultures and multiple coronaviruses in mice. *Sci Transl Med.* 2020; 12 (541): eabb5883.
20. Rosenke K, Okumura A, Lewis MC, Feldmann F, Meade-White K, Bohler WF, Griffin A, Rosenke R, Shaia C, A Jarvis MA, Feldmann H. Molnupiravir inhibits SARS-CoV-2 variants including Omicron in the hamster model. *JCI Insight.* 2022; 7 (13): e160108.
21. Yuan S, Ye ZW, Liang R, et al. Pathogenicity, transmissibility, and fitness of SARS-CoV-2 Omicron in Syrian hamsters. *Science.* 2022; 377 (6604): 428–33.

Литература

1. Yousuke F, Takashi K, Takaaki N. Favipiravir (T-705), a broad-spectrum inhibitor of viral RNA polymerase. *Proc Jpn Acad Ser B Phys Biol Sci.* 2017; 93 (7): 449–63.
2. McMahon JH, Lau JS, Coldham A, et al. Favipiravir in early symptomatic COVID-19, a randomised placebo-controlled trial. *EClinicalMedicine.* 2022; 20 (54): 101703.
3. Yanagisawa K, Takara K, Suga H, et al. The Assessment of the Efficacy and Safety of Favipiravir for Patients with SARS-CoV-2 Infection: A Multicenter Non-randomized, Uncontrolled Single-arm Prospective Study. *Intern Med.* 2022; 61 (21): 3197–204.
4. Bosaeed M, Alharbi A, Mahmoud E, et al. Efficacy of favipiravir in adults with mild COVID-19: a randomized, double-blind, multicentre, placebo-controlled clinical trial. *Clin Microbiol Infect.* 2022; 28 (4): 602–8.
5. Lee CC, Hsieh CC, Ko WC. Molnupiravir-A Novel Oral Anti-SARS-CoV-2 Agent. *Antibiotics (Basel).* 2021; 10 (11): 1294.
6. Toots M, Yoon JJ, Hart M, Natchus MG, Painter GR, Plemper RK. Quantitative efficacy paradigms of the influenza clinical drug candidate EIDD-2801 in the ferret model. *Transl Res.* 2020; 218: 16–28.
7. Yoon JJ, Toots M, Lee S, et al. Orally Efficacious Broad-Spectrum Ribonucleoside Analog Inhibitor of Influenza and Respiratory Syncytial Viruses. *Antimicrob Agents Chemother.* 2018; 62 (8): e00766–18.
8. Sheahan TP, Sims AC, Zhou S, et al. An orally bioavailable broad-spectrum antiviral inhibits SARS-CoV-2 in human airway epithelial cell cultures and multiple coronaviruses in mice. *Sci Transl Med.* 2020; 12 (541): eabb5883.
9. Wahl A, Gralinski LE, Johnson CE, et al. SARS-CoV-2 infection is effectively treated and prevented by EIDD-2801. *Nature.* 2021; 591 (7850): 451–7.
10. Painter WP, Holman W, Bush JA, Almazedi F, Malik H, Eraut NC, Morin MJ, Szewczyk LJ, Painter GR. Human Safety, Tolerability, and Pharmacokinetics of Molnupiravir, a Novel Broad-Spectrum Oral Antiviral Agent with Activity Against SARS-CoV-2. *Antimicrob Agents Chemother.* 2022; 65 (5): e02428–20.
11. Imran M, Arora MK, Asdaq SM, et al. Discovery, Development, and Patent Trends on Molnupiravir: A Prospective Oral Treatment for COVID-19. *Molecules.* 2021; 26 (19): 5795.
12. Kabinger A, Stiller C, Schmitzová J, Dienemann C, Kocic G, Hillen HS, Höbartner C, Cramer P. Mechanism of molnupiravir-induced SARS-CoV-2 mutagenesis. *Nat Struct Mol Biol.* 2021; 28 (9): 740–746.
13. Mohapatra RK, Kuppli S, Suvvari TK, et al. SARS-CoV-2 and its variants of concern including Omicron: A never ending pandemic. *Chem Biol Drug Des.* 2022; 99 (5): 769–88.
14. Gushchin VA, Pochtovyi AA, Kustova DD, et al. Dynamics of SARS-CoV-2 Major Genetic Lineages in Moscow in the Context of Vaccine Prophylaxis. *Int J Mol Sci.* 2022; 23 (23): 14670.
15. Siniavin AE, Streltsova MA, Nikiforova MA, et al. Snake venom phospholipase A2s exhibit strong virucidal activity against SARS-CoV-2 and inhibit the viral spike glycoprotein interaction with ACE2. *Cell Mol Life Sci.* 2021; 78 (23): 7777–94.
16. Driouch JS, Cochin M, Lingas G, et al. Favipiravir antiviral efficacy against SARS-CoV-2 in a hamster model. *Nat Commun.* 2021; 12 (1): 1735.
17. Abdelnabi R, Foo CS, Kaptein SJ, et al. The combined treatment of Molnupiravir and Favipiravir results in a potentiation of antiviral efficacy in a SARS-CoV-2 hamster infection model. *EBioMedicine.* 2021; 72: 103595.
18. Wang M, Cao R, Zhang L, Yang X, Liu J, Xu M, Shi Z, Hu Z, Zhong W, Xiao G. Remdesivir and chloroquine effectively inhibit the recently emerged novel coronavirus (2019-nCoV) in vitro. *Cell Res.* 2020; 30 (3): 269–71.
19. Sheahan TP, Sims AC, Zhou S, et al. An orally bioavailable broad-spectrum antiviral inhibits SARS-CoV-2 in human airway epithelial cell cultures and multiple coronaviruses in mice. *Sci Transl Med.* 2020; 12 (541): eabb5883.
20. Rosenke K, Okumura A, Lewis MC, Feldmann F, Meade-White K, Bohler WF, Griffin A, Rosenke R, Shaia C, A Jarvis MA, Feldmann H. Molnupiravir inhibits SARS-CoV-2 variants including Omicron in the hamster model. *JCI Insight.* 2022; 7 (13): e160108.
21. Yuan S, Ye ZW, Liang R, et al. Pathogenicity, transmissibility, and fitness of SARS-CoV-2 Omicron in Syrian hamsters. *Science.* 2022; 377 (6604): 428–33.

AMBIENT MS PROFILING OF MENINGIOMAS: INTRAOPERATIVE ONCOMETABOLITE-BASED MONITORING

Bormotov DS¹, Shamraeva MA¹, Kuzin AA¹, Shamarina EV¹, Elifirov VA¹, Silkin SV¹, Zhdanova EV¹, Pekov SI^{2,3}✉, Popov IA¹

¹ Moscow Institute of Physics and Technology, Dolgoprudny, Russia

² Skolkovo Institute of Science and Technology, Moscow, Russia

³ Siberian State Medical University, Tomsk, Russia

The primary method of initial treatment of meningiomas is radical neurosurgical intervention. Various methods of intraoperative diagnostics currently in development aim to improve resection efficiency; we focus on methods based on molecular profiling using ambient ionization mass spectrometry. Such methods have been proven effective on various tumors, but the specifics of the molecular structure and the mechanical properties of meningiomas raise the question of applicability of protocols developed for other conditions for this particular task. The study aimed to compare the potential clinical use of three methods of ambient ionization in meningioma sample analysis: spray from tissue, inline cartridge extraction, and touch spherical sampler probe spray. To this end, lipid and metabolic profiles of meningioma tissues removed in the course of planned neurosurgical intervention have been analyzed. It is shown that in clinical practice, the lipid components of the molecular profile are best analyzed using the inline cartridge extraction method, distinguished by its ease of implementation and highest informational value. Analysis of oncometabolites with low molecular mass is optimally performed with the touch spherical sampler probe spray method, which scores high in both sensitivity and mass-spectrometric complex productivity.

Keywords: mass spectrometry, ambient ionization, electrospray ionization, meningioma, lipids, oncometabolites

Funding: The study was conducted as part of the state task of the Ministry of Science and Higher Education (agreement №075-00337-20-02, project № 0714-2020-0006), using the equipment of the N. N. Semenov Federal Research Center for Chemical Physics of the Russian Academy of Sciences.

Author contribution: Bormotov DS — experiment, data analysis, manuscript editing; Shamraeva MA — data analysis, preparation of illustrations, manuscript writing; Kuzin AA — experiment; Shamarina EV — experiment, ion source development; Elifirov VA — ion source development; Silkin SV — experiments, data analysis; Zhdanova EV — data analysis; Pekov SI — study concept, manuscript writing; Popov IA — search for sources of funding, project management, manuscript editing.

Compliance with ethical standards: the study was approved by the Ethics Committee of N. N. Burdenko National Medical Research Center of Neurosurgery (protocols №40 of 12 April 2016 and №131 of 17 July 2018) and conducted in accordance with the Declaration of Helsinki (2000 and subsequent revisions). All patients signed a voluntary informed consent form to participate in the study with use of biomaterials for research purposes.

✉ **Correspondence should be addressed:** Stanislav I. Pekov
Bolshoy Blvd., 30, стр. 1, 121205, Moscow, Russia; stanislav.pekov@forwe.ru

Received: 27.11.2022 **Accepted:** 14.12.2022 **Published online:** 30.12.2022

DOI: 10.24075/brsmu.2022.072

ПРЯМОЕ МАСС-СПЕКТРОМЕТРИЧЕСКОЕ ПРОФИЛИРОВАНИЕ МЕНИНГИОМ: ИНТРАОПЕРАЦИОННЫЙ МОНИТОРИНГ НА ОСНОВЕ ОНКОМЕТАБОЛИТОВ

Д. С. Бормотов¹, М. А. Шамраева¹, А. А. Кузин¹, Е. В. Шамарина¹, В. А. Елиферов¹, С. В. Силкин¹, Е. В. Жданова¹, С. И. Пеков^{2,3}✉, И. А. Попов¹

¹ Московский физико-технический институт, Долгопрудный, Россия

² Сколковский институт науки и технологий, Москва, Россия

³ Сибирский государственный медицинский университет, Томск, Россия

Основным методом лечения менингиом на первом этапе является нейрохирургическое вмешательство с максимальной радикальностью. Для повышения полноты резекции в настоящее время разрабатывают различные подходы интраоперационной диагностики, в частности, опирающиеся на принципы молекулярного профилирования. Основанные на масс-спектрометрии с прямой ионизацией, подобные методы демонстрируют свою эффективность на различных видах опухолей, однако особенности молекулярного строения и механические характеристики менингиом не позволяют напрямую транслировать протоколы, разработанные для других нозологий. Целью работы было провести сравнение возможностей применения трех методов прямой ионизации для исследования образцов менингиом: метода прямого спрея с ткани, метод картриджной экстракции и метода ионизации с поверхности сферического пробоотборника. Для этого анализировали липидный и метаболический профиль тканей менингиом, иссеченных в ходе планового нейрохирургического вмешательства. Было показано, что для анализа липидных компонент молекулярного профиля оптимальным для клинического применения оказывается метод картриджной экстракции, отличающийся наиболее простой реализацией и максимальной информативностью. Для анализа онкометаболитов с малой молекулярной массой лучшим выбором является метод ионизации с поверхности сферического пробоотборника, обеспечивающий высокую чувствительность и наилучшую производительность масс-спектрометрического комплекса.

Ключевые слова: масс-спектрометрия, прямая ионизация, электрораспылительная ионизация, менингиома, липиды, онкометаболиты

Финансирование: работа выполнена в рамках государственного задания Министерства науки и высшего образования (соглашение № 075-00337-20-02, проект № 0714-2020-0006), с использованием оборудования ЦКП ФИЦ ХФ им. Н. Н. Семенова РАН.

Вклад авторов: Д. С. Бормотов — проведение эксперимента, анализ данных, редактирование статьи; М. А. Шамраева — анализ данных, подготовка иллюстраций, написание статьи; А. А. Кузин — проведение эксперимента; Е. В. Шамарина — проведение эксперимента, разработка ионных источников; В. А. Елиферов — разработка ионных источников; С. В. Силкин — проведение экспериментов, анализ данных; Е. В. Жданова — анализ данных; С. И. Пеков — концепция, написание статьи; И. А. Попов — поиск источников финансирования, руководство, редактирование статьи.

Соблюдение этических стандартов: исследование одобрено этическим комитетом НМИЦН имени Н. Н. Бурденко (протоколы № 40 от 12 апреля 2016 г. и № 131 от 17 июля 2018 г.), проведено в соответствии с принципами Хельсинкской декларации (2000 г.) и ее последующих пересмотров. Все пациенты подписали добровольное информированное согласие на участие в исследовании и использование биоматериалов в исследовательских целях.

✉ **Для корреспонденции:** Станислав Игоревич Пеков
Большой бульвар, д. 30, стр. 1, Москва, 121205, Россия; stanislav.pekov@forwe.ru

Статья получена: 27.11.2022 **Статья принята к печати:** 14.12.2022 **Опубликована онлайн:** 30.12.2022

DOI: 10.24075/vrgmu.2022.072

Of all the meningeal tumors of the central nervous system (CNS), meningiomas are the most clinically significant. These brain tumors commonly occur in adults and account for over 36% of the total number of newly diagnosed CNS tumors [1, 2]. They are predominantly discovered by chance, i. e. the disease develops asymptotically at the initial stage, but clinical symptoms can be observed in 15% of cases. Incidence of meningiomas increases with age; in addition, they are unusually common in females of reproductive age (~3 : 1 female predominance in this age group) [3]. This may be due to the peculiarities of the hormonal profile of women. Clinical symptoms are highly variable and depend on the location of the tumor. As with other intracranial tumors, meningiomas may present with manifestations of intracranial hypertension in the form of headache, nausea, vomiting, and reduced visual acuity [4].

Treatment of symptomatic meningioma begins with radical microsurgical or endoscopic removal of afflicted tissue [5, 6]. Although many brain tumor visualization methods have been developed in recent time, tumor delimitation is not performed in real time in most clinical cases. MRI methods, applied primarily prior to the operation, are presently employed in both diagnosis and operation navigation. As of other clinically relevant methods, use of fluorescent molecular imaging [7] is limited mainly by the specificity and sensitivity of the study being performed, and intraoperative ultrasound is not applicable if tumor density is close to that of intact tissue. Histopathological methods are the gold standard in tumor assessment and provide diagnostic information during surgery within half an hour, but they are usually limited to one segregated sample (or a small number thereof) from each operation and are not used to delimit tumors.

Various intraoperative diagnostic methods currently in development aim to increase the efficiency of surgical intervention [8, 9], enabling control over composition of the excised tissue; some methods are based on molecular profiling [10–13]. For example, gangliosides are used to differentiate astrocytoma [14]. Lipid profiles, oncometabolites, and specific neurometabolites such as n-acetylaspartate (NAA) are also used to delimit tumors [15, 16].

Ambient MS allows to analyze excised tissues almost in real time. The registered molecular profiles contain information both on the metabolic profile of tissues and on the change in the ratio of various lipids, which makes it possible to facilitate automatic classification by presence and proportion of malignant cells in the test sample [17, 18]. Thus, using rapid extraction of lipids and metabolites from tissue [13, 17, 19] or touch spray ionization [15, 20, 21], methods have been developed to differentiate various tumors from intact tissue. However, choice of a direct ionization method that is optimal for further development of methods for intraoperative meningioma monitoring is non-trivial due to the specifics of the molecular structure of meningeal tumors. The aim of this work was to compare three methods of mass spectrometric profiling and determine their applicability for solving the problems of differentiating afflicted and intact tissue in patients with meningioma.

METHODS

Histologically annotated and anonymized samples of meningiomas were provided by the N. N. Burdenko National Medical Research Center of Neurosurgery. All samples were obtained as part of planned operations for resection of pathological brain tissue.

Three methods of molecular profiling have been applied to the samples: spray from tissue (SFT) [22, 23], inline cartridge extraction (ICE) [17], and touch spherical sampler probe spray (SSP) [21].

To analyze meningioma samples using SFT [22, 23], a sample about 2 mm in size is placed on the tip of a disposable injection needle located at a distance of 10 mm from the vacuum interface of the mass spectrometer (Fig. 1).

The solvent is fed through a fused silica capillary with a flow rate of 3 $\mu\text{l}/\text{min}$ directly onto the surface of the sample to extract lipids and metabolites. The molecules are ionized immediately after extraction by a voltage of up to 4–6 kV applied to the injection needle (selected empirically based on the geometric parameters of the sample), which ensures the formation of a Taylor cone and electrospray at the end of the needle.

To implement ICE [17], a disposable cartridge with a sample is inserted into the solvent supply line using common HPLC fittings for supplying solutions (Fig. 2).

The cartridge is a stainless steel tube with an internal diameter of 1.8 mm. A sample sized approximately 1 mm^2 is placed in the cartridge. The molecules from the sample are extracted by the solvent flowing through the solvent supply line at 2 $\mu\text{l}/\text{min}$. To connect to the line, two short sections of PEEK (polyether ether ketone) capillary are inserted into the tube and crimped to prevent leaks. The glass fiber filter in the cartridge prevents macroscopic parts of the sample from entering the line and blocking it. A standard commercially available electrospray ion source is installed at the end of the line after the cartridge. The voltage on the ion source is 3 kV in the positive-ion mode and 4 kV in the negative-ion mode.

SSP [21] uses fibrous samplers of spherical shape followed by electrospray ionization directly from their surface. A sampler is a rod of cleaned and pressed polymer fibers (specifically polyethylene terephthalate) 10 mm long, 2 mm in diameter. A sample is taken through a swab touch using the aforementioned porous sampler. The sampler is then fixed in a special ion source, where the solvent (80 μl) and high voltage (5 kV) are supplied for electrospraying.

To compare the effectiveness of the various direct ionization methods, we analyzed three meningioma samples obtained from three patients. Each meningioma sample was divided into three parts and analyzed by each of the proposed methods. The results of the study were validated on samples of meningiomas obtained from three different patients. The experiments were performed using an LTQ XL Orbitrap ETD hybrid mass spectrometer (ThermoFisher; USA) in full scan mode with m/z 100–2000. Mass spectra were obtained using both low resolution mass analyzers (LTQ XL ion trap in "normal" scan mode) and high resolution mass analyzers (Orbitrap with 30,000 FWHM resolution at $m/z = 400$). The temperature of the heating capillary at the entrance to the mass spectrometer was 220°C. The extraction solvent consisted of methanol (MeOH, > 99.9% HPLC; Merck KgaA; Germany), isopropanol (i-PrOH, > 99.9% HPLC; Merck KGaA, Germany), acetonitrile (ACN, > 99.9% HPLC; Merck KgaA, Germany), and deionized water (H_2O , $\rho \geq 17 \text{ M}\Omega \times \text{cm}$) in a ratio of 3 : 3 : 3 : 1 (vol.), with the addition of 0.1% (vol.) acetic acid (CH_3COOH , >99%; Merck KgaA, Germany), which is optimal for extraction of lipid molecules and metabolites from soft fabrics, as well as suitable for use in electrospray ionization sources.

The most intense peaks were additionally annotated with exact mass readings using the LipiDex software [24], and with isotopic distribution using the Xcalibur™ software (Thermo Scientific-Jose; USA).

RESULTS

For all three methods (SFT (Fig. 3), ICE (Fig. 4A) and SSP (Fig. 4B)), the high-resolution mass spectra in the positive-ion mode are

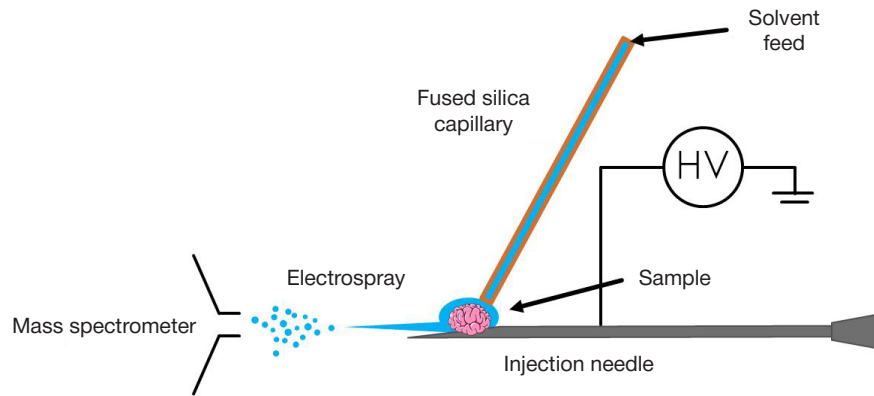


Fig. 1. SFT installation diagram

characterized by similar composition and relative intensity of the spectra of ions associated with lipids ($600 < m/z < 900$). Positive ions are registered in the form of protonated ions or ions cationized with sodium or potassium. The ICE and SSP spectra showed an additional intense group of peaks ($1450 < m/z < 1650$), where two groups of peaks (one characteristic of cardiolipins, the other for membrane lipid dimers) superposed. While the SFT and ICE spectra exhibit close signal-to-noise ratios, the same indicator is two to four times lower for SSP spectra, complicating discovery and analysis of low-intensity peaks.

Low resolution in the positive-ion mode yields similar spectra. SFT spectra additionally revealed an approximately 2.5 times higher intensity of lipid peaks (Fig. 5A), and, accordingly, a lower relative (but not absolute) intensity of peaks in m/z 100–400 in comparison with the ICE spectra (Fig. 5B). SSP spectra showed a reduced intensity in the region of the spectrum characteristic of lipids, but an increased intensity and diversity of peaks in low masses, where metabolites were recorded (Fig. 5C).

Characteristic lipid peaks were detected in all high-resolution spectra in the negative-ion mode (Figs. 6 and 7). The signal intensities of molecules of different classes vary between the three methods to a much lesser extent than in the positive-ion mode. However, only two methods of direct ionization (ICE and SSP) registered ions corresponding to the NAA neurometabolite, characteristic of intact nervous tissue [25, 26], in the spectra. The presence of this metabolite indicates that the studied samples were taken from the border of the

tumor. The low-resolution spectra in the negative-ion mode are similar to each other in terms of the lipid ions (the results are completely identical to the corresponding high-resolution mass spectra and are not presented here). However, NAA could not be identified in any of the spectra obtained in this mode.

DISCUSSION

Rapid tissue analysis using ambient mass spectrometry is currently in consideration as a tool for molecular diagnosis of CNS tumors. While the idea of embedding molecular profiling methods in a surgical instrument [11, 19] is indeed attractive, its implementation is associated with disadvantages similar to those of intraoperative tomography. The need to equip each operating room with an expensive mass spectrometer, in addition to the complexity of certification of such complexes, makes it difficult to introduce them into clinical practice. At the same time, offline analysis methods [13, 17], in which a tissue sample is taken *in vivo* during resection and then analyzed *ex vivo* in a pathological laboratory, can be easily integrated into routine practice, which provides quick feedback to the surgeon and enables precise tumor excision. When integrated as a standard practice in rapid histological examination of clinical images, molecular profiling provides information on excised tissue within minutes, where the primary rate-limiting factor is the time required for transit of the sample between the operating room and the laboratory.

Each of the presented methods of ambient ionization of tumor tissues has a set of characteristic features. SFT

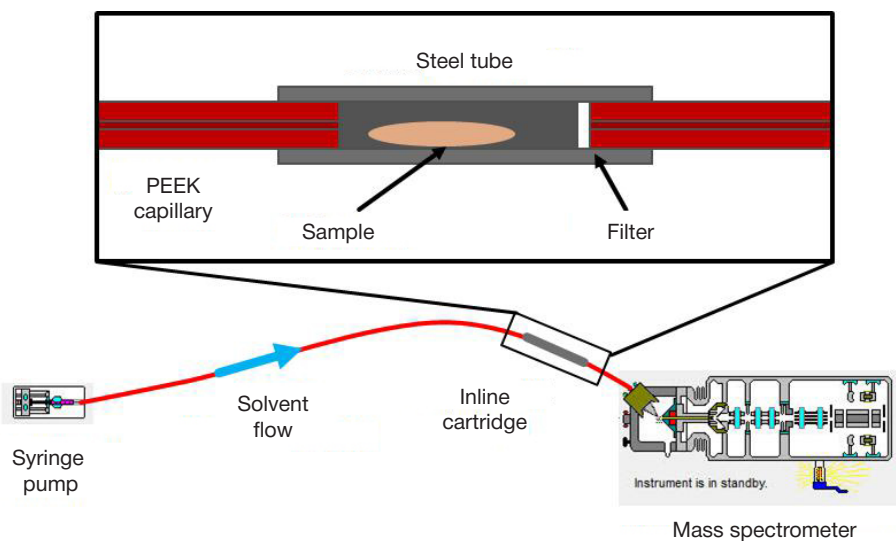


Fig. 2. ICE installation diagram

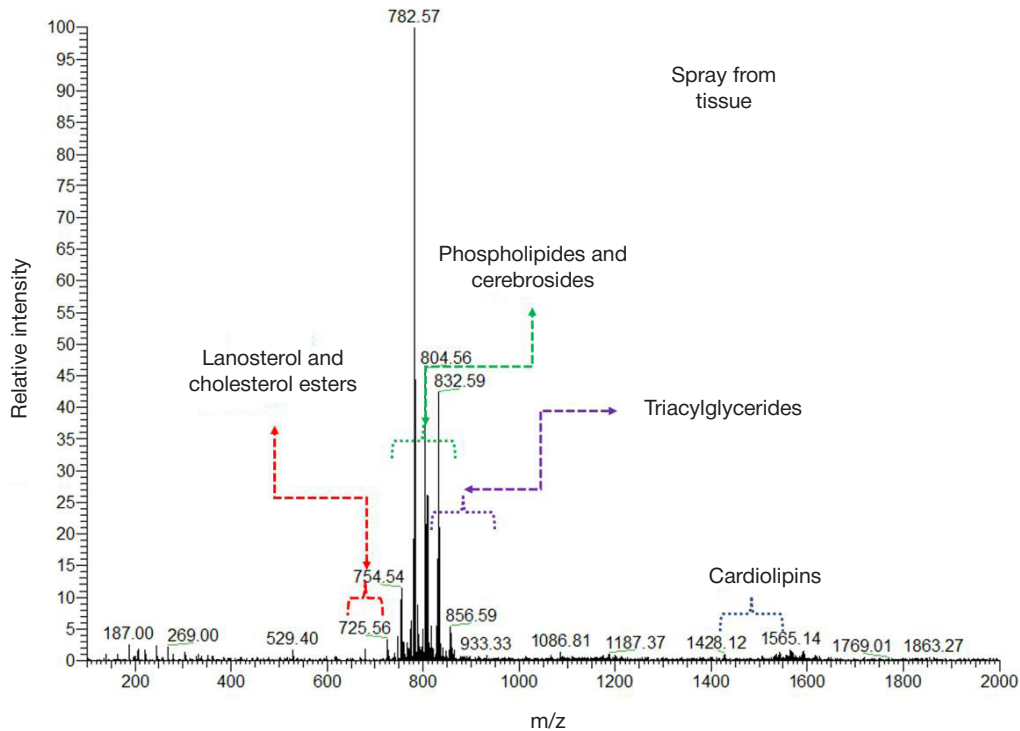


Fig. 3. Positive-ion high-resolution mass spectra of meningioma samples: SFT

completely eliminates the possibility of cross-contamination (i.e., the presence of residual molecules of the previous sample in the analysis of the current one, and their effect on the mass spectrum), since the only elements of the ion source that come into contact with the analyzed image completely disposable. However, the stability of ionization, which is important for obtaining reliable and repeatable test results, depends on the shape of the analyzed tissue sample. Since meningeal brain tumors generally have low mechanical rigidity and high plasticity, it is difficult to control the shape and size of the sample; therefore, additional adjustment of the voltage in the ion source is required for each sample, which reduces efficiency and requires additional staff qualifications.

ICE enables a highly stable ionization process due to the use of a standard mass spectrometer electrospray source. Ion sources of this type are widespread and are used to analyze various biological molecules, including those used in medical diagnostics. However, the need to flush the ion source between samples reduces performance of the method, since insufficient

cleaning of the ion source can lead to cross-contamination between samples and, consequently, erroneous identification of oncometabolites in the test sample.

SSP, which employs disposable samplers, eliminates the problem of sample cross-contamination, which is characteristic of ICE, and simplifies the analysis process in comparison with SFT. The spherical shape of the rigid samplers ensures the geometry of the ion source is constant and simplifies the sampling process, which consists only of touching the sample with the tip of the sampler. The inertness of the materials from which the sampler is made also makes it possible to use it for sampling directly in the operating room, if appropriate certification is carried out. Despite these advantages, SSP is less efficient for the analysis of the lipid component of the molecular profile in the positive-ion mode. Importantly, this includes phosphatidylcholines and other components of cell membranes, which change significantly in the process of malignancy. However, in the negative-ion mode in the spectrum of the lipid component, phosphatidylserines in particular are

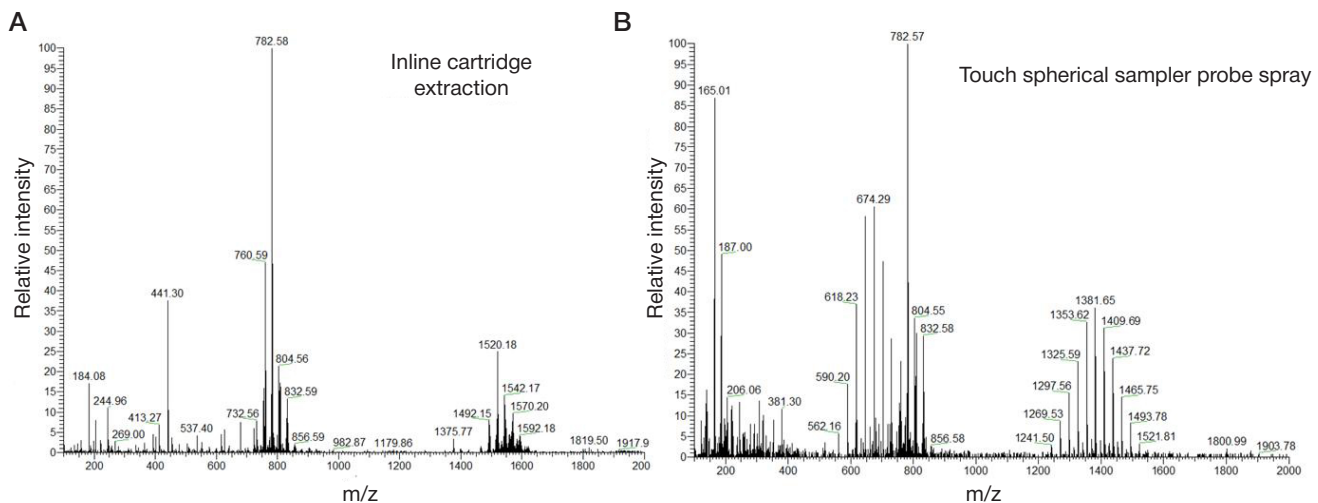


Fig. 4. Positive-ion high-resolution mass spectra of meningioma samples: ICE (A) and SSP (B)

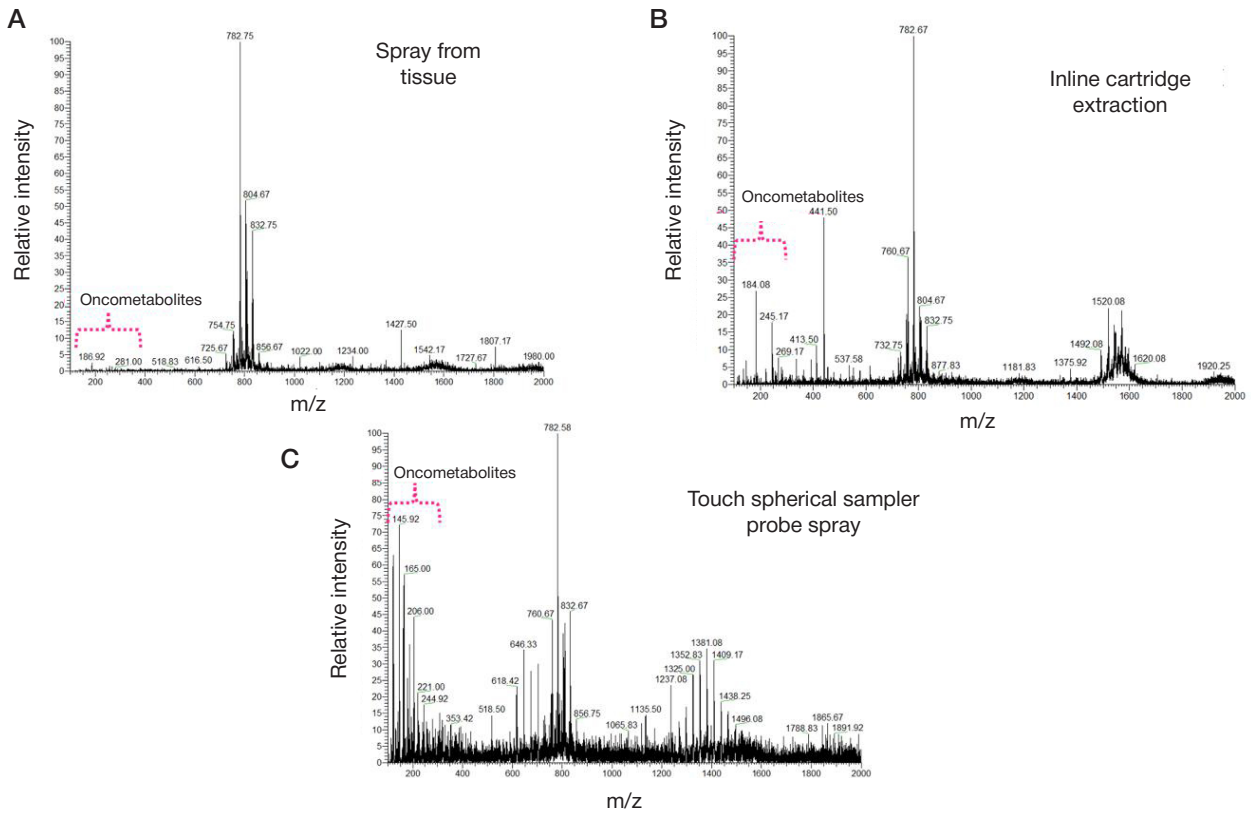


Fig. 5. Positive-ion low-resolution mass spectra of meningioma samples: SFT (A), ICE (B), and SSP (C)

observed, which make up a significant proportion of lipids in the cell membranes of intact brain tissue, which makes it possible to use SSP to differentiate tumor and intact tissue using molecular profiling data.

In contrast to the lipid component, the efficiency of ionization of low-mass metabolites ionized in the m/z range 100–400 turned out to be comparable for all ionization methods. However, the metabolic profile obtained using SFT

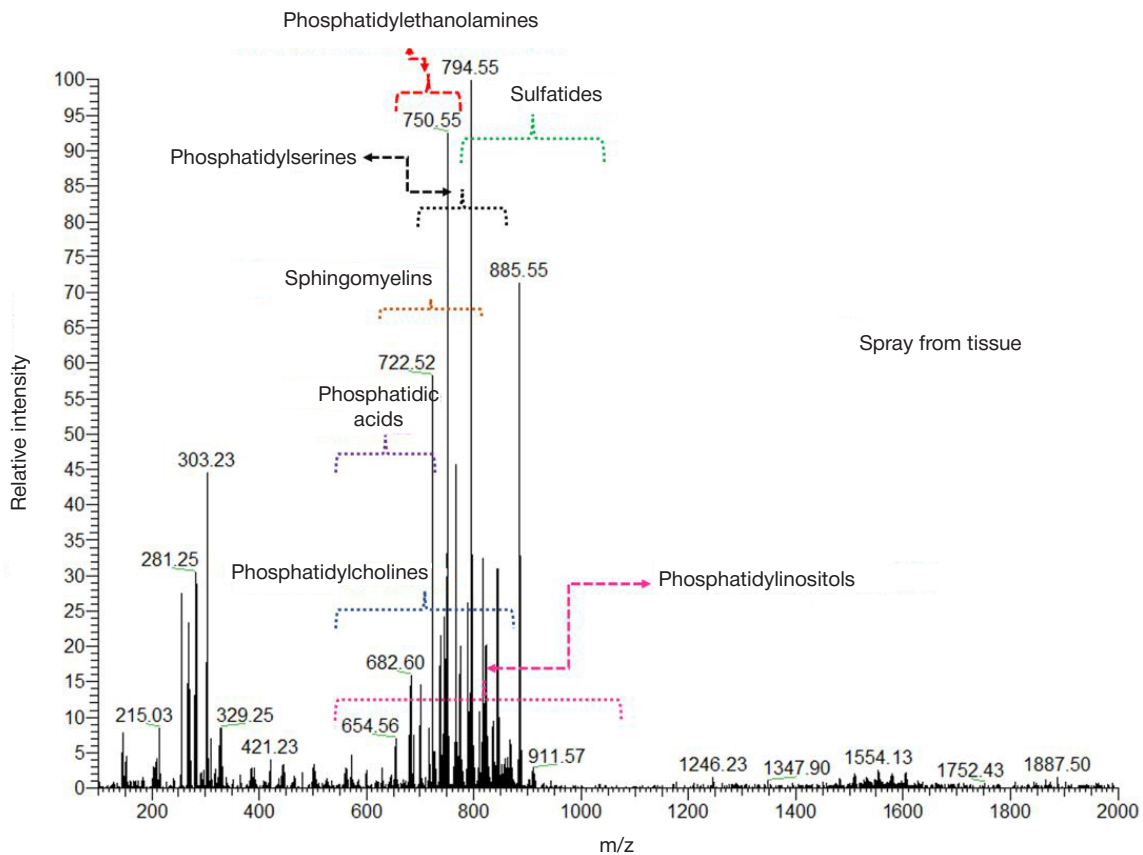


Fig. 6. Negative-ion high-resolution mass spectra of meningioma samples: SFT

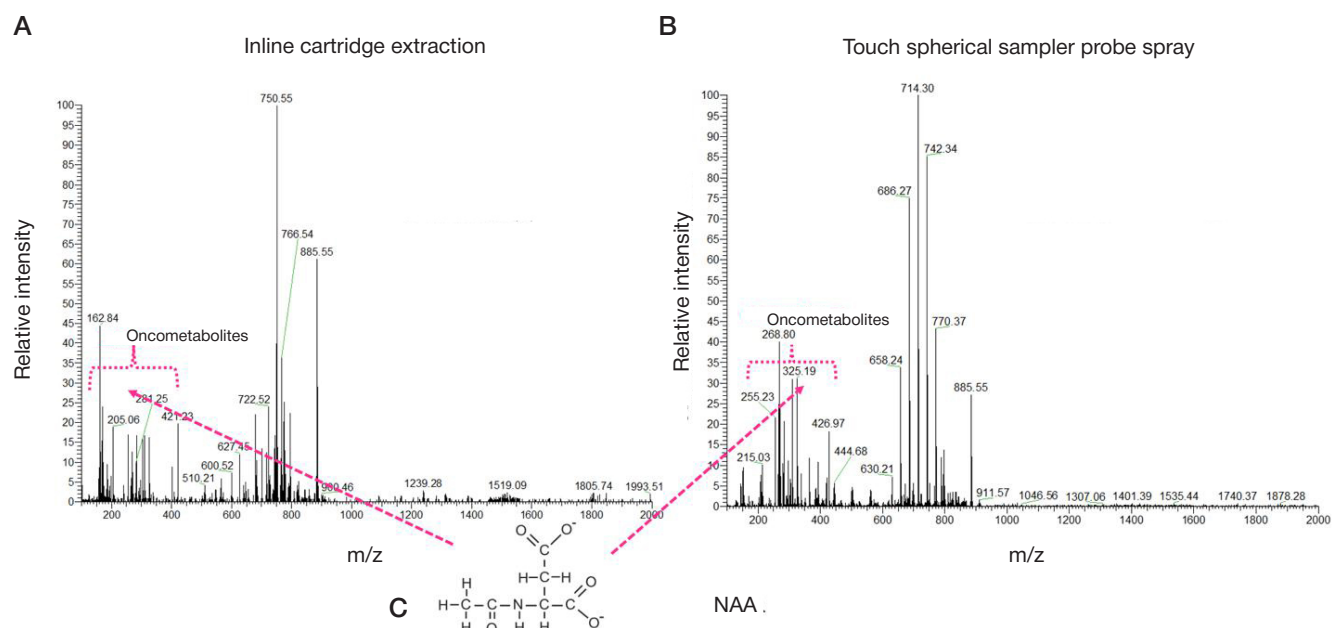


Fig. 7. Negative-ion high-resolution mass spectra of meningioma samples: ICE (A) and SSP (B). C. Structural formula of the neurometabolite NAA

was less diverse, as it showed less mass-spectrometric peaks. Significantly, none of the experiments using this method detected NAA, which was registered when these samples were simultaneously examined using other ionization methods. This result is likely associated with lower efficiency of extraction of water-soluble metabolites from a whole tissue sample by washing the sample with a solvent during ionization compared to a more complete cartridge-aided extraction, or to efficient transfer of moderately hydrophobic analytes to the surface of a fibrous sampler.

SSP in the negative-ion mode, in turn, appears promising for express surgical evaluation of the tumor resection margin. Due to the relatively high ion intensity in this range, it seems possible to detect an oncometabolite, in particular NAA, and provide an assessment of tumor infiltration, which is of paramount importance when trying to maximize glioma resection (a favorable prognostic factor for patients with glioma).

CONCLUSIONS

The use of various ambient ionization methods for studying CNS meningeal tumor samples makes it possible to obtain a molecular profile sufficiently intense to be suitable for differentiating tumor tissues from intact ones, as was previously demonstrated for glial tumors. Spray from tissue is a highly productive method of obtaining spectra of the lipid component of tissues. Inline cartridge extraction is the simplest to implement, but has the lowest analysis productivity. Touch spherical sampler probe spray has limited application in analysis of the lipid fraction, but it is suitable for detection of onco- and neurometabolites, and is likewise easy to implement. The choice of an ionization method for clinical use thus directly depends on the requirements for ease of implementation and analysis performance imposed on the laboratory, and on the set of classes of biological molecules, lipids or water-soluble metabolites that best characterize a particular condition, accounting for its degree of malignancy.

References

- Islim AI, Mohan M, Moon RDC, Srikandarajah N, Mills SJ, Brodbelt AR, et al. Incidental intracranial meningiomas: a systematic review and meta-analysis of prognostic factors and outcomes. *J Neurooncol.* 2019; 142: 211–21. Available from: <https://doi.org/10.1007/s11060-019-03104-3>.
- Ostrom QT, Patil N, Cioffi G, Waite K, Kruchko C, Barnholtz-Sloan JS. CBTRUS Statistical Report: Primary Brain and Other Central Nervous System Tumors Diagnosed in the United States in 2013–2017. *Neuro Oncol.* 2020; 22: iv1–96. Available from: <https://doi.org/10.1093/neuonc/noaa200>.
- Buerki RA, Horbinski CM, Kruser T, Horowitz PM, James CD, Lukas R v. An overview of meningiomas. *Future Oncology.* 2018; 14: 2161–77. Available from: <https://doi.org/10.2217/fon-2018-0006>.
- Ogasawara C, Philbrick BD, Adamson DC. Meningioma: A Review of Epidemiology, Pathology, Diagnosis, Treatment, and Future Directions. *Biomedicines.* 2021; 9: 319. Available from: <https://doi.org/10.3390/biomedicines9030319>.
- Nguyen PX, Thi-Ngoc Doan H, van Vu H. Neuronavigation in falcine meningiomas are surgery: Initial results from a Vietnamese multicenter study. *Annals of Medicine and Surgery.* 2022: 104905. Available from: <https://doi.org/10.1016/j.amsu.2022.104905>.
- Bir SC, Konar SK, Maiti TK, Thakur JD, Guthikonda B, Nanda A. Utility of Neuronavigation in Intracranial Meningioma Resection: A Single-Center Retrospective Study. *World Neurosurg.* 2016; 90: 546–555.e1. Available from: <https://doi.org/10.1016/j.wneu.2015.12.101>.
- Stummer W, Koch R, Valle RD, Roberts DW, Sanai N, Kalkanis S, et al. Intraoperative fluorescence diagnosis in the brain: a systematic review and suggestions for future standards on reporting diagnostic accuracy and clinical utility. *Acta Neurochir (Wien).* 2019; 161: 2083–98. Available from: <https://doi.org/10.1007/s00701-019-04007-y>.
- Iifa DR, Eberlin LS. Ambient ionization mass spectrometry for cancer diagnosis and surgical margin evaluation. *Clin Chem.* 2016; 62: 111–23. Available from: <https://doi.org/10.1373/clinchem.2014.237172>.
- Kiritani S, Yoshimura K, Arita J, Kokudo T, Hakoda H, Tanimoto M, et al. A new rapid diagnostic system with ambient mass spectrometry and machine learning for colorectal liver metastasis. *BMC Cancer.*

- 2021; 21: 262. Available from: <https://doi.org/10.1186/s12885-021-08001-5>.
10. Huang Y-C, Chung H-H, Dutkiewicz EP, Chen C-L, Hsieh H-Y, Chen B-R, et al. Predicting Breast Cancer by Paper Spray Ion Mobility Spectrometry Mass Spectrometry and Machine Learning. *Anal Chem.* 2020; 92: 1653–7. Available from: <https://doi.org/10.1021/acs.analchem.9b03966>.
 11. Phelps DL, Balog J, Gildea LF, Bodai Z, Savage A, El-Bahrawy MA, et al. The surgical intelligent knife distinguishes normal, borderline and malignant gynaecological tissues using rapid evaporative ionization mass spectrometry (REIMS). *Br J Cancer.* 2018; 118: 1349–58. Available from: <https://doi.org/10.1038/s41416-018-0048-3>.
 12. Ogrinc N, Attencourt C, Colin E, Boudahi A, Tebbakha R, Salzet M, et al. Mass Spectrometry-Based Differentiation of Oral Tongue Squamous Cell Carcinoma and Nontumor Regions With the SpiderMass Technology. *Frontiers in Oral Health.* 2022; 3. Available from: <https://doi.org/10.3389/froh.2022.827360>.
 13. Pekov SI, Bormotov DS, Nikitin PV, Sorokin AA, Shurkhay VA, Eliferov VA, et al. Rapid estimation of tumor cell percentage in brain tissue biopsy samples using inline cartridge extraction mass spectrometry. *Anal Bioanal Chem.* 2021; 413: 2913–22. Available from: <https://doi.org/10.1007/s00216-021-03220-y>.
 14. Eberlin LS, Dill AL, Golby AJ, Ligon KL, Wiseman JM, Cooks RG, et al. Discrimination of human astrocytoma subtypes by lipid analysis using desorption electrospray ionization imaging mass spectrometry. *Angewandte Chemie — International Edition.* 2010; 49: 5953–6. Available from: <https://doi.org/10.1002/anie.201001452>.
 15. Pirro V, Llor RS, Jarmusch AK, Alfaro CM, Cohen-Gadol AA, Hattab EM, et al. Analysis of human gliomas by swab touch spray-mass spectrometry: Applications to intraoperative assessment of surgical margins and presence of oncometabolites. *Analyst.* 2017; 142: 4058–66. Available from: <https://doi.org/10.1039/c7an01334e>.
 16. Jarmusch AK, Pirro V, Baird Z, Hattab EM, Cohen-Gadol AA, Cooks RG. Lipid and metabolite profiles of human brain tumors by desorption electrospray ionization-MS. *Proceedings of the National Academy of Sciences.* 2016; 113: 1486–91. Available from: <https://doi.org/10.1073/pnas.1523306113>.
 17. Pekov SI, Eliferov VA, Sorokin AA, Shurkhay VA, Zhvansky ES, Vorobyev AS, et al. Inline cartridge extraction for rapid brain tumor tissue identification by molecular profiling. *Sci Rep.* 2019; 9: 18960. Available from: <https://doi.org/10.1038/s41598-019-55597-7>.
 18. Pirro V, Jarmusch AK, Alfaro CM, Hattab EM, Cohen-Gadol AA, Cooks RG. Utility of neurological smears for intrasurgical brain cancer diagnostics and tumour cell percentage by DESI-MS. *Analyst.* 2017; 142: 449–54. Available from: <https://doi.org/10.1039/c6an02645a>.
 19. Keating MF, Zhang J, Feider CL, Retaileau S, Reid R, Antaris A, et al. Integrating the MasSpec Pen to the da Vinci Surgical System for in Vivo Tissue Analysis during a Robotic Assisted Porcine Surgery. *Anal Chem.* 2020; 92: 11535–42. Available from: <https://doi.org/10.1021/acs.analchem.0c02037>.
 20. Shamraeva MA, Pekov SI, Bormotov DS, Levin RE, Larina IM, Nikolaev EN, et al. The lightweight spherical samplers for simplified collection, storage, and ambient ionization of drugs from saliva and blood. *Acta Astronaut.* 2022; 195: 556–60. Available from: <https://doi.org/10.1016/j.actastro.2022.03.026>.
 21. Shamraeva MA, Bormotov DS, Shamarina EV, Bocharov KV, Peregudova OV, Pekov SI, et al. Spherical Sampler Probes Enhance the Robustness of Ambient Ionization Mass Spectrometry for Rapid Drugs Screening. *Molecules.* 2022; 27: 945. Available from: <https://doi.org/10.3390/molecules27030945>.
 22. Chagovets V, Wang Z, Kononikhin A, Starodubtseva N, Borisova A, Salimova D, et al. A Comparison of Tissue Spray and Lipid Extract Direct Injection Electrospray Ionization Mass Spectrometry for the Differentiation of Eutopic and Ectopic Endometrial Tissues. *J Am Soc Mass Spectrom.* 2017; 6–8. Available from: <https://doi.org/10.1007/s13361-017-1792-y>.
 23. Adamyan L, Starodubtseva N, Borisova A, Stepanian A, Chagovets V, Salimova D, et al. Direct Mass Spectrometry Differentiation of Ectopic and Eutopic Endometrium in Patients with Endometriosis. *J Minim Invasive Gynecol.* 2017. Available from: <https://doi.org/10.1016/j.jmig.2017.08.658>.
 24. Hutchins PD, Russell JD, Coon JJ. LipiDex: An Integrated Software Package for High-Confidence Lipid Identification. *Cell Syst.* 2018; 6: 621–5.e5. Available from: <https://doi.org/10.1016/j.cels.2018.03.011>.
 25. Bogner-Strauss JG. N-acetylaspartate metabolism outside the brain: Lipogenesis, histone acetylation, and cancer. *Front Endocrinol (Lausanne).* 2017; 8: 1–5. Available from: <https://doi.org/10.3389/fendo.2017.00240>.
 26. Pirro V, Alfaro CM, Jarmusch AK, Hattab EM, Cohen-Gadol AA, Cooks RG. Intraoperative assessment of tumor margins during glioma resection by desorption electrospray ionization-mass spectrometry. *Proceedings of the National Academy of Sciences.* 2017; 114: 201706459. Available from: <https://doi.org/10.1073/pnas.1706459114>.

Литература

1. Islim AI, Mohan M, Moon RDC, Srikantharajah N, Mills SJ, Brodbelt AR, et al. Incidental intracranial meningiomas: a systematic review and meta-analysis of prognostic factors and outcomes. *J Neurooncol.* 2019; 142: 211–21. Available from: <https://doi.org/10.1007/s11060-019-03104-3>.
2. Ostrom QT, Patil N, Cioffi G, Waite K, Kruchko C, Barnholtz-Sloan JS. CBTRUS Statistical Report: Primary Brain and Other Central Nervous System Tumors Diagnosed in the United States in 2013–2017. *Neuro Oncol.* 2020; 22: iv1–96. Available from: <https://doi.org/10.1093/neuonc/noaa200>.
3. Buerki RA, Horbinski CM, Kruser T, Horowitz PM, James CD, Lukas R v. An overview of meningiomas. *Future Oncology.* 2018; 14: 2161–77. Available from: <https://doi.org/10.2217/fo-2018-0006>.
4. Ogasawara C, Philbrick BD, Adamson DC. Meningioma: A Review of Epidemiology, Pathology, Diagnosis, Treatment, and Future Directions. *Biomedicines.* 2021; 9: 319. Available from: <https://doi.org/10.3390/biomedicines9030319>.
5. Nguyen PX, Thi-Ngoc Doan H, van Vu H. Neuronavigation in falxine meningiomasare surgery: Initial results from a Vietnamese multi-center study. *Annals of Medicine and Surgery.* 2022: 104905. Available from: <https://doi.org/10.1016/j.amsu.2022.104905>.
6. Bir SC, Konar SK, Maiti TK, Thakur JD, Guthikonda B, Nanda A. Utility of Neuronavigation in Intracranial Meningioma Resection: A Single-Center Retrospective Study. *World Neurosurg.* 2016; 90: 546–555.e1. Available from: <https://doi.org/10.1016/j.wneu.2015.12.101>.
7. Stummer W, Koch R, Valle RD, Roberts DW, Sanai N, Kalkanis S, et al. Intraoperative fluorescence diagnosis in the brain: a systematic review and suggestions for future standards on reporting diagnostic accuracy and clinical utility. *Acta Neurochir (Wien).* 2019; 161: 2083–98. Available from: <https://doi.org/10.1007/s00701-019-04007-y>.
8. Ila DR, Eberlin LS. Ambient ionization mass spectrometry for cancer diagnosis and surgical margin evaluation. *Clin Chem.* 2016; 62: 111–23. Available from: <https://doi.org/10.1373/clinchem.2014.237172>.
9. Kiritani S, Yoshimura K, Arita J, Kokudo T, Hakoda H, Tanimoto M, et al. A new rapid diagnostic system with ambient mass spectrometry and machine learning for colorectal liver metastasis. *BMC Cancer.* 2021; 21: 262. Available from: <https://doi.org/10.1186/s12885-021-08001-5>.
10. Huang Y-C, Chung H-H, Dutkiewicz EP, Chen C-L, Hsieh H-Y, Chen B-R, et al. Predicting Breast Cancer by Paper Spray Ion Mobility Spectrometry Mass Spectrometry and Machine Learning. *Anal Chem.* 2020; 92: 1653–7. Available from: <https://doi.org/10.1021/acs.analchem.9b03966>.
11. Phelps DL, Balog J, Gildea LF, Bodai Z, Savage A, El-Bahrawy MA,

- et al. The surgical intelligent knife distinguishes normal, borderline and malignant gynaecological tissues using rapid evaporative ionisation mass spectrometry (REIMS). *Br J Cancer*. 2018; 118: 1349–58. Available from: <https://doi.org/10.1038/s41416-018-0048-3>.
12. Ogrinc N, Attencourt C, Colin E, Boudahi A, Tebbakha R, Salzet M, et al. Mass Spectrometry-Based Differentiation of Oral Tongue Squamous Cell Carcinoma and Nontumor Regions With the SpiderMass Technology. *Frontiers in Oral Health*. 2022; 3. Available from: <https://doi.org/10.3389/froh.2022.827360>.
 13. Pekov SI, Bormotov DS, Nikitin PV, Sorokin AA, Shurkhay VA, Eliferov VA, et al. Rapid estimation of tumor cell percentage in brain tissue biopsy samples using inline cartridge extraction mass spectrometry. *Anal Bioanal Chem*. 2021; 413: 2913–22. Available from: <https://doi.org/10.1007/s00216-021-03220-y>.
 14. Eberlin LS, Dill AL, Golby AJ, Ligon KL, Wiseman JM, Cooks RG, et al. Discrimination of human astrocytoma subtypes by lipid analysis using desorption electrospray ionization imaging mass spectrometry. *Angewandte Chemie — International Edition*. 2010; 49: 5953–6. Available from: <https://doi.org/10.1002/anie.201001452>.
 15. Pirro V, Llor RS, Jarmusch AK, Alfaro CM, Cohen-Gadol AA, Hattab EM, et al. Analysis of human gliomas by swab touch spray-mass spectrometry: Applications to intraoperative assessment of surgical margins and presence of oncometabolites. *Analyst*. 2017; 142: 4058–66. Available from: <https://doi.org/10.1039/c7an01334e>.
 16. Jarmusch AK, Pirro V, Baird Z, Hattab EM, Cohen-Gadol AA, Cooks RG. Lipid and metabolite profiles of human brain tumors by desorption electrospray ionization-MS. *Proceedings of the National Academy of Sciences*. 2016; 113: 1486–91. Available from: <https://doi.org/10.1073/pnas.1523306113>.
 17. Pekov SI, Eliferov VA, Sorokin AA, Shurkhay VA, Zhvansky ES, Vorobyev AS, et al. Inline cartridge extraction for rapid brain tumor tissue identification by molecular profiling. *Sci Rep*. 2019; 9: 18960. Available from: <https://doi.org/10.1038/s41598-019-55597-7>.
 18. Pirro V, Jarmusch AK, Alfaro CM, Hattab EM, Cohen-Gadol AA, Cooks RG. Utility of neurological smears for intrasurgical brain cancer diagnostics and tumour cell percentage by DESI-MS. *Analyst*. 2017; 142: 449–54. Available from: <https://doi.org/10.1039/c6an02645a>.
 19. Keating MF, Zhang J, Feider CL, Retailleau S, Reid R, Antaris A, et al. Integrating the MasSpec Pen to the da Vinci Surgical System for in Vivo Tissue Analysis during a Robotic Assisted Porcine Surgery. *Anal Chem*. 2020; 92: 11535–42. Available from: <https://doi.org/10.1021/acs.analchem.0c02037>.
 20. Shamraeva MA, Pekov SI, Bormotov DS, Levin RE, Larina IM, Nikolaev EN, et al. The lightweight spherical samplers for simplified collection, storage, and ambient ionization of drugs from saliva and blood. *Acta Astronaut*. 2022; 195: 556–60. Available from: <https://doi.org/10.1016/j.actaastro.2022.03.026>.
 21. Shamraeva MA, Bormotov DS, Shamarina EV, Bocharov KV, Peregudova OV, Pekov SI, et al. Spherical Sampler Probes Enhance the Robustness of Ambient Ionization Mass Spectrometry for Rapid Drugs Screening. *Molecules*. 2022; 27: 945. Available from: <https://doi.org/10.3390/molecules27030945>.
 22. Chagovets V, Wang Z, Kononikhin A, Starodubtseva N, Borisova A, Salimova D, et al. A Comparison of Tissue Spray and Lipid Extract Direct Injection Electrospray Ionization Mass Spectrometry for the Differentiation of Eutopic and Ectopic Endometrial Tissues. *J Am Soc Mass Spectrom*. 2017; 6–8. Available from: <https://doi.org/10.1007/s13361-017-1792-y>.
 23. Adamyant L, Starodubtseva N, Borisova A, Stepanian A, Chagovets V, Salimova D, et al. Direct Mass Spectrometry Differentiation of Ectopic and Eutopic Endometrium in Patients with Endometriosis. *J Minim Invasive Gynecol*. 2017. Available from: <https://doi.org/10.1016/j.jmig.2017.08.658>.
 24. Hutchins PD, Russell JD, Coon JJ. LipiDex: An Integrated Software Package for High-Confidence Lipid Identification. *Cell Syst*. 2018; 6: 621–5.e5. Available from: <https://doi.org/10.1016/j.cels.2018.03.011>.
 25. Bogner-Strauss JG. N-acetylaspartate metabolism outside the brain: Lipogenesis, histone acetylation, and cancer. *Front Endocrinol (Lausanne)*. 2017; 8: 1–5. Available from: <https://doi.org/10.3389/fendo.2017.00240>.
 26. Pirro V, Alfaro CM, Jarmusch AK, Hattab EM, Cohen-Gadol AA, Cooks RG. Intraoperative assessment of tumor margins during glioma resection by desorption electrospray ionization-mass spectrometry. *Proceedings of the National Academy of Sciences*. 2017; 114: 201706459. Available from: <https://doi.org/10.1073/pnas.1706459114>.

EFFECTS OF VARIOUS MRNA-LNP VACCINE DOSES ON NEUROINFLAMMATION IN BALB/C MICE

Kirshina AS¹, Kazakova AA¹, Kolosova ES¹, Imasheva EA¹, Vasileva OO¹, Zaborova OV^{1,2}, Terenin IM^{1,3}, Muslimov AR^{1,4}, Reshetnikov VV^{1,5} ✉¹ Research Center for Translational Medicine, Sirius University of Science and Technology, Sirius, Russia² Lomonosov Moscow State University, Moscow, Russia³ Belozersky Institute of Physico-Chemical Biology, Lomonosov Moscow State University, Moscow, Russia⁴ Pavlov First St. Petersburg State Medical University, St. Petersburg, Russia⁵ Institute of Cytology and Genetics, Novosibirsk, Russia

It has been proven that mRNA vaccines are highly effective against the COVID-19 outbreak, and low prevalence of side effects has been shown. However, there are still many gaps in our understanding of the biology and biosafety of nucleic acids as components of lipid nanoparticles (LNPs) most often used as a system for intracellular delivery of mRNA-based vaccines. It is known that LNPs cause severe injection site inflammation, have broad biodistribution profiles, and are found in multiple tissues of the body, including the brain, after administration. The role of new medications with such pharmacokinetics in inflammation developing in inaccessible organs is poorly understood. The study was aimed to assess the effects of various doses of mRNA-LNP expressing the reporter protein (0, 5, 10, and 20 µg of mRNA encoding the firefly luciferase) on the expression of neuroinflammation markers (*Tnfa*, *Il1β*, *Gfap*, *Aif1*) in the prefrontal cortex and hypothalamus of laboratory animals 4, 8, and 30 h after the intramuscular injection of LNP nanoemulsion. It was shown that mRNA-LNP vaccines in a dose of 10–20 µg of mRNA could enhance *Aif1* expression in the hypothalamus 8 h after vaccination, however, no such differences were observed after 30 h. It was found that the *Gfap*, *Il1β*, *Tnfa* expression levels in the hypothalamus observed at different times in the experimental groups were different. According to the results, mRNA-LNPs administered by the parenteral route can stimulate temporary activation of microglia in certain time intervals in the dose-dependent and site specific manner.

Keywords: mRNA vaccine, neuroinflammation, lipid nanoparticles, *Aif1*, *Gfap***Funding:** the study was supported by the Ministry of Science and Higher Education of the Russian Federation (agreement № 075-10-2021-113, project ID RF--193021X0001).**Author contribution:** Kirshina AS — RNA extraction, conducting PCR; Kazakova AA, Kolosova ES, Imasheva EA, Vasileva OO — generating genetic constructs, RNA extraction, manuscript writing; Zaborova OV — RNA formulation in LNP, manuscript writing; Terenin IM — RNA synthesis, manuscript writing; Muslimov AR — animal experiment, manuscript editing; Reshetnikov VV — animal experiment, data analysis, preparing illustrations, manuscript wr**Compliance with ethical standards:** the study was approved by the Ethics Committee of Pavlov First St. Petersburg State Medical University (protocol № 83 of 21 September 2022); it was conducted in accordance with the European Convention for the Protection of Vertebrate Animals used for Experimental and other Scientific Purposes (ETS No. 123, Strasbourg, 1986, with the 2006 Appendix), international convention on the humane treatment of animals (1986), Guide for the Care and Use of Laboratory Animals, 8th ed. (2010); Directive 2010/63/EU of the European Parliament and of the Council on the protection of animals used for scientific purposes (2010), Principles of Good Laboratory Practice (2016).✉ **Correspondence should be addressed:** Vasily V. Reshetnikov
Olimpiyskiy prospekt, 1, Sochi, 354340, Russia; reshetnikov.vv@talantiuspeh.ru**Received:** 01.12.2022 **Accepted:** 15.12.2022 **Published online:** 30.12.2022**DOI:** 10.24075/brsmu.2022.068

ВЛИЯНИЕ РАЗЛИЧНЫХ ДОЗ МРНК-ЛНЧ-ВАКЦИН НА НЕЙРОВОСПАЛЕНИЕ У BALB/C МЫШЕЙ

А. С. Киршина¹, А. А. Казакова¹, Е. С. Колосова¹, Е. А. Имашева¹, О. О. Васильева¹, О. В. Заборова^{1,2}, И. М. Теренин^{1,3}, А. Р. Муслимов^{1,4}, В. В. Решетников^{1,5} ✉¹ Научный центр трансляционной медицины, «Научно-технологический университет «Сириус», Сириус, Россия² Московский государственный университет имени М. В. Ломоносова, Москва, Россия³ Научно-исследовательский институт физико-химической биологии имени А. Н. Белозерского Московского государственного университета имени М. В. Ломоносова, Москва, Россия⁴ Первый Санкт-Петербургский государственный медицинский университет имени И. П. Павлова, Санкт-Петербург, Россия⁵ Институт цитологии и генетики, Новосибирск, Россия

Доказана высокая эффективность мРНК-вакцин в борьбе с эпидемией COVID-19, продемонстрирована низкая частота развития побочных эффектов. Тем не менее существует еще много пробелов в нашем понимании биологии и биобезопасности нуклеиновых кислот в составе липидных наночастиц (ЛНЧ), наиболее часто используемых в качестве системы внутриклеточной доставки вакцин на основе мРНК. Известно, что ЛНЧ приводят к сильному воспалительному ответу в месте введения, имеют широкий профиль биораспределения и обнаруживаются после введения во многих тканях организма, в том числе в головном мозге. Роль новых препаратов с такой фармакокинетикой в воспалительных процессах, развивающихся в забарьерных органах изучена недостаточно. Целью исследования было оценить влияние различных доз мРНК-ЛНЧ, экспрессирующих репортерный белок (0, 5, 10 и 20 мкг мРНК, кодирующей люциферазу светлячка) на экспрессию маркеров нейровоспаления (*Tnfa*, *Il1β*, *Gfap*, *Aif1*) в префронтальной коре и гипоталамусе лабораторных животных через 4, 8 и 30 ч после внутримышечной инъекции наноэмульсии ЛНЧ. Показано, что мРНК-ЛНЧ-вакцины в дозе 10–20 мкг мРНК способны усиливать экспрессию *Aif1* в гипоталамусе через 8 ч после вакцинации, но через 30 ч эти различия не определялись. Обнаружено, что уровень экспрессии *Gfap*, *Il1β*, *Tnfa* в экспериментальных группах различался в различных временных точках в гипоталамусе. Согласно полученным результатам, введенные парентерально мРНК-ЛНЧ могут стимулировать временную активацию микроглии в определенных временных промежутках дозо- и регион-зависимым образом.

Ключевые слова: мРНК-вакцины, нейровоспаление, липидные наночастицы, *Aif1*, *Gfap***Финансирование:** исследование выполнено при поддержке Министерства науки и высшего образования Российской Федерации (соглашение № 075-10-2021-113, уникальный идентификатор проекта РФ----193021X0001).**Вклад авторов:** А. С. Киршина — выделение РНК, постановка ПЦР реакций; А. А. Казакова, Е. С. Колосова, Е. А. Имашева, О. О. Васильева — получение генетических конструкций, выделение РНК, написание статьи; О. В. Заборова — формуляция РНК в ЛНЧ, написание статьи; И. М. Теренин — синтез РНК, написание статьи; А. Р. Муслимов — эксперимент с животными, редактирование текста; В. В. Решетников — эксперимент с животными, анализ данных, подготовка рисунков, написание статьи.**Соблюдение этических стандартов:** исследование одобрено этическим комитетом ПСПбГМУ им. И. П. Павлова (протокол № 83 от 21 сентября 2022 г.); проведено в соответствии с Европейской конвенцией ETS № 123 о защите позвоночных животных, используемых для экспериментов или в научных целях (Страсбург) (1986 г. с приложением от 2006), Международным соглашением о гуманном обращении с животными (1986 г.), Guide for the care and use of laboratory animals, 8th ed. (Руководством по уходу и использованию лабораторных животных, 2010 г.); Directive 2010/63/EU of the European parliament and of the council on the protection of animals used for scientific purposes, 2010 г.; «Правилами надлежащей лабораторной практики» (2016 г.).✉ **Для корреспонденции:** Василий Владимирович Решетников
Олимпийский пр-кт, д. 1, г. Сочи, 354340, Россия; reshetnikov.vv@talantiuspeh.ru**Статья получена:** 01.12.2022 **Статья принята к печати:** 15.12.2022 **Опубликована онлайн:** 30.12.2022**DOI:** 10.24075/vrgmu.2022.068

Advances in the development of mRNA (LNP) vaccines have made it possible to obtain two FDA approved vaccines (Pfizer/BioNTech and Moderna) against the SARS-CoV-2 virus in less than a year [1, 2]. The LNP-mRNA-based medications can be used for both treatment of a number of socially significant disorders and as vaccines for prevention of infections caused by many pathogens. The mRNA-LNP platform flexibility is due to the possibility of specific selection of the antigenic sequence comprised in the mRNA molecule, it is also due to different variants of the lipid composition and their ratios in LNPs that can modulate the mRNA vaccine efficiency and immunogenicity [3]. The Pfizer/BioNTech and Moderna lipid particles comprise charged ionized lipids, neutral ionized lipids, poly(ethylene glycol)-containing lipids, cholesterol, and distearoylphosphatidylcholine (DSPC) [4]. LNPs ensure mRNA-LNP internalization into the cell and play an adjuvant role, stimulating a moderate increase in the injection site inflammation. It has been shown that different variants of ionizable lipids recognized by the toll-like receptor 4 (TLR4) play a central role in the induction of inflammation caused by LNPs [5]. Furthermore, the mRNA molecule being a vaccine component can exert pro-inflammatory activity via TLR-3,7,8, RIG-I, MDA5 [6, 7]. Moderate pro-inflammatory activity contributes to effective antigen presentation of the antigen-presenting cells, as well as to the humoral and T-cell immunity formation. However, inflammation may sometimes cause adverse effects. In particular, recent studies have shown that LNPs cause severe injection site inflammation, have a broad biodistribution profile, and are found in multiple tissues of the body, including the brain [4, 8]. Uninhibited crossing the blood-brain barrier together with pro-inflammatory activity can cause adverse effects in the form of immune activation in the central nervous system. The study was aimed to perform the dynamic assessment of neuroinflammatory markers in the prefrontal cortex and hypothalamus of the Balb/c mice after administration of various mRNA-LNP vaccine doses.

METHODS

Experimental design

The conventional experiment involved 75 adult Balb/c males (age 9–10 weeks, body weight 19–22 g) obtained from

the Rappolovo Breeding Nursery of the Russian Academy of Medical Sciences (St. Petersburg, Russia) and kept at the Center of Experimental Pharmacology, St. Petersburg State Chemical and Pharmaceutical University, under fixed lightning conditions (12.00 : 12.00 h). The animals had free access to the standard food (granules) and water. The animals were distributed into the study groups by randomization before the study. Intramuscular injections of 30 μ L of various doses of mRNA-LNP (three concentrations: 5, 10, and 20 μ g of RNA) or control (empty) LNPs in phosphate buffer were performed. The animals inhaled the 2.0% isoflurane (Laboratories Karizoo, S.A.; Spain) mixed with oxygen for 5 min and were subsequently decapitated within 4, 8, and 30 h after administration of the particle suspension (Fig. 1). The samples of the hypothalamus and prefrontal cortex (PFC) were obtained as earlier reported [9]. The same volume (30 μ L) of phosphate buffer was administered to the control animals. Five animals per experimental point were used in each group.

Cloning

Amplification of the target gene comprising the 5'-UTR Moderna (gggaaataagagagaaaagaagagtaagaagaaat aagaccccgccgcccacc) encoding the firefly (*Photinus pyralis*) luciferase and the 3'-UTR Moderna (gctggagcctcgg tggcctagcttctgtcccctgggctccccagcccctctcccctctctgc acccgtagcctgtctttgaataaagtctgagtgggcgga) sequences was performed via linking together three fragments by the overlapping primer-based PCR. Then the resulting fragment was incubated with the EcoRI and BglIII restriction endonucleases, purified from agarose gel and ligated to the pSmart commercial vector (Lucigen; USA) prepared by the same method. The vector comprised a polyA-tail with the size of 110. A NEB-stable *E. coli* strain (New England Biolabs; UK) was used for transformation. Clones were selected from the colonies by PCR, and the sequence of the insert was confirmed by sequencing. To generate the verified plasmid, *E. coli* was grown in the incubator shaker at 30 °C and 180 rpm. Then plasmid DNA was extracted from bacterial cells using the QIAGEN Plasmid Maxi Kit (Qiagen; USA). The resulting plasmid preparation was linearized by the unique SpeI restriction site and subsequently visualized in agarose gel.

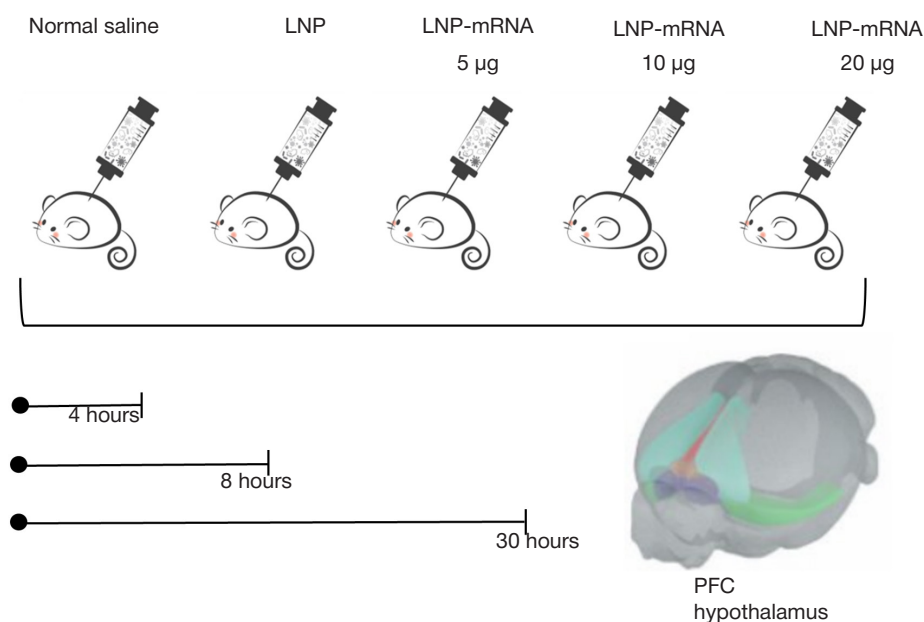


Fig. 1. Experimental design

Table. Nucleotide sequences of primers and probes

Gene	Sequence 5'→3'	
<i>Aif1</i>	Probe	ROX-AGAGAGGCTGGAGGGGATC-BHQ2
	For	GCTTTTGGACTGCTGAAGGC
	Rev	GAAGGCTTCAAGTTTGGACG
<i>Gfap</i>	Probe	ROX-GCAAGAGACAGAGGAGTGG-BHQ-2
	For	CCTGAGAGAGATTTCGCACTC
	Rev	GACTCCAGATCGCAGGTCAAG
<i>TNFα</i>	Probe	ROX-CGAGTGACAAGCCTGTAGC-BHQ2
	For	CATCAGTTCTATGGCCAGACCCT
	Rev	GCTCCTCCACTTGGTGGTTTGCTA
<i>Il1β</i>	Probe	ROX-CTGCTTCCAACCTTTGACCTGG-BHQ2
	For	CCTGTTCTTTGAAGTTGACGG
	Rev	CTGAAGCTCTTGTGATGTGC
<i>Gapdh</i>	Probe	CCATCAACGACCCCTTCATTGACCTC
	For	TGCAGTGGCAAAGTGGAGAT
	Rev	TGCCGTGAGTGGAGTCATACT

***In vitro* mRNA transcription**

In vitro transcription was carried out in the buffer solution containing 20 mmol of DTT, 2 mmol of spermidine, 80 mmol of HEPES-KOH (pH 7.4), 24 mmol of MgCl₂. The reaction mixture also contained 3 mmol of each ribonucleoside triphosphate (Biosan; Russia), 12 mmol of anti-reverse cap analog (ARCA) (Biolabmix; Russia). Other components per 100- μ L reaction volume: 40 units of the RiboCare ribonuclease inhibitor (Evrogen; Russia), 500 units of the T7 RNA polymerase (Biolabmix; Russia), 5 μ g of the linearized plasmid, and 1 μ L of the enzyme mix from the RiboMAX Large Scale RNA Production System kit (Promega; USA) as the source of inorganic pyrophosphatase. The reaction was carried out for 2 h at a temperature of 37 °C, then another 3 mmol of each ribonucleoside triphosphate were added to the reaction and incubated for 2 h. DNA was hydrolyzed using the RQ1 nuclease (Promega; USA), RNA was precipitated by adding LiCl to a concentration of 0.32 mol and EDTA (pH 8.0) to a concentration of 20 mmol with subsequent incubation on ice for an hour. Then the solution was centrifuged for 15 min (25,000 g, 4 °C). RNA precipitate was washed with 70% ethanol, diluted in the ultrapure water and once more precipitated by alcohol using the standard method. RNA concentration was defined by spectrophotometry based on absorbance at a wavelength of 260 nm.

Formulation of LNPs containing mRNA

Encapsulation of mRNA into lipid nanoparticles was performed by mixing the 0.2 mg/mL mRNA aqueous solution (10 mmol citrate buffer, pH 3.0) with the alcohol solution of the lipid mixture in the microfluidic cartridge using the NanoAssemblr Benchtop system (Precision Nanosystems; USA). The lipid mixture contained the following components: ALC-0315 ionizable lipidoid (BroadPharm; USA), distearoylphosphatidylcholine (DSPC) (Avanti Polar Lipids; USA), cholesterol (Sigma-Aldrich; USA), DMG-PEG-2000 (BroadPharm; USA) in a molar ratio (%) of 46.3 : 9.4 : 42.7 : 1.6. The amount of lipids per unit of mRNA was calculated based on the following ratio: N/P = 6 (ALC-0315 ionizable lipidoid/mRNA base). To generate particles of the desired size, the aqueous and alcohol phases were mixed in a ratio of 3 : 1 v/v with the total mixing speed of

10 mL/min. After mixing the phases the resulting water-alcohol particle suspension was dialyzed in 300 volumes of phosphate buffered saline (pH 7.4, 18 h, +15 °C). After dialysis the particle suspension was concentrated using the Amicon Ultra-4 10,000 Da molecular weight cutoff filter. Then particles were filtered through the filter with the 0.22 μ m PES membrane (Merck; USA) and stored at 4 °C. Empty LNPs were obtained by mixing the 10 mmol citrate buffer (pH 3.0) with the lipid mixture alcohol solution in the microfluidic cartridge by the same method that was used to obtain the mRNA-loaded LNPs.

After filtration, the quality of the particles generated was assessed based on two parameters: mRNA load and particle size. The concentration of mRNA loaded into lipid nanoparticles was defined based on the differences in the fluorescence signal levels obtained for the particle suspension stained with the RiboGreen reagent (Thermo Fischer Scientific; USA) before and after the particle disruption. The Triton X-100 detergent (Sigma-Aldrich; USA) was used to disrupt the particles. The LNP size was defined by the dynamic light scattering method in the Zetasizer Nano ZSP system (Malvern Panalytical; USA).

Estimation of gene expression in the brain

Total RNA was extracted from the PFC and hypothalamus using the kit for column-based RNA isolation (Biolabmix; Russia) in accordance with the manufacturer's protocol. RNA concentration and purity were assessed with the NanoDrop OneC spectrophotometer (Thermo Scientific; USA).

To carry out the reverse transcription reaction, 500 ng of RNA and the OT-M-MuLV-RH reverse transcription kit (Biolabmix; Russia) with random hexanucleotide primers were used. The resulting cDNA was used to assess gene expression. Expression levels of the genes encoding pro-inflammatory cytokines and interleukins (*Il1 β* , *Tnfa*), marker genes of microglia (*Aif1*) and astroglia (*Gfap*) activation were assessed as neuroinflammation markers. The study involved the use of quantitative PCR with fluorescent Taq-man probes. The sequences of primers and probes are provided in Table 1.

The expression was assessed relative to mRNA of the housekeeping gene (*Gapdh*). PCR was carried out using the BioMaster HS-qPCR (2 \times) kit (Biolabmix; Russia) in the Real-Time CFX96 Touch system (Bio-Rad Laboratories; USA) in

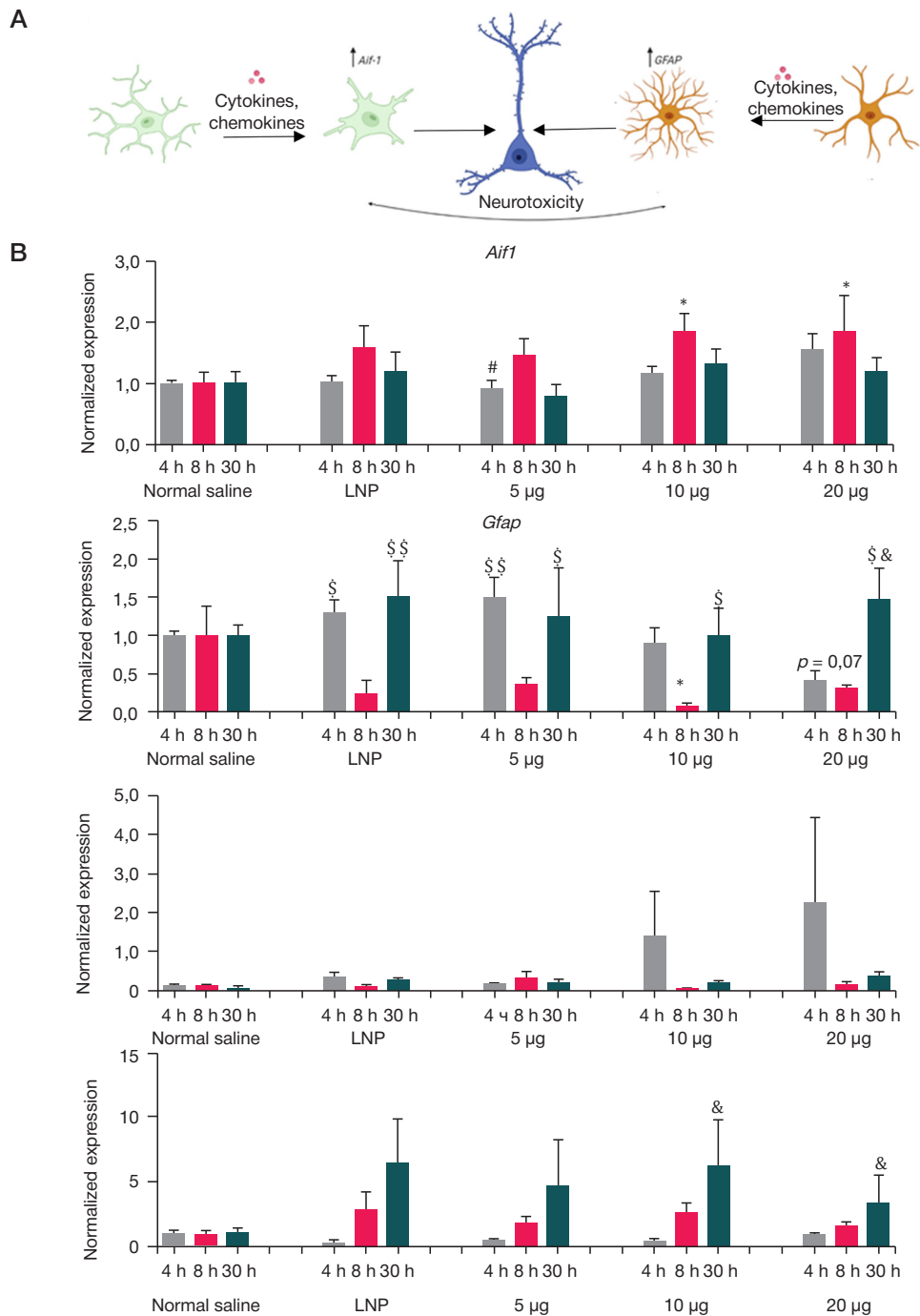


Fig. 2. Expression of neuroinflammatory marker genes in the hypothalamus **A.** Astroglial and microglial response to acute inflammation. **B.** Relative expression of genes encoding pro-inflammatory cytokines (*Il1b*, *Trnfa*) and markers of glial activation (*Aif1*, *Gfap*) at various time points after the mRNA-LNP vaccine administration. The data are presented as mean ± standard error. * — $p < 0.05$, ** — $p < 0.01$, compared to the group that received normal saline at the same time point; # — $p < 0.05$, compared to the group that received 20 µg of mRNA-LNP at the same time point; \$ — $p < 0.05$, \$\$ — $p < 0.01$, compared to the point within 8 hours after administration; & — $p < 0.05$, compared to the point within 4 hours after administration. Post hoc analysis using the Fisher's LSD test

accordance with the following protocol: 95 °C for 15 s, 60 °C for 20 s. Three iterations of all tests per cDNA sample were performed. The expression was quantified by the $\Delta\Delta C_t$ method.

Statistical analysis

Statistical processing of the results was performed by ANOVA (the “group” and “time after administration” were used as factors) and Fisher's least significant difference (LSD) test as a post hoc test. The differences between the experimental groups were considered significant at $p < 0.05$, while at the level of trends these were considered significant at $p < 0.1$.

Data analysis was performed using the Statistica 8.0 software package (Statsoft Inc.; USA).

RESULTS

The findings show that various mRNA-LNP vaccine doses induce activation of *Aif1* in the hypothalamus (Fig. 2), but not in the prefrontal cortex (Fig. 3). The two-way analysis of variance (ANOVA) made it possible to reveal significant effects of the “group” and “time after administration” factors on the *Aif1* expression in the hypothalamus ($F(4.70) = 2.866$ at $p = 0.032$; $F(2.72) = 4.246$ at $p = 0.019$). In the groups of mice that

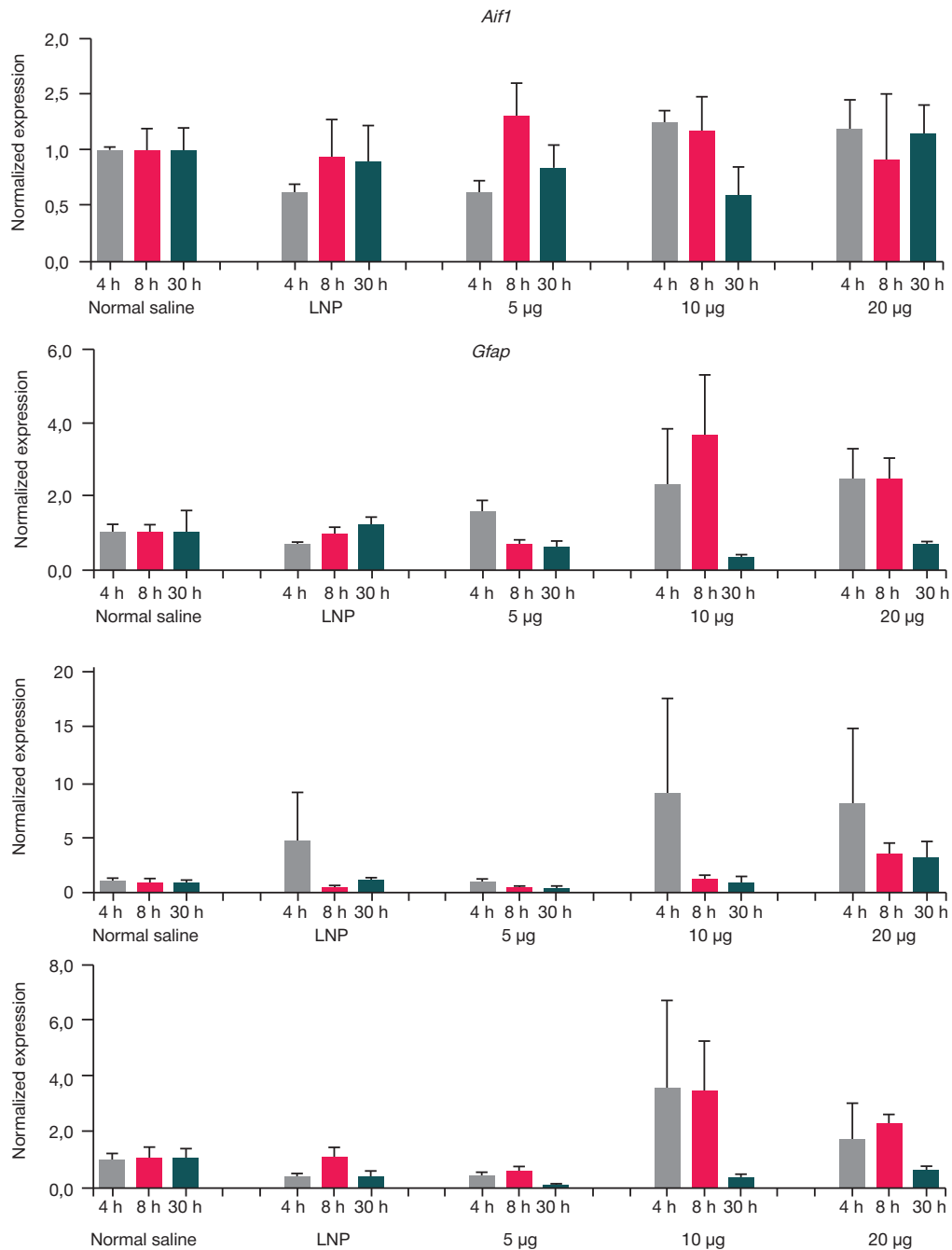


Fig. 3. Relative expression of genes encoding pro-inflammatory cytokines (*Il1β*, *Tnfa*) and markers of glial activation (*Aif1*, *Gfap*) at various time points after the mRNA-LNP vaccine administration in the prefrontal cortex

received 10 μg of mRNA and 20 μg of RNA as part of the mRNA-LNP vaccine, the expression of *Aif1* mRNA within 7 h after the vaccine administration was about 80% higher than in the control group that received phosphate buffer ($p > 0.05$). It is interesting to note that the groups that received 5 μg of RNA as part of the mRNA-LNP vaccine and empty LNPs (with no mRNA) also showed elevated expression of *Aif1* (by 40–55%) within 8 h, however, these differences were non-significant. No differences in the hypothalamic *Aif1* expression between animals of different groups were observed 30 h after the vaccine administration. No significant effects of the “group” factor or the interaction of the “group” and “time after administration” factors on the expression of other assessed genes in the hypothalamus (*Tnfa*, *Il1β*, *Gfap*) and gene expression in the prefrontal cortex were revealed. Thus, we observed moderate mRNA-LNP effects on the neuroinflammation associated with

the elevated expression of the markers of active microglia in the hypothalamus, but not in the prefrontal cortex. Furthermore, these effects were dose-dependent.

Comparison of gene expression at various time points between animals of various groups after administration of the mRNA-LNP vaccine showed that *Il1β* expression was dramatically increased 4 h after vaccination in both hypothalamus and prefrontal cortex of certain animals in the groups that received 10 μg of mRNA and 20 μg of RNA as part of the mRNA-LNP vaccine. However, no such effects were observed in the later measurement points. Despite the profound effects on the *Il1β*, these differences were non-significant, since only a few animals in the groups showed a pronounced response. Such results demonstrate heterogeneity of the response to the mRNA-LNP vaccine associated with individual characteristics of the animals.

The effect of the “time after administration” factor on the *Gfap* and *Tnfa* expression in the hypothalamus was revealed ($F(2.72) = 10.179$ at $p < 0.0001$; $F(2.72) = 5.181$ at $p = 0.008$). The *Gfap* expression decreased within 8 h in all experimental groups, however, it increased in 30 h. It is interesting that the *Tnfa* expression also increased in 30 h after vaccination compared to the levels observed within 4 h in the majority of experimental groups. Such results suggest that mice in the experimental group develop the second wave of pro-inflammatory activation involving astrocytes and interleukin $TNF\alpha$.

DISCUSSION

The findings show that mRNA–LNP vaccines with the mRNA doses of 10–20 μg are capable of increasing the *Aif1* expression within 8 h in the hypothalamus, but not in the prefrontal cortex. We have found that experimental groups demonstrate the differences in the *Gfap*, *Il1b*, *Tnfa* expression levels measured at various time points in the hypothalamus, which is also an indirect evidence of the fact that the expression levels of these genes may be correlated to the mRNA–LNP vaccine administration.

The mRNA–LNP vaccine can cause both local and systemic inflammation [4, 8]. Inflammation can be caused by various vaccine components: mRNA molecules, lipids forming part of LNPs or protein product encoded by mRNA. The mRNA–LNPs most often transfect cells near the injection site, after that LNPs are rapidly transported to the proximal lymph nodes by passive drainage and are also actively transported by the professional antigen-presenting cells and neutrophils [10, 11]. Then mRNA–LNP can reach any cell of the body via systemic circulation; low amounts of mRNA–LNP are found in the brain, thus suggesting its capability of crossing the blood-brain barrier [12, 13].

It is known that peripheral inflammatory stimuli can also cause immune response in the brain that results in activation of astrocytes, the main immunocompetent cells of the brain [14]. Because of their cytokine-producing and phagocytic activity, these cells affect the development and maturation of the CNS structures [15], participate in the normal formation and development of neural circuits during ontogenesis [16], maintain the pool of neurons, mediate synapse maturation and reduction, thereby regulating the number of synapses and receptor expression [17].

Thus, the signs of microglia activation we have found in certain experimental groups may be both evidence of mRNA–LNP directly crossing the blood-brain barrier and triggering neuroinflammation, and the result of the increasing peripheral inflammation. Since our study does not involve assessment of the peripheral immune activation parameters, we cannot answer this question explicitly.

Significant differences in the *Aif1* expression revealed 8 h after immunization are consistent with the data showing that the peak of microglia activation falls between 6–24 h after induction of inflammation [14, 18–20]. At the same time, the peak of cytokine activation after induction by inflammatory agents, such as bacterial lipopolysaccharide or the synthetic analog of double-stranded RNA (Poly I:C), falls between 1.5–3.0 after administration of inflammatory mimetics. That is why the lack of significant effects on the expression of *Il1b* and *Tnfa* observed across the groups may be due to the fact that peak activation of gene expression is passed. At the same time, a number of studies show that elevated cytokine levels in the brain and periphery may persist up to 24 h after inflammation induction by mimetics.

In our study we assessed the expression of pro-inflammatory genes in two brain structures. The more pronounced effects were observed in the hypothalamus, while prefrontal cortex showed no significant alterations. The hypothalamus is an important brain structure that functions as a metabolic center responsible for regulation of multiple fundamental physiological processes involved in metabolism of the whole body, including food intake, regulation of appetite, energy consumption; thus, the hypothalamus plays a crucial role in systemic homeostatic regulation [22]. Clinical data have shown that various stimuli, such as peripheral inflammation or the increased intake of saturated fatty acids, may cause neuroinflammation in this brain structure [23–25]. Furthermore, the hypothalamus contains various cell populations of microglia and astroglia [26]. Taken together, these data show that the hypothalamus may be a kind of the peripheral inflammation sensor and respond to pro-inflammatory signals more actively than the prefrontal cortex.

CONCLUSIONS

The mRNA–LNP vaccine can activate the hypothalamic *Aif1* expression 8 h after vaccination in a dose-dependent manner. However, no significant effects of mRNA–LNP vaccines on the gene expression have been found in the prefrontal cortex. Despite the fact that alterations in the *Aif1* expression observed within 30 h after vaccination are non-significant, these findings show that mRNA–LNP vaccine can induce neuroinflammation. Further experiments involving larger groups of animals and focused on assessing the parameters of peripheral inflammation and broader analysis of neuroinflammation involving the use of immunoassays and immunohistochemistry for assessment of pro-inflammatory agents and microglial cell morphology in the hypothalamus and other brain structures are required to understand the mechanisms underlying the mRNA–LNP vaccine capability of inflammation stimulation.

References

1. Baden LR, et al. Efficacy and Safety of the mRNA-1273 SARS-CoV-2 Vaccine. *N Engl J Med.* 2021; 384 (5): 403–16.
2. Polack FP, et al. Safety and Efficacy of the BNT162b2 mRNA Covid-19 Vaccine. *N Engl J Med.* 2020; 383 (27): 2603–15.
3. Kon E, Elia U, Peer D. Principles for designing an optimal mRNA lipid nanoparticle vaccine. *Curr Opin Biotechnol.* 2022; 73: 329–36.
4. Ndeupen S, et al. The mRNA-LNP platform's lipid nanoparticle component used in preclinical vaccine studies is highly inflammatory. *iScience.* 2021; 24 (12): 103479.
5. Parhiz H. et al. Added to pre-existing inflammation, mRNA-lipid nanoparticles induce inflammation exacerbation (IE). *J Control Release.* 2022; 344: 50–61.
6. Mu X, Hur S. Immunogenicity of In Vitro-Transcribed RNA. *Acc Chem Res.* 2021; 54 (21): 4012–23.
7. Heil F. et al. Species-specific recognition of single-stranded RNA via toll-like receptor 7 and 8. *Science.* 2004; 303 (5663): 1526–9.
8. Trougakos IP, et al. Adverse effects of COVID-19 mRNA vaccines: the spike hypothesis. *Trends Mol Med.* 2022; 28 (7): 542–54.
9. Reshetnikov VV, et al. Social defeat stress in adult mice causes alterations in gene expression, alternative splicing, and the epigenetic landscape of H3K4me3 in the prefrontal cortex: An impact of early-life stress. *Prog Neuropsychopharmacol Biol Psychiatry.* 2021; 106: 110068.
10. Bahl K, et al. Preclinical and Clinical Demonstration of Immunogenicity by mRNA Vaccines against H10N8 and H7N9 Influenza Viruses. *Mol Ther.* 2017; 25 (6): 1316–27.

11. Liang F, et al. Efficient Targeting and Activation of Antigen-Presenting Cells In Vivo after Modified mRNA Vaccine Administration in Rhesus Macaques. *Mol Ther.* 2017; 25 (12): 2635–47.
12. Maugeri M, et al. Linkage between endosomal escape of LNP-mRNA and loading into EVs for transport to other cells. *Nat Commun.* 2019; 10 (1): 4333.
13. Pardi N, et al. Expression kinetics of nucleoside-modified mRNA delivered in lipid nanoparticles to mice by various routes. *J Control Release.* 2015; 217: 345–1.
14. Hoogland IC, et al. Systemic inflammation and microglial activation: systematic review of animal experiments. *J Neuroinflammation.* 2015; 12: 114.
15. Billimoria PM, Stevens B. Microglia function during brain development: New insights from animal models. *Brain Res.* 2015; 1617: 7–17.
16. Chen Z, et al. Microglial displacement of inhibitory synapses provides neuroprotection in the adult brain. *Nat Commun.* 2014; 5: 4486.
17. Ji K, et al. Microglia actively regulate the number of functional synapses. *PLoS One.* 2013; 8 (2): e56293.
18. Biesmans S, et al. Systemic immune activation leads to neuroinflammation and sickness behavior in mice. *Mediators Inflamm.* 2013; 2013: 271359.
19. Buttini M, Limonta S, Boddeke HW. Peripheral administration of lipopolysaccharide induces activation of microglial cells in rat brain. *Neurochem Int.* 1996; 29 (1): 25–35.
20. Mutovina A, et al. Unique Features of the Immune Response in BTBR Mice. *Int J Mol Sci.* 2022; 23 (24).
21. Cunningham C, et al. The sickness behaviour and CNS inflammatory mediator profile induced by systemic challenge of mice with synthetic double-stranded RNA (poly I:C). *Brain Behav Immun.* 2007; 21 (4): 490–502.
22. Goldstein DS, Kopin IJ. Homeostatic systems, biocybernetics, and autonomic neuroscience. *Auton Neurosci.* 2017; 208: 15–28.
23. Burfeind KG, Michaelis KA, Marks DL. The central role of hypothalamic inflammation in the acute illness response and cachexia. *Semin Cell Dev Biol.* 2016; 54: 42–52.
24. Rahman MH, et al. Hypothalamic inflammation and malfunctioning glia in the pathophysiology of obesity and diabetes: Translational significance. *Biochem Pharmacol.* 2018; 153: 123–33.
25. de Git KC, Adan RA. Leptin resistance in diet-induced obesity: the role of hypothalamic inflammation. *Obes Rev.* 2015; 16 (3): 207–24.
26. Mendes NF, et al. Hypothalamic Microglial Heterogeneity and Signature under High Fat Diet-Induced Inflammation. *Int J Mol Sci.* 2021; 22 (5).

Литература

1. Baden LR, et al. Efficacy and Safety of the mRNA-1273 SARS-CoV-2 Vaccine. *N Engl J Med.* 2021; 384 (5): 403–16.
2. Polack FP, et al. Safety and Efficacy of the BNT162b2 mRNA Covid-19 Vaccine. *N Engl J Med.* 2020; 383 (27): 2603–15.
3. Kon E, Elia U, Peer D. Principles for designing an optimal mRNA lipid nanoparticle vaccine. *Curr Opin Biotechnol.* 2022; 73: 329–36.
4. Ndeupen S, et al. The mRNA-LNP platform's lipid nanoparticle component used in preclinical vaccine studies is highly inflammatory. *iScience.* 2021; 24 (12): 103479.
5. Parhiz H, et al. Added to pre-existing inflammation, mRNA-lipid nanoparticles induce inflammation exacerbation (IE). *J Control Release.* 2022; 344: 50–61.
6. Mu X, Hur S. Immunogenicity of In Vitro-Transcribed RNA. *Acc Chem Res.* 2021; 54 (21): 4012–23.
7. Heil F, et al. Species-specific recognition of single-stranded RNA via toll-like receptor 7 and 8. *Science.* 2004; 303 (5663): 1526–9.
8. Trougakos IP, et al. Adverse effects of COVID-19 mRNA vaccines: the spike hypothesis. *Trends Mol Med.* 2022; 28 (7): 542–54.
9. Reshetnikov VV, et al. Social defeat stress in adult mice causes alterations in gene expression, alternative splicing, and the epigenetic landscape of H3K4me3 in the prefrontal cortex: An impact of early-life stress. *Prog Neuropsychopharmacol Biol Psychiatry.* 2021; 106: 110068.
10. Bahl K, et al. Preclinical and Clinical Demonstration of Immunogenicity by mRNA Vaccines against H10N8 and H7N9 Influenza Viruses. *Mol Ther.* 2017; 25 (6): 1316–27.
11. Liang F, et al. Efficient Targeting and Activation of Antigen-Presenting Cells In Vivo after Modified mRNA Vaccine Administration in Rhesus Macaques. *Mol Ther.* 2017; 25 (12): 2635–47.
12. Maugeri M, et al. Linkage between endosomal escape of LNP-mRNA and loading into EVs for transport to other cells. *Nat Commun.* 2019; 10 (1): 4333.
13. Pardi N, et al. Expression kinetics of nucleoside-modified mRNA delivered in lipid nanoparticles to mice by various routes. *J Control Release.* 2015; 217: 345–1.
14. Hoogland IC, et al. Systemic inflammation and microglial activation: systematic review of animal experiments. *J Neuroinflammation.* 2015; 12: 114.
15. Billimoria PM, Stevens B. Microglia function during brain development: New insights from animal models. *Brain Res.* 2015; 1617: 7–17.
16. Chen Z, et al. Microglial displacement of inhibitory synapses provides neuroprotection in the adult brain. *Nat Commun.* 2014; 5: 4486.
17. Ji K, et al. Microglia actively regulate the number of functional synapses. *PLoS One.* 2013; 8 (2): e56293.
18. Biesmans S, et al. Systemic immune activation leads to neuroinflammation and sickness behavior in mice. *Mediators Inflamm.* 2013; 2013: 271359.
19. Buttini M, Limonta S, Boddeke HW. Peripheral administration of lipopolysaccharide induces activation of microglial cells in rat brain. *Neurochem Int.* 1996; 29 (1): 25–35.
20. Mutovina A, et al. Unique Features of the Immune Response in BTBR Mice. *Int J Mol Sci.* 2022; 23 (24).
21. Cunningham C, et al. The sickness behaviour and CNS inflammatory mediator profile induced by systemic challenge of mice with synthetic double-stranded RNA (poly I:C). *Brain Behav Immun.* 2007; 21 (4): 490–502.
22. Goldstein DS, Kopin IJ. Homeostatic systems, biocybernetics, and autonomic neuroscience. *Auton Neurosci.* 2017; 208: 15–28.
23. Burfeind KG, Michaelis KA, Marks DL. The central role of hypothalamic inflammation in the acute illness response and cachexia. *Semin Cell Dev Biol.* 2016; 54: 42–52.
24. Rahman MH, et al. Hypothalamic inflammation and malfunctioning glia in the pathophysiology of obesity and diabetes: Translational significance. *Biochem Pharmacol.* 2018; 153: 123–33.
25. de Git KC, Adan RA. Leptin resistance in diet-induced obesity: the role of hypothalamic inflammation. *Obes Rev.* 2015; 16 (3): 207–24.
26. Mendes NF, et al. Hypothalamic Microglial Heterogeneity and Signature under High Fat Diet-Induced Inflammation. *Int J Mol Sci.* 2021; 22 (5).

DRUG DESIGN STRATEGIES FOR THE TREATMENT OF CORONAVIRUS INFECTION

Terekhov SS¹, Shmygarev VI¹, PurtoV KV², Smirnov IV¹, Yampolsky IV^{1,3}, Tsarkova AS^{1,3} ✉¹ Shemyakin–Ovchinnikov Institute of Bioorganic Chemistry RAS, Moscow, Russia² Institute of Biophysics SB RAS, Federal Research Center “Krasnoyarsk Science Center SB RAS”, Krasnoyarsk, Russia³ Pirogov Russian National Research Medical University, Moscow, Russia

The increasing size and density of the human population is leading to an increasing risk of infectious diseases that threaten to spread yet another pandemics. The widespread use of vaccination has reduced morbidity and mortality associated with viral infections and in some cases eradicated the virus from the population entirely. Regrettably, some virus species retain the ability to mutate rapidly and thus evade the vaccine-induced immune response. New antiviral drugs are therefore needed for the treatment and prevention of viral diseases. Modern research into the structures and properties of viral proteases, which are of key importance in the life cycle of viruses, makes it possible, in our opinion, to turn these enzymes into promising targets for the development of effective viral disease control methods.

Keywords: antiviral drugs, viral proteases, protease inhibitors, prodrug design

Funding: This work was financially supported by grant № 075-15-2021-1049 from the Ministry of Science and Higher Education of the Russian Federation.

Author contribution: S.S. Terekhov, V.I. Shmygarev, K.V. PurtoV — literature analysis; I.V. Yampolsky, I.V. Smirnov — literature analysis, general project management; A.S. Tsarkova — literature analysis, data processing, project management, article writing.

✉ **Correspondence should be addressed:** Aleksandra S. Tsarkova
Miklukho-Maklay, 16/10, Moscow, 117997, Russia; altsarkova@gmail.com

Received: 05.12.2022 **Accepted:** 19.12.2022 **Published online:** 28.12.2022

DOI: 10.24075/brsmu.2022.067

СТРАТЕГИИ ДИЗАЙНА ЛЕКАРСТВЕННЫХ ПРЕПАРАТОВ ДЛЯ ЛЕЧЕНИЯ КОРОНАВИРУСНОЙ ИНФЕКЦИИ

С. С. Терехов¹, В. И. Шмыгарев¹, К. В. Пуртов², И. В. Смирнов¹, И. В. Ямпольский^{1,3}, А. С. Царькова^{1,3} ✉¹ Институт биоорганической химии имени М. М. Шемякина и Ю. А. Овчинникова Российской академии наук, Москва, Россия² Институт биофизики, Федеральный исследовательский центр «Красноярский научный центр СО РАН», Красноярск, Россия³ Российский национальный исследовательский медицинский университет имени Н. И. Пирогова, Москва, Россия

Возрастающие с каждым годом численность и плотность человеческой популяции приводит к увеличивающемуся риску распространения инфекционных заболеваний, что грозит возникновением все новых эпидемий по всему миру. Широкое использование вакцинации снизило заболеваемость и смертность, связанные с вирусными инфекциями, а в некоторых случаях полностью уничтожило вирус среди населения. К сожалению, некоторые виды вирусов сохраняют способность к быстрой мутации и таким образом ускользают от вызванного вакциной иммунного ответа. В связи с этим для лечения и профилактики вирусных заболеваний требуются новые противовирусные препараты. Современные исследования в области структур и свойств вирусных протеаз, имеющих ключевое значение в жизненном цикле вирусов, позволяют, на наш взгляд, превратить эти ферменты в перспективные мишени для разработки эффективных методов борьбы с вирусными заболеваниями.

Ключевые слова: противовирусные препараты, вирусные протеазы, ингибиторы протеаз, дизайн пролекарств

Финансирование: работа выполнена при поддержке гранта Министерства науки и высшего образования Российской Федерации № 075-15-2021-1049.

Вклад авторов: С. С. Терехов, В. И. Шмыгарев, К. В. Пуртов — анализ литературы; И. В. Ямпольский, И. В. Смирнов — анализ литературы, общее руководство проектом; А. С. Царькова — анализ литературы, обработка данных, руководство проектом, написание статьи.

✉ **Для корреспонденции:** Александра Сергеевна Царькова
ул. Миклухо-Маклая, д. 16/10, г. Москва, 117997, Россия; altsarkova@gmail.com

Статья получена: 05.12.2022 **Статья принята к печати:** 19.12.2022 **Опубликована онлайн:** 28.12.2022

DOI: 10.24075/vrgmu.2022.067

Together with cardiovascular and cerebrovascular diseases, infectious diseases caused by bacteria, viruses, parasites and fungi are the leading cause of death worldwide [1]. According to the World Health Organization, the global spread of coronavirus infection, which began in 2019 in China, has infected more than 600 million and killed more than 6.5 million people over three years [2]. The cause of the COVID-19 pandemic was a new coronavirus, SARS-CoV-2. Previously, members of the Coronaviridae family SARS-CoV and MERS-CoV caused outbreaks of severe acute respiratory syndrome (SARS) in 2002 and Middle East respiratory syndrome (MERS) in 2012 [3].

Several decades of studies of the family Coronaviridae have shown that the viral RNA genome is translated into two large polyproteins, pp1a and pp1ab, which, through their internal peptidase activity, are cleaved into several non-structural proteins (Nsp) required to enable transcription and replication of the viral genome [4]. Two cysteine proteases, papain-like

peptidase (PLP) [5] and chymotrypsin-like peptidase (3CL), also known as the major coronavirus protease (M^{Pro}), are critical for proteolytic degradation of polyproteins [6]. M^{Pro} peptidase consists of three domains: domains I and II form a chymotrypsin-like fold containing a substrate-binding site located in the cleft between the two domains, while domain III is required for homodimer formation and plays a critical role in the catalytic activity of the protease as the M^{Pro} monomer is inactive [7]. M^{Pro} of different coronaviruses share highly conserved substrate-binding sites recognizing the amino acid sequence of the polyprotein (Leu-Gln)↓(Ser/Ala/Gly), where the peptide bond after the glutamine residue is hydrolyzed [7, 8].

The development of inhibitors of cysteine proteases involved in coronavirus (CoV) replication represent an effective strategy against COVID-19 and other diseases caused by coronaviruses. M^{Pro} is a promising target for the development of antiviral drugs targeting SARS-CoV-2 and other CoV because of its important role in post-translational processing

of polyproteins. Moreover, the absence of human proteases cleaving proteins after the Gln residue is one of the advantages of M^{pro} as a target for inhibitor development, as it increases their specificity and limits the undesirable side-effects. Since the epidemic outbreaks caused by CoV in 2002 and 2012, various M^{pro} inhibitors have been proposed [9], but not until 2021 that the first drug candidates that successfully passed clinical trials have appeared [10, 11].

Another interesting strategy for antiviral drug development is the use of proteolysis to activate prodrugs [12]. Prodrugs are inactivated derivatives of drug molecules that can undergo enzymatic transformation to release the active compound *in vivo* [12]. A number of protease-activated prodrugs (PAPs) have been developed and successfully used in cancer treatment to improve drug delivery to malignant neoplasms,

where protease expression is higher than in healthy tissues [13]. However, the application of PAPs is not limited to the development of anti-cancer drugs; recent publications show that this approach can also be used to treat bacterial and viral infections [14, 15].

CONCLUSION

The combination of the two strategies could be a promising avenue in the development of drugs for the treatment of COVID-19. The use of inactivated cytotoxic and cytostatic drugs conjugated with both irreversible and reversible selective M^{pro} protease inhibitors can provide the targeted delivery and release of the active agents in infected cells and reduce the systemic toxicity of the developed drugs.

References

1. The top 10 causes of death, Geneva: World Health Organization c2022 [cited 2022 Nov 30]. Available from: <https://www.who.int/news-room/fact-sheets/detail/the-top-10-causes-of-death>.
2. WHO Coronavirus (COVID-19) Dashboard, Geneva: World Health Organization c2022 [cited 2022 Nov 30]. Available from: <https://covid19.who.int/>.
3. Zhou H, Yang J, Zhou C, Chen B, Fang H, Chen S, et al. A Review of SARS-CoV2: Compared With SARS-CoV and MERS-CoV. *Front Med.* 2021; 8: 628370.
4. Fehr AR, Perlman S. Coronaviruses: an overview of their replication and pathogenesis. *Methods Mol Biol.* 2015; 1282: 1–23.
5. Báez-Santos YM, St. John SE, Mesecar AD. The SARS-coronavirus papain-like protease: structure, function and inhibition by designed antiviral compounds. *Antiviral Res.* 2015; 115: 21–38.
6. Wang F, Chen C, Tan W, Yang K, Yang H. Structure of Main Protease from Human Coronavirus NL63: Insights for Wide Spectrum Anti-Coronavirus Drug Design. *Sci Rep.* 2016; 6: 22677.
7. Jin Z, Du X, Xu Y, Deng Y, Liu M, Zhao Y, et al. Structure of M^{pro} from SARS-CoV-2 and discovery of its inhibitors. *Nature.* 2020; 582: 289–93.
8. Zhang L, Lin D, Sun X, Curth U, Drosten C, Sauerhering L, et al. Crystal structure of SARS-CoV-2 main protease provides a basis for design of improved α -ketoamide inhibitors. *Science.* 2020; 368 (6489): 409–12.
9. Liu Y, Liang C, Xin L, Ren X, Tian L, Ju X, et al. The development of Coronavirus 3C-Like protease (3CLpro) inhibitors from 2010 to 2020. *Eur J Med Chem.* 2020; 206: 112711.
10. Owen DR, Allerton CMN, Anderson AS, Aschenbrenner L, Avery M, Berritt S, et al. An oral SARS-CoV-2 Mpro inhibitor clinical candidate for the treatment of COVID-19. *Science.* 2021; 374 (6575): 1586–93.
11. de Vries M, Mohamed AS, Prescott RA, Valero-Jimenez AM, Desvignes L, O'Connor R, et al. A comparative analysis of SARS-CoV-2 antivirals characterizes 3CLpro inhibitor PF-00835231 as a potential new treatment for COVID-19. *J Virol.* 2021; 95 (10): e01819–20.
12. Poreba M. Protease-activated prodrugs: strategies, challenges, and future directions. *FEBS J.* 2020; 287 (10): 1936–69.
13. Choi KY, Swierczewska M, Lee S, Chen X. Protease-activated drug development. *Theranostics.* 2012; 2 (2): 156–78.
14. Richter M, Leuthold MM, Graf D, Bartenschlager R, Klein CD. Prodrug activation by a viral protease: evaluating combretastatin peptide hybrids to selectively target infected cells. *ACS Med Chem Lett.* 2019; 10: 1115–21.
15. Boyce JH, Dang B, Ary B, Edmondson Q, Craik CS, Degrado WF, et al. Platform to Discover Protease-Activated Antibiotics and Application to Siderophore-Antibiotic Conjugates. *J Am Chem Soc.* 2020; 142 (51): 21310.

Литература

1. The top 10 causes of death, Geneva: World Health Organization c2022 [cited 2022 Nov 30]. Available from: <https://www.who.int/news-room/fact-sheets/detail/the-top-10-causes-of-death>.
2. WHO Coronavirus (COVID-19) Dashboard, Geneva: World Health Organization c2022 [cited 2022 Nov 30]. Available from: <https://covid19.who.int/>.
3. Zhou H, Yang J, Zhou C, Chen B, Fang H, Chen S, et al. A Review of SARS-CoV2: Compared With SARS-CoV and MERS-CoV. *Front Med.* 2021; 8: 628370.
4. Fehr AR, Perlman S. Coronaviruses: an overview of their replication and pathogenesis. *Methods Mol Biol.* 2015; 1282: 1–23.
5. Báez-Santos YM, St. John SE, Mesecar AD. The SARS-coronavirus papain-like protease: structure, function and inhibition by designed antiviral compounds. *Antiviral Res.* 2015; 115: 21–38.
6. Wang F, Chen C, Tan W, Yang K, Yang H. Structure of Main Protease from Human Coronavirus NL63: Insights for Wide Spectrum Anti-Coronavirus Drug Design. *Sci Rep.* 2016; 6: 22677.
7. Jin Z, Du X, Xu Y, Deng Y, Liu M, Zhao Y, et al. Structure of M^{pro} from SARS-CoV-2 and discovery of its inhibitors. *Nature.* 2020; 582: 289–93.
8. Zhang L, Lin D, Sun X, Curth U, Drosten C, Sauerhering L, et al. Crystal structure of SARS-CoV-2 main protease provides a basis for design of improved α -ketoamide inhibitors. *Science.* 2020; 368 (6489): 409–12.
9. Liu Y, Liang C, Xin L, Ren X, Tian L, Ju X, et al. The development of Coronavirus 3C-Like protease (3CLpro) inhibitors from 2010 to 2020. *Eur J Med Chem.* 2020; 206: 112711.
10. Owen DR, Allerton CMN, Anderson AS, Aschenbrenner L, Avery M, Berritt S, et al. An oral SARS-CoV-2 Mpro inhibitor clinical candidate for the treatment of COVID-19. *Science.* 2021; 374 (6575): 1586–93.
11. de Vries M, Mohamed AS, Prescott RA, Valero-Jimenez AM, Desvignes L, O'Connor R, et al. A comparative analysis of SARS-CoV-2 antivirals characterizes 3CLpro inhibitor PF-00835231 as a potential new treatment for COVID-19. *J Virol.* 2021; 95 (10): e01819–20.
12. Poreba M. Protease-activated prodrugs: strategies, challenges, and future directions. *FEBS J.* 2020; 287 (10): 1936–69.

13. Choi KY, Swierczewska M, Lee S, Chen X. Protease-activated drug development. *Theranostics*. 2012; 2 (2): 156–78.
14. Richter M, Leuthold MM, Graf D, Bartenschlager R, Klein CD. Prodrug activation by a viral protease: evaluating combretastatin peptide hybrids to selectively target infected cells. *ACS Med Chem Lett*. 2019; 10: 1115–21.
15. Boyce JH, Dang B, Ary B, Edmondson Q, Craik CS, Degrado WF, et al. Platform to Discover Protease-Activated Antibiotics and Application to Siderophore–Antibiotic Conjugates. *J Am Chem Soc*. 2020; 142 (51): 21310.